UNIVERSIDAD AUTONOMA DE MADRID

Facultad de Ciencias
Sección Departamental de Ingeniería Química

Carbones Activados Granulares a partir de Residuos mediante Activación por Ciclos de Oxidación-Desorción

Granular Activated Carbons from Residues by Activation Cycles of Oxidation-Desorption

Tesis Doctoral
Doctoral Thesis

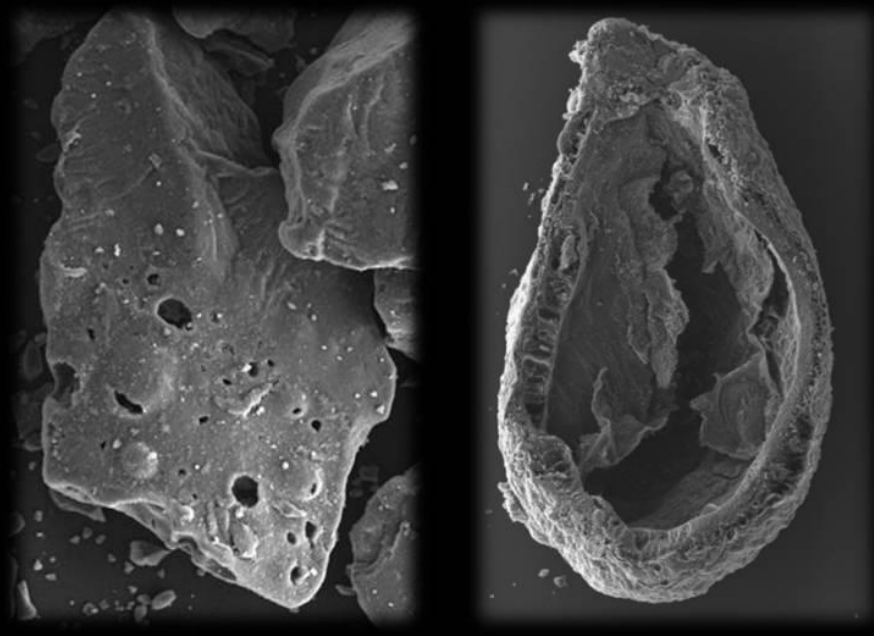

Diana Jiménez Cordero

Madrid 2013

UNIVERSIDAD AUTÓNOMA DE MADRID

FACULTAD DE CIENCIAS
SECCIÓN DEPARTAMENTAL DE INGENIERÍA QUÍMICA

CARBONES ACTIVADOS GRANULARES A PARTIR DE RESIDUOS MEDIANTE ACTIVACIÓN POR CICLOS DE OXIDACIÓN-DESORCIÓN

GRANULAR ACTIVATED CARBONS FROM RESIDUES BY ACTIVATION CYCLES OF OXIDATION-DESORPTION

MEMORIA

QUE PARA OPTAR AL GRADO DE

DOCTOR CON MENCIÓN INTERNACIONAL

PRESENTA

DIANA JIMÉNEZ CORDERO

DIRECTORES: DR. FRANCISCO HERAS MUÑOZ
DR. MIGUEL ÁNGEL GILARRANZ REDONDO

MADRID, 2013

D. Francisco Heras Muñoz, Profesor Contratado Doctor, y D. Miguel Ángel Gilarranz Redondo, Profesor Titular, ambos profesores de la Sección Departamental de Ingeniería Química y pertenecientes al Departamento de Química-Física Aplicada de la Universidad Autónoma de Madrid.

HACEN CONSTAR: que el presente trabajo titulado: “Carbones activados granulares a partir de residuos mediante activación por ciclos de oxidación-desorción”, presentado por Dña. Diana Jiménez Cordero, ha sido realizado bajo su dirección, en los laboratorios del Área de Ingeniería Química, en la Universidad Autónoma de Madrid y que, a su juicio, reúne los requisitos de originalidad y rigor científico necesarios para ser presentado como Tesis Doctoral.

Y para que conste a efectos oportunos, firmamos el presente informe en Madrid a siete de junio de dos mil trece.

Francisco Heras Muñoz Miguel Ángel Gilarranz Redondo

TODO LO QUE TIENE UN PRINCIPIO,
TIENE UN FINAL

Agradecimientos

En primer lugar, quisiera agradecer a mis directores de tesis Francisco Heras Muñoz y Miguel Ángel Gilarranz Redondo, por su confianza en mí y por darme la oportunidad de participar en los proyectos de neumáticos y de semillas de uva que han dado lugar a esta tesis. Gracias por vuestra dedicación, apoyo y consejos durante todos estos años.

Quiero agradecer también a Juan José Rodríguez Jiménez su ayuda y consejos que valoro enormemente.

Al Sr. Lázaro Alonso quisiera agradecer su colaboración al proporcionarnos más de 20 Kg de semillas de uva, sin los cuales esta tesis no hubiese sido posible. Y a Noe, por su simpatía y amistad, y por toda su ayuda durante todo este tiempo.

Gracias a Encarnación Raymundo Piñero por facilitarme la oportunidad de desarrollar parte de mi tesis en el CNRS en Orleans, por su cálido recibimiento y su ayuda tanto dentro como fuera del laboratorio. Gracias a Laurent y a Nicola por su ayuda en el laboratorio y a Juan, Indira y Leire por las quedadas para comer de todas las semanas.

Al servicio interdepartamental de investigación (SIdI), en especial a Pascual y Luis de análisis elemental y a Esperanza, Isi y Quique de SEM y del SEGAINVEX al taller de vidrio. Gracias a todos ellos por su trabajo y dedicación.

También quiero agradecer a mis compañeros de la sección departamental por estar siempre para ayudar, con una idea, un consejo, para dar ánimo en momentos de nervios antes de un congreso, traerme una tirita o llevarme al hospital, por los partidos de fútbol y por esos grandes momentos de risas que no olvidaré. De la planta piloto, a Cristian, Cristina, Elena P., Irene, Jesús, Nuria, Sonia, Vero y Luis. Del C-VI a Alex, Carmen, Gema, Jose, Jose Luis, Maca, María, Sandra y Sonia B. Y del C-XVI a Ari,

Carol, Elena, Jorge, Víctor y Zahara. No he podido tener mejores compañeros que vosotros.

En el ámbito personal, quiero agradecer a mis amigas, las de Leganés y las de Aldea, que siempre están cuando se las necesita, que aguantan mis historias del laboratorio y en algunos momentos hasta me han obligado a distraerme para dejar de pensar por un rato en esta tesis.

Para finalizar quisiera dar las gracias a mi familia. A mis padres por todo lo que me han ayudado y me ayudan. A mi hermano por ser mi amigo además de mi hermano, por apoyarme en cada cosa que he hecho a lo largo de mi vida y con el que siempre puedo contar, que se alegra como el que más con cada congreso y con cada cosa que publico, esta tesis también es un poco suya. A Inma, por ser mi amiga desde que llegó a la familia. Y por último, y no por ello menos importantes a Daniel y Marcos, a los que quiero con locura, sois mi alegría, sólo con pensar en vosotros no puedo evitar sonreír.

A tod@s, Gracias.

ÍNDICE / INDEX

RESUMEN / SUMMARY 7

CHAPTER 1. BACKGROUND 15

1.1. Residual materials 17
1.1.1. Waste tire 18
1.1.2. Grape seeds 21
1.2. The activated carbon 24
1.2.1. Obtaining activated carbon 27
1.3. Activation by cycles of oxidation-desorption 31
1.3.1. Oxidation with ozone 33
1.3.2. Oxidation in liquid phase 34
1.4. Applications 36
References 40

CHAPTER 2. MATERIALS, DEVICES AND METHODOLOGY 49

2.1. Materials 51
2.1.1. Starting materials 51
2.1.2. Other materials 52
2.2. Experimental Devices 53
2.2.1. Oil extraction from grape seeds 53
2.2.2. Pyrolysis system 54
2.2.3. Activation systems 55
2.3. Activation conditions 58
2.3.1. Gas phase oxidation 58
2.3.2. Liquid phase oxidation 59
2.4. Characterization methods 60
2.4.1. Differential weighting 61
2.4.2. Nitrogen adsorption-desorption isotherms 61
2.4.3. Argon adsorption-desorption isotherms 62
2.4.4. CO_2 adsorption isotherms 63

2.4.5. Mercury porosimetry 64
2.4.6. Elemental analysis and inductively coupled plasma mass spectrometry 64
2.4.7. X-ray photoelectron spectroscopy 64
2.4.8. Scanning electron microscopy 65
2.4.9. Fourier transform infrared spectroscopy 65
2.4.10. Thermogravimetric analysis 66
2.4.11. Temperature programmed desorption 66
2.4.12. Temperature programmed oxidation 67
2.4.13. Attrition tests 68
2.5. Application of activated carbons to the preparation of electric double-layer capacitors 68
2.5.1. Preparation of electrodes and capacitors 68
2.5.2. Electrochemical characterization 69
2.5.3. Cyclic voltammetry 70
2.5.4. Galvanostatic charge/discharge 70
2.5.5. Impedance spectroscopy 71
References 72

CHAPTER 3. PYROLYSIS OF GRAPE SEEDS 75

3.1. Abstract 77
3.2. Operating variables tested 78
3.3. Samples characterization 78
3.4. Results 79
3.4.1. Influence of pyrolysis variables 80
3.4.2. Specific surface area 85
3.4.3. Pore volume 90
3.4.4. Pore size distribution 93
3.4.5. Morphological analysis 95
3.4.6. Attrition tests 98
References 100

CHAPTER 4. ACTIVATION OF WASTE TIRES CHAR WITH AIR 103

4.1. Abstract 105
4.2. Materials and methods 106
4.2.1. Samples characterization 106
4.2.2. Cyclic activation conditions 107
4.3. Results 109
4.3.1. Burn-off in 6-cycle tests 109
4.3.2. Specific surface area in 6-cycle tests 110
4.3.3. Mean pore size in 6-cycle tests 112
4.3.4. Analysis of variance about influence of variables studied 115
4.3.5. Burn-off in 20-cycle tests 118
4.3.6. Specific surface area in 20-cycle tests 119
4.3.7. Pore volume in 20-cycle tests 121
4.3.8. Pore size distribution 123
4.3.9. Temperature programmed oxidation 125
4.3.10. Morphological analysis 127
4.3.11. Comparison with results in literature 128
References 129

CHAPTER 5. ACTIVATION OF GRAPE SEEDS CHAR WITH AIR 133

5.1. Abstract 135
5.2. Materials and methods 136
5.2.1. Samples characterization 136
5.2.2. Cyclic activation conditions 137
5.3. Results 137
5.3.1. Activation conditions 137
5.3.2. Burn-off 140
5.3.3. Specific surface area 141
5.3.4. Pore volume 147
5.3.5. Pore size distribution 150
5.3.6. Morphological analysis 153

5.3.7. Attrition tests 155
5.3.8. Comparison with results in literature 157
References 158

CHAPTER 6. ACTIVATION OF GRAPE SEEDS CHAR WITH OZONE 161

6.1. Abstract 163
6.2. Materials and methods 164
6.2.1. Samples characterization 164
6.2.2. Cyclic activation conditions 165
6.3. Results 165
6.3.1. Burn-off 166
6.3.2. Specific surface area 167
6.3.3. Pore volume 173
6.3.4. Pore size distribution 176
6.3.5. Fourier transform infrared spectroscopy 179
6.3.6. Morphological analysis 181
References 183

CHAPTER 7. ACTIVATION OF WASTE TIRE CHAR IN LIQUID PHASE OXIDATION 185

7.1. Abstract 187
7.2. Materials and methods 188
7.2.1. Samples characterization 188
7.2.2. Cyclic activation conditions 188
7.2.3. Experimental program 189
7.3. Results 191
7.3.1. Burn-off in 5-cycle tests 191
7.3.2. Specific surface area in 5-cycle tests 192
7.3.3. Pore volume in 5-cycle tests 193
7.3.4. Mean pore size in 5-cycle tests 194
7.3.5. Burn-off in 15-cycle tests 195
7.3.6. Specific surface area in 15-cycle tests 196

7.3.7. Pore volume in 15-cycle tests 197
7.3.7. Pore size distribution in 15-cycle tests 198
7.3.9. Morphological analysis 200
References 202

CHAPTER 8. ACTIVATION OF GRAPE SEEDS CHAR IN LIQUID PHASE OXIDATION 203

8.1. Abstract 205
8.2. Materials and methods 206
8.2.1. Samples characterization 206
8.2.2. Cyclic activation conditions 206
8.3. Results 207
8.3.1. Burn-off 207
8.3.2. Specific surface area 208
8.3.3. Pore volume 211
8.3.4. Pore size distribution 213
8.3.5. Fourier transform infrared spectroscopy 216
8.3.6. Morphological analysis 218
References 220

CHAPTER 9. APPLICATION OF GRAPE SEEDS-BASED ACTIVATED CARBONS AS STARTING MATERIAL FOR ELECTRODES USED IN SUPERCAPACITORS 221

9.1. Abstract 223
9.2. Materials and methods 224
9.2.1. Chemical and textural characterization 224
9.2.2. Electrochemical characterization 225
9.3. Results 225
9.3.1. Chemical and textural characterization 225
9.3.2. Electrochemical characterization 235
References 251

CONCLUSIONES / CONCLUSIONS **253**

APPENDICES **267**

9.1. Appendix 1. Nomenclature **269**

9.2. Appendix 2. Diffusion of results **271**

NOTES **277**

RESUMEN

SUMMARY

Resumen

La tesis que se presenta se ha centrado en la obtención y caracterización de sólidos carbonosos (*char*) mediante pirólisis de semillas de uva y neumáticos fuera de uso (NFU), así como su posterior uso para la preparación y caracterización de carbones activados (AC) con diversas posibilidades de aplicación. Para ello se propone un método de activación por ciclos de oxidación-desorción, que permite una activación y un desarrollo de porosidad controlados. En la etapa de oxidación se han utilizado varios agentes oxidantes, como son aire y ozono en fase gas, y ácido nítrico, peróxido de hidrógeno y persulfato de amonio, en fase líquida.

En el capítulo 2 se realiza una breve descripción de los materiales, las instalaciones experimentales y los métodos de caracterización utilizados a lo largo de la tesis.

En el capítulo 3 se evalúa la influencia de las distintas variables de operación sobre los rendimientos y las propiedades texturales de los *char* obtenidos a partir de la pirólisis de semillas de uva. Las variables que se han estudiado son la extracción del aceite presente en las semillas, la temperatura de pirólisis (300 – 1000 ºC) y la velocidad de calentamiento (lenta -10 $^{o}Cmin^{-1}$- y súbita o *flash*). La caracterización de los *char* se ha realizado empleando diferentes técnicas como son el análisis elemental, isotermas de adsorción-desorción de nitrógeno y argón, isotermas de adsorción de CO_2, porosimetría por intrusión de mercurio y microscopía electrónica de barrido. También se ha realizado un test de atrición para determinar la resistencia mecánica de las partículas de *char* y estudiar las propiedades texturales de las distintas capas de las semillas pirolizadas. El trabajo de caracterización ha permitido seleccionar las condiciones óptimas de pirólisis, en las que se ha obtenido el *char* utilizado para preparar los carbones activados granulares que se describen en los capítulos dedicados a la activación.

El capítulo 4 presenta los resultados del estudio de la influencia de la temperatura de desorción (550, 650 y 750 ºC) y el tamaño de partícula (0.5, 1, y 2 mm) en la activación de *char* de NFU mediante ciclos de oxidación-desorción, usando aire como agente activante. En una primera aproximación se realizó un estudio a 6 ciclos de activación, que permitió seleccionar las tres combinaciones de condiciones de operación que proporcionan los mayores desarrollos de superficie específica. En estas tres condiciones, se realizaron estudios más extensos, hasta completar 20 ciclos de activación. Los carbones activados obtenidos se caracterizaron mediante isotermas de adsorción-desorción de nitrógeno, oxidación térmica programada y microscopía electrónica de barrido.

El capítulo 5 aborda la activación del *char* obtenido a partir de semillas de uva mediante ciclos de oxidación-desorción usando aire como agente activante. Aquí, las variables estudiadas son el número de ciclos de activación (hasta 10 ciclos), la temperatura de oxidación (200, 250 y 275 ºC) y la temperatura de desorción (550, 675, 850 y 950 ºC). Estos intervalos de temperaturas se establecieron a partir de ensayos de termogravimetría y desorción térmica programada realizados al *char*. Los carbones activados obtenidos se sometieron a caracterización textural, morfológica y de atrición, mediante las mismas técnicas indicadas para el *char*.

Para finalizar con la activación en fase gas, el capítulo 6 describe la preparación de carbón activado a partir de *char* de semillas de uva usando ozono como agente activante. De nuevo, se han estudiado la temperatura de oxidación (250 y 275 ºC), la temperatura de desorción (850 y 950 ºC) y el número de ciclos de activación aplicados (hasta 10 ciclos). En este caso, además de las técnicas de caracterización empleadas con los materiales descritos arriba, se utilizó la espectroscopía de infrarrojos por transformada de Fourier (FTIR) para determinar los principales grupos funcionales presentes en la superficie del carbón activado.

Los capítulos 7 y 8 tratan también de la obtención de carbones activados mediante ciclos de oxidación-desorción, pero con la característica

de que la etapa de oxidación se lleva a cabo en fase líquida usando diferentes agentes oxidantes.

En primer lugar se realiza la activación del *char* de NFU en dos series de experimentos. En la primera serie las variables de estudio son el agente activante (ácido nítrico, peróxido de hidrógeno y persulfato amónico), el tamaño de partícula (1 y 2 mm) y el número de ciclos de activación (hasta 5 ciclos). En la segunda serie de experimentos se estudió el agente activante (ácido nítrico y peróxido de hidrógeno) y su concentración (15 y 30 % en peso) y el número de ciclos (hasta 15), fijándose el tamaño de partícula en 2 mm.

En la activación de *char* de semillas de uva mediante oxidación en fase líquida, las variables de estudio fueron el agente activante (ácido nítrico, peróxido de hidrógeno y persulfato amónico), la temperatura de desorción (850 y 950 ºC) y el número de ciclos de activación (10 máximo). Las propiedades texturales, químicas superficiales y morfológicas fueron caracterizadas como en anteriores etapas del trabajo (capítulo 6).

Para finalizar el apartado de resultados experimentales, en el capítulo 9 se recogen los resultados obtenidos durante la aplicación de carbones activados, obtenidos a partir de semillas de uva, como material de partida para fabricar electrodos utilizados en supercapacitores, con el fin de evaluar sus propiedades electroquímicas en el almacenamiento de energía. El comportamiento de los electrodos se analizó usando voltametría cíclica, carga/descarga galvanostática y espectroscopía de impedancia, empleando tres electrolitos acuosos diferentes (Na_2SO_4, KOH y H_2SO_4). Para este estudio, se seleccionaron los carbones activados que presentaron mayor desarrollo de superficie específica y diferentes propiedades texturales y distribuciones de tamaño de poro.

Summary

This thesis is focused on the preparation and characterization of carbonaceous materials (char) by pyrolysis of grape seeds and waste tires rubber (WTR), as well as on their use for the preparation of activated carbons with different potential applications. An activation method based on cycles of oxidation-desorption is proposed, allowing for controlled activation and porosity development. In the oxidation stage, different oxidizing agents were used, namely air and ozone in gas phase, and nitric acid, hydrogen peroxide and ammonium persulphate, in liquid phase.

Chapter 2 shows a brief description of the materials, experimental devices and the characterization methods used throughout the thesis. In chapter 3, the influence of the different operation variables on the textural properties of the char obtained from pyrolysis of grape seeds was evaluated. The variables studied were the extraction of the seed oil, pyrolysis temperature (300 – 1000 ºC) and heating rate (slow -10 ºCmin^{-1}- and flash). The characterization of chars was carried out using different techniques: elemental analysis, nitrogen and argon adsorption-desorption isotherms, CO_2 adsorption isotherms, mercury intrusion porosimetry and scanning electron microscopy. An attrition test was also performed to determine the mechanic resistance of char particles and to study the textural properties of different layers of pyrolyzed seeds. The characterization work allowed to identify the optimum pyrolysis conditions to obtain a char suitable for the preparation of granular activated carbons described in activation chapters.

Chapter 4 deals with the study of the influence of desorption temperature (550, 650 and 750 ºC) and particle size (0.5, 1, and 2 mm) on the activation of waste tire char by oxidation-desorption cycles using air as oxidizing agent. In a first approach, a study for 6 activation cycles was carried out, which allowed to select the three sets of operating conditions providing better results in terms of surface area development. Under such conditions, an extensive study of 20 activation cycles was performed. The activated carbons obtained were characterized by nitrogen adsorption-desorption

isotherms, temperature programmed oxidation and scanning electron microscopy.

Chapter 5 is dedicated to the activation of grape seeds char by cycles of oxidation-desorption using air as oxidizing agent. The variables studied were the number of activation cycles (up to 10 cycles), the oxidation temperature (200, 250 and 275 ºC) and the desorption temperature (550, 675, 850 and 950 ºC). These temperature ranges were established from thermogravimetric and temperature programmed desorption analysis of the grape seeds char. The textural properties, morphology and attrition resistance of the activated carbons obtained were studied by the same procedures applied to the char (chapter 3).

The evaluation of gas phase oxidants is completed in chapter 6, where the preparation of activated carbon from grape seeds char using ozone as oxidizing agent is studied. As in previous chapters, the oxidation temperature (250 and 275 ºC), the desorption temperature (850 and 950 ºC) and the number of cycles applied (up to 10 cycles) were the studied variables. In this case, in addition to the characterization techniques described above, Fourier transform infrared spectroscopy (FTIR) was used to determine the main oxygenated functional groups present on the activated carbon surface.

Chapters 7 and 8 are also devoted to the preparation of activated carbons by cycles of oxidation-desorption, but using different liquid phase oxidizing agents in the oxidation step. The activation of waste tires char (chapter 7) was performed in two series of experiments. In the first series, the variables studied were the oxidizing agent (nitric acid, hydrogen peroxide and ammonium persulphate), the particle size (1 and 2 mm) and the number of activation cycles (up to 5 cycles). In the second series, the influence of the oxidizing agent (nitric acid and hydrogen peroxide), its concentration (15 and 30 %v) and the number of cycles (up to 15 cycles) in the development of porosity were evaluated. In the activation of grape seeds char (chapter 8) by liquid phase oxidation, the parameters studied were the oxidizing agent (nitric acid, hydrogen peroxide and ammonium persulphate), the desorption

temperature (850 and 950 ºC) and the number of activation cycles (up to 10 cycles).

As a last approach, chapter 9 presents the results achieved using the activated carbons obtained from grape seeds in the preparation of electrodes used in supercapacitors, with the aim of evaluating their electrochemical properties in energy storage. The behavior of the electrodes was analyzed using cyclic voltammetry, galvanostatic charge/discharge and impedance spectroscopy with three aqueous electrolytes. To carry out this study, the activated carbons with the highest porosity development, but different textural properties and pore size distribution were selected.

CAPÍTULO 1 / CHAPTER 1

INTRODUCCIÓN

BACKGROUND

1.1. Materiales residuales

La masiva generación de residuos supone en la actualidad uno de los grandes retos ambientales. Sólo en España se produjeron más de 137 millones de toneladas de residuos [1], por lo que se hace imprescindible el desarrollo de soluciones eficaces que podrán ser muy diversas dependiendo del tipo de residuo considerado.

Los residuos son el último eslabón de cualquier actividad, ya sea doméstica, industrial, agrícola, etc. Se considera residuo cualquier sustancia u objeto que su poseedor deseche o tenga la intención o la obligación de desechar [2]. Así, el desarrollo de métodos y procedimientos destinados a la reutilización o revalorización de los residuos se ha consolidado como una de las áreas de investigación y desarrollo más importantes en los últimos años. Dado que la energía interviene en la inmensa mayoría de procesos de fabricación, transporte, etc., recuperar toda o parte de esa energía cuando un material deja de ser útil y se desecha no sólo es un reto desde un punto de vista científico y tecnológico, sino también un compromiso medioambiental [3].

Las bases de una gestión de residuos sostenible parten de minimizar su generación desde el origen, lo que puede requerir actuaciones como: mejoras en los métodos de fabricación, sustitución de materias primas, mejorar el aprovechamiento de los recursos, fomentar cambios hacia hábitos de consumo más sostenibles o la valorización de los residuos una vez producidos, entre otras.

Las alternativas básicas son la *reducción* en origen de la cantidad de residuos generada, la *recuperación* de todas aquellas materias o componentes que puedan volver a usarse directamente (donde se puede incluir la incineración con recuperación energética, o *valorización energética*, cuando sea la alternativa más interesante o la única posible) y el *reciclaje* (en el que el material residual se somete a una transformación mediante diversas técnicas para darle un nuevo uso), quedando la *eliminación* segura

de los residuos sin recuperación de materia o energía (siendo la incineración en condiciones adecuadas la opción más interesante) y con el almacenamiento en *vertederos* (que presenta problemas asociados de olores, plagas de animales, contaminación del suelo y aguas, degradación del paisaje, etc.) como últimas y menos deseables opciones, que deben emplearse cuando el reciclaje o la reutilización no son posibles [4].

En este trabajo, se han utilizado dos materiales residuales de gran producción en España, como son los neumáticos fuera de uso y las semillas de uva.

1.1.1. Neumáticos fuera de uso

La masiva fabricación de neumáticos, y las dificultades que presenta su correcta gestión una vez usados, constituyen uno de los más graves problemas medioambientales de los últimos años en todo el mundo. De acuerdo con estadísticas recientes, anualmente se generan en España en torno a 10 millones de neumáticos usados, lo que supone unas 314.000 toneladas [5]. La deposición de NFU en vertederos es un peligro potencial para la salud y el medioambiente (plagas de insectos, posibilidad de incendios, etc.) además de ocupar grandes espacios y de constituir un ineficaz medio de gestión al no recuperar ningún tipo de valor del residuo. Por ello, se desarrolló y se publicó el Real Decreto 1619/2005, de 30 de Diciembre, que posteriormente se ha dado continuidad con el II Plan Nacional de Neumáticos Fuera de Uso, el cual forma parte del Plan Nacional Integrado de Residuos 2008 – 2015. Entre otras medidas, obliga a los productores a garantizar la recogida y a realizar una correcta gestión y valorización de los NFU, mediante procedimientos que permitan reciclar o recuperar materiales y/o energía y, en consecuencia, usar con moderación los recursos naturales.

El aprovechamiento de los NFU actualmente comprende la reutilización (mediante recauchutado de los neumáticos que estén en buen

estado), fabricación de combustible alternativo (principalmente para uso en cementeras) y el reciclado (mediante la molienda de los NFU y separación de los metales y textiles para obtener un granulado de caucho que se utiliza como aditivo de los asfaltos para carreteras, para fabricar suelos de pistas deportivas, parques infantiles, bandas de retención de tráfico, etc. (Figura 1.1) [6].

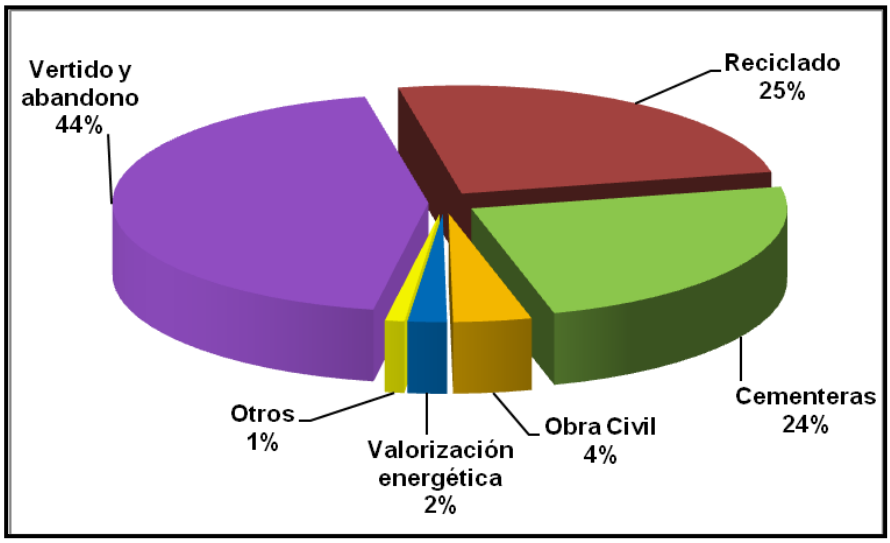

Figura 1.1. Destino de los NFU en España.

Los neumáticos están compuestos por más de 100 sustancias diferentes, siendo los principales componentes el caucho (50 %), negro de humo (25 %), metales (10 %), azufre (1 %), óxido de zinc (1 %) y muchos otros aditivos [7]. Esta proporción puede variar en función de las propiedades que se deseen conseguir según el tipo de neumático, pero una característica esencial es que el elemento principal presente en los neumáticos es el carbono (Tabla 1.1). Los cauchos utilizados son una mezcla de caucho natural y cauchos sintéticos, principalmente copolímero Estireno-Butadieno (SBR) [8].

Tabla 1.1. Composición elemental de los neumáticos.

Carbono	55 – 85 %
Hidrógeno	6 – 7 %
Nitrógeno	0.3 – 0.5 %
Azufre	1.7 – 2 %

Además de los procesos de valorización de neumáticos comentados anteriormente, otros métodos basados en la pirólisis o gasificación del caucho de los NFU han sido extensamente estudiados. La Tabla 1.2 muestra la composición de los productos de pirólisis de neumáticos [9, 10].

La composición química de las fases líquida y gaseosa ha sido ampliamente estudiada con el fin de recuperar compuestos químicos valiosos, como los aromáticos y las olefinas. Sin embargo, el bajo coste de producción petroquímica de estos compuestos hace que la recuperación a partir de pirólisis de NFU resulte antieconómica. Por el contrario, el elevado poder calorífico de estas fracciones (en torno a 35 $MJ(Nm^{-3})$ y 40 $MJkg^{-1}$ para fracción gaseosa y la líquida respectivamente [9, 11]), similar al de combustibles convencionales como el petróleo o el carbón (en torno a 30 – 40 $MJkg^{-1}$) y muy superior al del gas natural (unos 5 $MJkg^{-1}$), hace que su utilización como combustible sea una opción viable e interesante desde la perspectiva económica.

Tabla 1.2. Composición de los productos de pirólisis de NFU.

Fracciones obtenidas		Composición
25 – 30 %	Gases	COx, H_2, metano, etano, etileno, propano, propileno y butenos
25 – 30 %	Líquidos oleosos	Monómeros (isopreno, estireno, butadieno), oligómeros, poliaromáticos (alquitranes)
30 – 50 %	Sólidos	Residuo carbonoso ("*char*")

Pero una especial atención merece la valorización del residuo sólido, el *char*. En general, los *char* producidos a partir de neumáticos fuera de uso no poseen características apropiadas para su uso directo en aplicaciones comerciales. Por esta razón, varios métodos han sido estudiados con el objetivo de modificar las propiedades de estos *char* para ser utilizados como negro de humo, carbones activados u otro tipo de materiales. Por ejemplo, los carbones activados obtenidos a partir de NFU han sido probados satisfactoriamente como adsorbentes en el tratamiento de aguas residuales [9] y separación de gases [12].

1.1.2. Semillas de uva

Los residuos procedentes de la agricultura, silvicultura y, en general, todos los residuos biomásicos están siendo cada vez más considerados como recursos alternativos para la obtención de energía, productos químicos y materiales tales como los materiales de carbón. Estos subproductos han demostrado ser prometedoras materias primas para la producción de carbón activado a causa de su buena disponibilidad a bajo coste [13].

La biomasa está formada por una compleja mezcla de materia orgánica y, en menor medida, materia inorgánica. Esa materia orgánica está

compuesta principalmente por celulosa, hemicelulosa y lignina, mientras que la materia inorgánica está formada por especies minerales de diferentes clases como silicatos, sulfatos, óxidos, carbonatos, fosfatos, nitratos, etc. La composición química elemental de los residuos biomásicos comprende los siguientes elementos, en orden decreciente de contenido: C > O > H > N > Ca > K > Si > Mg > Al > S > Fe > P > Cl > Na > Mn > Ti [14].

Las variaciones de composición que presentan los distintos tipos de biomasa pueden afectar a las propiedades y la estructura porosa de los carbones activados que se preparen con ellos. Así, hay estudios en los que se demuestra que materiales con un alto contenido en lignina desarrollan carbones activados con estructura principalmente macroporosa, mientras que materiales con un mayor porcentaje de celulosa conducen a carbones activados con una estructura predominantemente microporosa [13].

Existe abundante bibliografía sobre preparación de carbones activados a partir de gran variedad de residuos biomásicos, como la turba [15], huesos de aceituna [16], madera de abedul [17], residuos de trigo [18] y de algodón [19], cáscara de almendras [13, 20], huesos de melocotón [13, 20] y cereza [13, 21], semillas de uva [13, 15], cáscaras de avellanas, nueces [13, 20], cacahuetes [22], coco [23], etc. De especial interés en nuestro país son las semillas de uva, ya que representan hasta un 15 % de los residuos sólidos procedentes de la industria vitivinícola [24, 25]. Según la FAO (*Food and Agriculture Organization of the United Nations*), en España se producen anualmente en torno a 6 millones de toneladas de uva para la producción de vino [26], por lo que la cantidad de residuos de semillas de uva que se genera es notable.

Hasta ahora los residuos vitivinícolas se han utilizado para producir material para compostaje y para la producción de biocombustibles. Concretamente, las semillas de uva se usan habitualmente para producir combustible y alimento para ganado. De ellas también se extrae aceite de gran calidad para el consumo humano [24, 25], si bien esta aplicación es aún minoritaria.

Con todo ello, las semillas de uva constituyen un material de partida económico, abundante y con una alta disponibilidad, que recientemente ha recibido atención para su valorización mediante pirólisis, pudiendo ser una fuente interesante para la producción de combustibles líquidos y gaseosos y materiales carbonosos como el carbón activado.

Los dos tipos principales de procesos de conversión usados para obtener productos de valor añadido a partir de biomasa son los termoquímicos y los bioquímicos. La conversión termoquímica de la biomasa incluye la gasificación, la combustión y la pirólisis. Las propiedades texturales y el contenido de cenizas de los *char* obtenidos por pirólisis de semillas de uva proporcionan un material de partida interesante para la preparación de carbones activados mediante distintos métodos de activación tanto físicos como químicos.

Los char y carbones activados obtenidos a partir de residuos agrícolas y del procesado de frutas, como las semillas, cáscaras o pieles [15, 27, 28], ampliamente disponibles a bajo coste, han demostrado que no sólo el precursor, sino también las condiciones de pirolisis, tienen un importante efecto sobre las características del *char* producido [21, 29], lo que afecta significativamente a la calidad de los carbones activados obtenidos a partir de esos *char*. Así, materiales de partida con inadecuadas morfologías o composiciones (contenidos en cenizas o carbono, principalmente) no resultan recomendables para la preparación de carbones activados. Por otra parte, condiciones de operación mal seleccionadas, como una excesiva temperatura, pueden conducir al colapso de la estructura porosa por estrés térmico u otros inconvenientes [30].

El interés de evaluar el potencial de las semillas de uva como material de partida para la preparación de carbón activado (u otros materiales carbonosos) se basa tanto en su morfología singular como en su distribución de tamaño de poro, características importantes para la posible aplicación de los carbones como tamices moleculares para separación de gases [29] captura de CO_2 [31] o en sistemas de almacenamiento de energía [32].

1.2. El Carbón Activado

El carbón activado se puede obtener a partir de una gran variedad de precursores con alto contenido en carbono y bajo en materia inorgánica; además es interesante que sea de alta disponibilidad y bajo coste. El AC se consigue cuando el precursor se trata para mejorar sus propiedades texturales y/o químicas. Los materiales de partida utilizados son muy diversos: materiales naturales (como la turba [15], la madera [17], el carbón o cáscaras de coco [23]), residuos (huesos de aceituna [33], neumáticos fuera de uso [34], residuos de polímeros, lodos de fábricas de papel, lodos de depuradora [35], sub-productos agrícolas [27]), etc.

Los carbones activados pueden clasificarse atendiendo al tamaño de partícula en carbón activado en polvo, cuando las partículas tienen un tamaño inferior a 0.18 mm [36], y carbón activado granular (GAC), cuyo tamaño medio de partícula está habitualmente entre 1 y 5 mm. Actualmente también se pueden encontrar en otros formatos como fibras, telas o monolitos (Figura 1.2).

Figura 1.2. Diferentes formatos de carbones activados [37].

Dependiendo del precursor, del método de activación y del grado de activación, los carbones activados tendrán una determinada estructura porosa que se puede clasificar en función de los tamaños de poro (d_{poro}). Según la IUPAC (*International Union of Pure and Applied Chemistry*), a partir de datos de isotermas de adsorción de N_2, pueden distinguirse microporos (d_{poro} < 2 nm), mesoporos (2 nm < d_{poro} < 50 nm) y macroporos (d_{poro} > 50 nm) (Figura 1.3). A su vez, los microporos han sido clasificados en dos subgrupos: ultramicroporos (d_{poro} < 0,7 nm) y supermicroporos (0,7 nm < d_{poro} < 2 nm) [38, 39].

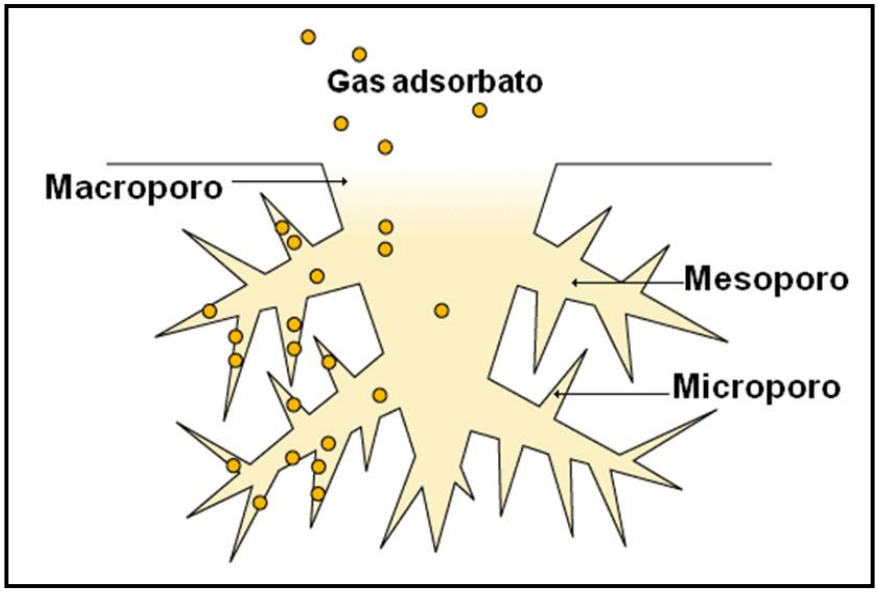

Figure 1.3. Representación esquemática de los tipos de poro [40].

Las propiedades de adsorción del carbón activado no sólo están determinadas por la estructura porosa sino también por su composición química superficial. La superficie del carbón activado puede adsorber moléculas en fase líquida o gas, sin embargo, también existe la posibilidad de quimisorción, en la que moléculas del adsorbato se fijan a los centros activados de la superficie mediante enlace químico. Por lo tanto, la eficacia del carbón activado depende tanto de su área superficial accesible, donde tiene lugar la adsorción física, como de la presencia de sitios activados en los que ocurre la quimisorción [41]. La superficie de los carbones puede presentar, en mayor o menor proporción, heteroátomos como oxígeno, nitrógeno, azufre, metales, etc., formando diferentes grupos superficiales. Éstos pueden proceder del material de partida, de los procesos de activación o de tratamientos de oxidación.

La oxidación es uno de los métodos más utilizados para modificar AC mediante generación de grupos superficiales carbono—oxígeno (Figura 1.4),

siendo los grupos más frecuentes los carboxílicos, fenoles, quinonas, lactonas y anhídridos. Los métodos de oxidación más comunes comprenden la utilización de gases oxidantes, como el dióxido de carbono, el vapor de agua y el oxígeno, o disoluciones oxidantes, como el ácido nítrico, peróxido de hidrógeno, etc. Pero tanto la oxidación en fase gas como en fase líquida pueden producir cambios en la estructura porosa de un material que afecte a su comportamiento [42].

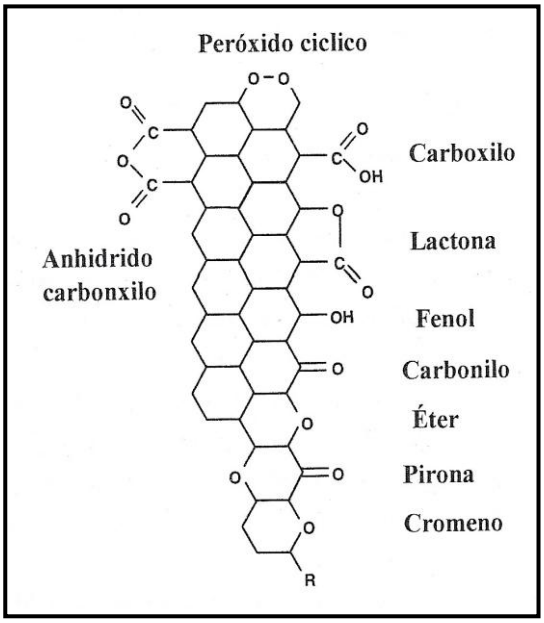

Figura 1.4. Grupos funcionales oxigenados que pueden estar presentes en la superficie carbonosa [43].

1.2.1. Obtención del carbón activado

Se han estudiado diferentes métodos con el fin de modificar las propiedades de los *char,* que consisten básicamente en desarrollar la porosidad de un material carbonoso para dar como resultado un aumento de

la superficie específica disponible, obteniendo así el carbón activado [23]. En principio, los métodos para preparar carbones activados pueden dividirse en dos categorías: activación física y activación química. La Figura 1.5 muestra un esquema de las etapas que se llevan a cabo en cada uno de estos procedimientos de activación.

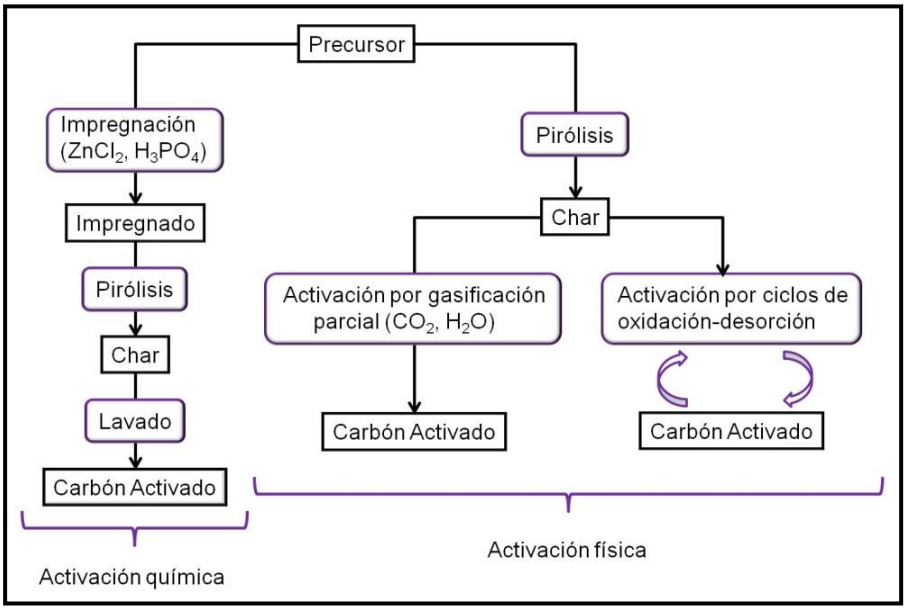

Figura 1.5. Etapas en la activación química y física para la producción de carbón activado.

En la activación química, el material de partida es impregnado con un agente químico activante, siendo habituales los agentes deshidratantes como H_2SO_4 [13], $ZnCl_2$ [44], KOH [22], y H_3PO_4 [45]. El material impregnado se carboniza a alta temperatura en atmósfera inerte (si bien estas temperaturas suelen ser inferiores a las utilizadas en activación física [44]) produciéndose simultáneamente la pirólisis y el desarrollo de porosidad. Finalmente, es necesaria una etapa de lavado de la muestra para eliminar el

agente activante. Estos reactivos químicos pueden promover la formación de una matriz rígida, menos propensa a la pérdida de volátiles y a la contracción del volumen de partícula a pesar del calentamiento a altas temperaturas [22].

Girgis et al. [22] prepararon carbón activado a partir de cáscaras de cacahuete mediante activación química por impregnación con H_3PO_4, $ZnCl_2$ y KOH del precursor antes de la pirólisis y con posterior activación con vapor de agua a 700 – 900 ºC. Consiguieron un gran desarrollo de porosidad, alcanzando valores de superficie específica BET (S_{BET}) de 1177, 420 y 268 m^2g^{-1} con valores de *burn-off* de 78, 70 y 73 % respectivamente, presentando las muestras, además, un alto grado de microporosidad. Aygün et al. [20] evaluaron la activación con cloruro de zinc sobre varios precursores biomásicos (cáscaras de almendras, de avellanas, de nueces y huesos de albaricoques) con posterior pirólisis en atmósfera inerte a 750 – 850 ºC, con resultados similares (S_{BET} de 736 – 793 m^2g^{-1} para valores de *burn-off* en torno al 70 %).

En la activación física, el primer paso para la obtención del carbón activo es la pirólisis. Este proceso consiste en la carbonización del material inicial a alta temperatura y en ausencia de oxígeno, para obtener un residuo sólido carbonoso (*char*) que servirá de precursor para obtener el carbón activado. Las variables de pirólisis tales como la temperatura, duración, velocidad de calentamiento y la atmósfera empleada (habitualmente se realiza en atmósfera de nitrógeno o helio) son de gran importancia ya que en función de éstas se obtendrá un *char* con una estructura y reactividad determinada. El *char* obtenido tendrá unas propiedades y una composición muy diferentes con respecto el material de partida pero, en general, aunque presenta una porosidad incipiente sigue teniendo una estructura porosa pobre, con lo que no tendrá unas características adecuadas para ser usadas directamente en aplicaciones comerciales. Por esta razón es necesaria una etapa de activación en la que se desarrolla esa porosidad inicial.

La activación física requiere, tras la pirólisis del precursor carbonoso, la activación del *char* obtenido. Este proceso se realiza generalmente a

elevada temperatura en presencia de algún oxidante, siendo los más utilizados el dióxido de carbono [9, 46] y vapor de agua [7, 45], aunque también pueden emplearse aire [47], ozono [48] o mezclas de ellos. A pesar de que el aire (oxígeno) es con mucho la opción más económica, raramente se usa debido a su elevada reactividad con los *char*, que dificulta un control efectivo del proceso de activación [34]. La activación con aire comúnmente transcurre bajo el control de la difusión de las moléculas de oxígeno hacia el interior de los poros, que conduce a un pobre desarrollo de área superficial centrado mayoritariamente en la formación de macroporos y asociado a altos valores de *burn-off* (entendiendo *burn-off* como pérdida indeseable de masa de carbón debido a la combustión) [9]. Así, Helleur et al. [9] usaron una mezcla de O_2/N_2 2/98 (vol.) como agente activante sin lograr un significativo desarrollo de S_{BET} con un *burn-off* del 15 %.

En la bibliografía existente sobre activación física de *char* obtenido a partir de NFU, se muestra que es difícil conseguir valores de S_{BET} superiores a 300 – 400 m^2g^{-1} sin un elevado *burn-off*. Como ejemplo, mediante activación con CO_2, se han obtenido valores de S_{BET} entre 200 y 300 m^2g^{-1} para *burn-off* de 10 – 40 % operando a 900 ºC, y de 200 – 1100 m^2g^{-1} con valores de *burn-off* en torno al 80 %, a 950 – 1100 ºC [9, 49, 50]. Valores tan elevados de *burn-off* suponen la casi total destrucción del material. Además, los carbones activados obtenidos son esencialmente mesoporosos.

Las semillas de uva se han usado anteriormente como precursor de carbón activado, obteniéndose valores de S_{BET} en torno a 400 m^2g^{-1}, con *burn-off* del 75 %, mediante una sola etapa de pirólisis/activación a 800 ºC con vapor de agua [27]. Savova et al. [13] en las mismas condiciones, consiguieron carbón activado a partir de semillas de uva con valores de S_{BET} en torno a 500 m^2g^{-1} con un *burn-off* de 74 % y con una distribución de tamaño de poro heterogénea, presentando un significativo volumen de macro, meso y microporo (0,28, 0,18 y 0,12 cm^3g^{-1} respectivamente).

Todos estos trabajos demuestran que no sólo la elección del material de partida, sino también el agente activante y las condiciones de activación

son importantes a la hora de preparar un carbón activado con unas características determinadas.

En el trabajo presentado en esta tesis se utilizó un novedoso método de activación alternativo a los métodos tradicionales ya descritos: la activación mediante ciclos de oxidación – desorción.

1.3. Activación mediante ciclos de oxidación – desorción

Este método consiste en una sucesión de ciclos formados por dos etapas. La primera etapa, la etapa de oxidación, se realiza a temperatura moderada en atmósfera oxidante, mientras que la segunda, la etapa de desorción, tiene lugar a alta temperatura en atmósfera inerte. Esta secuencia (ciclo de activación) es repetida hasta alcanzar el desarrollo de porosidad deseado. La Figura 1.6 muestra un esquema de este proceso.

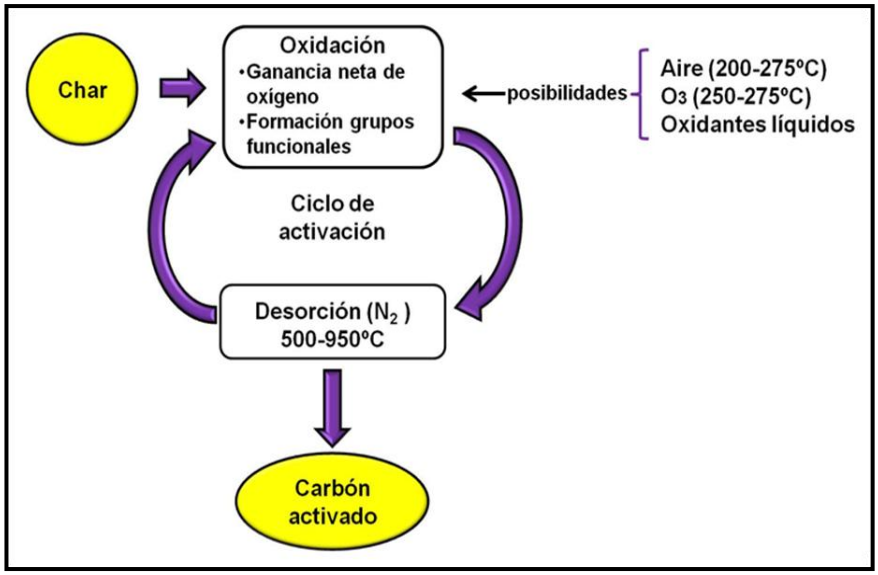

Figure 1.6. Esquema del proceso de activación por ciclos de oxidación-desorción.

Las variables críticas en el proceso de activación por ciclos de oxidación-desorción son la temperatura y el tiempo para cada etapa, lo que requiere que deban ser convenientemente estudiadas y optimizadas. Cuando el *char* es calentado en presencia de un oxidante, las reacciones de quimisorción por un lado, y de desorción y combustión por otro, son fenómenos competitivos. A baja temperatura la oxidación prevalece, mientras que la desorción/combustión es el proceso dominante a altas temperaturas. La temperatura de oxidación condiciona la cantidad de oxígeno adsorbido (grupos funcionales formados) respecto de la pérdida de masa por desorción/combustión, mientras que la de desorción influye no sólo en la cantidad de carbón que es desorbido como CO y/o CO_2 sino también en el tipo de grupos oxigenados superficiales que se descomponen generando porosidad [51].

Este método ha sido poco estudiado, lo que se pone de manifiesto por las escasas referencias bibliográficas existentes; sin embargo, puede ser

una alternativa interesante a los métodos tradicionales, ya que puede proporcionar una manera eficiente de crear porosidad a partir de un precursor poco poroso manteniendo la integridad física de la partícula, lo que permitiría obtener carbón activado granular [34]. Además, este método hace posible el uso de aire como agente activante, soslayando los inconvenientes derivados de su alta reactividad en procesos convencionales de activación física, lo cual impide seriamente un control efectivo del proceso de activación.

Py et al. [52] en el 2003 publicaron sobre este método de activación basada en ciclos de oxidación-desorción para controlar la alta reactividad del oxígeno como agente activante. Demostraron, por un lado, la gran importancia de encontrar unas condiciones de operación adecuadas. Por otra parte, que permite modificar la porosidad a lo largo de los ciclos, aumentando el volumen y el tamaño medio de poro, posibilitando el "diseño" o modificación del tamaño de poro en función de la aplicación que se le quiera dar al carbón activado producido. Esta capacidad para personalizar la porosidad de los carbones activados es de gran interés para numerosas aplicaciones [53].

1.3.1. Oxidación con ozono

Por otra parte, puede encontrarse abundante bibliografía presentando estudios sobre el efecto de la oxidación con ozono para el desarrollo de porosidad en materiales carbonosos. Álvarez et al. [54] informan de la degradación de la estructura porosa en carbones activados comerciales cuando se oxidan con ozono en fase gas, aumentando el efecto con la concentración de ozono. Observaron reducciones de S_{BET} y volumen de poro inferiores al 10 % usando aire enriquecido con ozono (40 mgL^{-1}) a 100 ºC, con un valor de *burn-off* en torno al 13 %. Belyaeva et al. [55] estudiaron la modificación de carbones activados granulares comerciales mediante oxidación a 25 ºC utilizando aire con 1.5 % de ozono durante 1 h, y

obtuvieron un significativo aumento de S_{BET} (de 683 a 885 m^2g^{-1}) y de volumen de poro total, debido a la formación de nuevos microporos. Una oxidación más prolongada da lugar a un proceso destructivo en la superficie de los micro y mesoporos que favorece su ensanchamiento, junto con un bloqueo parcial en la boca de los poros por los productos de oxidación. Este efecto de obstrucción de los microporos fue también observado por Rivera-Utrilla y Sánchez-Polo [56], como reducción de la superficie específica de carbones activados comerciales cuando se tratan con ozono en fase gas, a 25 ºC, de 20 a 120 min.

Estos trabajos [54 – 56] muestran, además, que la oxidación por ozono de los materiales carbonosos produce un considerable aumento de grupos oxigenados superficiales. Esta elevada capacidad oxidante del ozono, que posibilita la modificación tanto de la porosidad como la composición química superficial, lo convierte en un candidato muy prometedor para su uso en la etapa de oxidación en el proceso de activación cíclica.

1.3.2. Oxidación en fase líquida

Otro método que puede emplearse para modificar la superficie de carbones es la oxidación en fase líquida. Aunque en general, se utiliza para modificar la química superficial de carbones que han sido activados por otros métodos (generalmente con CO_2, vapor de agua o KOH), en este trabajo se presenta como una opción a evaluar, no sólo para modificar o crear grupos oxigenados superficiales sino también para desarrollar porosidad en materiales carbonosos sin activar (*char*) mediante el método de activación por ciclos de oxidación-desorción. Los oxidantes en fase líquida más utilizados son el ácido nítrico, el peróxido de hidrógeno y el persulfato amónico [42, 57 – 65].

La oxidación en fase líquida ha sido ampliamente utilizada en carbones activados comerciales [57 – 59] y obtenidos a partir de precursores

biomásicos [42, 60 – 65]. El grado de modificación depende tanto de la estructura del carbón como de las condiciones de oxidación y el agente oxidante. En general, el orden en cuanto a poder oxidante es HNO_3 > H_2O_2 > $(NH_4)_2S_2O_8$ [57, 60, 65]. La acción oxidante del HNO_3 aumenta como resultado de la fluidez de la solución ácida que permite una gran difusión y en los poros del AC. En cambio, para H_2O_2 y $(NH_4)_2S_2O_8$ no sólo la descomposición en disolución acuosa sino también el mayor tamaño molecular afecta negativamente a la acción oxidante [42] (tamaños moleculares: 59,09, 38,80 y 205,18 $Å^3$ para el ácido nítrico, peróxido de hidrógeno y persulfato amónico, respectivamente)[1].

En todos los casos, la oxidación produce un descenso tanto en superficie específica como en el volumen de poro, generalmente explicada por la restricción del volumen de poro disponible para la adsorción de N_2. Esta restricción está causada por la formación de grupos oxigenados en la entrada y/o pared de los microporos y por la posible destrucción de las paredes de los poros (y su posterior colapso) cuando se crean los grupos oxigenados superficiales, especialmente cuando se usa HNO_3 como oxidante [57, 60 – 62, 64].

La oxidación en fase líquida de carbones activados conduce a la formación de varios grupos funcionales comunes para los tres oxidantes ya mencionados: carboxilos, lactonas, fenoles y carbonilos. Sin embargo, se observan diferencias en su abundancia relativa, que puede ser estudiada mediante espectroscopía de infrarrojo [57, 59 – 62, 64, 65].

Dependiendo de la capacidad de las moléculas de los diferentes oxidantes para difundir dentro de los poros, los grupos superficiales generados pueden localizarse en diferentes zonas de la superficie carbonosa. Parece que se encuentran preferentemente en la superficie externa del carbón cuando se oxida con H_2O_2 y $(NH_4)_2S_2O_8$ mientras que cuando se usa ácido nítrico como agente oxidante, se crean más grupos en

[1] Valores obtenidos mediante software de simulación molecular COSMO-RS.

la superficie interna de las partículas del carbón [57, 61, 64, 65], debido a una mayor erosión de la superficie de las partículas que facilita la entrada de las moléculas de oxidante y a la mayor capacidad para difundir dentro de los poros del HNO_3 [60, 61, 65].

Mysyk et al. [58] utilizaron la activación por ciclos de oxidación-desorción usando H_2O_2 como agente oxidante en fase líquida y posterior desorción a 900 ºC en atmósfera inerte, obteniendo carbones activados microporosos a partir de sacarosa y celulosa, con superficies específicas entre 950 y 1600 m^2g^{-1} (calculados por el método de Dubinin-Radushkevich –S_{DR}– a partir de la isoterma de adsorción de N_2 a 77 K), a valores de *burn-off* entre el 18 y el 39 %. Los autores concluyen que este método de activación proporciona materiales con propiedades texturales idóneas para su uso como capacitores electroquímicos.

1.4. Aplicaciones

Los carbones activados tienen numerosas utilidades aunque los principales usos son la adsorción de impurezas en fase líquida como el tratamiento de aguas residuales [9], adsorción en fase gas como la captura de CO_2 [31] o la separación de gases [66], su uso como soporte de catalizadores [57] y otros que actualmente están suscitando gran interés, como su aplicación para el almacenamiento de energía mediante la producción de capacitores o supercapacitores [32].

Los capacitores electroquímicos de doble capa (EDLC), a menudo conocidos como “supercapacitores”, han recibido mucha atención en los últimos años. El supercapacitor más empleado es el denominado simétrico, el cual es un dispositivo formado por dos electrodos iguales sumergidos en electrolito orgánico o acuoso y separados físicamente por una barrera porosa denominada “separador”, a través de la cual los iones pueden moverse. Este separador puede ser de papel, fibra de vidrio o membrana polimérica. En estos capacitores los electrodos están compuestos de carbón

activado, que recubre un colector de corriente generalmente de aluminio u oro para los electrolitos orgánicos, o de acero inoxidable si el electrolito es acuoso. Además, para preparar un electrodo es necesario un aglutinante que mantenga unidas las partículas del carbón, siendo los más utilizados el fluoruro de polivinilideno, la carboximetilcelulosa y el poli-tetrafluoretileno. Por último, también es necesario un aditivo que mejore la conductividad del carbón activado, para lo cual suele emplearse el negro de humo [67].

El mecanismo de almacenamiento de energía en los supercapacitores se basa en la atracción electroestática entre cargas a lo largo de la doble capa formada en la interfase electrodo/electrolito. Cuando se conecta el EDLC a una fuente de alimentación y se aplica un voltaje entre los dos electrodos, éstos se cargan y atraen a los iones de carga opuesta, formando una doble capa de iones en la superficie de cada electrodo (Figura 1.7).

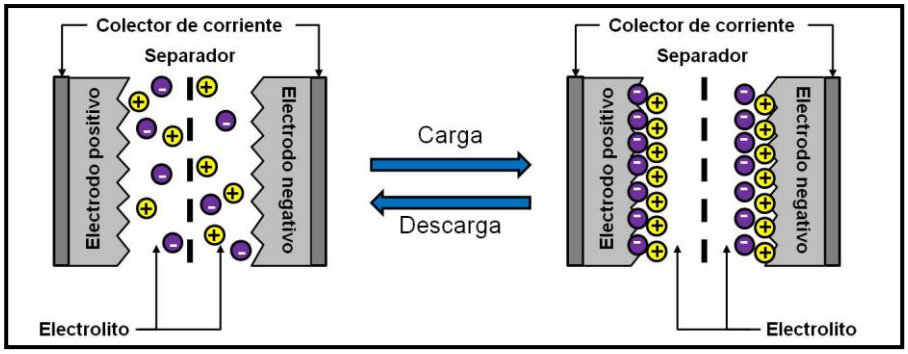

Figura 1.7. Estados de carga y descarga de un supercapacitor [67].

Dado que este fenómeno está controlado por la superficie específica del material constituyente del electrodo, los carbones activados son los materiales más usados para la fabricación de electrodos para supercapacitores, ya sea en forma de polvo, nanotubos, aerogeles, fullerenos, etc. [68]. Además de su elevada área superficial específica (SSA),

los carbones activados tienen otras ventajas como su alta disponibilidad y el coste relativamente bajo de la mayoría de los precursores y las tecnologías de producción [69, 70]. La utilización como electrodos para supercapacitores requiere de estos materiales que cumplan determinadas condiciones como son una alta conductividad (para asegurar alta densidad de carga), una distribución de tamaño de poro adecuada (principalmente con un tamaño medio de poro inferior a 1 nm). Por otra parte, una gran cantidad de grupos oxigenados superficiales puede ser una fuente de capacitancia adicional, denominada pseudo-capacitancia, ya que algunos de estos grupos podrían dar lugar a rápidas reacciones redox que mejoren la capacitancia cuando se trabaja con electrolitos acuosos como H_2SO_4 o KOH [71].

Los tamaños de los iones y los poros, así como el tipo de conexión entre los poros y la superficie externa de las partículas de carbón, pueden influir de manera importante en los valores de capacitancia, especialmente bajo condiciones de operación de alta densidad de carga de los supercapacitores. Raymundo-Piñero et al. [70] han estudiado el efecto del tamaño de poro en electrolitos acuosos y orgánicos usando una serie de carbones porosos preparados a partir del mismo precursor, texturalmente similares salvo en el tamaño medio de poro. Encontraron que la capacitancia específica de esos carbones aumenta cuando el tamaño medio de poro disminuye, dando como resultado que no sólo la SSA sino también la distribución de la porosidad en la zona de microporos influye sobre las propiedades electroquímicas del material. Chmiola et al. obtuvieron resultados similares usando carbones derivados de carburos (CDC) en electrolitos orgánicos o líquidos iónicos [72].

Otros autores (Guo et al. [73] y Yang et al. [74]) han preparado carbones activados con alta SSA a partir de cáscaras de arroz y de nueces respectivamente, y han estudiado como las diferentes condiciones de activación, que conducen a diferentes estructuras porosas de los carbones, pueden afectar a su comportamiento electroquímico. Se encontró que la capacitancia específica no era proporcional a la SSA y las muestras con

mesoporo ancho dieron lugar a los valores de capacitancia más bajos. Así, concluyeron que la estructura porosa, especialmente la distribución de tamaño de poro, tiene una influencia significativa en el rendimiento de los supercapacitores.

El comportamiento de los supercapacitores puede ser analizado usando varias técnicas electroquímicas. La voltametría cíclica se usa habitualmente para una rápida determinación de la electroactividad y la reversibilidad electroquímica de los materiales de los electrodos, mientras que la técnica de carga/descarga galvanostática se considera más fiable para medir la capacitancia, la reversibilidad farádica, la caída óhmica y la ciclabilidad en supercapacitores [67]. Además, la espectroscopía de impedancia es una técnica útil para la caracterización de capacitores, dando información complementaria, como la resistencia equivalente en serie (ESR) y la resistencia equivalente distribuida (EDR), que miden la resistencia a la conductividad entre el electrodo y el electrolito y la resistencia a la difusión de los iones dentro de los poros, respectivamente.

El rendimiento de un sistema electroquímico de almacenaje de energía puede ser caracterizado mediante el diagrama de Ragone, el cual representa la densidad de energía (que mide la cantidad de energía disponible) frente a la densidad de potencia (que mide la velocidad a la que el sistema libera la energía), generalmente expresadas en términos de $WhKg^{-1}$ y Wkg^{-1}, respectivamente [75].

Debido a la baja densidad de energía de los supercapacitores, en comparación con las baterías recargables comerciales, es necesario aumentar la capacitancia de los supercapacitores. Así, diseñar la estructura porosa de un carbón activado se convierte en un objetivo necesario para la optimización de los supercapacitores [76].

Bibliografía / References

[1] Base de datos de Eurostat. http://epp.eurostat.ec.europa.eu/portal/page/portal/waste/waste_generation_management/generation

[2] Ley 22/2011, del 28 de Julio, de residuos y suelos contaminados. BOE 181/2011 de 29 de Julio.

[3] X.E. Castells. Reciclaje de residuos industriales. Ed. Díaz de Santos. 2000. P. 1 – 32, 495.

[4] VI Programa de acción en materia de Medio Ambiente. http://europa.eu/youreurope/business/doing-business-responsibly/keeping-to-environmental-rules/index_es.htm

[5] F.A. López, T. Álvarez Centeno, F.J. Alguacil. *Aprovechamiento energético de residuos: el caso de los neumáticos fuera de uso*. www.energia2012.es

[6] Sistema Integrado de Gestión de Neumáticos Usados (Signus Ecovalor). Memoria de gestión 2011.

[7] A. Aranda, R. Murillo, T. García, M.S. Callén, A.M. Mastral. *Steam activation of tyre pyrolytic carbon black: Kinetic study in a thermobalance*. Chem. Eng. J. 2007; 126(2 – 3): 79 – 85.

[8] http://tecnologiadelosplasticos.blogspot.com.es/2011/07/caucho-sbr.html

[9] R. Helleur, N. Popovic, M. Ikura, M. Stanciulescu, D. Liu. *Characterization and potential applications of pyrolytic char from ablative pyrolysis of used tires*. J. Anal. Appl. Pyrolysis 2001; 58: 813 – 824.

[10] M. Arabiourrutia, G. López, G. Elordi, M. Olazar, R. Aguado, J. Bilbao. *Product distribution obtained in the pyrolysis of tyres in a conical spouted bed reactor*. Chem. Eng. Sci. 2007; 62(18 – 20): 5271 – 5275.

[11] D.C.K. Ko, E.L.K. Mui, K.S.T. Lau, G. McKay. *Production of activated carbons from waste tire-Process design and economical analysis*. Waste Manage. 2004; 24 (9): 875 – 888.

[12] T.A. Brady, M.J. Rostam-Abadi. Rood. *Applications for activated carbons from waste tires: natural gas storage and air pollution control*. Gas. Sep. Purif. 1996; 10(2): 97 – 102.

[13] D. Savova, E. Apak, E. Ekinci, F. Yardim, N. Petrov, T. Budinova, M. Razvigorova, V. Minkova. *Biomass conversion to carbon adsorbents and gas*. Biomass Bioenergy 2001; 21(2): 133 – 142.

[14] S.V. Vassilev, D. Baxter, L.K. Andersen, C.G. Vassileva, T.J. Morgan. *An overview of the organic and inorganic phase composition of biomass*. Fuel 2012; 94(1): 1 – 33.

[15] J.M. Encinar, F.J. Beltrán, A. Bernalte, A. Ramiro, J.F. González. *Pyrolysis of two agricultural residues: olive and grape bagasse. Influence of particle size and temperature*. Biomass Bioenergy 1996; 11(5): 397 – 409.

[16] A.H. El-Sheikh, A.P. Newman, H.K. Al-Daffaee, S. Phull, N. Cresswell. *Characterization of activated carbon prepared from a single cultivar of Jordanian Olive stones by chemical and physicochemical techniques*. J. Anal. Appl. Pyrolysis 2004; 71(1): 151 – 164.

[17] V. Minkova, M. Razvigorova, E. Bjornbom, R. Zanzi, T. Budinova, N. Petrov. *Effect of water vapour and biomass nature on the yield and quality of the pyrolysis products from biomass*. Fuel Proc. Technol. 2001; 70(1): 53 – 61.

[18] M. Lanzetta, C. Di Blasi. *Pyrolysis kinetics of wheat and corn straw*. J Anal. Appl. Pyrolysis 1998; 44(2): 181 – 92.

[19] B.S. Girgis, M.F. Ishak. *Activated carbon from cotton stalks by impregnation with phosphoric acid*. Mater. Letter. 1999; 39(2): 107 – 114.

[20] A. Aygun, S. Yenisoy-Karakas, I. Duman. *Production of granular activated carbon from fruit stones and nutshells and evaluation of their physical, chemical and adsorption properties*. Micro. Meso. Mater. 2003; 66(2 – 3): 189 – 195.

[21] C.J. Duran-Valle, M. Gómez-Corzo, J. Pastor-Villegas, V. Gómez-Serrano. *Study of cherry stones as raw material in preparation of carbonaceous adsorbents*. J. Anal. Appl. Pyrolysis 2005; 73(1): 59 – 67.

[22] B.S. Girgis, S.S. Yunis, A.M. Soliman. *Characteristics of activated carbon from peanut hulls in relation to conditions of preparation*. Mater. Letter. 2002; 57(1): 164 – 172.

[23] S. Guo, J. Peng, W. Li, K. Yang, L. Zhang, S. Zhang, H. Xia. *Effects of CO_2 activation on porous structures of coconut shell-bases activated carbons*. Appl. Surf. Sci. 2009; 255(20): 8443 – 8449.

[24] A. Molero Gómez, C. Pereyra López, E. Martínez de la Ossa. *Recovery of grape seed oil by liquid and supercritical carbon dioxide extraction: a comparison with conventional solvent extraction*. Chem. Eng. J. 1996; 61(3): 227 – 231.

[25] J.M. Luque-Rodríguez, M.D. Luque de Castro, P. Pérez-Juan. *Extraction of fatty acids from grape seed by superheated hexane*. Talanta 2005; 68(1): 126 – 130.

[26] http://www.fao.org/corp/statistics/es/.

[27] S. Uçar, S. Karagöz. *The slow pyrolysis of pomegranate seeds: The effect of temperature on the product yields and bio-oil properties.* J. Anal. Appl. Pyrolysis 2009; 84(2): 151 – 156.

[28] R. Arriagada, G. Bello, R. García, F. Rodríguez-Reinoso, A. Sepúlveda-Escribano. *Carbon molecular sieves from hardwood carbon pellets. The influence of carbonization temperature in gas separation properties*. Micro. Meso. Mater. 2005; 81(1 – 3): 161 – 167.

[29] M. Polyakov, M. Poisot, W.E. Maurits, T. Drescher, A. Lotnik, L. Kienle, W. Bensch, M. Muhler, W. Grunert. *Carbon-stabilized mesoporous MoS2 - structural and surface characterization with spectroscopic and catalytic tools*. Catal. Commun. 2010; 12(3): 231 – 237.

[30] A. Wahby, J. Silvestre-Albero, A. Sepúlveda-Escribano, F. Rodríguez-Reinoso. *CO_2 adsorption on carbon molecular sieves*. Micro. Meso. Mater. 2012; 164(SI): 280 – 287.

[31] M.P. Bichat, E. Raymundo-Piñero, F. Béguin. *High voltage supercapacitor built with seaweed carbons in neutral aqueous electrolyte*. Carbon 2010; 48(15): 4351 – 4361.

[32] J.D. López-González, F. Martínez-Vilchez, F. Rodríguez-Reinoso. *Preparation and characterization of active carbons from olive stones*. Carbon 1980; 18(6): 413 – 418.

[33] F. Heras, N. Alonso-Morales, D. Jiménez-Cordero, M.A. Gilarranz, J.J. Rodríguez. *Granular mesoporous activated carbons from waste tires by cyclic oxygen chemisorption-desorption*. Ind. Eng. Chem. Research. 2012; 51(6): 2609 – 2614.

[34] X. Chen, S. Jeyaseelan, N. Graham. *Physical and chemical properties study of the activated carbon made from sewage sludge*. Waste. Manag. 2002; 22(7): 755 – 760.

[35] K. Gergova, N. Petrov, S. Eser. *Adsorption properties and microstructure of activated carbons produced from agricultural by-products by steam pyrolysis*. Carbon 1994; 32(4): 693 – 702.

[36] H. Marsh, E. Heinz, F. Rodríguez-Reinoso. *Introduction to carbon Technologies.* Universidad de Alicante. 1997; 2: 41 – 44.

[37] http://articulos.aquamillfactory.com/?p=619

[38] K.S.W. Sing, D.H. Everett, R.A.W. Haul, L. Moscow, R.A. Pierotti, J. Rouquerol and T. Siemieniewska. *Reporting physisorption data for gas/solid systems with special reference to the determination of surface area and porosity*. Pure Appl. Chem. 1985; 57(4): 603 – 619.

[39] K.S.W. Sing. *Principles and applications of pore structural characterization*. Edited by J.M Haynes and P. Rossi-Doria (J.W. Arrowsmith Ltd., Bristol, 1985), p. 1.

[40] http://www.bat-science.com/groupms/sites/BAT_7AWFH3.nsf/vwPagesWebLive/DO7AXGBN?opendocument&SKN=1.

[41] F. Rodríguez-Reinoso, M. Molina-Sabio, M.A. Muñecas. *Modification in Porous Texture and Oxygen Surface Groups of Activated Carbons by Oxidation.* J. Phys. Chem. 1991; 62: 329 – 339.

[42] J. Jaramillo, P. Modesto Álvarez, V. Gómez-Serrano. *Oxidation of activated carbon by dry and wet methods surface chemistry and textural modifications*. Fuel Process. Technol. 2010; 91(11): 1768 – 1775.

[43] J.C. Cortés, L. Giraldo, A.A. García, C. García, J.C. Moreno. *Oxidación de un carbón activado comercial y caracterización del contenido de grupos ácidos superficiales*. Rev. Colomb. Quim. 2008; 37(1): 55 – 65.

[44] W.T. Tsai, C.Y. Chang, S.L. Lee. *A low cost adsorbent from agricultural waste corn cob by zinc chloride activation*. Bioresour. Technol. 1998; 64(3): 211 – 217.

[45] T. Budinova, E. Ekinci, F. Yardim, A. Grimm, E. Björnbon, V. Minkova, M. Goranova. *Characterization and application of activated carbon produced by H_3PO_4 and water vapor activation*. Fuel Process. Technol. 2006; 87(10): 899 – 905.

[46] A. Min, A.T. Harris. *Influence of carbon dioxide partial pressure and fluidization velocity on activated carbons prepared from scrap car tyre in a fluidized bed.* Chem. Eng. Sci. 2006; 61(24): 8050 – 8059.

[47] M. Olivares-Marín, C. Fernández-Gonzalez, A. Macías-García, V. Gómez-Serrano. *Preparation of activated carbon from cherry stones by physical activation in air. Influence of the chemical carbonization with H_2SO_4*. J. Anal. Appl. Pyrolysis. 2012; 94: 131 – 137.

[48] V. Gómez-Serrano, P.M. Álvarez, J. Jaramillo, F.J. Beltrán. *Formation of oxygen complexes by ozonation of carbonaceous materials prepared from cherry stones I. Thermal effects*. Carbon 2002; 40(4): 513 – 522.

[49] G. San Miguel, G.D. Fowler, C.J. Sollars. *A study of the characteristics of activated carbons produce by steam and carbon dioxide activation of waste tyre rubber*. Carbon 2003; 41(5): 1009 – 1016.

[50] E.L.K. Mui, D.C.K. Ko, G. McKay. *Production of active carbons from waste tyres - A review*. Carbon 2004; 42(14): 2789 – 2805.

[51] F. Heras, N. Alonso, M.A. Gilarranz, J.J. Rodríguez. *Activation of waste tire char upon cyclic oxygen chemisorption-desorption*. Ind. Eng. Chem. Res. 2009; 48(10): 4664 – 4670.

[52] X. Py, A. Guillot, B. Cagnon. *Activated carbon porosity tailoring by cyclic sorption/decomposition of molecular oxygen*. Carbon 2003; 41 (8): 1533 – 1543.

[53] P. Solís-Fernández, J.I. Paredes, A. Cosío, A. Martínez-Alonso, J.M.D. Tascón. *A comparison between physically and chemically driven etching in the oxidation of graphite surfaces.* J. Colloid Interface Sci. 2010; 344(2): 451 – 459.

[54] O.V. Belyaeva, T.A. Krasnova, S.A. Semenova. *Effect of Modification of Granulated Activated Carbons with ozone on their properties*. Russian J. Appl. Chem. 2011; 84(4): 597 – 601.

[55] J. Rivera-Utrilla, M. Sánchez-Polo. *Adsorbent-adsorbate interactions in the adsorption of organic and inorganic species on ozonized activated carbons: a short review.* Adsorption 2011; 17(3): 611 – 620.

[56] P. Krawczyk. *Effect of ozone treatment on properties of expanded graphite*. Chem. Eng. J. 2011; 172(2 – 3): 1096 – 1102.

[57] L. Calvo, M.A. Gilarranz, J.A. Casas, A.F. Mohedano, J.J. Rodríguez. *Hydrodechlorination of 4-chlorophenol in aqueous phase using Pd/AC catalysts prepared with modified active carbon supports.* Appl. Cat. B-Environ. 2006; 67(1 – 2): 68 – 76.

[58] R. Mysyk, Q. Gao, E. Raymundo-Piñero, F. Béguin. *Microporous carbons finely-tuned by cyclic high pressure low-temperature oxidation and their use in electrochemical capacitors.* Carbon 2012; 50(9): 3367 – 3374.

[59] J.L. Figueiredo, M.F.R. Pereira, M.M.A. Freitas, J.J.M. Órfao. *Modification of the surface chemistry of activated carbons.* Carbon 1999; 37(9): 1379 – 1389.

[60] ANA. El-Hendawy. *Influence of HNO_3 oxidation on the structure and adsorptive properties of corncob-based activated carbon*. Carbon 2003; 41(4): 713 – 722.

[61] X. Lu, J. Jiang, K. Sun, X. Xie, Y. Hu. *Surface modification, characterization and adsorptive properties of a coconut activated carbon.* Appl. Surf. Sci. 2012; 258(20): 8247 – 8252.

[62] M. Belhachemi, R.V.R.A. Rios, F. Addoun, J. Silvestre-Albero, A. Sepúlveda-Escribano, F. Rodríguez-Reinoso. *Preparation of activated carbon from date pits: Effect of the activation agent and liquid phase oxidation*. J. Anal. Appl. Pyrolysis 2009; 86(1): 168 – 172.

[63] A. Gil, G. de la Puente, P. Grange. *Evidence of textural modifications of an activated carbon on liquid-phase oxidation treatments*. Micro. Mater. 1997; 12(1 – 3): 51 – 61.

[64] X. Song, H. Liu, L. Cheng, Y. Qu. *Surface modification of coconut-based activated carbon by liquid-phase oxidation and its effects on lead ion adsorption.* Desalination 2010; 255(1 – 3): 78 – 83.

[65] C. Moreno-Castilla, M.V. López-Ramón, F. Carrasco-Marín. *Changes in surface chemistry of activated carbons by wet oxidation*. Carbon 2000; 38(14): 1995 – 2001.

[66] P.S. Tin, T-S. Chung, Y. Liu, R. Wang. *Separation of CO_2/CH_4 trough carbon molecular sieve membranes derived from P84 polymide*. Carbon 2004; 42(15): 3123 – 3131.

[67] F. Béguin, E. Frackowiak. *Carbons for electrochemical energy storage and conversion systems*. CRC Press; 2010. P. 19, 34 – 35 y 330 – 358.

[68] H.A. Andreas, B.E. Conway. *Examination of the double-layer capacitance of an high specific area C-cloth electrode as titrated from acidic to alkaline pHs*. Electroch. Acta 2006; 51(28): 6510 – 6520.

[69] R. Mysyk, E. Raymundo-Piñero, J. Pernak, F. Béguin. *Confinement of Symmetric Tetraalkylammonium Ions in Nanoporous Carbon Electrodes of Electric Double-Layer Capacitors*. J. Phys. Chem. 2009; 113(30): 13443 – 13449.

[70] E. Raymundo-Piñero, K. Kierzek, J. Machnikowski, F. Béguin. *Relationship between the nanoporous texture of activated carbons and their capacitance properties in different electrolytes*. Carbon 2006; 44(12): 2498 – 2507.

[71] E.J. Ra, E. Raymundo-Piñero, Y.H. Lee, F. Béguin. *High power supercapacitors using polyacrylonitrile-based carbon nanofiber paper*. Carbon 2009; 47(13): 2984 – 2992.

[72] J. Chmiola, G. Yushin, Y. Gogotsi, C. Portet, P. Simon, P.L. Taberna. *Anomalous Increase in Carbon Capacitance at Pore Sizes Less Than 1 Nanometer*. Science 2006; 313(5794): 1760 – 1763.

[73] Y. Guo, J. Qi, Y. Jiang, S. Yang, Z. Wang, H. Xu. *Performance of electrical double layer capacitors with porous carbons derived from rice husk*. Materials Chemistry and Physics 2003; 80(3): 704 – 709.

[74] J. Yang, Y. Liu, X. Chen, Z. Hu, G. Zhao. *Carbon electrode material with high densities of energy and power*. Acta Physica-Chimica Sinica 2008; 24(1): 13 – 19.

[75] E. Raymundo-Piñero, F. Béguin. *Interface science and technology, Volume 7. Chapter 6: Application of nanotextured carbons for supercapacitors and hydrogen storage*. Academic Press 2006. P. 293 – 308.

[76] O. Barbieri, M. Hahn, A. Herzog, R. Kötz. *Capacitance limits of high surface area activated carbons for double layer capacitors*. Carbon 2005; 43(6): 1303 – 1310.

CAPÍTULO 2 / CHAPTER 2

MATERIALES, INSTALACIÓN EXPERIMENTAL Y METODOLOGÍA

MATERIALS, DEVICES AND METHODOLOGY

2.1 Materials

In this work two materials have been used as starting materials for the preparation of porous carbons: waste tires rubber (WTR) and grape seeds (GS). Both of them are readily available and maintain essentially intact their morphology after pyrolysis.

2.1.1. Starting materials

Figure 2.1 shows the typical parts of a tire. In this study the external surface in contact with the floor, i.e. tread strip, was the only part of the tire used. The waste rubber from the tread strip was separated and grinded after freezing with liquid nitrogen in a blade grinder IKA model MF10 basic. Three different fractions were separated by sieving of 0.5, 1, and 2 mm of average particle diameter.

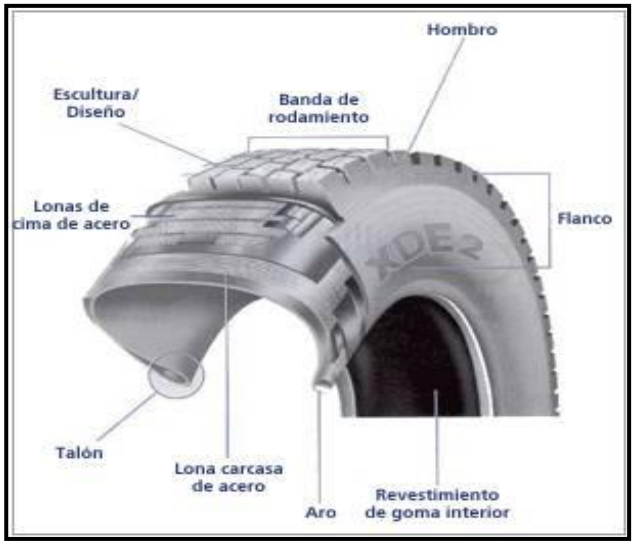

Figure 2.1. Parts of a tire.

The grape seeds used in this study were collected from grapes of the red variety “Tinta de Toro” harvested in Toro (Zamora, Spain). The seeds were separated just after the fermentation of the must (grape juice), and were not treated with any chemical additive. The seeds were washed with distilled water repeatedly until no turbidity was observed, dried at 105 ºC for 1 day and stored at room temperature until use. The size of the raw seeds was between 2 – 3 mm.

2.1.2. Other materials

Hexane with a purity of 95 % supplied by Sigma-Aldrich was used to extract the oil from grape seeds before pyrolysis. For the characterization of the textural properties of samples nitrogen, CO_2 and Argon with a purity of 99.999 % supplied by Praxair were used.

The oxidant agents used in the gas phase oxidation of the activation method were oxygen (air) and ozone, the air was obtained from a compressor. Ozone was produced from air using an ozone generator GMB PRO003 rated at 300 mgh^{-1}. The oxidant agents used in liquid phase oxidation were nitric acid (35 %), hydrogen peroxide (30 %) and ammonium persulfate, all of them supplied by Sigma-Aldrich (with purity >98 %).

2.2. Experimental Devices

2.2.1. Oil extraction from grape seeds

Before pyrolysis, part of the grape seeds was subjected to n-hexane extraction for 24h in a Soxhlet apparatus (Figure 2.2) to remove oil [1]. After extraction the seeds were washed with distilled water and dried at 105 ºC for 1 day.

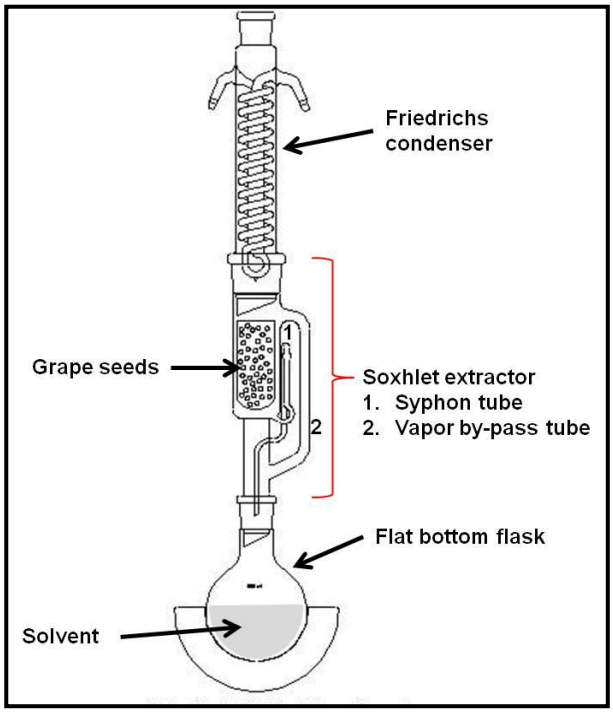

Figure 2.2. Soxhlet extractor.

2.2.2. Pyrolysis system

Figure 2.3 shows a schematic diagram of the pyrolysis unit. Pyrolysis was carried out in a vertical quartz tube (68 cm length and 4.8 cm i.d.) placed in a sandwich-type electrical furnace. A 100 $mLmin^{-1}$ nitrogen flow was continuously passed downward. Two K-type thermocouples placed on the furnace wall and at the central part of the reactor (hot zone) were used to control the pyrolysis temperature. A quartz basket with 7 – 8 g of the starting material was maintained for air removal in the cold zone of the furnace from there it was displaced to the hot zone by means of a rod. After the heat treatment the basket was cooled in the cold zone and finally the char was recovered and weighted to determine burn-off [2]. For the slow-heating samples, the basket was placed in the central part of the reactor, air was purged and then heating of the system was started. For the flash-heating samples, the basket with the grape seeds was kept in the cold zone of the reactor until the central part reached the desired pyrolysis temperature; then the basket was moved into the hot zone, so that the sample reached the operating temperature in few seconds. The conditions for the preparation of the flash heating samples can be considered as flash pyrolysis conditions. Flash pyrolysis has been defined as a process characterized by rapid devolatilization in an inert atmosphere, at high heating rate and reaction temperatures between 450 and 1000 ºC [3].

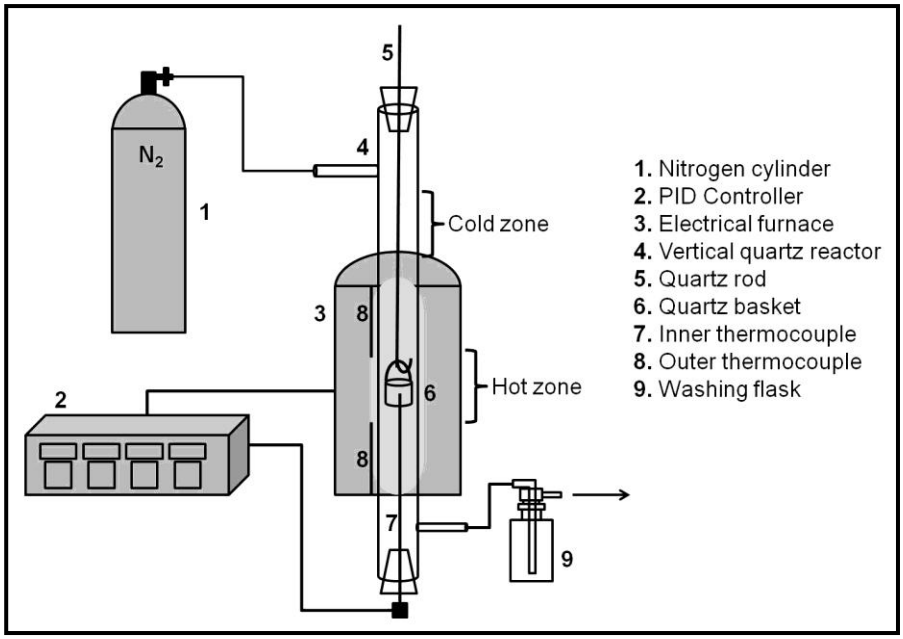

Figure 2.3. Schematic diagram of pyrolysis system.

2.2.3. Activation systems

For the activation of chars two furnaces with different configuration were used. The first of them (Figure 2.4), based on manual operation, was used for the activation with air of the char from waste tire, the activation with ozone of grape seeds char and the desorption stage after liquid phase oxidation of waste tire char. The system consists of a vertical quartz tube (45 cm length and 2.2 cm diameter) placed in a sandwich-type electrical furnace. Two K-type thermocouples, placed on the furnace wall and at the inner central part of the reactor, were used to control the temperature. Heating rate, temperature and gas flow were controlled using a PID controller and mass flow meters.

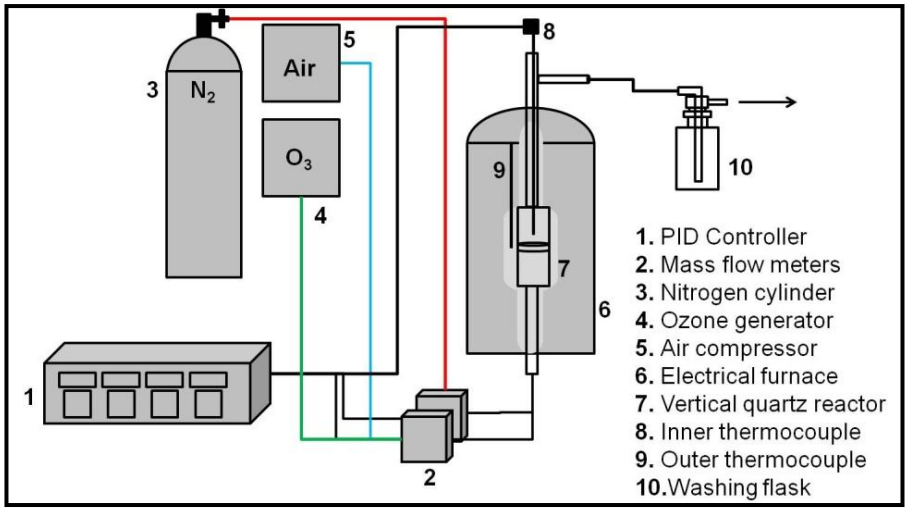

Figure 2.4. Schematic diagram of activation system with manual control.

The second activation system (automatic activation system, Figure 2.5) was used for the activation with air of grape seeds char and for the desorption stage in liquid phase experiments with the same precursor. The system consists of a vertical quartz tube (70 cm length and 3.5 cm diameter) placed in a sandwich-type electrical furnace. Three K-type thermocouples, two of the placed on the furnace wall at the top and at the bottom and the third one situated at the central inner part of the reactor, were used to control the temperature. Heating rate, temperature and gas flow were controlled using PID controllers, mass flow meters and a control software. The system was provided by PID Eng&Tech.

After each activation cycle the reactor was cooled under nitrogen flow and the activated carbon was collected to estimate the burn-off and perform the textural characterization.

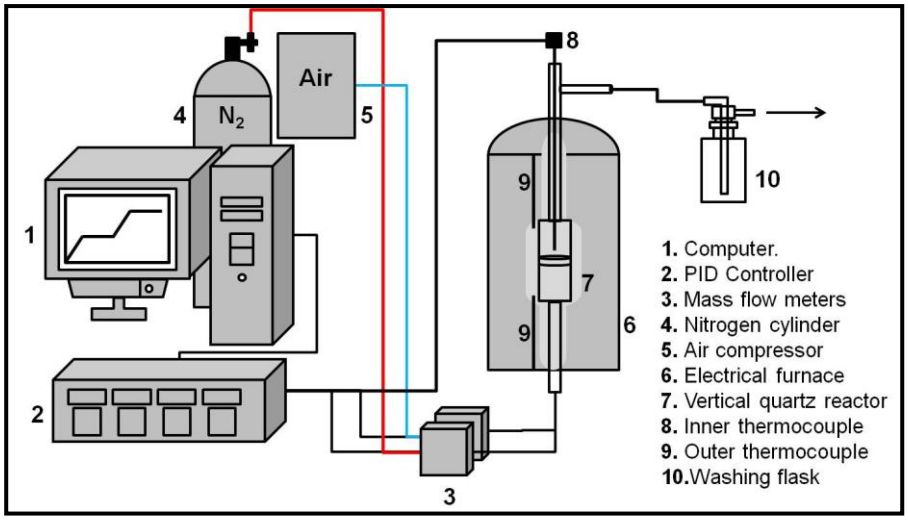

Figure 2.5. Schematic diagram of the automatic activation system.

2.3. Activation conditions

2.3.1. Gas phase oxidation

In the activation with air of waste tire rubber char (WTR char) the operating conditions for oxidation step of each cycle were the same for all the experiments, 210 ºC during 200 min with an air flow of 80 $NmLmin^{-1}$. The desorption step was carried out at three different temperatures (550, 650 and 750 ºC) using a flow rate of 100 $NmLmin^{-1}$ of nitrogen and 2 h of reaction time in all the cases. The switch from chemisorption to desorption was carried out at a heating rate of 10 $ºCmin^{-1}$ under nitrogen flow in all cases.

For the experiments of grape seeds char (GS char) activation with air, the activation conditions were three different oxidation temperatures (200, 250 and 275 ºC) for 2 h under a 100 $NmLmin^{-1}$ air flow, while the desorption step was carried out at four different temperatures (500, 675, 850 and 950 ºC) using a flow rate of 100 $NmLmin^{-1}$ of nitrogen and 2 h of desorption time. The switch from oxidation to desorption was carried out at a heating rate of 10 $ºCmin^{-1}$ under nitrogen flow.

For ozone activation of GS char the oxidation step of each cycle was carried out at 250 and 275 ºC for 2 h using a gas flow of ozone of 50 $mLmin^{-1}$ and the desorption step was performed at 850 and 950 ºC using a flow rate of 100 $mLmin^{-1}$ of nitrogen for 2 h. The switch from oxidation to desorption steps was carried out at a heating rate of 10 $ºCmin^{-1}$ under nitrogen flow.

2.3.2. Liquid phase oxidation

The procedure for the oxidation step was different depending on the oxidant used. Oxidation with HNO_3 was carried out by boiling under reflux for 20 min. Oxidation with H_2O_2 and $(NH_4)_2S_2O_8$ was performed at 20 ºC for 24 h. For all the oxidant agents the oxidation step consisted in contacting the oxidant and the carbon (10 mL of oxidant solution per gram of carbon) in an orbital shaker followed by filtration, washing with distilled water until neutrality and drying in a muffle at 105 ºC.

Operating conditions for the desorption step in the experiments with WTR char were 650 °C for 2 h with 100 $NmLmin^{-1}$ nitrogen flow and a heating rate of 10 $ºCmin^{-1}$. While in activation of GS char, the desorption conditions were 850 and 950 ºC for 2 h with 100 $NmLmin^{-1}$ nitrogen flow and a heating rate of 10 $ºCmin^{-1}$.

After each activation cycle the reactor was cooled under nitrogen flow, the activated carbon was collected, and the burn-off and textural properties were determined before starting a new cycle.

2.4. Characterization methods

The characterization of the starting material, char and activated carbons was performed using several techniques. Table 2.1 summarizes the techniques and equipment used for the characterization of samples.

Table 2.1. Techniques and equipment used for the characterization of samples.

Characterization technique	Equipment used
• Argon adsorption-desorption isotherms • CO_2 adsorption isotherms • N_2 adsorption-desorption isotherms	Micromeritics TriStar II 3020
Attrition tests	Orto Arlesa vibrating sifter
Differential Weighting	Analytical balance Sartorius CP124s
Elemental analysis (EA)	LECO CHNS-932 analyzer LECO VTF-900 analyzer
Fourier transform infrared spectroscopy (FTIR)	FTIR Bruker IFS66v with MCT detector
Inductively coupled plasma mass spectrometry (ICP-MS)	Elan 6000 Perkin-Elmer Sciex
Mercury porosimetry	Quantachrome Poremaster 33
Scanning electron microscopy (SEM)	Hitachi S-3000N Metallizer Sputter Caoter SC502
Temperature programmed desorption (TPD)	Siemems Ultramat 22 detector
Temperature programmed oxidation (TPO)	LECO-RC 412
Thermogavimetric analysis (TGA)	Mettler Toledo TGA/SDTA851^e
X-Ray photoelectron spectroscopy (XPS)	VG ESCALAB 250

In the following sections the procedure for the characterization of samples is detailed.

2.4.1. Differential weighting

The differential weighting was used to determine the burn-off and yield after pyrolysis and activation cycles. The burn-off is the value that determines the loss of mass of the sample after a high temperature treatment. The burn-off and yield values were calculated as indicated in equations 2.1 and 2.2, respectively.

$$BO(\%) = 100 - \left(\frac{w_f}{w_i} \cdot 100 \right) \qquad [2.1]$$

$$Yield\ (\%) = 100 - BO \qquad [2.2]$$

Where w_f is the final weight of the sample after heat treatment and w_i is the initial weight of the sample before heat treatment.

2.4.2. Nitrogen adsorption-desorption isotherms

The textural characterization from nitrogen adsorption-desorption isotherms was based in the measurement of the volume of nitrogen adsorbed at 77 K at different values of relative pressure in a range from 10^{-5} to 0.995, and of the volume desorbed in a relative pressure range of 0.995 - 0.1. Data processing provided relevant information on the structure of the materials analyzed.

- Specific surface area:
    - BET surface area (S_{BET}): The Brunauer-Emmet-Teller equation was used to calculate the surface area [4].
    - The Dubinin-Radushkevich surface area (S_{DR}) was calculated by the Dubinin-Radushkevich equation [5].
- Pore volume:

  - Micropore volume ($V_{microN2}$) was calculated by the t-plot method [6].
  - Narrow mesopore volume ($V_{Narrow\text{-}meso}$) and total mesopore volume ($V_{mesoTOTAL}$) were calculated by the BJH method [7].

- Mean mesopore size (d_{meso}), calculated by the BJH method [7].
- Mean micropore size (L_0), calculated by the Stoeckli equation [8].
- Pore size distribution (PSD). It was assumed that each pore acts independently, so that each pore size in the sample contributes to the total adsorption isotherm in the same percentage it contributes to the total surface area. PSD was obtained in a pore size range from 1 to 50 nm by the Non-Local Density Functional Theory ($NLDFT_{N2}$) [9].

2.4.3. Argon adsorption-desorption isotherms

This technique is based in the measurement of the volume of argon adsorbed at 77 and 87 K in a relative pressure range from 10^{-5} to 0.995. These isotherms provide complementary information about the pore structure. Due to the low mesoporosity found in grape seeds char characterization by both nitrogen and argon adsorption-desorption was used to confirm the contribution of mesopores to the surface area of char samples. The surface area from Ar adsorption-desorption was calculated with BET equation.

2.4.4. CO_2 adsorption isotherms

This technique is based in the measurement of the volume of CO_2 adsorbed at 273 K in the 10^{-5} – 0.03 relative pressure range, thus providing information on the micropore structure. Before adsorption the samples were degassed for 7 h at 150 ºC and atmospheric pressure in a VacPrep 061 degas system. The parameters obtained were the following, all of them calculated by the Dubinin-Astakhov model [4]:

- Specific surface area (S_{DA}).
- Micropore volume ($V_{microCO2}$).
- Mean micropore size (d_{micro}).
- Pore size distribution. It was obtained in a pore size range from 0.4 to 1 nm by the Non-local Density Functional Theory ($NLDFT_{CO2}$) [9].

The Dubinin-Radushkevich (DR) and Dubinin-Astakhov (DA) equations have been used to describe micropores filling and the energetic heterogeneity of porous solids [5]. While several studies [10, 11] postulated that the DR equation applies only to solids with a uniform structure of micropores, others [5, 12 - 15] proposed a modification of this equation when a microporous solid possesses micropores of the same shape but of different sizes. One of them is the well-known DA equation, which can be applied to the description of the adsorption on structurally heterogeneous solids [16, 17]. In this work the DA method is used for grape seeds derived samples because of the heterogeneous structure of the samples and the better regression coefficient obtained in all cases, while the DR is the method used with waste tire derived samples.

2.4.5. Mercury porosimetry

Mercury intrusion porosimetry was used as complementary technique to complete the textural characterization, i.e. to determine the mesopore and macropore volume (V_{macro}) and pore size distribution of the chars and activated carbons obtained from grape seeds.

2.4.6. Elemental analysis and Inductively coupled plasma mass spectrometry

The elemental analysis (EA) is based in the total oxidation of the sample by a complete and instantaneous combustion that transform the sample in combustion products such as CO_2, H_2O, N_2 and SO_2. These products are dragged in Helium up to individuals sensors and they are subsequently measured to determine the C, H, N and S content of the sample.

Inductively coupled plasma mass spectrometry (ICP-MS) is a technique for inorganic analysis that is able to determine and quantify most of the elements of the periodic table in a linear dynamic range of 8 orders of magnitude, being ideal to analyze trace elements.

The elemental analysis was used to determine to determine the C, H, N and S content of char and activated carbon samples. Inductively coupled plasma mass spectrometry was used to determine other significant elements.

2.4.7. X-ray photoelectron spectroscopy

In X-ray photoelectron spectroscopy (XPS) analysis a sample irradiated with x-rays later emits photoelectrons from its sample surface. The binding energy of the photoelectrons is determined by an electron energy analyzer. As a function of the binding energy and intensity of a photoelectron

peak, the elemental identity, chemical state, and quantity of an element are determined [18].

In this work, the XPS technique was used to complete the elemental composition of activated carbons following different oxidative treatments on grape seeds char.

2.4.8. Scanning Electron Microscopy

The scanning electronic microscopy (SEM) is a technique that allows the observation and characterization of organic and inorganic materials by the study of surfaces, evaluating their morphology.

The morphology of the grape seeds, waste tire, chars and activated carbons was evaluated by SEM. The specimens for SEM observation were metalized with gold to prevent electrical charging during examination using a Sputter Coater SC502. Imaging was done in the high vacuum mode under an accelerating voltage of 20 kV, using secondary electrons.

2.4.9. Fourier transform infrared spectroscopy

The Fourier transform infrared (FTIR) spectroscopy is the study of the interaction of electromagnetic radiation with matter. For the study of the infrared spectrum of solid and liquid samples only changes between states of vibration energy are taken into account, which makes possible the characterization of the major functional groups in the molecular structure. Usually the spectrum ranges from 4000 to 500 cm^{-1}.

The FTIR was used to characterize the main functional groups of the activated carbons surface for the AC produced by ozone and liquid phase oxidation of grape seeds char.

2.4.10. Thermogravimetric analysis

The thermogravimetric analysis (TGA) measures the weight change and change rate of a sample with temperature and/or time in a controlled atmosphere, providing characterization of materials that lose o gain weight due to decomposition, oxidation or dehydration.

In the chapters devoted to pyrolysis, this technique was used to determine the range of temperature and time pyrolysis tests. In the chapters on the activation with air, this technique was used to establish the most adequate oxidation and desorption temperature.

2.4.11. Temperature programmed desorption

In the characterization of oxygen surface groups by temperature programmed desorption (TPD) the sample is heated up to 900 – 1000 ºC in inert atmosphere and the amounts CO and CO_2 released are quantified. The information is presented in form of TPD curves that usually show various peaks. The maximum of these peaks (maximum temperature) provides information to identify the specific oxygenated functional groups evolved at each temperature. Table 2.2 collects the temperature desorption intervals for the assignation of different surface oxygen groups reported in literature [19].

Table 2.2. Oxygenated functional groups detected with TPD tests.

Temperature (ºC)	Desorbed species	Functional groups
100 – 400	CO_2	Carboxylic
350 – 650	CO, CO_2	Anhydrides
500 – 700	CO_2	Lactones
600 – 700	CO	Phenol
700 – 900	CO	Carbonyls and quinones
750 – 800	CO	Ethers and chromenes
800 – 1100	CO_2	Pyrones

The effect of oxygen chemisorption of waste tire char was studied by temperature programmed desorption (TPD) to identify the type of oxygen surface groups on the samples after oxidation and desorption.

2.4.12. Temperature programmed oxidation

The temperature programmed oxidation (TPO) is a useful technique to quantify the different types of carbonaceous solids in a sample according to their reactivity with oxygen. TPO curves provide a direct measurement of the amount of carbon gasified depending on the oxidation temperature, quantifying the CO_2 released during oxidation of sample in oxygen atmosphere. To learn about the presence of carbon domains of different reactivity was performed the TPO test for waste tire char air activation.

2.4.13. Attrition tests

The grape seeds char and some of the activated carbons produced by cyclic activation with air were subjected to attrition tests to study their mechanical strength. The samples were subjected to attrition on a sieve (1 mm opening) in an Orto Alresa vibrating sifter operating at a frequency of 42 s^{-1}. During the attrition tests three and five fractions of the powder passing through the sieve openings were collected at regular intervals of 2 h, for char and activated carbons respectively.

2.5. Application of activated carbons to the preparation of supercapacitors

A selection of activated carbon prepared from grape seeds char by different methods were tested for the preparation of supercapacitors. The procedure for the preparation of capacitors and their testing is described below.

2.5.1. Preparation of electrodes and capacitors

The electrodes used for the measurements were prepared by mixing the activated carbons (previously grinded in an agate mortar) with powdered carbon black (PURE-BLACK Carbon, Superior Graphite Co.) as conductivity additive and a solution of Polytetrafluoroethylene (PTFE), used as a binder, in an 8:1:1 ratio (%w) in the dry electrode. Ethanol was added to allow a good homogenization. The mixture was stretched to obtain a thin film. Electrodes with 10 mm diameter were cut and pressed to obtain 8 – 13 mg pellets with a thickness of 300 ± 50 nm. The carbon pellets were dried in a muffle furnace at 120 ºC to remove humidity and the remaining ethanol.

The supercapacitor consisted in two-electrode cells that were assembled using two identical carbon pellets (electrodes), stainless steel current collectors, a porous membrane separator, and a Teflon Swagelok airtight system (Figure 2.6).

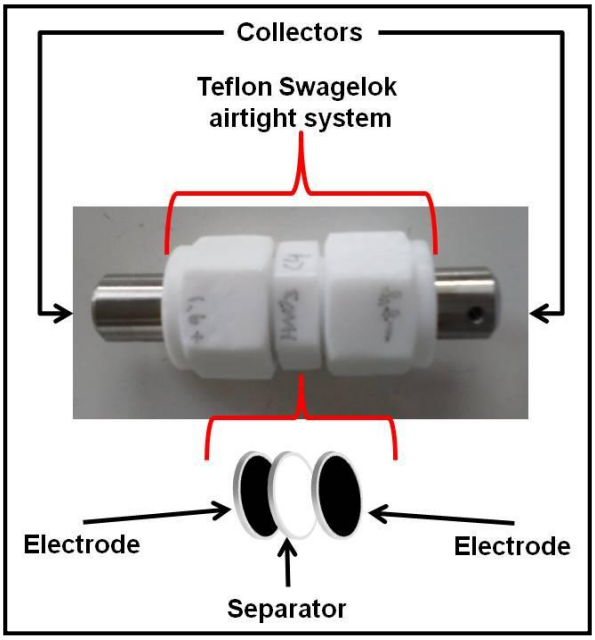

Figure 2.6. Schematic diagram of a supercapacitor.

2.5.2. Electrochemical characterization

The electrochemical performance of the materials was evaluated in three aqueous electrolytes Na_2SO_4 0.5 $molL^{-1}$, KOH 6 $molL^{-1}$ and H_2SO_4 1 $molL^{-1}$ by cyclic voltammetry (CV) at 2 mVs^{-1}. Galvanostatic charge/discharge (GA) was evaluated at first using 200 mAg^{-1} using different range of operating voltage (0.6 – 2.0 V for Na_2SO_4 and 0.6 – 1.4 V for KOH and H_2SO_4) and later at a scan rate of 10 mVs^{-1} with only one voltage value and a variable

current density from 100 to 30000 mAg^{-1} using a VMP multichannel generator (Biologic, France).

By the impedance spectroscopy were evaluated the equivalent series resistance (ESR) and the equivalent distributed resistance (EDR), obtained in 100 kHz to 300 mHz interval by a VMP 2 device (Biologic, France).

2.5.3. Cyclic voltammetry

Cyclic voltammetry (CV) is frequently used for a quick determination of the range of electroactivity, capacity and electrochemical reversibility. The effectiveness of CV results from its capability for rapidly observing the redox behavior over a wide potential range. The resulting voltammogram shows the current density vs potential with a constant sweep rate [20, 21].

2.5.4. Galvanostatic charge/discharge

In the galvanostatic charge/discharge (GA) technique, the supercapacitor is charged at a constant current (I) until a chosen voltage (V) is reached. Then, the current is reversed and discharge takes place. The efficiency of the capacitor can be calculated as the ratio between the discharge and charge times. Thus, the gravimetric capacitance (C) measured in Farads per gram (Fg^{-1}) was calculated by the equation 2.3. The specific surface capacitance (Cs) is calculated referring the gravimetric capacitance to the BET surface area (eq. 2.4), being the usual units used μFcm^{-2}.

$$Capaci\tan ce = \frac{dq}{dV} = \frac{I \cdot dt}{dV} \qquad [2.3]$$

$$Specific\_Capacitance = \frac{C}{S_{BET}} \qquad [2.4]$$

2.5.5. Impedance spectroscopy

The impedance spectroscopy is a useful technique for the characterization of capacitors. In this technique a small voltage is applied (often in the range of 5 to 10 mV) and the change in phase over a range frequency is measured [22]. Thus, the electrical series resistance (ESR) and the electrical distributed resistance (EDR) that measure the conductivity resistance between the electrode and the electrolyte and the resistance to the diffusion of ions within the pores, respectively, can be evaluated.

References

[1] A. Molero Gómez, C. Pereyra López, E. Martínez de la Ossa. *Recovery of grape seed oil by liquid and supercritical carbon dioxide extraction: a comparison with conventional solvent extraction.* Chem. Eng. J. 1996; 61(3): 227 - 231.

[2] F. Heras, N. Alonso-Morales, M.A. Gilarranz, J.J. Rodríguez. *Activation of waste tire char upon cyclic oxygen chemisorption-desorption.* Ind. Eng. Chem. Res. 2009; 48(10): 4664 – 4670.

[3] M.I. Jahirul, M.G. Rasul, A.A. Chowdhury, N. Ashwath. *Production through biomass pyrolysis – A technological review*. Energies 2012; 5(12): 4952 – 5001.

[4] S. Brunauer, E. Emmett, E. Teller. *Adsorption of gases in multimolecular layers.* J. Am. Chem. Soc. 1938; 60: 309 – 319.

[5] M. Jaroniec, R.K. Gilpin, K. Kaneko. *Evaluation of energetic heterogeneity and microporosity of activated carbon-fibers on the basis of gas-adsorption isotherms.* Langmuir 1991; 7(11): 2719 – 2722.

[6] M. Kruk, M. Jaroniec, Y. Bereznitski. *Adsorption study of porous structure development in carbon blacks.* J. Colloid. Int. Sci. 1996; 182: 282 – 288.

[7] E.P. Barret, L.G. Joyner, P.P. Halenda. *The determination of pore volume and area distributions in porous substances. I. Computations from nitrogen isotherms.* J. Am. Chem. Soc. 1951; 73(1): 373 – 380.

[8] F. Stoeckli, E. Daguerre, A. Guillot. *The development of micropore volumes and widths during physical activation of various precursors*. Carbon 1999; 37: 2075 – 2077.

[9] J. Jagiello, M. Thommes. *Comparison of DFT characterization methods based on N_2, Ar, CO_2 and H_2 adsorption applied to carbons with various pore size distributions.* Carbon 2004; 42(7): 1227 – 1232.

[10] H.F. Soeckli. *A generalization of the Dubinin-Radushkevich equation for the filling of heterogeneous micropore systems.* J. Colloid Interface Sci. 1977; 59(1): 184 – 185.

[11] M. Jaroniec, J. Piotrowska. *Isotherm equations for adsorption on heterogeneous microporous solids.* Monatsh. Chem. 1986; 117(1): 7 – 19.

[12] M.M. Dubinin. *Inhomogeneous microporous structures of carbonaceous adsorbents.* Carbon 1981; 19(4): 321 – 324.

[13] M. Rodwadowski, R. Wojsz. *An attempt at determination of the structural heterogeneity of microporous adsorbents.* Carbon 1984; 22(4 – 5): 363 – 367.

[14] M. Jaroniec, J. Choma. *On the characterization of structural heterogeneity of microporous solids by discrete and continuous micropore distribution functions.* Mater. Chem. Phys. 1988; 19(3): 267 – 289.

[15] A. Gil, M. Montes. *Analysis of the microporosity in pillared clays.* Langmuir 1994; 10(1): 291 – 297.

[16] A. Gil, P. Grange. *Application of the Dubinin-Radushkevich and Dubinin-Astakhov equations in the characterization of microporous solids.* Colloids Surf A Physicochem. Eng. Asp. 1996; 113(1 – 2): 39 – 50.

[17] M. Carrasco-Marin, M.V. Lopez-Ramon, C. Moreno-Castilla. *Applicability of the Dubinin-Radushkevich equation to carbon dioxide adsorption on activated carbons.* Langmuir 1993; 9(11): 2758 – 2760.

[18] http://www.phi.com/surface-analysis-techniques/xps.html

[19] J.L. Figueiredo, M.F.R. Pereira, M.M.A. Freitas, J.J.M. Órfao. *Modification of the surface chemistry of activated carbons.* Carbon 1999; 37: 1379 – 1389.

[20] F. Béguin, E. Frackowiak. *Carbons for electrochemical energy storage and conversion systems.* CRC Press; 2010. P. 12 – 35.

[21] P.T. Kissinger, WR Heineman. *Cyclic voltammetry. Journal of chemical education* 1983; 60(9): 702 – 707.

[22] E. Raymundo-Piñero, F. Béguin. *Interface science and technology, Volume 7. Chapter 6: Application of nanotextured carbons for supercapacitors and hydrogen storage*. Academic Press 2006. P. 293 – 308.

CAPÍTULO 3 / CHAPTER 3

PIRÓLISIS DE SEMILLAS DE UVA

PYROLYSIS OF GRAPE SEEDS

3.1. Resumen / Abstract

En este capítulo se estudia la influencia de las condiciones de operación utilizadas en la pirólisis de semillas de uva sobre la morfología y las propiedades texturales del *char* obtenido. Se han utilizado pirólisis flash y convencional (con velocidad de calentamiento de 10 $^{o}Cmin^{-1}$) en un intervalo de temperatura de 300 a 1000 ºC. También se ha estudiado el efecto del pre-tratamiento de extracción del aceite de las semillas de uva. La estructura porosa del *char* se ha caracterizado por isotermas de adsorción de N_2 a 77 K, Ar a 77 y 87 K y CO_2 a 273 K, así como por porosimetría de intrusión de mercurio. La morfología se ha analizado por microscopía electrónica de barrido. Todos los materiales preparados revelan una estructura esencialmente microporosa con una pobre contribución de mesoporos. Al aumentar la temperatura de pirólisis se alcanza una mayor superficie específica y un menor tamaño medio de poro. Los valores más altos de superficie específica se han obtenido en el intervalo de 700 a 800 ºC, alcanzando valores de hasta 500 m^2g^{-1} con tamaños de poro entre 0.4 y 1.1 nm. No se observan cambios significativos en la morfología del *char* obtenidos tras la pirólisis, obteniéndose materiales granulares con tamaño similar al de las semillas de uva iniciales. La estructura hueca del *char*, con la mayoría del material situado en la periferia de los gránulos puede ayudar a superar la limitación de transferencia de masa que habitualmente tienen los carbones activados granulares. A la par el *char* mostró una buena resistencia mecánica durante los test de atrición. Los materiales obtenidos presentan propiedades interesantes como precursores para la preparación de tamices moleculares carbonosos o carbones activados.

3.2. Operating variables tested

The seeds used as starting materials were separated in two fractions. The first of them was pyrolyzed after their washing and drying, as described in Chapter 2. These seeds were designated as NEX (non-extracted). The other fraction was subjected to n-hexane extraction for 24 h in a Soxhlet apparatus to remove oil [1]. After extraction the seeds were washed with water and dried at 105 ºC for 1 day. These seeds were designated as EX (extracted).

Oil mass fraction of grape seeds depends on grape variety, though the usual range is a mass fraction of 10 – 16 % of the dry seed [1], though in this instance it is less than 9 %.

The others operating variables tested were the heating rate (slow heating (SH): 10 ºCmin^{-1} and FH: flash heating) and temperature from 300 to 1000 ºC.

Thus, the samples were designated by the pretreatment, pyrolysis temperature and heating rate. As e.g. for the char sample EX800FH, the sample was subjected to remove oil and pyrolyzed at 800 ºC by flash heating.

3.3. Samples characterization

The ash mass fraction of the raw material was determined by calcinations at 800 ºC in a crucible for 2 h. The samples were characterized by TGA before pyrolysis. The elemental composition of chars was also analyzed. Specific surface area and pore volume of the chars were measured by adsorption of N_2 at 77 K, Ar at 77 K and 87 K, and CO_2 at 273 K. The surface area of the samples was calculated from N_2 isotherms using BET equation and the t-method for the micropore volume, whereas DA model was applied to the CO_2 isotherms to determine the DA surface area and

micropore volume and the Non-Local Density Functional Theory was used to calculate the micropore size distribution. The mercury intrusion porosimetry was used to obtain the macropore volume.

The morphology of the grape seeds and the chars was evaluated by Scanning Electron Microscopy and the attrition test was carried out in a sifter.

3.4. Results

Prior to pyrolysis runs, the specimens were characterized by TGA runs with a heating rate of 10 ºCmin^{-1} until 900 ºC under 100 mLmin^{-1} N_2 flow during 200 min. Figure 3.1 shows the TG curve of EX sample. This curve is representative of all samples showing that the greatest weight loss occurs between 300 and 500 ºC. These results indicate that at temperatures below 500 ºC pyrolysis can be considered incomplete. A pyrolysis time of 2 h was considered acceptable for the rest of the study.

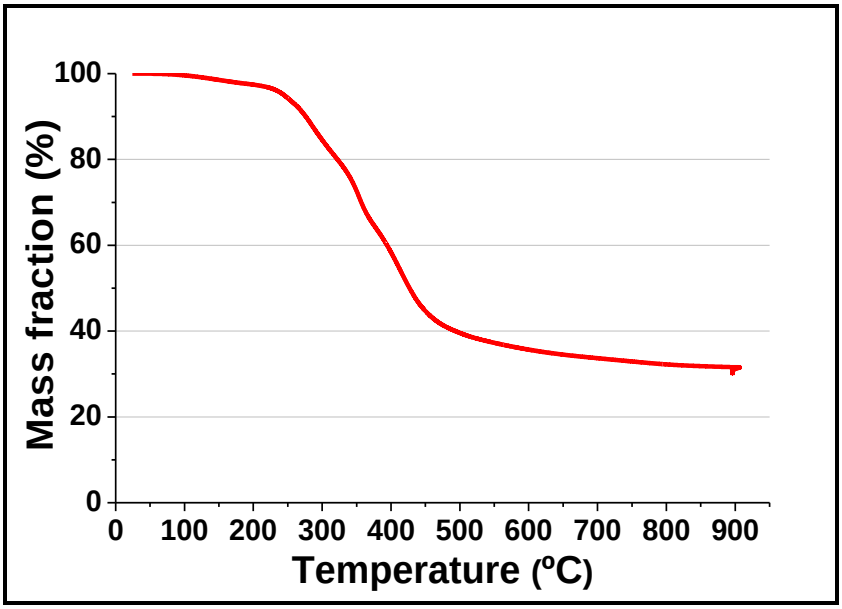

Figure 3.1. TG of EX seeds at 10 ºCmin^{-1} heating rate in N_2 atmosphere during 200 min.

3.4.1. Influence of pyrolysis variables

Table 3.1 summarizes the pyrolysis yields (dry oil-free basis). In the 300 to 1000 ºC thermal range, the yield values obtained are from 70 to 30 %. The pyrolysis yield (calculated by equations 2.1 and 2.2) showed as a general trend to decrease when the temperature was increased. Previous studies on biomass pyrolysis reported the same trend [2 – 14], showing a high yield of biochar at low pyrolysis temperatures as a results of incomplete pyrolysis [3, 4]. No significant differences were observed between SH and FH samples, although, in general FH provided slightly lower yields. This observation suggests that sudden devolatization gives rise to lower residence time of volatile products within the seeds somewhat diminishing the amount of carbonaceous solid formed upon condensation of pyrolysis products [12, 13].

Table 3.1. Mass fraction char yield (dry oil free basis).

Pyrolysis Temperature (ºC)	Yield (%)			
	EX-SH	EX-FH	NEX-SH	NEX-FH
300	71	68	63	69
400	41	40	41	44
500	36	33	36	37
600	35	31	35	34
700	32	28	33	32
800	31	28	33	31
900	29	27	33	30
1000	28	29	33	29

The elemental composition of the char samples is summarized in Table 3.2. Consistently with the TG curve (Figure 3.1) and yield (Table 3.1), the carbon percentage of the chars undergoes a significant increase within the 300 – 500 ºC range up to around 80 % and then a progressively slower thermal decomposition allows approaching to 90 % as a final charring level. Moreover the trend to increase slightly with the pyrolysis temperature is clearly shown even taking into account the results dispersion (around 1 – 2 %) that is typical of usual heterogeneity of biomass materials. Finally, as carbon percentage increased, hydrogen mass fraction decreased from 6 to less than 1 %. Previous studies on pyrolysis of different types of biomass showed the same trend in the evolution of carbon and hydrogen relative mass fractions [4 – 8, 15, 16].

The carbon mass fraction of the EX chars are somewhat higher than those of NEX, suggesting that the pyrolysis of the oil fraction generates a carbonaceous residue with lower carbon mass fraction than the oil-free matter of the seeds. No clear influence of the heating rate on the elemental

composition of the chars can be concluded in spite of the results in Table 3.2, where flash pyrolysis seems to provoke a somewhat more intense thermal decomposition leading to lower yield values. It is important to remark the almost negligible sulphur mass fraction of the starting grape seeds, which even diminishes in the chars. With regard to nitrogen mass fraction, a significant reduction is observed upon pyrolysis and the chars show in general percentages lower than 2 %.

The ash mass fraction of the raw material of the NEX and EX seeds are 2 and 8 % respectively with a elemental composition of C, H, N and S of 0.06, 0.2, 0.01 and 0.06 % respectively for NEX ashes and 0.07, 0.18, 0.03 and 0.16 %, respectively for EX ashes.

Table 3.2. Carbon, Hydrogen, Nitrogen and Sulfur as element mass fractions of starting materials and their chars.

Pyrolysis Temperature (ºC)	Elemental Composition							
	%C				%H			
	EX-SH	EX-FH	NEX-SH	NEX-FH	EX-SH	EX-FH	NEX-SH	NEX-FH
300	67.9	71.0	69.7	67.6	6.0	6.2	5.9	6.2
400	75.2	75.5	72.6	74.1	3.6	3.6	3.7	3.9
500	81.6	81.5	81.2	79.7	2.9	2.8	2.9	3.1
600	86.2	86.5	81.2	82.3	2.2	2.1	2.5	2.3
700	87.3	87.3	84.9	84.6	1.3	1.3	1.6	1.8
800	90.3	85.6	88.3	86.8	0.9	1.0	1.4	1.2
900	89.9	87.1	86.8	86.0	1.2	1.5	1.0	0.9
1000	90.0	90.3	89.8	86.1	0.7	0.8	0.9	0.9
Starting Material	49.7		50.6		5.9		6.3	

Table 3.2. Cont.

Pyrolysis Temperature (ºC)	Elemental Composition							
	%N				%S			
	EX-SH	EX-FH	NEX-SH	NEX-FH	EX-SH	EX-FH	NEX-SH	NEX-FH
300	2.2	2.0	2.4	2.0	0.03	0.06	0.10	0.10
400	2.6	1.7	2.1	1.4	0.01	0.02	0.09	0.09
500	2.3	2.1	2.0	1.5	0.02	0.03	0.05	0.02
600	1.5	1.5	2.0	2.3	0.05	0.05	0.09	0.01
700	1.9	1.9	2.0	1.9	0.03	0.02	0.06	0.10
800	1.8	1.7	1.9	1.8	0.03	0.04	0.04	0.05
900	1.8	1.5	2.2	1.9	0.03	0.04	0.02	0.04
1000	2.0	1.8	1.7	1.8	0.02	0.05	0.02	0.05
Starting Material	1.4		1.1		0.07		0.2	

3.4.2. Specific surface area

Figure 3.2 shows the 77 K N_2 adsorption isotherms of the chars obtained at different temperatures.

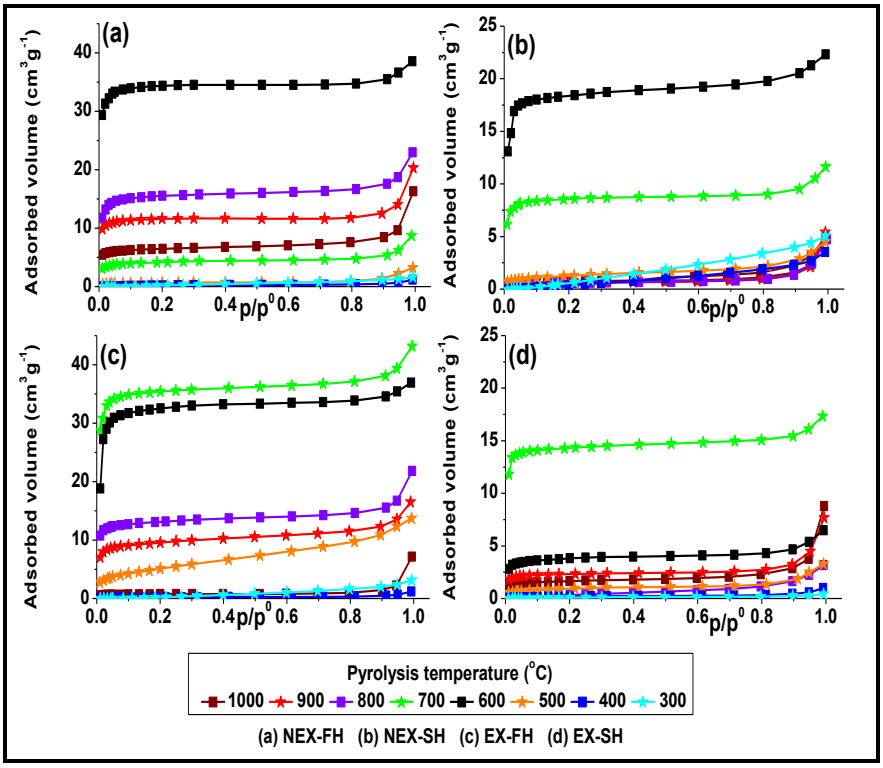

Figure 3.2. 77 K N_2 adsorption isotherms of grape seeds chars obtained at different temperatures.

The BET surface areas calculated by N_2 adsorption of the chars are summarized in Table 3.3. Most temperatures tested show that chars of FH series lead to higher specific surface area than SH series, particularly for the extracted seeds. The highest adsorption values correspond to the chars obtained by flash pyrolysis at an intermediate temperature of 600 – 700 ºC. Below that temperature a very poorly developed SSA can be observed in spite of the fact that devolatilization occurs mostly at lower temperature. The extraction of oil from the grape seeds does not show a clear effect in the development of S_{BET}. The porous structure is dominated by microporosity according to the shape of the isotherms with a sharp increase of N_2 adsorption at low relative pressures followed by a quasi-horizontal branch up to $P/P_0 \approx 0.95$ (Figure 3.2).

Table 3.3. BET Surface area values of raw seeds and chars obtained under different conditions from N_2 and Ar isotherms.

Pyrolysis temperature (ºC)	S_{BET} (m^2g^{-1})											
	N_2 (77 K)				Ar (77 K)				Ar (87 K)			
	EX-SH	EX-FH	NEX-SH	NEX-FH	EX-SH	EX-FH	NEX-SH	NEX-FH	EX-SH	EX-FH	NEX-SH	NEX-FH
300	1	7	15	6	<1	4	5	<1	5	5	4	5
400	1	1	15	1	<1	2	<1	3	1	2	1	13
500	3	18	5	2	2	14	2	3	23	58	45	5
600	13	110	34	120	13	57	37	320	60	290	205	310
700	51	124	31	15	27	66	5	60	24	161	60	260
800	1	47	2	54	1	38	1	31	1	128	1	85
900	8	33	2	50	2	24	2	33	14	44	2	57
1000	6	3	2	22	5	6	2	52	6	2	2	31
Starting Material	3		1		1		<1		12		4	

The characterization of the mesoporous range of the char samples was also carried out by Ar isotherms at 77 and 87 K. As can be read in Table 3.3 the results of specific surface area of the isotherms of Ar at 87 K are slightly higher than at 77 K due to the increased mobility of Ar molecules. The low values of specific surface area measured by Ar adsorption reveals the low contribution of mesopores to the surface area and corroborate the results obtained with N_2.

To learn more on the microporous structure of the chars, the CO_2 adsorption isotherms were obtained at 273 K. As an example, Figure 3.3 shows the CO_2 isotherms of the chars obtained at 800 ºC.

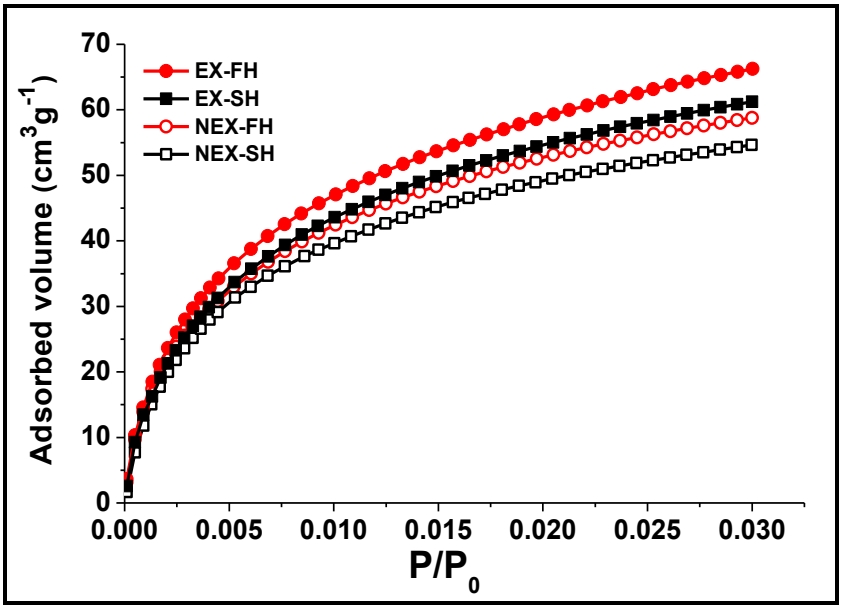

Figure 3.3. 273 K CO_2 adsorption isotherms of the chars obtained at 800 ºC.

The values of surface area obtained from the DA method are summarized in Table 3.4. These values are significantly higher than those reported in Table 3.3 from N_2 adsorption, which indicates the existence of a

narrow microporosity that become more important as the pyrolysis temperature increases. Temperatures below 500 ºC yielded low values of surface area which is another evidence of the incomplete pyrolysis at those temperatures [3, 4]; understanding this as the incomplete removal of volatile matter from the samples, which affects negatively the development of porosity. The surface area increased with temperature markedly from 400 – 500 ºC, peaking around 800 ºC for both NEX and EX samples. From 900 ºC the microporous structure seems to collapse during pyrolysis, as evidenced by the dramatic loss of specific surface area. Similarly to the results observed for the BET surface area [11, 17, 18]. Flash pyrolysis of the extracted grape seeds yielded the highest values of the CO_2-DA surface area.

Table 3.4. CO_2-DA surface area values of raw seeds and the chars obtained under different conditions.

Pyrolysis temperature (ºC)	S_{DA} (m^2g^{-1})			
	EX-SH	**EX-FH**	**NEX-SH**	**NEX-FH**
300	28	51	42	30
400	236	237	219	184
500	345	361	358	338
600	407	424	400	398
700	431	454	445	438
800	499	505	389	479
900	428	432	104	404
1000	63	108	26	155
Starting Material	5		7	

3.4.3. Pore volume

Figure 3.4 shows the micropore volume of the chars obtained under different conditions plotted versus pyrolysis temperature. As can be seen no significant development of porosity occurs below 600 ºC. The mesopore volumes were always negligible with adsorbed volumes lower than 0.01 cm^3g^{-1} for all the temperature range.

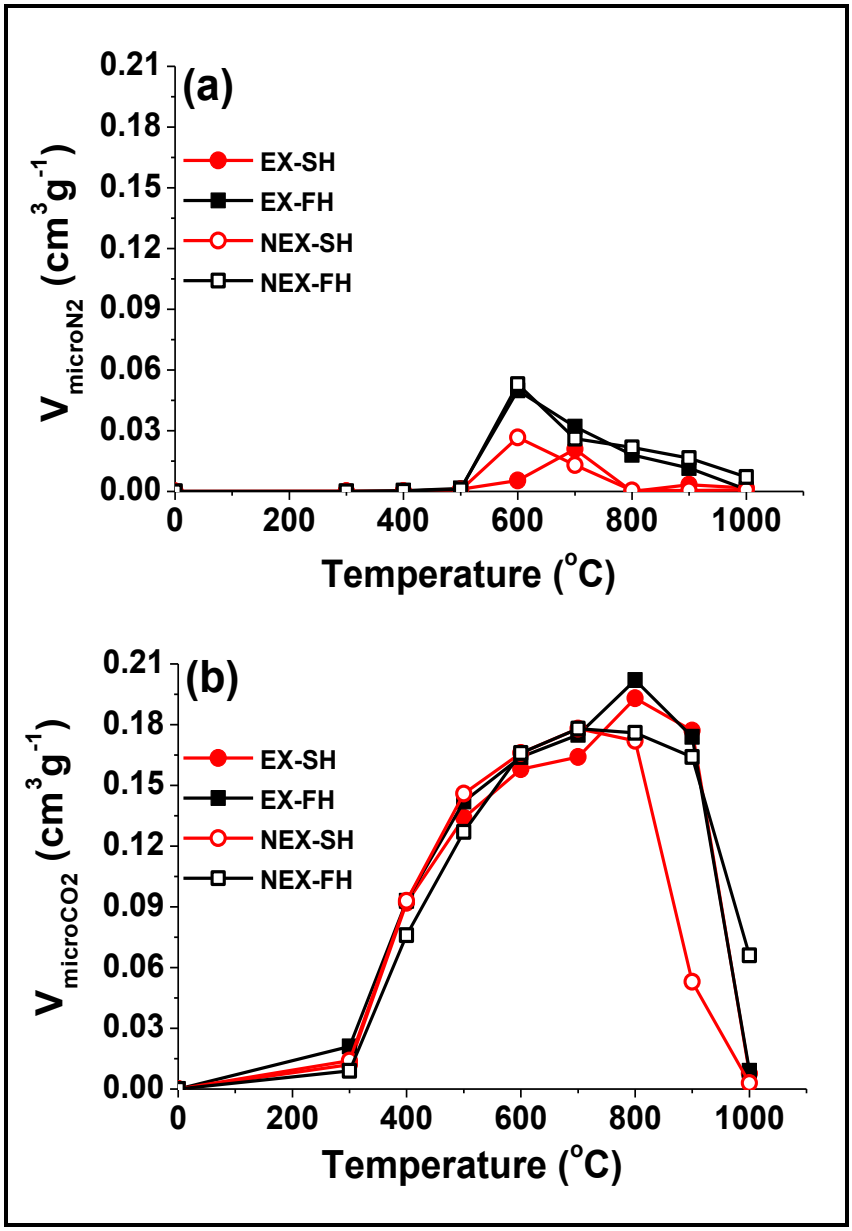

Figure 3.4. Micropore volume of the chars obtained under different conditions calculated from (a) N_2 and (b) CO_2 isotherms.

The micropore volume from CO_2 isotherms increases with temperature peaking around 800 ºC for both NEX and EX samples. From 900 ºC the microporous structure seems to collapse during pyrolysis, as evidenced by the dramatic loss of porosity [14, 20, 21]. The comparison between N_2 and CO_2 micropore volume indicates that pyrolysis temperatures of 800 – 900 ºC maximize the contribution of narrow microporosity (microporosity below 1 nm diameter). No significant influence of heating rate and seeds pretreatment was observed in the micropore volume obtained from CO_2 isotherms (Figure 3.4b).

Figure 3.5 shows the macropore volume determined by mercury intrusion porosimetry in the 0.01 – 4 μm pore size range for the chars prepared by flash pyrolysis at different temperatures. A gradual increase can be observed with pyrolysis temperature peaking around 800 ºC. The porosity is, in general, higher for the chars prepared from extracted seeds.

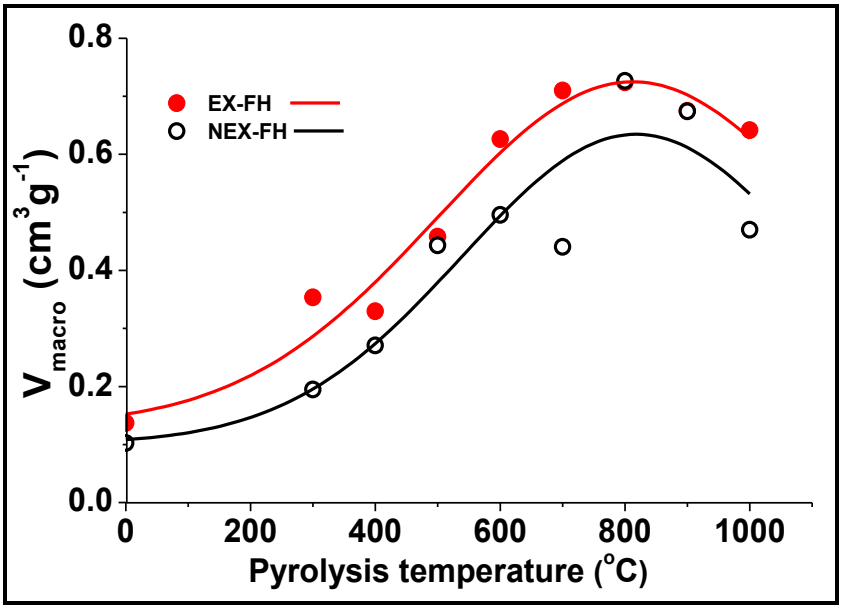

Figure 3.5. Macropore volume results from mercury porosimetry for EX-FH and NEX-FH series.

3.4.4. Pore size distribution

The pore size distribution is a key element in the characterization of porous carbons and a number of methods were developed for the PSD analysis. The Non-Local Density Functional Theory is widely used for the characterization of pore structure of activated carbons and other porous materials.

The micropore size distributions calculated from CO_2 isotherms by the NLDFT method are shown in Figure 3.6. For simplicity only the range from 600 to 900 ºC of pyrolysis temperature is evaluated since this is the temperature range where the relevant porosity development was achieved.

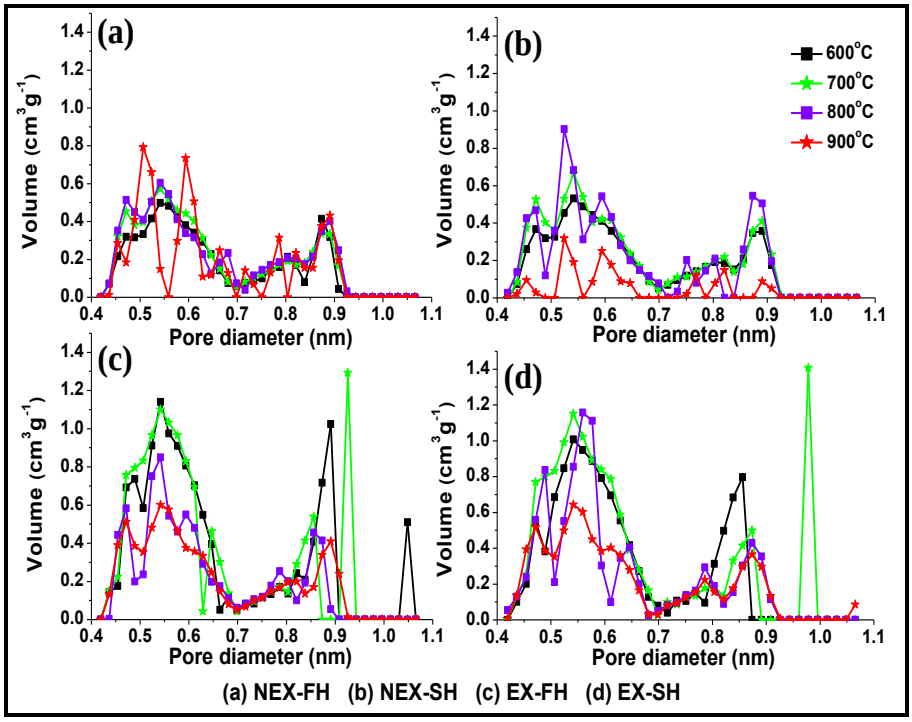

Figure 3.6. Micropore size distribution of grape seeds char.

No significant differences were found in the pattern of the PSD profiles with heating rate within the NEX or EX series. On the contrary a sharp difference can be seen between the EX and NEX samples in terms of differential pore volume, which is much higher for the EX series. This behavior may indicate that the residue of pyrolyzed oil present in the NEX samples blocks some pores leading to lower development of microporosity in the micropore lower than 1 nm. Although Figure 3.5 shows different PSD profiles depending on the pyrolysis temperature, it can be seen that the micropores show diameters falling mainly within the 0.40 to 0.95 nm range for all series. Furthermore these PSD profiles can be considered as bimodal due to the maxima of the adsorbed volume curves observed around 0.55 and 0.9 nm pore diameter.

Figure 3.7 shows the mercury intrusion porosimetry characterization of the samples obtained for a pyrolysis temperature of 800 ºC. The plotted data correspond to the volume of intruded mercury in the 0.01 – 4 μm pore size range. As can be observed, all the samples showed an important contribution of macropores and negligible volume of mesopores. The higher volume was obtained for the samples from flash pyrolysis reaching values above 0.5 cm^3g^{-1} and showing profiles centered around 0.4 μm. Samples obtained by slow heating showed values of adsorbed volume much lower, particularly in the mesopore range, and with a pore diameter centered around 0.2 – 0.3 μm. The higher porosity of the samples obtained by flash heating can be attributed to sudden release of pyrolysis gases that leads to channeling [19].

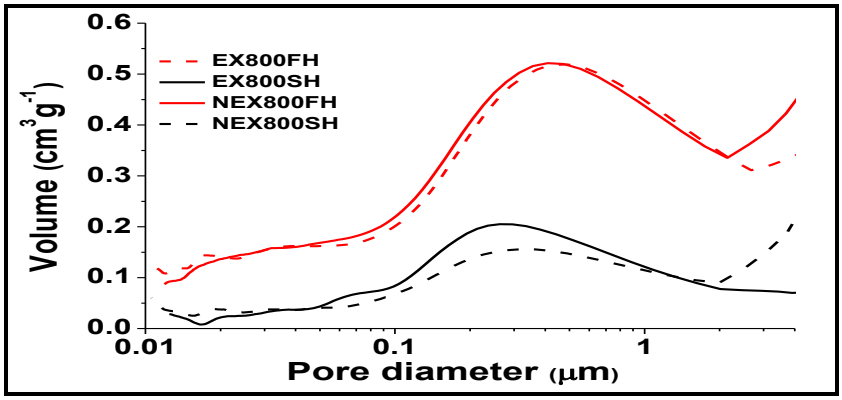

Figure 3.7. Macropore size distribution for 800 ºC pyrolyzed samples.

3.4.5. Morphological analysis

The grape seeds were examined by scanning electron microscopy to study their morphology and surface structure. Figure 3.8 shows the raw grape seed and the char produced by flash pyrolysis at 800 ºC of extracted seeds. For all the specimens examined the char maintained the granular morphology of the raw seed with no significant changes in size, even upon the most severe pyrolysis conditions, although some of the specimens showed opening of the coat (Figure 3.8b), presumably due to internal overpressure during pyrolysis.

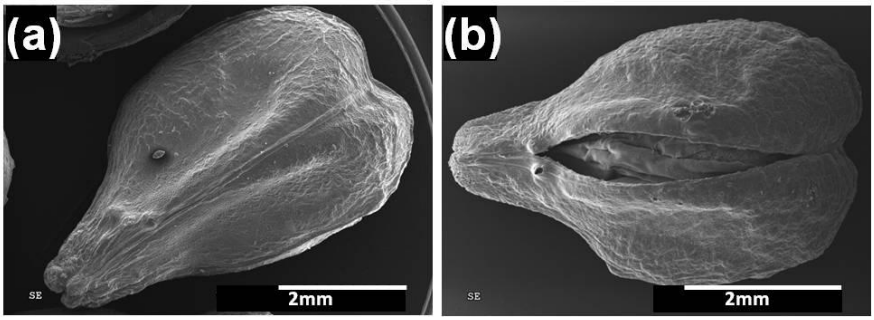

Figure 3.8. SEM image of grape seed raw (a) and char from extracted seed (EX800FH) (b).

A detail of the opening of the coat is shown in Figure 3.9a. The outer surface exhibits smooth and homogeneous texture (Figure 3.9b) resulting from the carbonization of the cuticle tissue of the coat, with no relevant presence of cracks and large macropores, that show that the structure of the outer surface was preserved in the char after pyrolysis [14]. Depending on the applications of the char, the outer layer can be an undesirable resistance for the diffusion of molecules, or can be potentially a barrier for separation. On the contrary, the inner layers exposed by the opening of the outer layers of the coat (Figure 3.9c) showed a well-developed network of channels and macropores that can provide favorable conditions for diffusion [20].

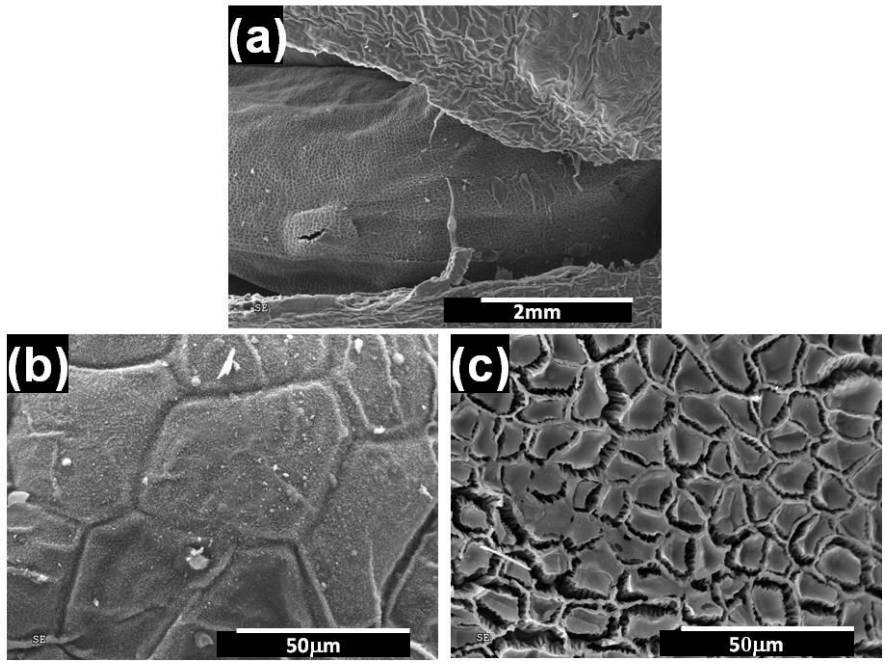

Figure 3.9. SEM images of the detail of opening of the outer layers of the coat (a), the outer surface of EX800FH sample (b) and the texture of the carbonized inner tissue (EX800FH) (c).

The material allocated inside the coat, i.e. albumen and embryo, is mostly removed during pyrolysis due to the high content in volatile components, resulting in a low density or carbon foam-like material, as can be seen in Figure 3.10a. A closer view of the carbonized coat (Figure 3.10b) shows that it has an average thickness of around 500 µm, and it is composed of three layers of differentiated structure, all of them with an important presence of channels and macropores. Therefore, the char has a hollow core structure, which together with the macroporous structure can favor the diffusion of molecules in adsorption or catalysis applications [20].

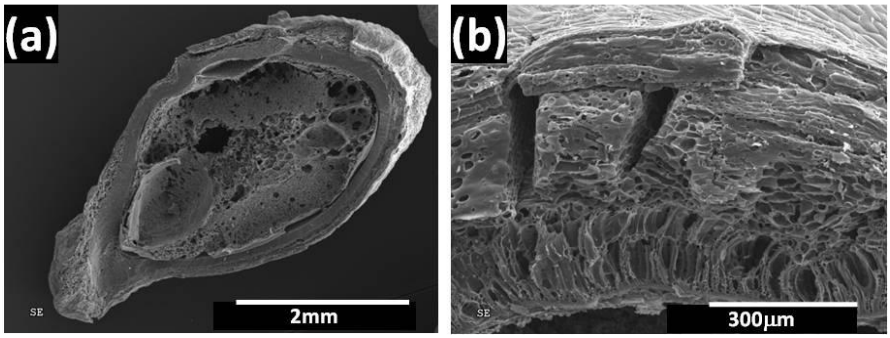

Figure 3.10. SEM images of the cross section of a grape seed after pyrolysis (EX800FH) (a) and the carbonized seed coat (EX800FH) (b).

3.4.6. Attrition tests

To study the pore structure of the different layers of the char particles, EX800FH sample was subjected to attrition in a vibrating sifter. The samples have a suitable balance between surface area and burn-off, so that the integrity and strength of the particles can be preserved. During the attrition tests three fractions of the powder passing through the sieve openings (<1 mm) were collected at regular intervals of 2 h. The results in Table 3.5 show a rather homogeneous development of surface area throughout the particle wall. The most noticeable differences can be found for S_{BET}, the outer layers showing significantly lower values of S_{BET}, which suggest the prevailing generation of narrow porosity in the inner layers. In the case of S_{DA} a similar behavior was observed.

It is also remarkable that the char particles have a good resistance to attrition, since only 7.5 % of the initial mass was lost in the first 2 h of the test, this resistance increasing in the inner layers. The strength of the particles is of great importance for the sake of handling and performance in potential applications.

Table 3.5. Specific surface area and mass fraction loss of EX800FH sample.

Sample	S_{BET} (m^2g^{-1})	S_{DA} (m^2g^{-1})	Mass loss (%)
EX800FH	47	505	
Fraction 1	4	465	7.5
Fraction 2	5	483	3.5
Fraction 3	12	633	1.2
Final sample	36	622	

References

[1] A. Molero Gómez, C. Pereyra López, E. Martínez de la Ossa. *Recovery of grape seed oil by liquid and supercritical carbon dioxide extraction: a comparison with conventional solvent extraction.* Chem. Eng. J. 1996; 61(3): 227 – 231.

[2] K. Açikalin, F. Karaka, E. Bolat. *Pyrolysis of pistachio shell: Effects of pyrolysis conditions and analysis of products.* Fuel 2012; 95(1): 169 – 177.

[3] S. Katyal, K. Thambimuthu, J. Valix. *Carbonisation of bagasse in a fixed bed reactor: influence of process variables on char yield and characteristics*. Renew. Energy 2003; 28(5): 713 – 725.

[4] D. Angin. *Effect of pyrolysis temperature and heating rate on biochar obtained from pyrolysis of safflower seed press cake*. Bioresour. Technol. 2013; 128: 593 – 597.

[5] W.M.A.W. Daud, W.S.W. Ali, M.Z. Sulaiman. *Effect of carbonization temperature on the yield and porosity of char produced from palm shell*. J. Chem. Technol. Biotechnol. 2001; 76(12): 1281 – 1285.

[6] A. Demirbas. *Effects of temperature and particle size on bio-char yield from pyrolysis of agricultural residues*. J. Annal. Appl. Pyrolysis 2004; 72(2): 243 – 248.

[7] G. Duman, C. Okutucu, S. Ucar, R. Stahl, J. Yanik. *The slow and fast pyrolysis of cherry seed*. Bioresour. Technol. 2011; 102(2): 1869 – 1878.

[8] W. Song, M. Guo. *Quality variations of poultry litter biochar generated at different pyrolysis temperatures*. J. Annal. Appl. Pyrolysis 2012; 94: 138 – 145.

[9] I. Demiral, E.A. Ayan. *Pyrolysis of grape bagasse: Effect of pyrolysis conditions on the product yields and characterization of the liquid product.* Bioresour. Technol. 2011; 102(4): 3946 – 3951.

[10] W. Li, K. Yang, J. Peng, L. Zhang, S. Guo, H. Xia. *Effects of carbonization temperatures on characteristics of porosity in coconut shell chars and activated carbons derived from carbonized coconut shell chars.* Ind. crops Prod. 2008; 28(2): 190 – 198.

[11] A.C. Lua, J. Guo. *Preparation and characterization of chars from oil palm waste.* Carbon 1998; 36(11): 1663 – 1670.

[12] A.E. Pütün, N. Özbay, E.A. Varol, B.B. Uzun, F. Ates. *Rapid and slow pyrolysis of pistachio shell. Effect of pyrolysis conditions on the product yields and characterization of the liquid product.* Int. J. Energy Res. 2007; 31(5): 506 – 514.

[13] S. Sensöz, D. Angin. *Pyrolysis of safflower seed press cake: Part 1. The effects of pyrolysis parameters on the product yields*. Bioresour. Technol. 2008; 99(13): 5492 – 5497.

[14] I. Uzunov, S. Uzunova, D. Angelova, A. Gigova. *Effects of the pyrolysis process on the oil sorption capacity of rice husk.* J. Annal. Appl. Pyrolysis 2012; 98: 166 – 176.

[15] P.R. Bonelli, P.A. Della Rocca, E.G. Cerrella, A.L. Cukierman. *Effect of pyrolysis temperature on composition, surface properties and thermal degradation rates of Brazil Nut shells.* Bioresour. Technol. 2001; 76(1): 15 – 22.

[16] B.B. Uzun, A.E. Pütün, E. Pütün. *Composition of products obtained via fast pyrolysis of olive-oil residue: Effect of pyrolysis temperature.* J. Anal. Appl. Pyrolysis 2007; 79(1-2): 147 – 153.

[17] M. Polyakov, M. Poisot, W.E. Maurits, T. Drescher, A. Lotnik, L. Kienle. *Carbon-stabilized mesoporous MoS2 - structural and surface characterization with spectroscopic and catalytic tools.* Catal Commun 2010; 12(3): 231 – 237.

[18] S. Guo, J. Peng, W. Li. *Effects of CO_2 activation on porous structures of coconut shell-based activated carbons*. Appl. Surf Sci. 2009; 255(20): 8443 – 8449.

[19] E. Cetin, R. Gupta, B. Moghtaderi. *Effect of pyrolysis pressure and heating rate on radiata pine char structure and apparent gasification reactivity.* Fuel 2005; 84(10): 1328 – 1334.

[20] M.J. Prauchner, F. Rodríguez-Reinoso. *Chemical versus physical activation of coconut shell: A comparative study.* Micro Meso Mater 2012; 152: 163 – 171.

CAPÍTULO 4 / CHAPTER 4

ACTIVACIÓN DE CHAR DE NFU

CON AIRE

ACTIVATION OF WASTE TIRES CHAR

WITH AIR

4.1 Resumen / Abstract

La activación mediante ciclos de oxidación-desorción con oxígeno (Aire) ha demostrado ser un método eficaz para desarrollar porosidad con bajos valores de *burn-off* en *char* de NFU. En este capítulo, se estudia la influencia del tamaño de partícula de *char*, la temperatura de desorción y el número de ciclos.

Los mayores valores de *burn-off* y superficie específica se han obtenido para el tamaño de partícula más grande (diámetro de 2 mm) y una temperatura de desorción intermedia (650 ºC). En esas condiciones se alcanzan valores en torno a 500 m^2g^{-1} con un *burn-off* del 30 %, y cerca de 600 m^2g^{-1} con un *burn-off* del 45 %, lográndose un tamaño medio de poro de 10 nm y un volumen de microporo de 0.08 cm^3g^{-1}. Aunque el área superficial es moderada, el bajo *burn-off* y la elevada relación S_{BET} por unidad de *burn-off* hace posible mantener la morfología granular inicial de las partículas de *char* de NFU incluso después de 20 ciclos de activación.

4.2. Materials and methods

The waste tire rubber was sieved in three different fractions of 0.5, 1, and 2 mm of average particle diameter. The char used as starting material for air activation was obtained by flash pyrolysis of the rubber from waste tires at 800 ºC for 20 min under nitrogen atmosphere at 100 $NmLmin^{-1}$ prepared in the pyrolysis furnace described in Chapter 2, according to the results of a previous work [1].

4.2.1. Samples characterization

The elemental composition of initial char was characterized by elemental analysis to determine C, H, N and S content and by inductively coupled plasma mass spectrometry to determine other significant elements.

The burn-off after each cycle was determined by sample weighting, as indicated in equation 2.1. Surface area and total pore volume of the samples were obtained by adsorption of N_2 at 77 K. The surface area was calculated from the N_2 isotherm using the BET equation and the t-method was used for the micropore volume. The mesopore volume and average mesopore diameter was obtained by BJH method. Temperature programmed oxidation was used to learn about the presence of carbon domains of different reactivity in 20-cycles samples and char. The Non-Local Density Functional Theory was used to calculate the pore size distribution. The morphology of grape seeds char and activated carbons was analyzed by Scanning Electron Microscopy.

4.2.2. Cyclic activation conditions

The cyclic activation was carried out in the furnace with manual control described in Chapter 2. The operating conditions for oxidation step of each cycle were the same for all the experiments. 210 ºC during 200 min with an air flow of 80 $NmLmin^{-1}$, these conditions were determined as the optimum conditions in a previous work [2]. The desorption step was carried out at three different temperatures (550, 650 and 750 ºC) using a flow rate of 100 $NmLmin^{-1}$ of nitrogen and 2 h of reaction time in all the cases. The switch from oxidation to desorption was carried out at a heating rate of 10 $ºCmin^{-1}$ under nitrogen flow in all cases.

The series activated carbons obtained were designated in function of average particle diameter with the letters S, M and L (for samples with particle diameter of 0.5, 1, and 2 mm, respectively), by the letter “A” from Air activation, followed by the desorption temperature in ºC. For instance, for the activated carbon series L-A650, from waste tire rubber with a diameter of 2 mm, the char was activated with air and a desorption temperature of 650 ºC was used.

In a first series of experiments, the influence of desorption temperature and particle size was studied using 6-cycle activation test. Later, depending on the results obtained, three series were chosen basis on surface area development for 20-cycles activation tests (Table 4.1).

Table 4.1. Conditions used in the activation experiments.

Rubber particle size (mm)	Desorption temperature (ºC)	Number of cycles
PREVIOUS TESTS		
0.5	550	6
1		
2		
0.5	650	6
1		
2		
0.5	750	6
1		
2		
POROSITY DEVELOPMENT STUDY		
2	650	20
0.5	750	20
2		

4.3. Results

Pyrolysis is a well-known step in the proposed process and it was optimized to obtain the maximum yield in char, about 42 %. This yield can be used as control parameter during pyrolysis. In this study, the char yield obtained for all the samples pyrolyzed was 41.4 ± 1.8 %.

Table 4.2 shows the elemental composition of char. As can be seen, in addition to the main elements that make up the rubber catalysts, inorganic charges, etc., that are used during tire manufacturing and are in enough composition to play a role in pyrolysis and/or activation processes.

Table 4.2 Composition of initial WTR char (% weight basis).

C	H	N	S	Si	Ca	Fe	Zn
89.3	0.5	0.3	2.1	0.7	1.1	0.1	1.9

4.3.1. Burn-off in 6-cycle tests

Figures 4.1 shows the evolution of burn-off upon the first series of experiments of 6 cycles duration. As can be observed, the burn-off increased progressively with the number of cycles. The final values of burn-off obtained were lower than 15 % for all the activation conditions studied.

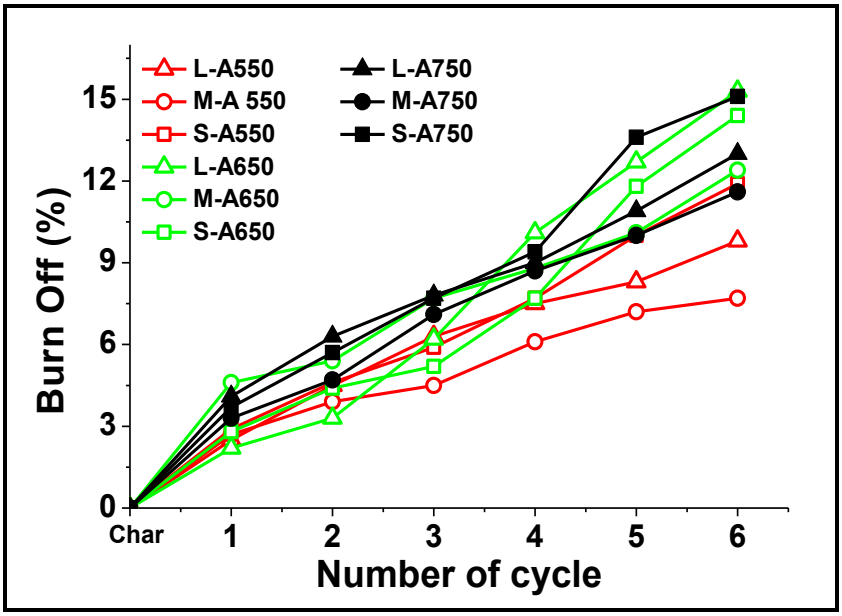

Figure 4.1. Burn-off vs number of cycles for 6-cycles tests.

4.3.2. Specific surface area in 6-cycle tests

Figures 4.2 shows the evolution of BET surface area upon the first series of experiments of 6 cycles duration. The S_{BET} also increased with the number of cycles and after 6 activation cycles, values between 110 and 260 m^2g^{-1} were achieved, except for the combination of L particle size and 650 ºC desorption temperature, which led to a S_{BET} value of 391 m^2g^{-1}. This combination also yielded the highest burn-off (15 %).

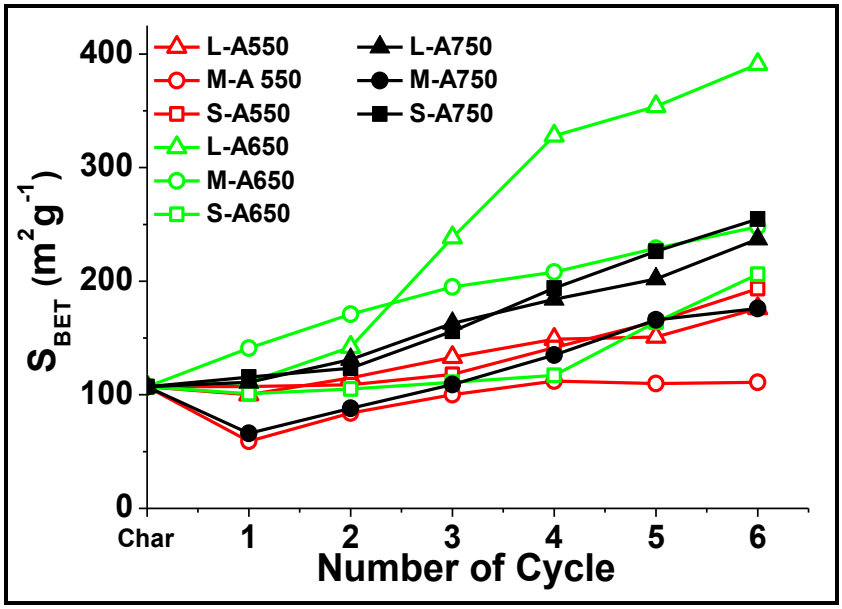

Figure 4.2. S_{BET} vs number of cycles for 6-cycles tests.

The values of the ratio S_{BET} / burn-off obtained (Figure 4.3) are in general greater those reported for air activation of waste tires chars [3], and similar to those obtained by Py et al. [4] using cyclic oxygen adsorption-desorption activation with less reactive precursors such as coal and tar pitch. In general, a monotonical decrease occur for all samples along the activation cycles with similar values except for the series with the combination of L particle size and 650 ºC of desorption temperature that shows a higher S_{BET} development per unit of burn-off.

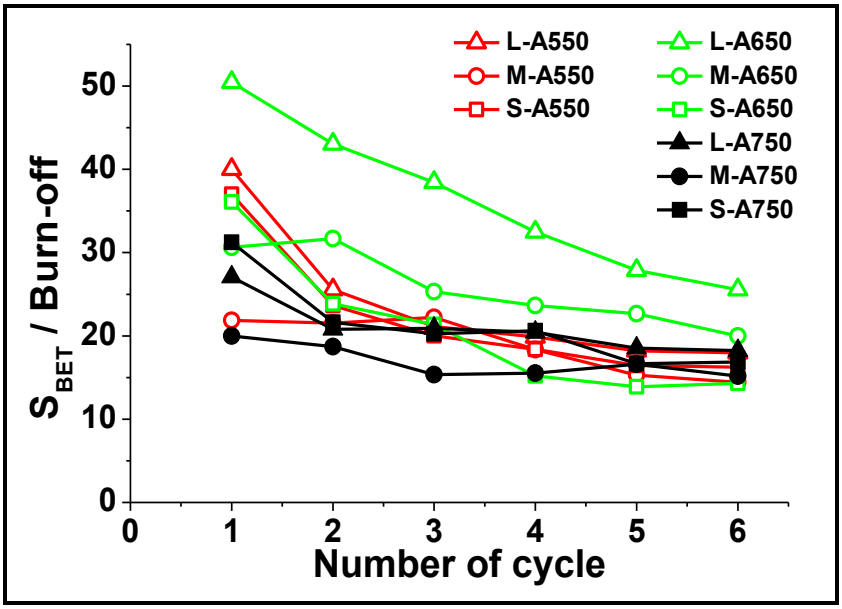

Figure 4.3. S_{BET} per burn-off unit vs number of cycles for 6-cycles tests.

4.3.3. Mean pore size in 6-cycle tests

The development of porosity was accompanied by a monotonic reduction of the mean mesopore size during the 6-cycle tests (Figure 4.4). After the first activation cycle a very important reduction of the d_{meso} took place for the series with M particle size and 550 and 750 ºC of desorption temperature, from this cycle, the decrease in the mean mesopore size was low. For the rest of the series a slight and gradual decrease was observed and the differences in mean pore size became higher with values between 12 and 30 nm.

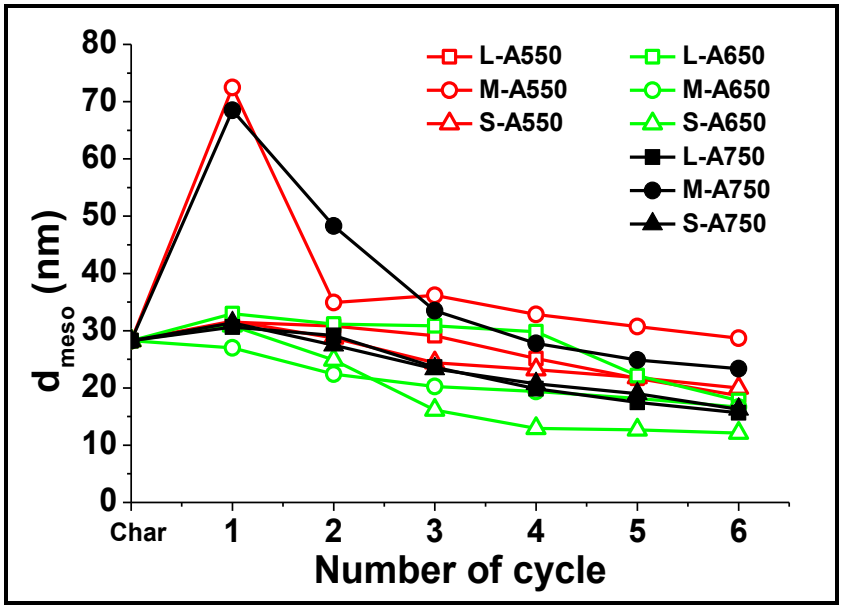

Figure 4.4. Average mesopore size vs number of cycles for 6-cycles tests.

Table 4.3. summarizes the results obtained after completion of the 6th activation cycle. In general, the high burn-off is associated with a higher BET surface area and a lower mean mesopore size.

Table 4.3. Results of activation after 6 cycles.

	BO (%)	S_{BET} (m^2g^{-1})	d_{meso} (nm)
S-A550	11.9	193	18.6
M-A550	7.7	111	28.7
L-A550	9.8	176	20.0
S-A650	14.4	206	17.8
M-A650	12.4	248	16.6
L-A650	15.3	391	12.1
S-A750	15.1	255	15.7
M-A750	11.6	176	23.4
L-A750	13.0	237	16.3

4.3.4. Analysis of variance about influence of variables studied

To analyze more in depth the influence of the particle size and desorption temperature, analysis of variance (ANOVA) was applied to the data of Table 4.3. The results are shown in Tables 4.4 and 4.5.

Table 4.4 Effects of the activation variables on burn-off and porosity development over the range tested.

	Burn-off (%)	**S_{BET} (m^2g^{-1})**	**d_{meso} (nm)**
Average	12.2 ± 0.2	239 ± 3	20.9 ± 0.1
Effect of the particle diameter (A)	-1.1 ± 0.2	50 ± 5	-1.2 ± 0.2
Effect of the desorption T (B)	3.4 ± 0.2	63 ± 5	-2.6 ± 0.2
2^{nd} order effect A·B	0 ± 0.3	-1 ± 6	-0.4 ± 0.3
2^{nd} order effect A·A	5.5 ± 0.4	129 ± 7	-19.9 ± 0.4
2^{nd} order effect B·B	-4.9 ± 0.4	-181 ± 7	17.6 ± 0.4

Table 4.5. Statistical parameters associated with the effects of the activation variables on burn-off and porosity development over the range tested[a].

	Burn-off		S_{BET}		d_{meso}	
	F-ratio	**P-value**	**F-ratio**	**P-value**	**F-ratio**	**P-value**
Particle diameter (A)	22.69	0.13	117.19	0.06	28.52	0.12
Desorption T (B)	221.02	0.04	184.08	0.05	126.75	0.06
AB	0.00	1.00	0.01	0.95	2.00	0.39
AA	218.29	0.04	302.01	0.04	2859.87	0.01
BB	177.12	0.05	599.09	0.03	2251.34	0.01
Lack-of-fit	13.23	0.20	144.20	0.06	548.57	0.03

[a]Note: degrees of freedom for effects and lack of fit are 1 and 3, respectively

That the mean effect of desorption temperature on burn-off, i.e., the average effect of increasing the desorption temperature from 550 to 750 ºC, is an increase of 3.4 % units of BO, being the statistical significance higher than 95 %. The high significance of the quadratic effect for desorption temperature and its sign indicates a higher BO for the runs carried out at an intermediate temperature of 650 ºC. This result suggests that the desorption of adsorbed oxygen at 650 ºC provides a better regeneration of the active sites for the oxidation step, leading to a higher accumulated burn-off after 6 activation cycles. The main effect of particle size shows a slight reduction of BO when increasing the particle diameter, although the significance for this effect is only 87 %.

The effect of desorption temperature on S_{BET} shows trends in accordance with the results for burn-off. Thus, the mean effect of desorption temperature is an increase of the S_{BET} with increasing temperature (significance 95 %) up to an intermediate temperature of 650 ºC when a maximum occurs. However, the curvature for S_{BET} is more marked than for burn-off. This results indicates that a desorption temperature of 650 ºC not only provides a better regeneration of active sites, but also a progressive generation of active sites at inner locations within the char structure. Therefore, at 650 ºC burn-off takes place with higher selectivity toward pore generation. In the case of S_{BET}, the main effect of particle diameter is significant (94 %) and its magnitude is equivalent to that of the desorption temperature. It can be observed that S_{BET} is generated more easily for the largest particles whereas minimum values are obtained for intermediate particle size.

The mean mesopore diameter after the 6-cycle tests is strongly influenced by the desorption temperature. The main effect of this variable is a reduction of the mean mesopore size with increasing desorption temperature up to 650 ºC where a minimum occurs. This result is in accordance with the enhanced generation of S_{BET} at this temperature. The ANOVA shows a

decrease in d_{meso} for higher particle diameters, however, the significance is low (88 %).

The discussion above indicates that the best results in terms of BO per cycle and development of S_{BET} can be obtained operating within the high range of desorption temperature (650 – 750 ºC) and for extreme particle size (S – L). It must also be pointed out that no interaction or synergy between desorption temperature and particle size was observed. Therefore, for the following series of long duration experiments tree combinations of the operating variables were selected: L-A650, S-A750 and L-A750.

4.3.5. Burn-off in 20-cycle tests

Figure 4.5 shows the results of burn-off for the series of experiments of 20-cycle duration. The burn-off values were in the range between 32 and 46 %, showing a nearly linear dependence on the number of cycles applied for samples S-A750 and L-A750, whereas for series L-A650 a decrease of the slope is observed beyond burn-off values around 35 %. Likewise, the increase of burn-off in each cycle is significantly higher at 650 ºC. When different initial particle sizes are compared at the same desorption temperature (750 ºC), the burn-off observed is higher for the smaller particles. The differences in burn-off were relatively small in the first 4 – 6 cycles and from then became more important.

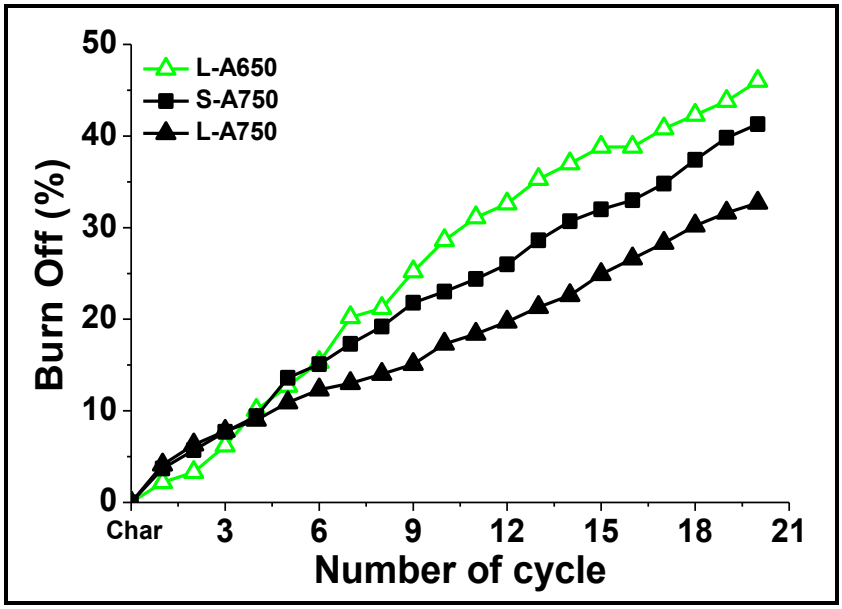

Figure 4.5. Burn-off vs number of cycles for 20-cycle tests.

4.3.6. Specific surface area in 20-cycle tests

As in the case of burn-off, the S_{BET} values increased with the number of cycles (Figure 4.6), although a progressive saturation effect can be observed as commonly occurs in activation processes. The best results in terms of surface area development were obtained with the largest particles (2 mm) at 650 ºC of desorption temperature (L-A650). It is noticeable there is considerably higher development of S_{BET} within the third-sixth cycle of that series, as compared with the two others despite that equivalent burn-off values are obtained up to that point, especially with respect to the S-A750 series.

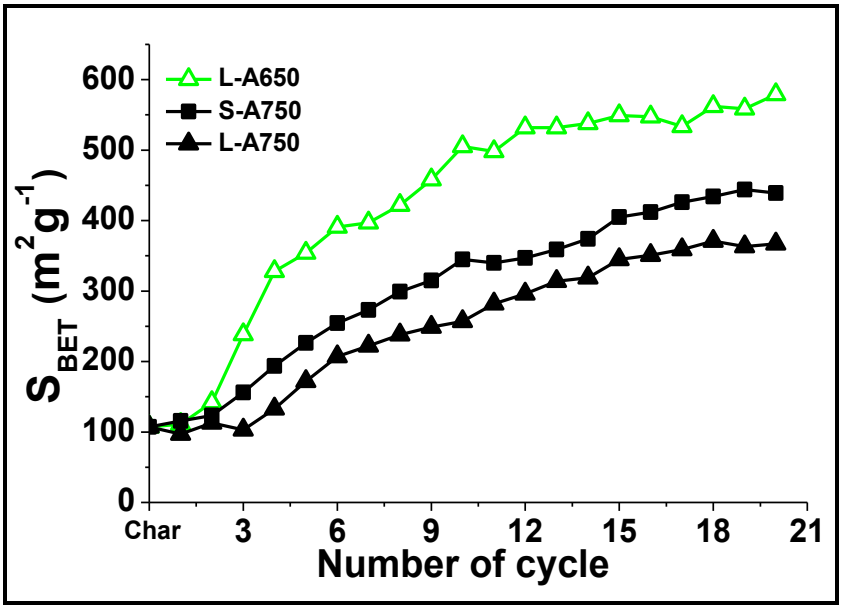

Figure 4.6. S_{BET} vs number of cycles for 20-cycle tests.

The important differences on the relative development of surface area of the L-A650 series in comparison with the two others can be better seen in Figure 4.7, where the S_{BET} / burn-off ratio versus number of cycles is depicted. After 7 – 8 cycles that ratio becomes fairly close for the three series.

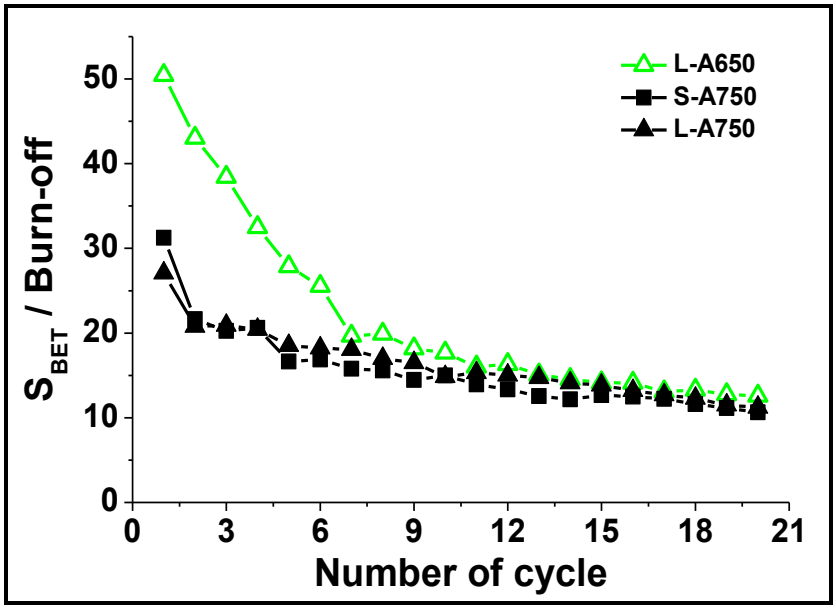

Figure 4.7. Variation of S_{BET} / burn-off versus number of cycles.

4.3.7. Pore volume in 20-cycle tests

As can be observed in Figure 4.8, the pore volume shows a very low contribution of microporosity compared with the mesoporosity (more than 66 % lower). The beginning of microporosity development depends on the operating conditions. For the L-A650 series the microporosity became measurable after the third activation cycle and increased steadily up to cycle 18. On the contrary, at least 6 and 10 activation cycles were needed for beginning the microporosity development in S-A750 and L-A750 series, respectively. In all cases a fairly low $V_{microN2}$ was obtained. On the opposite, the development of mesoporosity took place since the first activation cycle and significant mesopore volume values were achieved thus explaining the early development of surface area. The mesoporosity falls mostly within contribution of narrow mesoporosity (2 – 8 nm). Beyond the 6 - 10 cycles the development of mesoporosity was very low and the increase of S_{BET} is fundamentally associated with microporosity development.

According to the results obtained in the first cycles (third – tenth, depending on the operating conditions), mesoporosity is first developed and then micropores are created. This development pattern can be related to the presence of different types of carbon in the initial char, i.e., the different carbon domains of the original carbon black in the waste rubber and those from the carbonaceous material formed during the thermal decomposition of the rubber. In general carbon blacks are less reactive and are mainly embedded in the carbonaceous material from tires [5]. Therefore, the carbonaceous material from rubber can be expected to react more easily with oxygen and in earlier cycles than carbon black, being responsible for the formation of wider pores.

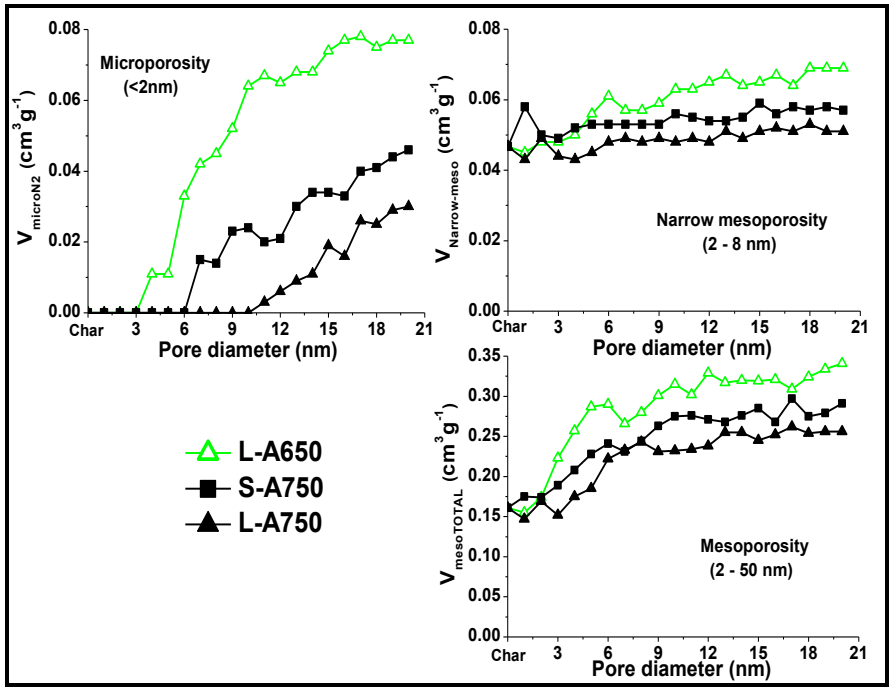

Figure 4.8. Micro, meso and narrow-meso volume versus number of cycles for 20-cycle series.

4.3.8. Pore size distribution in 20-cycle tests

The mean mesopore size after 20 activation cycles was very similar for the three series (see Figure 4.9). During the first 4 – 6 cycles an important decrease of the d_{meso} took place, which was quicker for the L-A650 series, in accordance with the higher development of surface area. After 4 – 6 activation cycles the mean mesopore size decreased slowly to around 10 nm after completion of the 20 activation cycles.

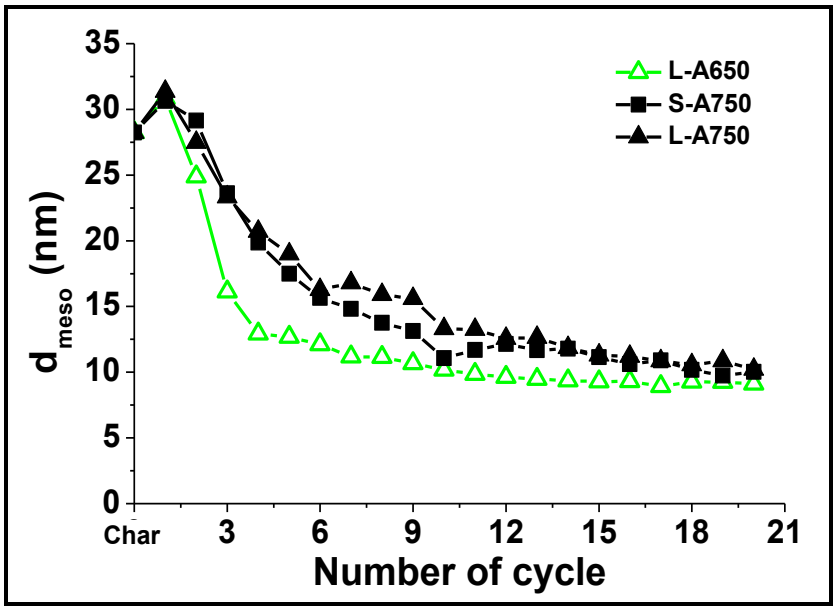

Figure 4.9. Average mesopore size versus number of cycles for 20-cycle series.

In order to have a deeper knowledge on the generation of porosity, the pore size distribution was calculated from N_2 isotherms by the NLDFT method for the char from waste tire rubber and for activated carbon of L-A650, S-A750 and L-A750 series samples after 20 activation cycles (Figure 4.10). As can be observed, the microporosity contribution is negligible

compared with the mesoporosity for all samples, while the mesoporosity shows similar patterns between samples but a notable increment of pore diameter for the samples activated, especially for those prepared with desorption temperature of 750 ºC. The distribution is characterized by the important contributions of mesopores centered at 14 and 17 nm for the char sample, at 20 nm for L-A650 C20 and at 28 and 35 nm for samples with 750 ºC of desorption temperature.

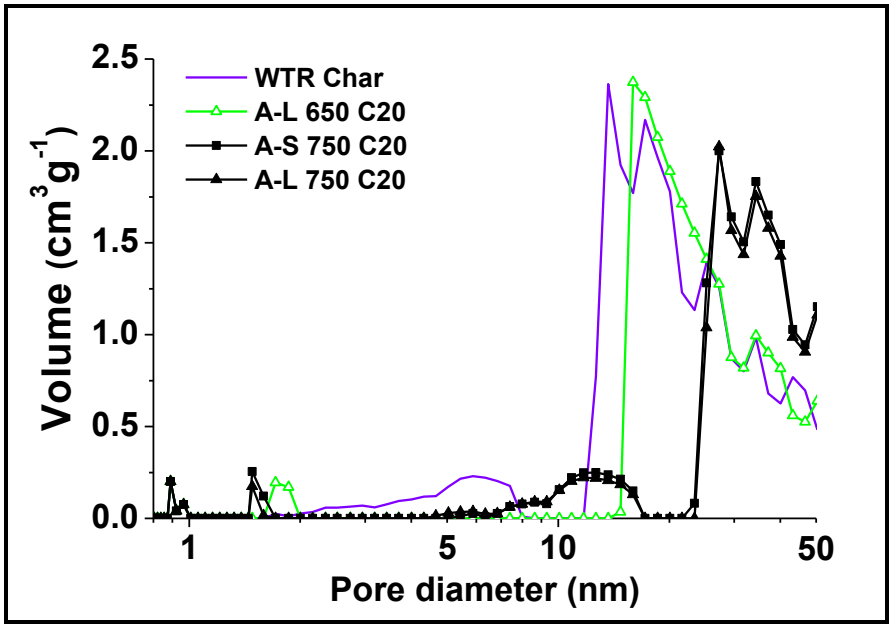

Figure 4.10. Pore size distribution by NLDFT method from N_2 isotherms for waste tire rubber char and the samples from L-A650, S-A750 and L-A750 series after 20 activation cycles.

4.3.9. Temperature programmed oxidation

To learn about the presence of carbon domains of different reactivity, TPO analysis of waste tire char and 20-cycles activated samples was carried out. Figure 4.11 shows that the TPO profiles are characterized by a rather narrow range of oxidation temperatures, which can be interpreted as a catalytic effect of the ash components of the samples (Zn, Ca, etc.) [6, 7]. However, significant differences can be observed among the samples studied. The initial char shows well-defined peaks that account for most of the carbon dioxide evolved during TPO analysis: two peaks between 520 and 525 ºC and a more important peak with a shoulder around 540 ºC. Smaller peaks in the initial char between 550 and 570 ºC disappeared and displaced to higher temperatures after activation. The application of 20 activation cycles led to the complete removal of the most reactive carbon of the initial char, i.e., that evolving as CO_2 at 520 and 525 ºC. This observation can be associated with the common activation pattern during the 4 – 6 first cycles and might be related to the initial development of mesoporosity. After 20 cycles the TPO of the samples showed a higher relative weight of somewhat less reactive carbon as burn-off increased. Then, the carbon domains in the initial char evolving below 540 ºC in the TPO analysis and those are missing in the activated samples could be responsible for the development of microporosity.

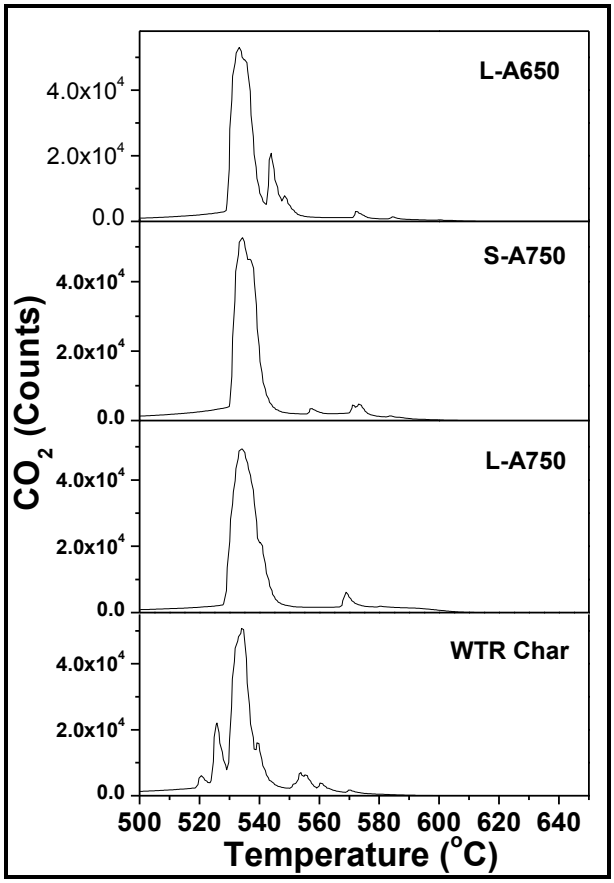

Figure 4.11. TPO profiles of the initial char and the samples L-A650, S-A750 and L-A750 after 20 activation cycles.

4.3.10. Morphological analysis

Figure 4.12. shows that morphology of the initial char particle is not significantly altered by the treatment even after 20 activation cycles due to the relatively low burn-off value achieved, which makes it possible to obtain granular carbons. The activation by cyclic oxidation-desorption with air can overcome the problems related to the high reactivity of waste tires char with oxygen providing porosity development and porous structure tailoring. Homogenous development of porosity is expected since the oxidation step avoids activation under oxygen-diffusion limitations.

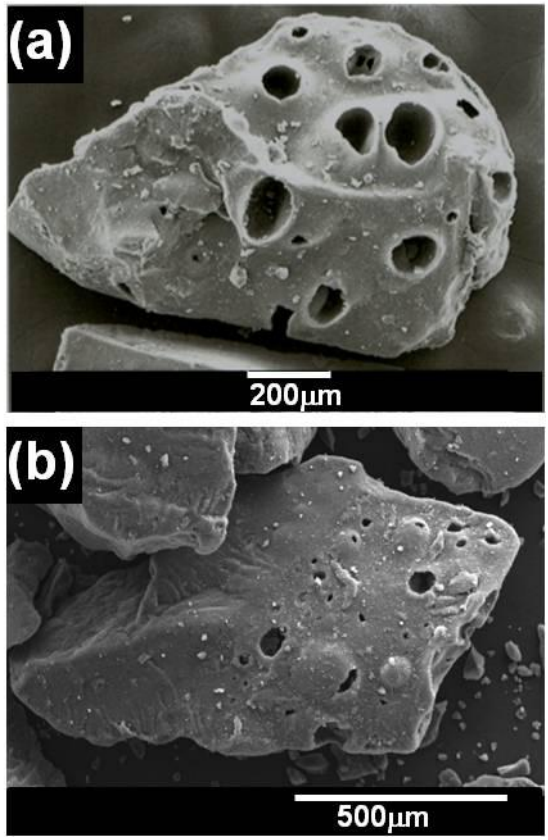

Figure 4.12. SEM images (20 kV) of the WTR char (a) and activated carbon particle of L-A650 after 20 activation cycles.

4.3.11 Comparison with results in literature

If the results of S_{BET} vs burn-off are compared with those obtained by other authors from physical activation of waste tire chars with steam [3, 8 – 17], CO_2 [3, 16 – 21] or steam–CO_2 mixtures [22] and from physicochemical activation with steam and HCl [12, 23] and combined treatments with heat, HNO_3 and H_2SO_4 [24] it can be concluded that the surface area values obtained by oxidation-desorption with air are moderate but they are achieved at low burn-off values and a high S_{BET}/ burn-off ratio (Figure 4.13). This is very interesting feature of cyclic activation because low burn-off values imply low destruction of the initial char particle, so that the method permits the preparation of granular activated carbons.

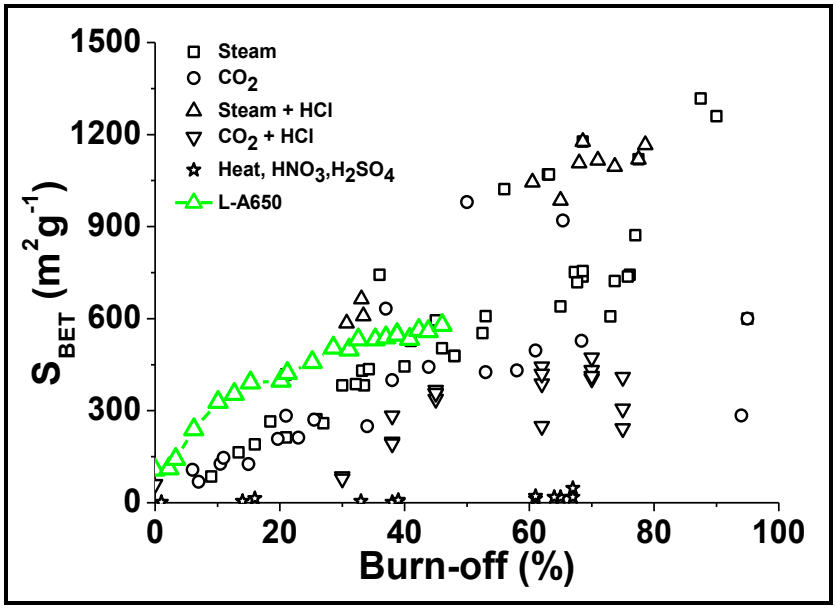

Figure 4.13. Comparison of S_{BET} vs Burn-off from oxygen cyclic activation of grape seeds char (L-A650 series) with literature results on the activation of waste tires [3, 8 – 24].

References

[1] N. Alonso-Morales, M.A. Gilarranz, F. Heras, V. González, J.J. Rodríguez. I*nfluence of operating variables on carbonization of waste tires*. 1st European Chemistry Congress, 2006, Bulgary.

[2] F. Heras, N. Alonso-Morales, M.A. Gilarranz, J.J. Rodríguez. *Activation of waste tires char upon cyclic oxygen oxidation-desorption*. Ind. Eng. Chem. Res. 2009; 48(10): 4664 – 4670.

[3] R. Helleur, N. Popovic, M. Ikura, M. Stanciulescu, D. Liu. *Characterization and potential applications of pyrolytic char from ablative pyrolysis of used tires*. J. Anal. Appl. Pyrolysis 2001; 58: 813 – 824.

[4] X. Py, A. Guillot, B. Cagnon. *Activated carbon porosity tailoring by cyclic sorption/decomposition of molecular oxygen*. Carbon 2003; 41(8): 1533 – 1543.

[5] J.B. Donnet. *Structure and reactivity of carbons: From carbon black to carbon composites*. Carbon 1982; 20(4): 267 – 282.

[6] J. Van Doorn, M.A. Vuurman, P.J.J. Tromp, D.J. Stufkens, J.A. Moulijn. *Correlation between Raman spectroscopic data and the temperature-programmed oxidation reactivity of coals and carbons*. Fuel Process. Technol. 1990; 24: 407 – 413.

[7] P.H. Matter, L. Zhang, U.S. Ozkan. *The role of nanostructure in nitrogen-containing carbon catalysts for the oxygen reduction reaction*. J. Catal. 2006; 239 (1): 83 – 96.

[8] J.F. González, J.M. Encinar, C.M. González-García, E. Sabio, A. Ramiro, J.L. Canito. *Preparation of activated carbons from used tires by gasification with steam and carbon dioxide*. Appl. Surf. Sci. 2006; 252(17): 5999 – 6004.

[9] A.M. Cunliffe, P.T. Williams. *Influence of process conditions on the rate of activation of chars derived from pyrolysis of used tires*. Energy Fuels 1999; 13(1): 166 – 175.

[10] S. Ogasawara, M. Kuroda, N. Wakao. *Preparation of activated carbon by thermal-decomposition of used automotive tyres*. Ind. Eng. Chem. Res. 1987; 26(12): 2552 – 2556.

[11] A.A. Merchant, M.A. Petrich. *Preparation and characterization of activated carbons from scrap tires, almond shells and Illinois coal*. Chem. Eng. Commun 1992; 118: 251 – 263.

[12] A.A. Merchant, M.A. Petrich. *Pyrolysis of scrap tires and conversion of chars to activate carbon*. AIChE J. 1993; 39(8): 1370 – 1376.

[13] P. Ariyadejwanich, W. Tanthapanichakoon, K. Nakagana, S.R. Mukai, H. Tamon. *Preparation and characterization of mesoporous activated carbon from waste tires*. Carbon 2003; 41(1): 157 – 164.

[14] J.L. Allen, J.L. Gatz, P.C. Eklund. *Applications for activated carbons from used tires: Butane working capacity*. Carbon 1999; 37(9): 1485 – 1489.

[15] G. San Miguel, G.D. Fowler, M. Dall'Orso, C.J. Sollars. *Porosity and surface characteristics of activated carbons produced from waste tyre rubber*. J. Chem. Technol. Biotechnol. 2002; 77(1): 1 – 8.

[16] G. San Miguel, G.D. Fowler, C.J. Sollars. *Adsorption of organic compounds from solution by activated carbons produced from waste tyre rubber*. Sep. Sci. Technol. 2002; 37(3): 663 – 676.

[17] A.A. Zabaniotou, G. Stavropoulos. *Pyrolysis of used automobile tires and residual char utilization*. J. Anal. Appl. Pyrolysis 2003; 70(2): 711 – 722.

[18] G. San Miguel, G.D. Fowler, C.J. Sollars. *A study of the characteristics of activated carbons produced by steam and carbon dioxide activation of waste tyre rubber*. Carbon 2003; 41(5): 1009 – 1016.

[19] H.S. Teng, M.A. Serio, M.A. Wojtowicz, R. Bassilakis, P.R. Solomon. *Reprocessing of used tires into activated carbon and other products*. Ind. Eng. Chem. Res. 1995; 34(9): 3102 – 3111.

[20] C.I. Sainz-Díaz, A.J. Griffiths. *Activated carbon from solid wastes using a pilot-scale batch flaming pyrolyser*. Fuel 2000; 79(15): 1863 -1871.

[21] R. Murillo, M.V. Navarro, T. García, J.M. López, M.S. Callen, E. Ayllon. *Production and application of activated carbons made from waste tire*. Ind. Eng. Chem. Res. 2005; 44(18): 7228 – 7233.

[22] A.A. Zabaniotou, G. Stavropoulos. *Active carbon production from used tire in two-stage procedure: industrial pyrolysis and bench scale activation with H_2O-CO_2 mixture*. J. Anal. Appl. Pyrolysis 2004; 72(2): 289 – 297.

[23] W. Tanthapanichakoon, P. Ariyadejwanich, P. Japthong, K. Nakagawa, S.R. Mukai. *Adsorption-desorption characteristics of phenol and reactive dyes from aqueous solution on mesoporous activated carbon prepared from waste tires*. Water Res. 2005; 39(7): 1347 – 1353.

[24] E. Manchón-Vizuete, A. Macías-García, A. Nadal-Gisbert, C. Fernández-González, V. Gómez-Serrano. *Preparation of mesoporous and macroporous materials from rubber of tyre wastes*. Microporous Mesoporous Mater. 2004; 67(1): 35 – 41.

Capítulo 5 / Chapter 5

Activación de char de Semillas de Uva con Aire

Activation of Grape Seeds char with Air

5.1. Resumen / Abstract

Los métodos de activación basados en ciclos de oxidación-desorción destacan por su capacidad para proporcionar un desarrollo controlado de la porosidad, requiriendo valores bajos de *burn-off*. Esta característica permite la utilización de agentes de activación baratos, pero de alta reactividad, como el oxígeno o el aire. En este capítulo se estudia la influencia de las temperaturas de oxidación y desorción y el número de ciclos sobre el desarrollo de porosidad en *char* de semillas de uva. Durante los dos primeros ciclos se observó un aumento importante de la S_{BET}, que se hizo menos acusado en los siguientes ciclos, aunque dicha superficie continuó aumentando. Con respecto a la S_{DA}, se observa un aumento menor a lo largo de los ciclos. El proceso de activación conduce al desarrollo tanto de micro como de mesoporosidad. Los valores más altos de *burn-off*, S_{BET} y S_{DA} se obtuvieron por la combinación de las temperaturas de oxidación y desorción más altas (275-850 ºC y 275-950 ºC). También se observó que la porosidad se desarrolla principalmente en la etapa de desorción. La caracterización morfológica mostró que el carbón activado obtenido mantiene la forma granular de las semillas incluso después de 10 ciclos de activación mostrando la misma estructura hueca que el *char* de partida pero con grietas más largas y profundas en la superficie exterior. Los carbones activados obtenidos muestran buena resistencia mecánica durante los test de atrición.

5.2. Materials and Methods

The grape seeds char used as starting material was obtained by flash pyrolysis of the extracted seeds at 800 ºC for 2 h under nitrogen atmosphere, according to the results of Chapter 3 [1].

5.2.1. Samples characterization

Prior to the study of activation cycles, isothermal and non isothermal thermogravimetric analyses of the char were carried out in order to establish the temperature ranges for the oxidation and desorption steps of the activation cycle. The gas flow (N_2) was 100 $NmLmin^{-1}$, whereas the heating rate was 10 $ºCmin^{-1}$. In the isothermal oxidation the nitrogen flow was maintained during heating until the working temperature was achieved. The effect of temperature in oxidation and desorption was also studied by TPD, where the samples were heated from 100 to 900 ºC at a rate of 10 $ºCmin^{-1}$ under a nitrogen flow of 100 $NmLmin^{-1}$.

Surface area and total pore volume of the samples were obtained by adsorption of N_2 at 77 K, and CO_2 at 273 K. The surface area was calculated from the N_2 isotherm BET equation and the t-method was used for the micropore volume, the mesopore volume and average mesopore diameter was obtained by BJH method. Whereas DA model was applied to the CO_2 isotherms to determine the S_{DA} and micropore volume. The macropore volume was obtained by mercury intrusion porosimetry. The Non-Local Density Functional Theory was used to calculate the pore size distribution.

The morphology of grape seeds char and activated carbons was analyzed by Scanning Electron Microscopy.

The activated carbon obtained was subjected to attrition test on a sifter to study the mechanical strength.

5.2.2. Cyclic activation conditions

The activation process was carried out in the furnace with automatic control described in Chapter 2. The oxidation step of each cycle was tested at three different temperatures (200, 250 and 275 ºC) for 2 h under a 100 $NmLmin^{-1}$ air flow. The desorption step was carried out at four different temperatures (500, 675, 850 and 950 ºC) using a flow rate of 100 $NmLmin^{-1}$ of nitrogen and 2 h of desorption time. The switch from oxidation to desorption was carried out at a heating rate of 10 $ºCmin^{-1}$ under nitrogen flow in all cases. The number of cycles applied (1 to 10) was also evaluated.

The activated carbons were designated by the letter “A” (from air), oxidation temperature, desorption temperature and the number of cycles used, e.g. for the activated carbon A200-500 C2, the sample was activated with air at 200 ºC of oxidation temperature with desorption temperature of 500 ºC and two activation cycles were performed.

5.3. Results

5.3.1. Activation conditions

The purpose of the oxidation step in this cyclic activation approach is the uptake of oxygen that can then be released combined with carbon in the subsequent desorption stage, thus leading to porosity development. The study of the oxidation step addressed to maximize the oxygen uptake, which would result, as a general trend, in higher burn-off and porosity development per cycle [2].

Isothermal TGA runs with char were carried out in nitrogen and air between 140 and 300 ºC until constant weight. The yield in inert atmosphere decreased as temperature increased due to the loss of volatile compounds remaining in the char after pyrolysis as well as adsorbed moisture. In the

TGA runs in air, this devolatilization takes place together with oxygen oxidation and further desorption of oxygen species. The net result observed was also a decrease of yield at increasing temperature, although the yield values were higher than in the case of TGA in nitrogen atmosphere due to oxygen uptake. Net oxygen uptake (NOU) was evaluated subtracting the TGA yield in inert atmosphere from that in air experiments (Figure 5.1). Beyond 200 ºC the NOU did not increase significantly due to partial evolution of uptaken oxygen. Working temperatures within the 200 – 300 ºC range maximized oxygen uptake, leading to weight gains around 2 % referred to the initial char weight (dry basis). So the temperature range between 200 and 300 ºC was identified as the most favorable for carrying out oxidation. Likewise, the isothermal TGA experiments carried out in air atmosphere showed that after 120 minutes the oxidation is completed and no further change in weight takes place, therefore this oxidation time was selected for the activation study.

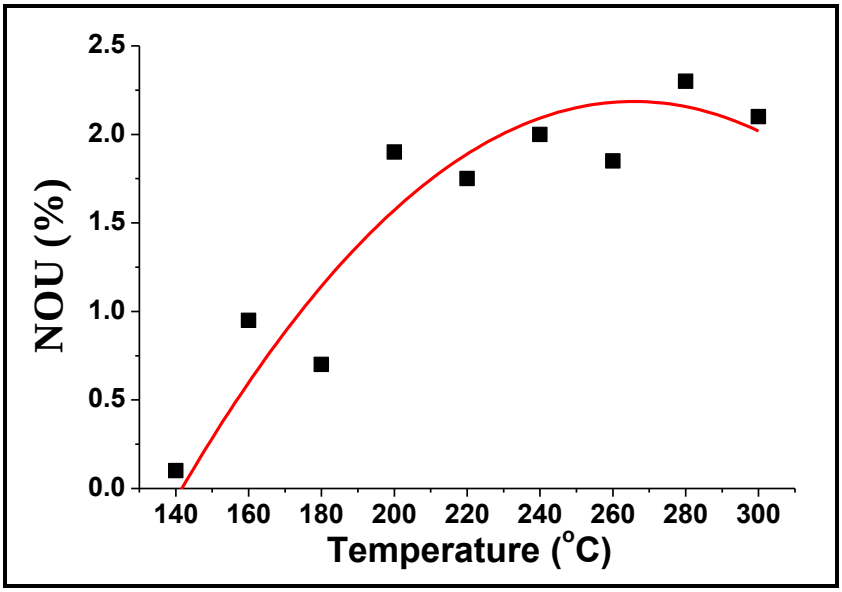

Figure 5.1. Net oxygen uptake at different oxidation temperatures (%w, dry initial char basis).

Although the whole range of oxidation temperature between 200 and 300 ºC seems convenient from the point of view of net oxygen uptake, different oxygen species may be generated at different oxidation temperatures. TPD was carried out to analyze the evolution of oxygen species generated at oxidation temperatures of 200 and 250 ºC. Though the amount of oxygen incorporated at both temperatures is similar, the corresponding TPD curves (Figure 5.2) suggest a different nature of the surface oxygen groups generated upon oxygen oxidation. Oxidation at 250 ºC leads to a TPD profile were the peak around that temperature is missing, indicating a lower presence of carboxylic acid groups. On the contrary, for an oxidation temperature of 250 ºC the contribution of groups that evolve upon TPD within the 600 – 700 ºC range is higher.

The TPD profiles also provide relevant information about the desorption step of the activation cycles. As can be seen in Figure 5.2, the oxygen adsorbed within the 200 – 250 ºC range has a high stability upon heating. At 500 ºC only 30 – 40 % of the CO_2-evolving groups are desorbed, that evolution being assessed mainly to carboxylic acid and carboxylic anhydride groups [3, 4].

Likewise, around 900 ºC, the desorption of CO_2 evolving groups is virtually completed, with a maximum in the TPD profile around 675 ºC, which can be attributed to phenol and lactones [3, 4]. The stability of the oxygen groups is higher for the species that evolve as CO. In this case the amount evolved peaks at 800 ºC, probably due to the decomposition of carbonyl and quinone groups.

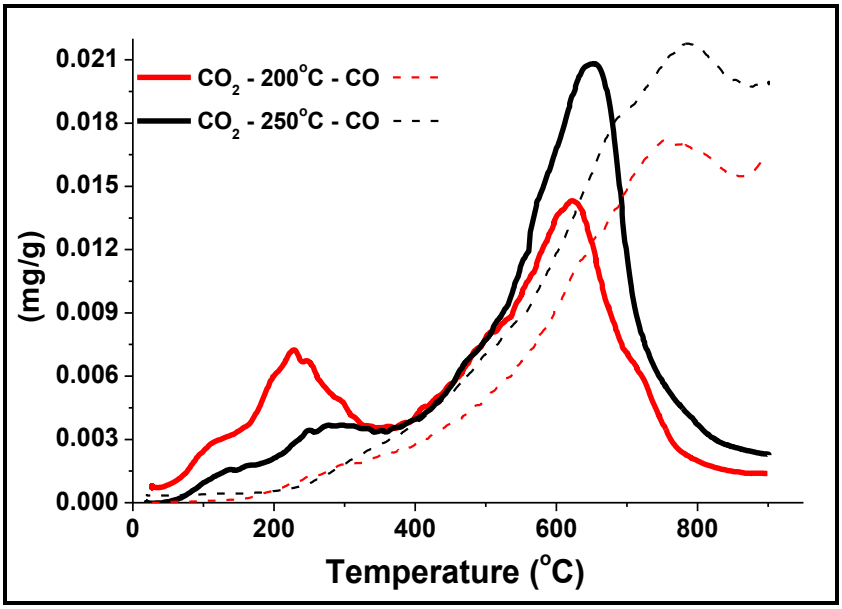

Figure 5.2. TPD profiles after oxygen oxidation at 200 and 250 ºC.

Taking into account the patterns in the TPD profiles indicated above, temperatures of 200, 250 and 275 ºC were selected for the oxidation step and 500, 675, 850 and 950 ºC for the desorption step of the activation cycles. From the TGA experiments a desorption time of 2 h was selected.

5.3.2. Burn-off

Under all the combinations of oxidation and desorption temperatures studied, the burn-off increased almost linearly with the number of activation cycles (Figure 5.3). As a general trend, BO increased with oxidation and desorption temperature, thus the highest burn-off was observed for the series prepared at a oxidation temperature of 275 ºC with a desorption temperature of 950 ºC.

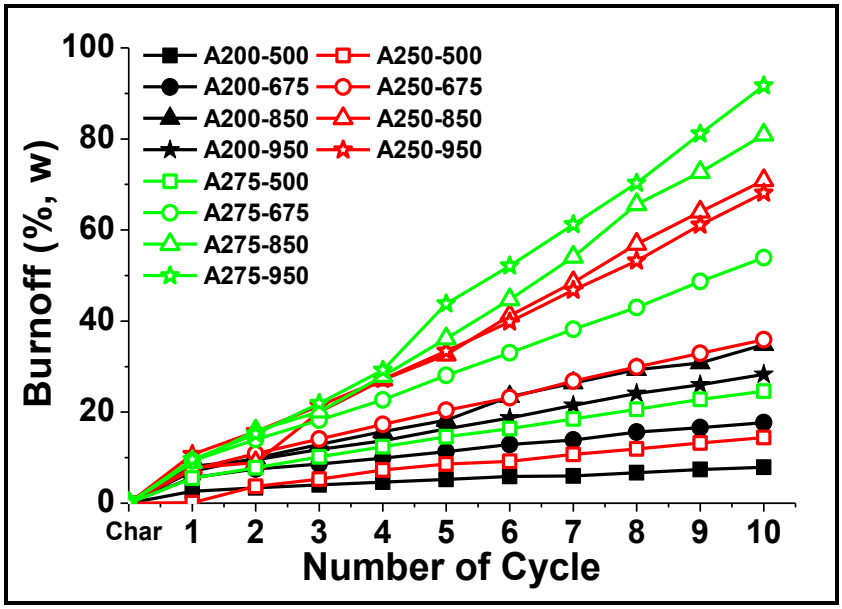

Figure 5.3. Burn-off vs number of activation cycles at different activation conditions.

5.3.3. Specific surface area

The starting char used in this work was mainly microporous with a S_{BET} of 47 m^2g^{-1} and a S_{DA} of 505 m^2g^{-1} [1]. Due to the narrow nature of the microporosity of the char, the porosity of the resulting activated carbons was analyzed by both the BET and DA methods.

The development of surface area with the number of cycles performed is depicted in Figure 5.4. For most of the samples an important development of porosity in terms of S_{BET} was observed in the first cycle, in all cases due to the widening of previously existing narrow micropores, since the S_{DA} values hardly increased, even decreased, after the first cycle. A monotonical increase of surface area was in general observed throughout the following cycles, which was more significant when combining the highest oxidation and desorption temperatures. This is consistent with the higher burn-off values

achieved (see Figure 5.3). As a general trend, the S_{DA} values are higher than the S_{BET} ones upon the successive cycles indicating that the development of porosity proceeds through the creation of new micropores in addition to the widening of existing ones.

The highest development of surface area corresponds to an oxidation temperature of 275 ºC combined with a desorption temperature of 950 ºC (1339 m^2g^{-1}, sample A275-950 C8). It can also be observed that under those conditions the development of porosity is very low in the last cycles and even a decrease of surface area occurs. This observation may be interpreted in terms of the collapse of pores taking place at high burn-off (c.a. 70 %), as it has been reported for the physical activation of other carbonaceous materials [5]. Likewise, Polyakov et al. [6] suggested that thermal stress induced a collapse of the microporous structure leading to the formation of mainly mesopores.

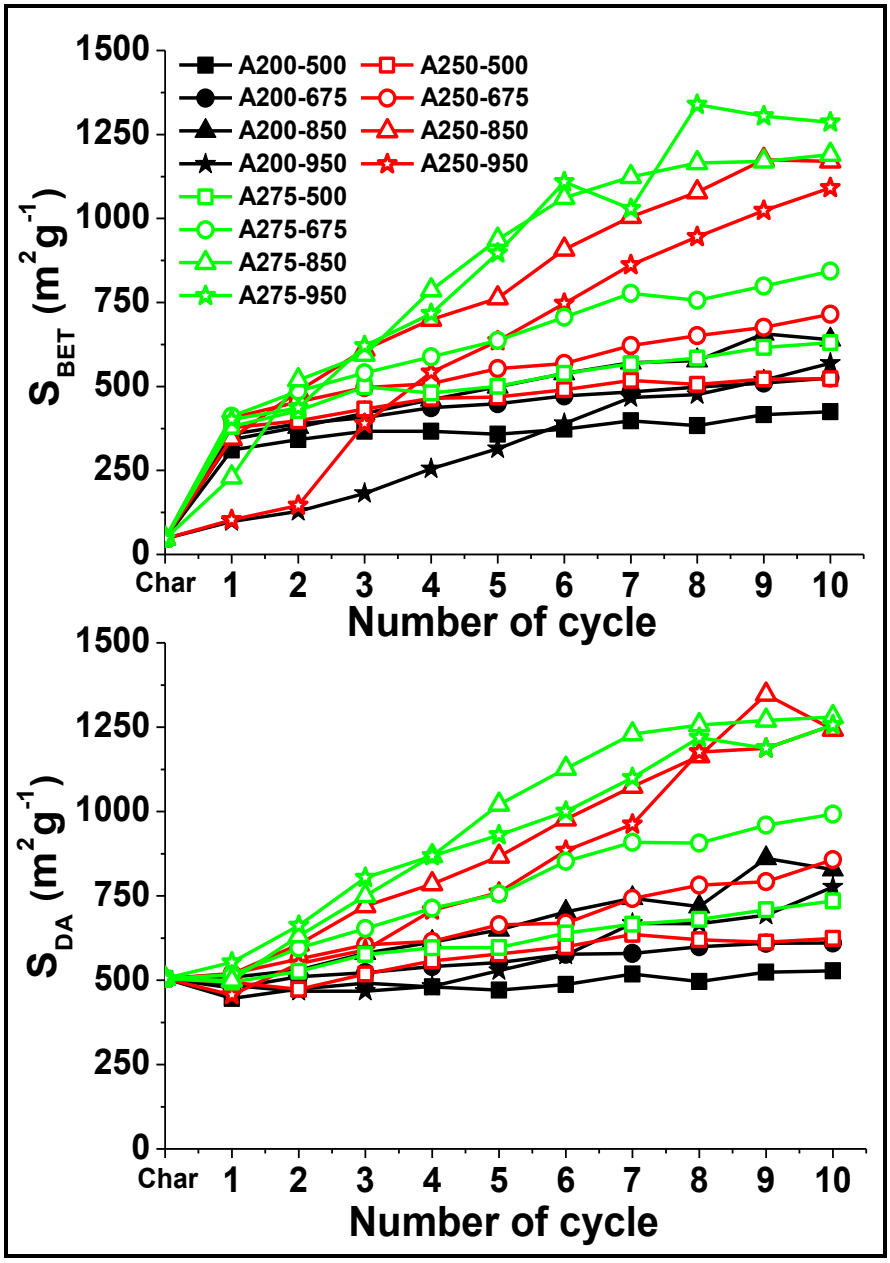

Figure 5.4. S_{BET} and S_{DA} vs number of cycles for 10-cycle test at different conditions.

Figure 5.5 shows that the BET surface area generated per burn-off, is quite different depending on the activation conditions, particularly in the first activation cycles. Thus, activated carbons with values of S_{BET} between 600 and 750 m^2g^{-1} can be obtained at burn-off between 25 and 35 %, depending on the activation conditions. Due to the different burn-off per cycle, S_{BET} values of 750 m^2g^{-1} are achieved after 4 – 5 cycles for combinations of high oxidation and desorption temperatures whereas up to 10 cycles are needed for combinations of low oxidation and desorption temperatures.

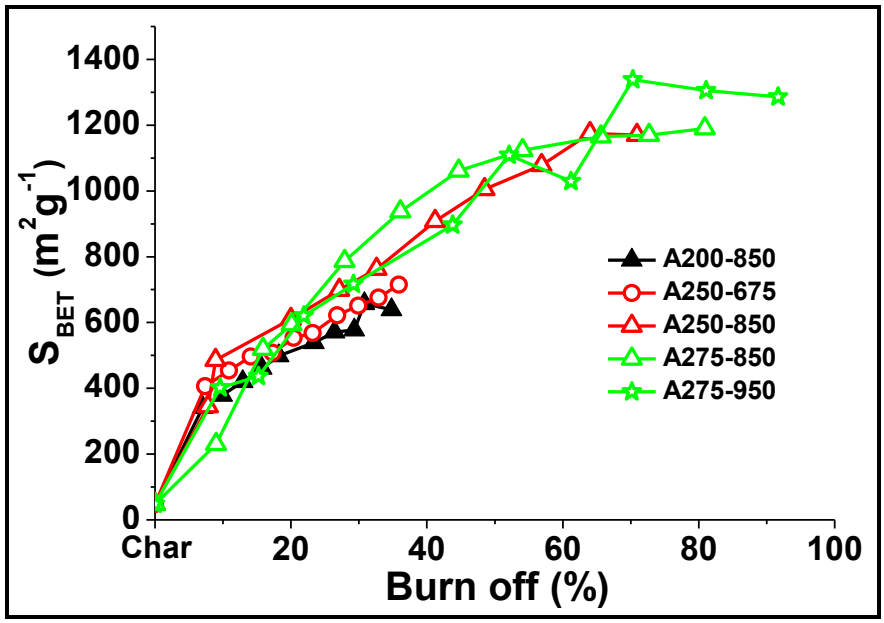

Figure 5.5. Variation of S_{BET} versus burn-off.

Figure 5.6 shows the development of S_{BET} per unit of burn-off along the 10-cycles test (a) and versus S_{BET} (b). It can be seen that the most important factor in that respect is the oxidation temperature. Thus, at low oxidation temperatures burn-off leads to a higher generation of porosity per unit of surface area. The differences with the results for higher oxidation temperatures become smaller as the number of cycles and the surface area developed increase. The type of oxygen surface groups formed during the

oxidation at low temperature, with a higher contribution of carboxylic acids, may be responsible for the higher generation of porosity.

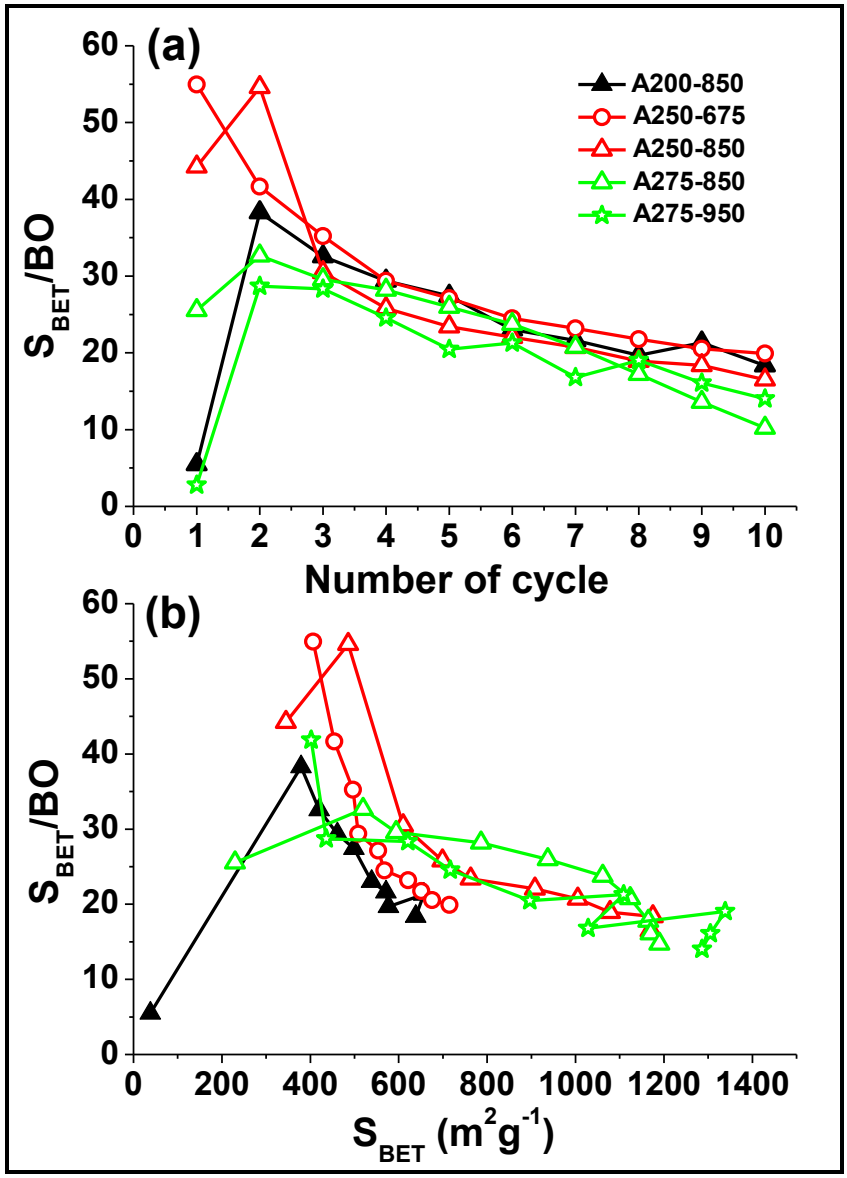

Figure 5.6. Variation of S_{BET} / burn-off versus number of cycles (a) and S_{BET} (b) at different activation conditions.

In an additional set of experiments the S_{BET} and S_{DA} were measured both after the oxidation and after the desorption step of each cycle for the A200-950 and the A275-950 series (Figure 5.7). The results confirm that the development of porosity takes place essentially in the desorption step of each cycle, whereas oxygen adsorption provokes in general no significant modification of surface area at the highest temperature tested (275 ºC), and even a considerable decrease at the lowest temperature (200 ºC), which can be associated to the location of oxygen at the pore mouths thus restricting the access of nitrogen in the S_{BET} determination. Such trend is not observed at an oxidation temperature of 275 ºC (series A275-950) due to earlier development of wider pores, as it was discussed above.

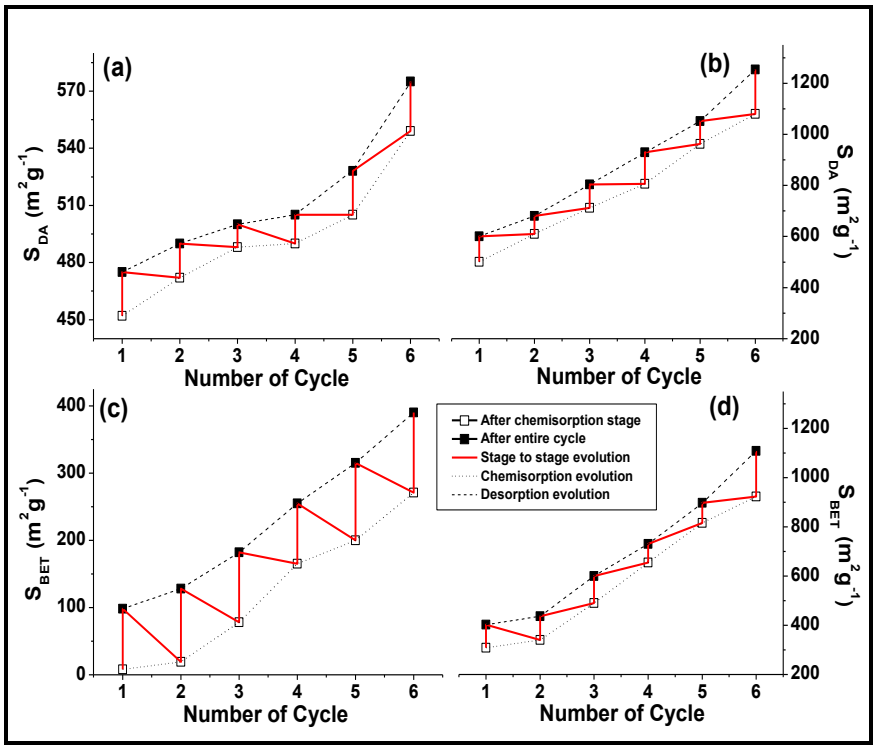

Figure 5.7. Evolution of S_{BET} and S_{DA} versus number of cycles after oxidation step and the entire cycle for the A200-950 (a and c) and A275-950 series (b and d).

5.3.4. Pore volume

The different response to the activation conditions is also of great interest for the preparation of activated carbons with different properties, as can be seen in Figure 5.8, where the evolution of micropore and mesopore volume along the cycles is shown. The resulting activated carbons are in all the cases essentially microporous solids with a fairly low contribution of mesopores that only for the samples obtained combining the highest oxidation and desorption temperatures has some significance, always modest. The development of mesopores is only significant after 2 – 3 cycles, which is in agreement with a mesopore formation mechanism based on the widening of previously created micropores [7]. Thus, mesoporosity development was observed once the activated carbons achieved a micropore volume of around 0.25 cm^3g^{-1}. After 10 activation cycles the samples of higher porosity ($V_{microN2}$: 0.57 cm^3g^{-1}) showed a total mesopore volume close to 0.1 cm^3g^{-1}.

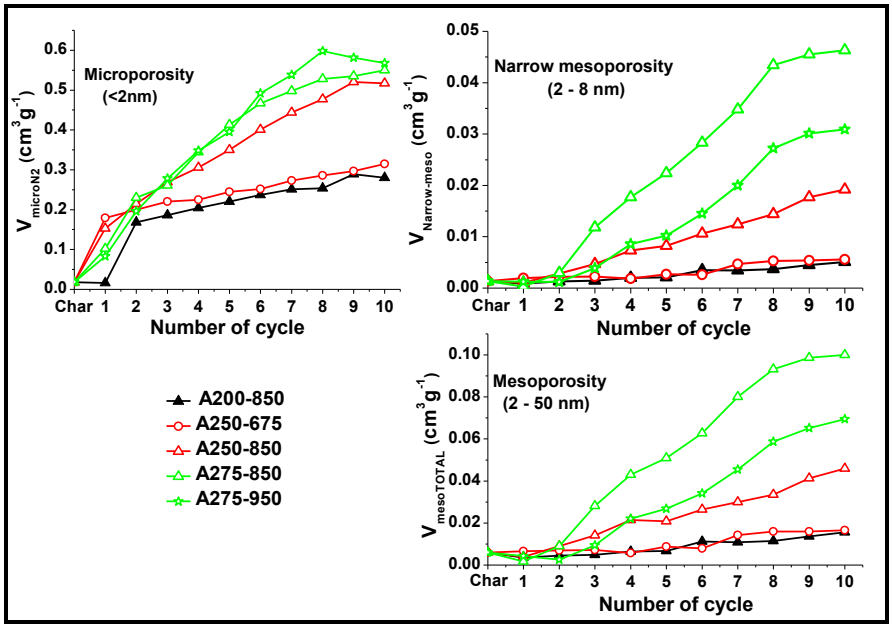

Figure 5.8. Pore volume development from N_2 isotherms along the cycles at different activation conditions.

Figure 5.9 shows the macropore volume determined by mercury intrusion porosimetry for all the activated carbon series after 10 activation cycles. As a general trend, the generation of macroporosity increases with both oxidation and desorption temperature (Figure 5.9a). The macropore volume generated correlates well with burn-off, showing little influence of the activation conditions (Figure 5.9b). Thus, whereas activation conditions are important for both the type and amount of pores generated in the micro and mesopore range, they do not seem to have noticeable influence on the pore distribution within the macropore range.

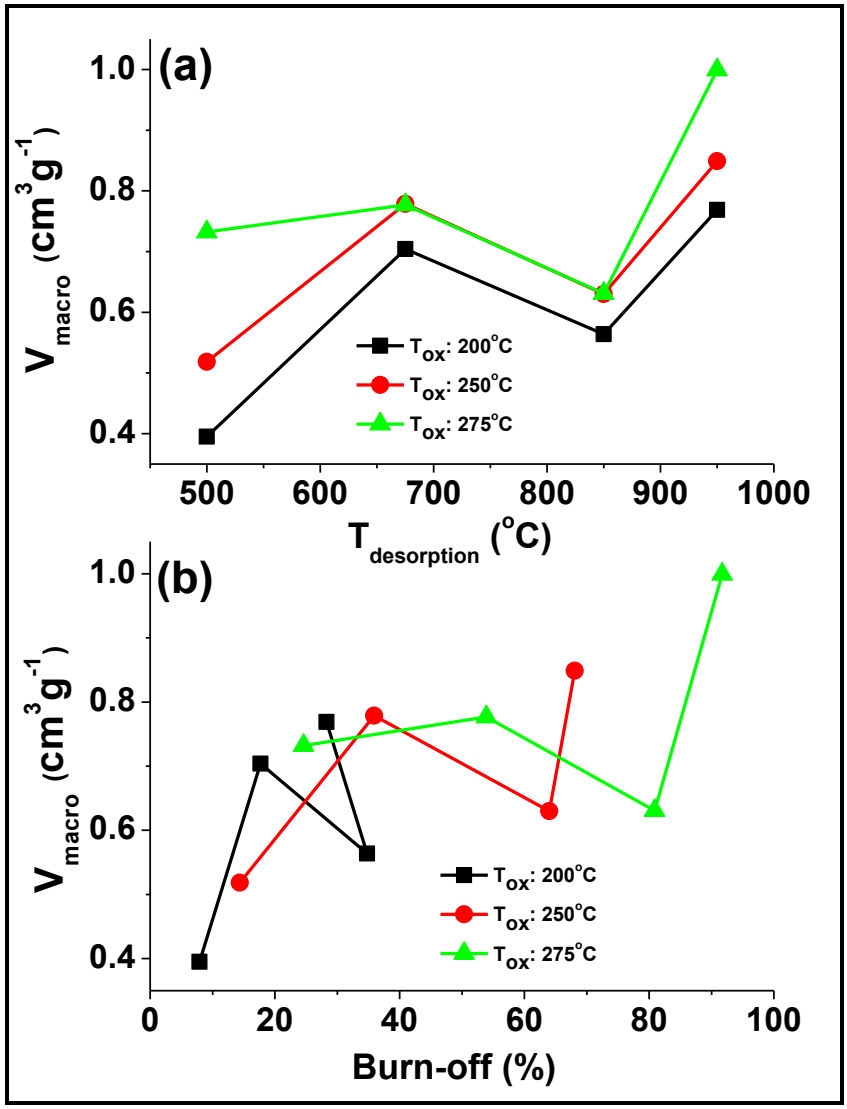

Figure 5.9. Macropore volume (4 μm > d > 0.05 μm) for the activation carbons samples after 10 activation cycles versus desorption temperature (a) and burn-off (b).

5.3.5. Pore size distribution

The pore size distribution is a key element in the characterization of porous carbons and a number of methods have been developed for the PSD analysis, the Non-Local Density Functional Theory being widely used for the characterization of the pore structure of activated carbons and other porous materials. However, global parameters such as the mean pore size are also commonly used to evaluate the type of porosity. Figures 5.10a and 5.10b shows that the mean micropore diameter increased with the number of cycles and with the burn-off, which is in agreement with the aforementioned widening of existing pores, the mean micropore diameter being higher for combinations of high oxidation and desorption temperatures. On the opposite, the mean diameter of mesopores (Figures 5.10c and 5.10d) decreases along the reaction cycles up to the lowest range from burn-off of about 30 %. The effect of operating conditions on the d_{meso} is almost negligible. The decrease of d_{meso} can be interpreted in terms of the creation of narrow mesopores as a result of micropores widening. Thus, the mean mesopore diameter remains higher for the activation conditions identified as less favorable for the development of mesoporosity (Figure 5.7), i.e. low oxidation and desorption temperatures.

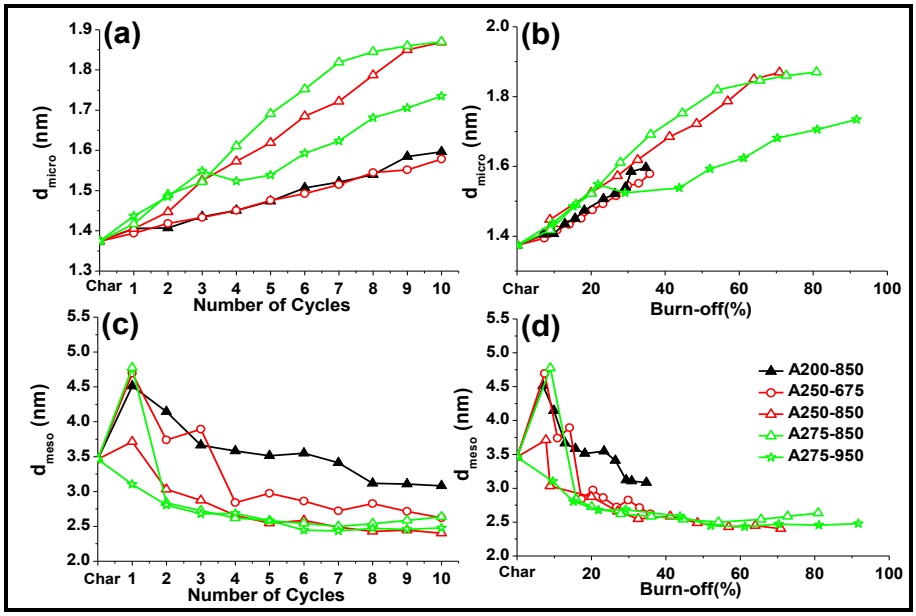

Figure 5.10. (a) and (b) mean micropore diameter versus number of cycles and burn-off. (c) and (d) mean mesopore diameter versus number of cycles and burn-off.

In order to have a deeper knowledge on the generation of porosity, the micropore size distribution was calculated from CO_2 isotherms and the mesopore size distribution from N_2 isotherms by the NLDFT method for five activated carbons prepared in different conditions but all of them with S_{BET} around 700 – 800 m^2g^{-1} and burn-off around 40 % (Figure 5.11). As can be observed, the microporosity pattern is quite similar for all the samples, with a fairly homogeneous distribution characterized by three important contributions centered at 0.45, 0.55 and 0.88 nm in all cases, even for the char. However, regarding the pore distributions there are significant differences between the samples prepared upon 4 activation cycles at more severe conditions and the samples prepared upon 8 – 9 cycles at milder conditions. Thus, the contribution of narrow mesoporosity is much lower for the 8 and 9 cycles samples, being essentially microporous materials and

good candidates for their application as molecular sieves and for electrochemical capacitors. For the 4-cycles a higher development of wide microporosity and narrow mesoporosity centered at 2.2 nm can be observed. Finally, no significant differences can be found in the pattern of mesoporosity within the 8 – 50 nm range, being this porosity probably already present in the starting char.

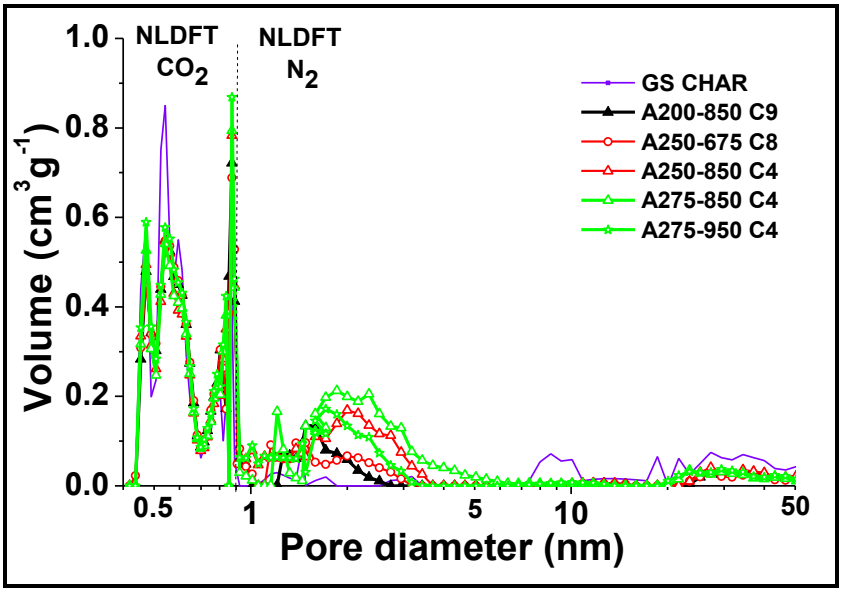

Figure 5.11. Pore size distribution by NLDFT method from CO_2 and N_2 isotherms for selected samples.

To provide a more complete sight on meso and macroporosity, pore size distribution of the activated carbons within the 0.01 μm to 4 μm range is depicted in Figure 5.12. As can be observed all the samples showed an equivalent pattern in the macropore range, being the pore volume in the mesopore range negligible in comparison with that of macropores.

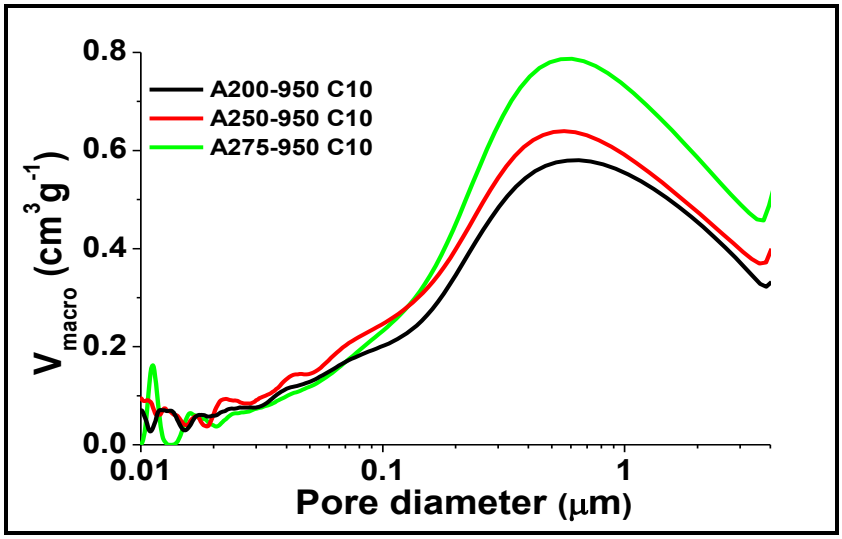

Figure 5.12. Macropore and mesopore size distribution for A200-950 C10, A250-950 C10 and A275-950 C10 samples.

5.3.6. Morphological analysis

The morphology of the activated carbons was evaluated by SEM, showing as the most relevant result that the granular morphology of the starting char is maintained along the activation cycles due to the controlled burn-off. Burn-off seems to take place preferentially at the outer layer of the particles, as can be inferred from the size reduction observed in Figure 5.13. Likewise, changes in the texture can be observed with a higher occurrence of large macropores, cracks and channels as the number of cycles is increased.

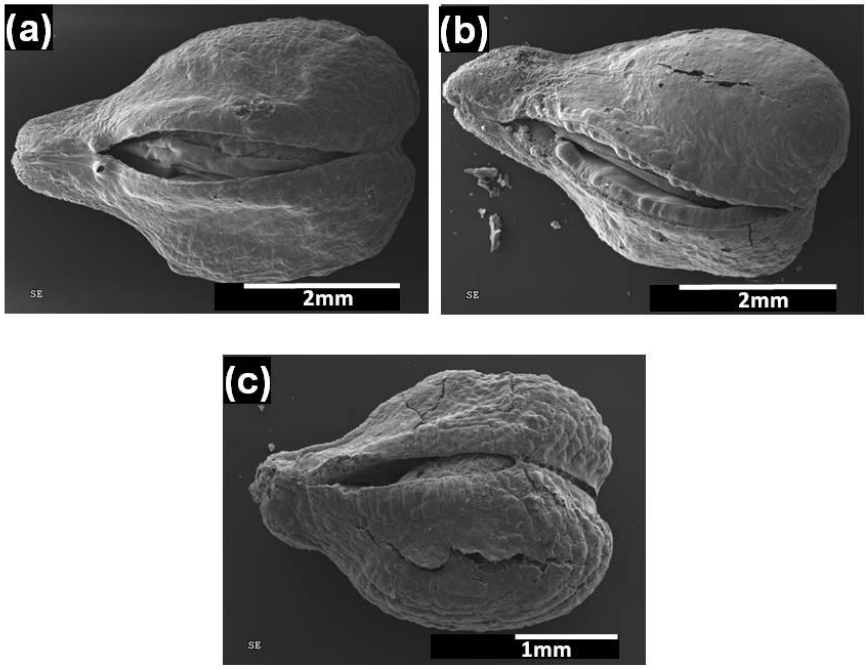

Figure 5.13. SEM micrographs of (a) Char from grape seed, (b) A275-850 C5 sample and (c) A275-850 C10 sample.

Figure 5.14 shows the SEM images of crushed particles showing the hollow core structure of the activated carbon particles resulting from the volatilization of the albumen and embryo during the pyrolysis stage. It can be observed that after 10 activation cycles both the outer layer and the carbonized tissue in the inner of the particle have been partially removed compared with the char SEM images (Figure 3.10). This indicates some homogeneity in the oxidation and burn-off resulting from the low temperature and long time of the oxidation stage. The activated carbon obtained has most of the carbonaceous material allocated in a shell thickness of around 250 μm, which is of great interest since the granular material prepared can combine easy handling and low pressure loss for packed bed applications with convenient mass transfer due to short diffusion path.

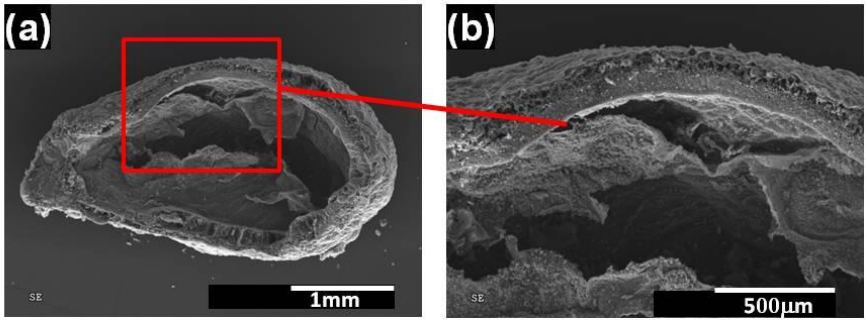

Figure 5.14. SEM micrographs of (a) Cross section of A275-850 C10 sample. (b) Detail of wall from A275-850 C10 sample.

5.3.7. Attrition tests

To study the pore structure of the different layers of the activated carbon particles A200-950 C4 and A275-950 C4 samples were subjected to attrition in a vibrating sifter. These samples are representative of the different materials that can be obtained by the use of different activation conditions. The samples also have a suitable balance between surface area and burn-off, so that the integrity and strength of the particles can be preserved. During the attrition tests five fractions of the powder passing through the sieve openings (<1 mm) were collected at regular intervals of 2 h. The results in Table 5.1 show a rather homogeneous development of surface area throughout the particle wall. The most noticeable differences can be found for S_{BET}, thus for the two samples studied the inner layers showed significantly lower values of S_{BET}, suggesting the preferential generation of narrow porosity in the outer layers. In the case of microporosity (S_{DA}) also preferential development of porosity is observed at the outer layers, the differences being higher for A275-950 C4.

It is also remarkable that the activated carbon particles have a good resistance to attrition, since only 2.2 % of the initial mass was lost in the first 2 h of the test. The strength of the particles is of great importance for the

sake of handling and performance in potential applications. The strength of the outer layers seems to be homogeneous according to the similar loss of mass upon 2 h shaking.

Table 5.1. Micropore and mesopore surface area and mass-loss of A200-950 C4 and A275-950 C4 samples.

SAMPLE	S_{BET} (m^2g^{-1})	S_{DA} (m^2g^{-1})	Mass loss (%)
A200-950 C4	255	482	
Fraction 1	169	567	2.2
Fraction 2	208	610	2.2
Fraction 3	227	636	1.8
Fraction 4	207	580	2.2
Fraction 5	188	557	2.2
Final Sample	84	475	
A275-950 C4	717	868	
Fraction 1	543	845	3.0
Fraction 2	560	750	3.0
Fraction 3	655	858	2.6
Fraction 4	646	812	2.5
Fraction 5	597	783	2.5
Final Sample	429	599	

5.3.8. Comparison with results in literature

In Figure 5.15 the results of S_{BET} vs burn-off are compared with the reported by other authors from physical activation of other agricultural by-products like apricot stones [8], cherry stones [8], olive stones [9], pecan shells [10], coconut shells [5] and other biomass residues, activated with steam [8, 9, 11 – 15] and CO_2 [5, 9, 15 – 20]. It can be observed that the BET surface area values obtained by activation cycles of oxidation−desorption with air of grape seeds covers the usual range of porosity for activated biomass materials, and that such porosity development can be achieved at burn-off values below the average results. Thus, cyclic activation by oxidation-desorption allows overcoming the drawback of low development of porosity characteristic of oxygen when used in conventional activation.

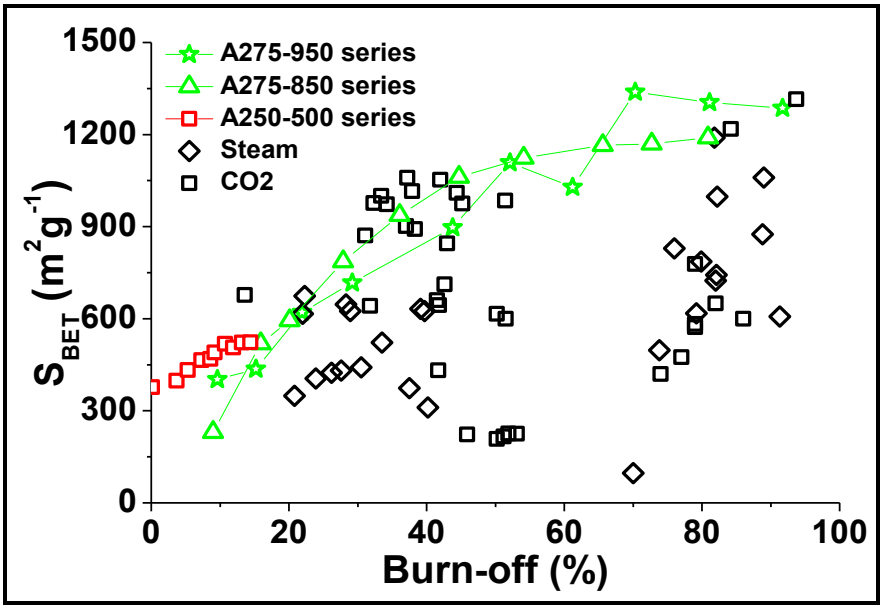

Figure 5.15. Comparison of S_{BET} vs Burn-off from oxygen cyclic activation of grape seeds char with literature results on the activation of biomass residues [5, 8 – 20].

References

[1] D. Jiménez-Cordero, F. Heras, N. Alonso-Morales, M.A. Gilarranz, J.J. Rodríguez. *Porous structure and morphology of granular chars from flash and conventional pyrolysis of grape seeds*. Biomass Bioenergy 2013; 54: 123 – 132.

[2] F. Heras, N. Alonso-Morales, M.A. Gilarranz, J.J. Rodríguez. *Activation of waste tire char upon cyclic oxygen oxidation-desorption*. Ind. Eng. Chem. Res. 2009; 48(10): 4664 – 4670.

[3] J.L. Figueiredo, M.F.R. Pereira. *The role of surface chemistry in catalysis with carbons*. Catal. Today 2010; 150(1 – 2): 2 – 7.

[4] S.A.C. Carabineiro, T. Thavorn-amornsri, M.F.R. Pereira, P. Serp, J.L. Figueiredo. *Comparison between activated carbon, carbon xerogel and carbon nanotube for the adsorption of the antibiotic cicrofloxacin*. Catal. Today 2012; 186(1): 29 – 34.

[5] S. Guo, J. Peng, W. Li et al. *Effects of CO_2 activation on porous structures of coconut shell-based activated carbons*. Appl. Surf. Sci. 2009; 255(20): 8443 – 8449.

[6] M. Polyakov, M. Poisot, W.E. Maurits, T. Drescher, A. Lotnik, L. Kienle, W. Bensch, M. Muhler, W. Grunert. *Carbon-stabilized mesoporous MoS2 - Structural and surface characterization with spectroscopic and catalytic tools*. Catal. Commun. 2010; 12(3): 231 – 237.

[7] R. Mysyk, Q. Gao, E. Raymundo-Piñero, F. Béguin. *Microporous carbons finely-tuned by cyclic high pressure low-temperature oxidation and their use in electrochemical capacitors*. Carbon 2012; 50(9): 3367 – 3374.

[8] D. Savova, E. Apak, E. Ekinci, F. Yardim, N. Petrov, T. Budinova, M. Razvigorova, V. Minkova. *Biomass conversion to carbon adsorbents and gas*. Biomass Bioenergy 2001; 21(2): 133 – 142.

[9] A.H. El-Sheikh, A.P. Newman, H.K. Al-Daffaee, S. Phull, N. Cresswell. *Characterization of activated carbon prepared from a single cultivar of Jordanian Olive stones by chemical and physicochemical techniques*. J. Anal. Appl. Pyrolysis 2004; 71(1): 151 – 164.

[10] M. Admedna, W.E. Marshall, R.M. Rao. *Production of granular activated carbons from select agricultural by-products and devaluation of their physical, chemical and adsorption properties*. Bioresour. Technol. 2000; 71(2): 113 – 123.

[11] B.S. Girgis, S.S. Yunis, A.M. Soliman. *Characteristics of activated carbon from peanut hulls in relation to conditions of preparation*. Mater. Lett. 2002; 57(1): 164 – 172.

[12] M. Fan, W. Marshall, D. Daugaard, R.C. Brown. *Steam activation of chars produced from oat hulls and corn stover*. Bioresour. Technol. 2004; 93(1): 103 – 107.

[13] A-NA. El-Hendawy, S.E. Samra, B.S. Girgis. *Adsorption characteristics of activated carbons obtained from corncobs*. Colloids Surf A Physicochem. Eng. Asp. 2001; 180(3): 209 – 221.

[14] M. Ahmedna , W.E. Marshall, A.A. Husseiny, R.M. Rao, I. Goktepe. *The use of nutshell carbons in drinking water filters for removal of trace metals*. Water Res. 2004; 38(4): 1062 – 1068.

[15] L.H. Wartelle, W.E. Marshall, C.A. Toles, M.M. Johns. *Comparison of nutshell granular activated carbons to commercial adsorbents for the purge-and-trap gas chromatographic analysis of volatile organic compounds*. J. Chromatogr. A 2000; 879(2): 169 – 175.

[16] A.C. Lua, T. Yang, J. Guo. *Effects of pyrolysis conditions on the properties of activated carbons prepared from pistachio-nut shells*. J. Anal. Appl. Pyrolysis 2004; 72(2) 279 – 287.

[17] A. Marcilla, S. García-García, M. Asensio, J.A. Conesa. *Influence of thermal treatment regime on the density and reactivity of activated carbons from almond shells*. Carbon 2000; 38(3) 429 – 440.

[18] E. Iniesta, F. Sánchez, A.N. García, A. Marcilla. *Influence of the holding temperature of the first heating step in a two-heating step carbonization process on the properties of chars and activated carbons from almond shells*. J. Anal. Appl. Pyrolysis 2001; 58 – 59: 967 – 981.

[19] T. Zhang, W.P. Walawender, L.T. Fan, M. Fan, D. Daugaard, R.C. Brown. *Preparation of activated carbon from forest and agricultural residues through CO_2 activation*. Chem. Eng. J. 2004; 105(1 – 2): 53 – 59.

[20] B.S. Girgis, A.M. Soliman, N.A. Fathy. *Development of micro-mesoporous carbons from several seed hulls under varying conditions of activation*. Microporous Mesoporous Mater. 2011; 142(2 – 3): 518 – 525.

Capítulo 6 / Chapter 6

Activación de char de Semillas de Uva con Ozono

Activation of Grape Seeds char with Ozone

6.1. Resumen / Abstract

En este capítulo, se ha utilizado también el método de activación por ciclos para activar *char* procedente de semillas de uva. En este caso la secuencia de activación ha consistido en una primera etapa de oxidación con ozono a baja temperatura seguida por otra etapa de desorción en atmósfera inerte a alta temperatura.

En el estudio se analiza la influencia de las condiciones de operación en el desarrollo de porosidad desde el *char* precursor (GS *Char*), que posee esencialmente una estructura microporosa, con S_{BET} de 47 m^2g^{-1} y una S_{DA} de 505 m^2g^{-1}, preparado por pirólisis flash a 800 ºC. Las variables estudiadas han sido la temperatura de oxidación (250 y 275 ºC), la temperatura de desorción (850 y 950 ºC) y el número de ciclos realizados (1 – 10).

El uso de temperaturas de oxidación elevadas da como resultado altos valores de *burn-off*, el cual aumenta de forma casi lineal con el número de ciclos de activación. El *burn-off* necesario para conseguir un alto desarrollo de superficie específica ha sido inferior al que habitualmente se requiere en la activación física convencional de materiales biomásicos de acuerdo con la bibliografía.

Después de 7 – 9 ciclos de activación se han obtenido carbones activados con valores de S_{BET} superiores a 1200 m^2g^{-1} y S_{DA} en torno a 1500 m^2g^{-1}. Todos los carbones activados preparados son altamente micro y macroporosos con una baja contribución de mesoporos. El diámetro medio de microporo (d_{micro}) va aumentando con el número de ciclos de activación debido al ensanchamiento de los poros ya existentes en la muestra, mientras que el diámetro medio de mesoporo (d_{meso}) disminuye a lo largo de los ciclos.

Las muestras con mayor desarrollo de porosidad ($V_{microN2}$ = 0.5cm^3g^{-1}) alcanzan un volumen de mesoporo de 0.07 cm^3g^{-1}. Este carbón activado también muestra una morfología granular singular con una estructura hueca

y una pared porosa, que se mantiene incluso después de 10 ciclos de activación.

6.2. Materials and Methods

The GS Char used as starting material was obtained by flash pyrolysis of the extracted seeds at 800 ºC for 2 h under nitrogen atmosphere, according to the results of Chapter 3 [1].

6.2.1. Samples characterization

Surface area and total pore volume of the samples were measured by 77 K N_2 adsorption/desorption and CO_2 adsorption at 273 K. The BET surface area of the samples was calculated from the N_2 isotherms using the BET equation, the t-method was used for the micropore volume and BJH method for mesopore mean size, whereas the DA model was applied to CO_2 isotherms to obtain the S_{DA} and micropore mean size. The mercury intrusion porosimetry was used to determine the macropore volume. The Non-Local Density Functional Theory was used to calculate the pore size distribution. Fourier transform infrared spectroscopy was used to characterize the main functional groups of the activated carbons surface.

The morphology of grape seeds char and activated carbons was evaluated by Scanning Electron Microscopy (SEM).

6.2.2. Cyclic activation conditions

The cyclic activation with ozone as activating agent was carried out in the furnace with manual control described in Chapter 2.

The activation conditions for the cycles were chosen according to the best results obtained in Chapter 5. The oxidation step of each cycle was carried out at 250 and 275 ºC for 2 h using a gas flow of ozone of 50 $mLmin^{-1}$ and the desorption step was performed at 850 and 950 ºC using a flow rate of 100 $mLmin^{-1}$ of nitrogen and 2 h of desorption time. The switch from oxidation to desorption steps was carried out at a heating rate of 10 $ºCmin^{-1}$ under nitrogen flow in all cases.

After each activation cycle the reactor was cooled under nitrogen flow and the activated carbon was recovered to estimate the burn-off (using the equation 2.1) and characterize the porous structure and surface composition.

The activated carbons were designated with the letter “O” from Ozone activation followed by the oxidation temperature, desorption temperature and the number of cycles applied, e.g. for the activated carbon O 250-850 C1, the sample was activated with ozone at 250 ºC of oxidation temperature and at 850 ºC of desorption temperature and one oxidation-desorption cycle was performed.

6.3. Results

The oxidation stage in cyclic activation results in oxygen uptake that can be released combined with carbon in the subsequent desorption stage, thus leading to porosity development. As a general trend, a higher oxygen uptake results in a higher burn-off and porosity development per cycle as reported for the activation with oxygen of grape seeds and waste tires chars (Chapters 4 and 5) [2].

6.3.2. Burn-off

Figure 6.1 shows that under all the combinations of oxidation and desorption temperatures tested, the burn-off increased almost linearly with the number of activation cycles. Average burn-off per cycle values between 4.9 and 7.6 % where achieved depending on the activation conditions. As a general trend, burn-off increased with oxidation temperature. The highest burn-off values were also obtained upon the combination of the highest oxidation temperature (275 ºC) and lowest desorption temperature (850 ºC) tested.

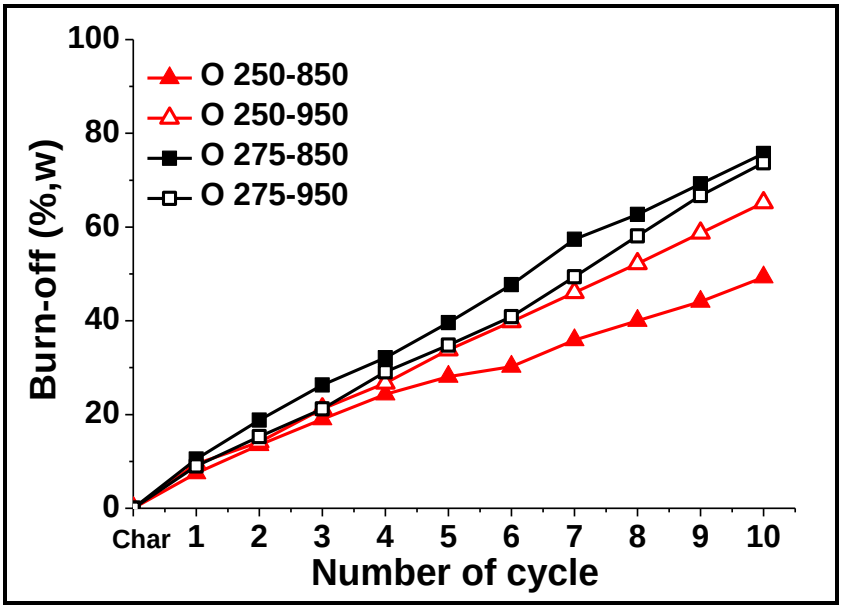

Figure 6.1. Burn-off vs number of activation cycles at different oxidation-desorption temperatures.

6.3.3. Specific surface area

The nitrogen adsorption isotherms of the starting char and the activated carbons resulting after five activation cycles are shown in Figure 6.2. The activated carbons yielded isotherms representative of essentially microporous solids with some small contribution of mesoporosity, these last increasing with burn-off as suggested by a more rounded knee and somewhat higher slope of the plateau-like region. The existence of slight hysteresis loops confirms a low development of mesopores.

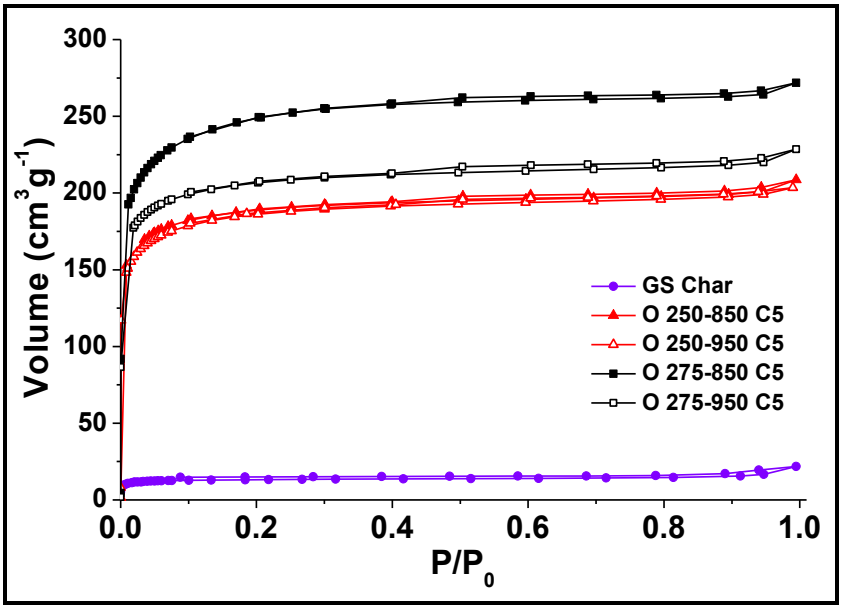

Figure 6.2. 77K N_2 adsorption-desorption isotherms of grape seed char and five-cycles activated carbons.

The starting char obtained from grape seeds used in this chapter was a mainly microporous solid with a S_{BET} of 47 m^2g^{-1} and a S_{DA} of 505 m^2g^{-1} (Chapter 3), with a narrow microporosity according to the difference between both surface areas [1].

Figure 6.3 depicts the development of surface area with the number of activation cycles for the four series of activated carbons evaluated. In general, a monotonical increase of S_{BET} (Figure 6.3a) was observed upon the successive cycles. For the series leading to the highest burn-off (O 275-850) a fairly important growth of BET surface area was observed in the first cycle, which can be explained by both widening of previously existing narrow micropores, but also as the creation of new ones since the S_{DA} also increased significantly in that first cycle (Figure 6.3b). On the opposite, the second activating cycle in that series produces essentially widening of narrow micropores since the increase of S_{BET} is accompanied by a decrease of S_{DA}.

That combination of an oxidation temperature of 275 ºC with a desorption temperature of 850 ºC led to the highest burn-off and also allowed to achieve the highest surface area, reaching maximum values of S_{BET} of 1209 m^2g^{-1} (9^{th} cycle) and 1524 m^2g^{-1} for S_{DA} (7^{th} cycle). The difference between both surface areas indicates that narrow micropores can still be found in the samples due to their creation upon the successive cycles. It can also be observed that for such activation conditions the development of porosity is significantly lower in the last cycles. This can likely be attributed to different effects of carbon ozonation: (i) widening of micropores and pore wall destruction as a result of gasification; (ii) partial blockage of micropores produced by surface oxygen groups fixed on the pore entrance [3, 4]. Polyakov et al. [5] also suggested that thermal stress induces a partial collapse of the microporous structure leading mainly to the formation of mesopores.

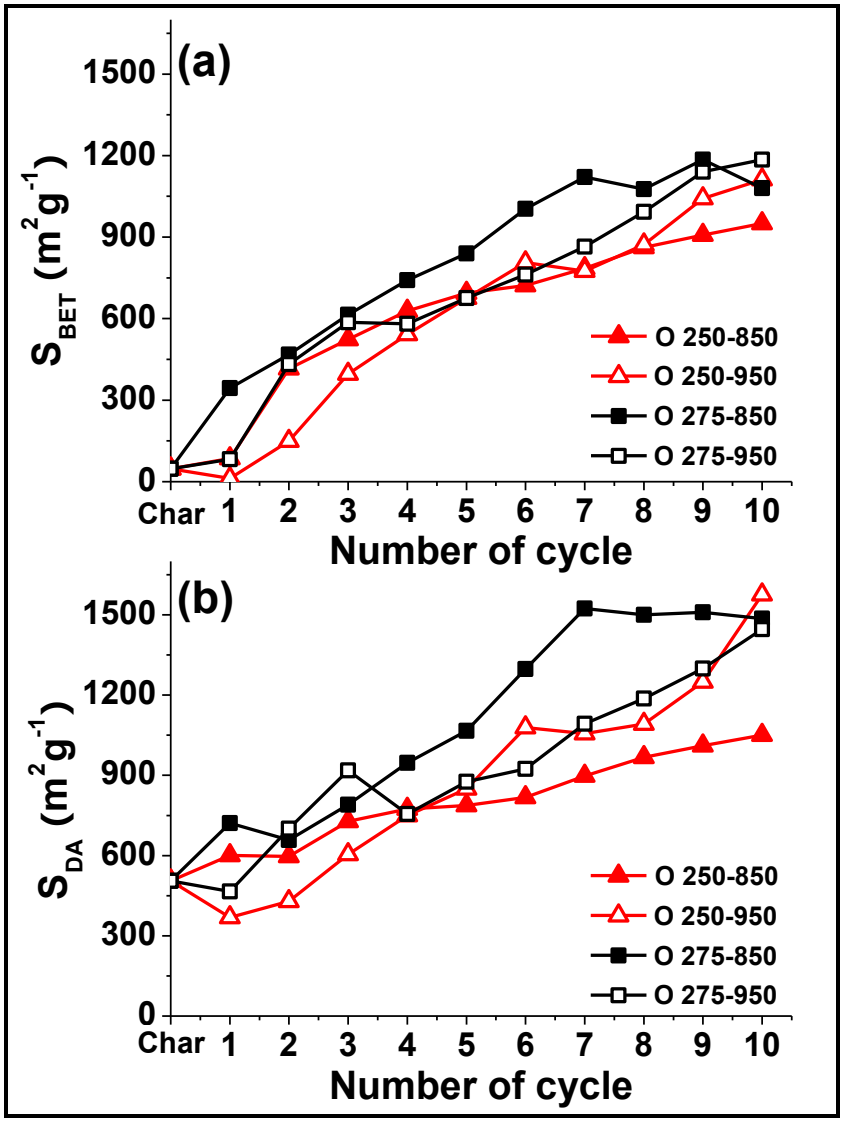

Figure 6.3. Evolution of S_{BET} (a) and S_{DA} (b) upon successive cycles of activation with ozone.

Figure 6.4 shows that the effectiveness of the activation cycles, i.e. the surface area generated at a certain burn-off, is different depending on the activation conditions, particularly in the first activation cycles, with a higher effectiveness when a desorption temperature of 950 ºC was used. Fairly similar combinations of S_{BET} and burn-off values can be obtained for all activated carbon series in the 600 – 800 m^2g^{-1} range, although the number of cycles needed vary with activation conditions.

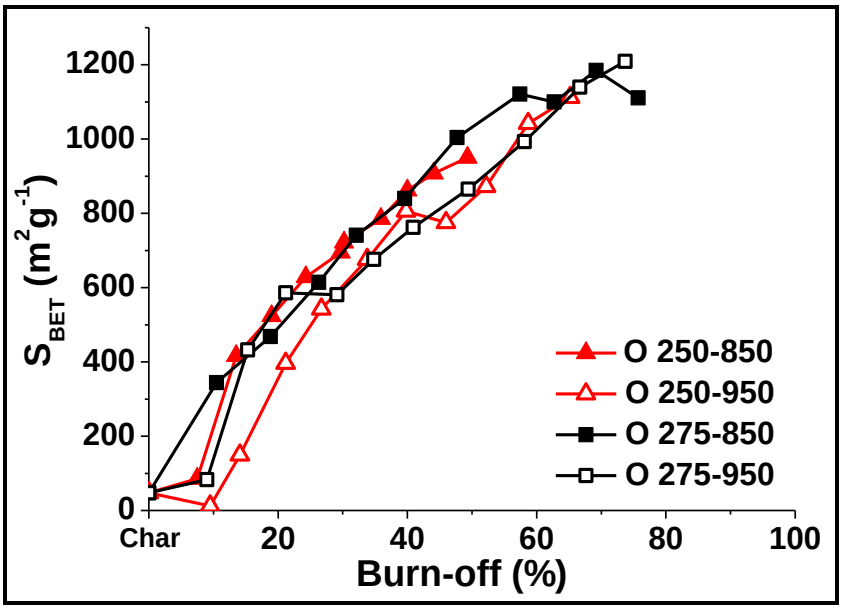

Figure 6.4. Variation of S_{BET} versus burn-off.

Figure 6.5 shows the development of S_{BET} per unit of burn-off versus the number of cycles (a) and S_{BET} (b). These graphics confirm that the first activation cycles are more effective in terms of generation of BET surface area per unit of burn-off. Such effectiveness decreases as more cycles are applied and increased surface area is developed, even though the burn-off per cycle remains essentially constant, as shown in Figure 6.1. It must be

taken into account that as the activated carbons develops S_{BET} in form of micropores, additional burn-off leads in some extent to the collapse of micropore walls. Therefore the generation of S_{BET} per unit of burn-off declines with the number of cycles as well as with increasing S_{BET} (Figure 6.5b).

In Figure 6.5 it can also be seen that the factor that mostly affects to the S_{BET} to burn-off ratio is the desorption temperature. Thus, a higher effectiveness in the development of porosity is achieved through the combination of low oxidation and desorption temperatures, within the range tested.

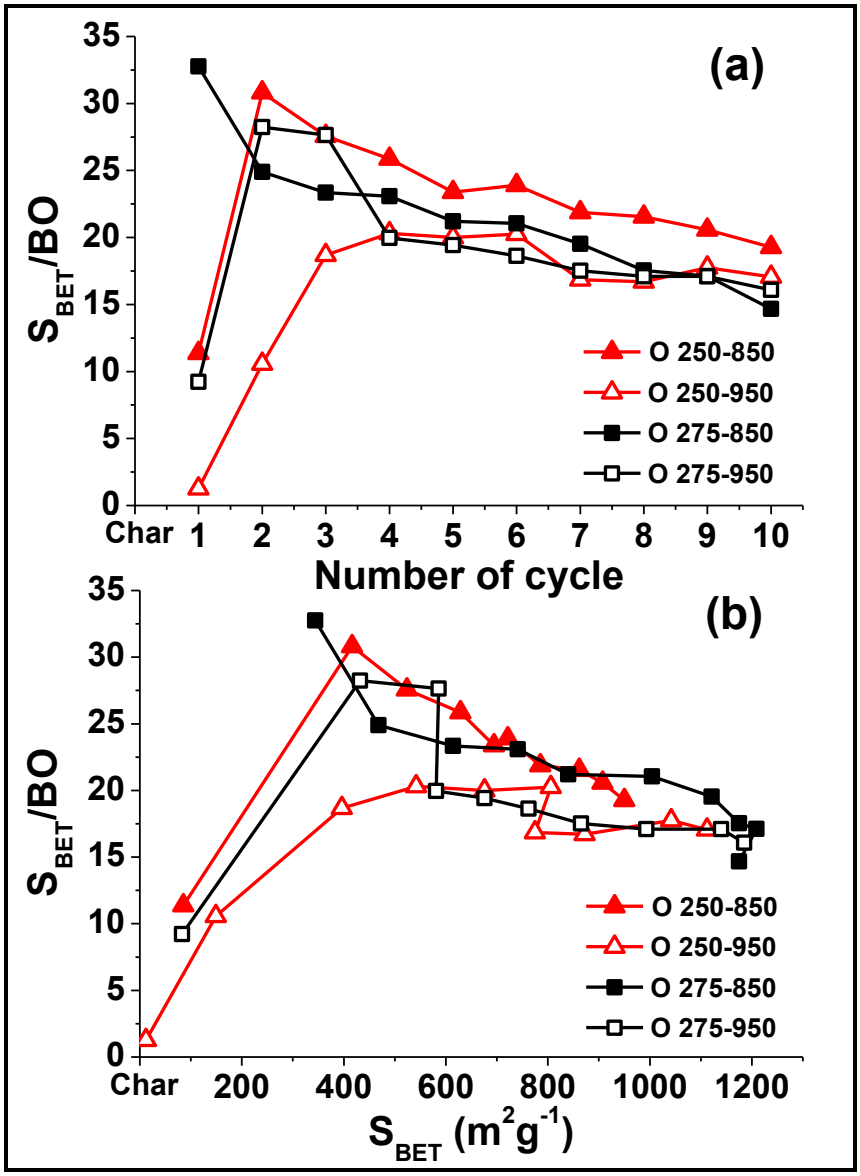

Figure 6.5. Variation of S_{BET}/burn-off ratio versus number of cycles (a) and S_{BET} (b) at different activation conditions.

6.3.3. Pore Volume

The different response to the activation conditions is of great interest for the preparation of activated carbons of different characteristics, as can be seen in Figure 6.6, where the evolution of micro and mesopore volume with the number of cycles is shown. In all cases a fairly low mesopore volume was obtained whereas an important development of microporosity occurred from the first activation cycle. It is relevant that the narrow (2 – 8 nm) and wide (8 – 50 nm) mesoporosity were only developed in some extent (always fairly modest) after the third-fourth cycle, which is in agreement with a mesopore formation mechanism based in the widening of previously formed micropores [6]. Thus, mesoporosity development was observed once the activated carbons achieved a micropore volume of around 0.25 cm^3g^{-1}. After 10 activation cycles with ozone, the samples of highest micropore volume (0.52 cm^3g^{-1}) showed a total mesopore volume of almost 0.07 cm^3g^{-1}. The so well marked transition observed between the development of micro and mesoporosity makes possible tailoring the type of porosity by an appropriate selection of the activation conditions and the number of cycles applied.

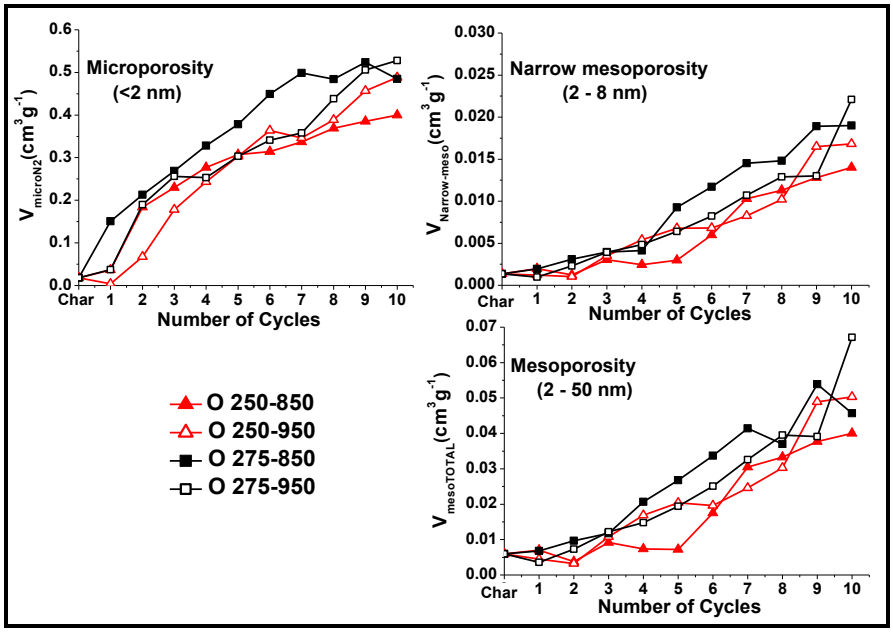

Figure 6.6. Micro and mesopore volume development along the cycles at different activation conditions.

Figure 6.7 shows the macropore volume determined by mercury porosimetry for all the activated carbon series after 1, 4, 7 and 10 activation cycles. The generation of macropore volume increases with the number of activation cycles and with the corresponding burn-off. The macropore volume correlates well with burn-off, showing low influence of the activation conditions.

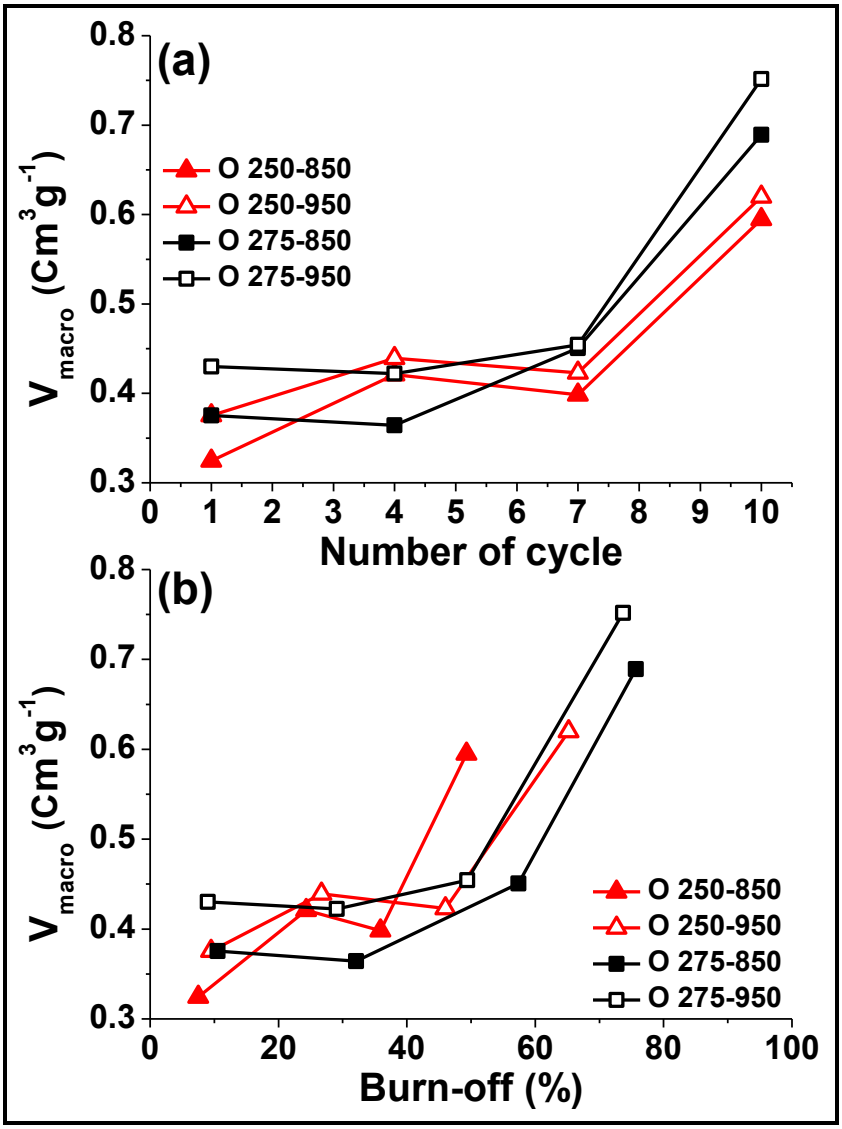

Figure 6.7. Macropore volume (0.05 – 4 μm pore size) from mercury intrusion porosimetry for all series evaluated versus number of cycles (a) and versus burn-off (b).

6.3.4. Pore size distribution

Figure 6.8a shows that the micropore mean size (d_{micro}) increases with the number of cycles, which is in agreement with the aforementioned widening of existing micropores, the micropore mean size being higher for the combination of 275 and 850 ºC as oxidation and desorption temperatures, respectively. Likewise, Figure 6.8b shows higher micropore mean size values are observed at higher values of burn-off. With regard to the evolution of the mesopore mean size (d_{meso}), a decrease can be observed with both number of cycles and burn-off (Figures 6.8c and 6.8d). This decrease can be interpreted in terms of the creation of narrow mesopores upon micropores widening.

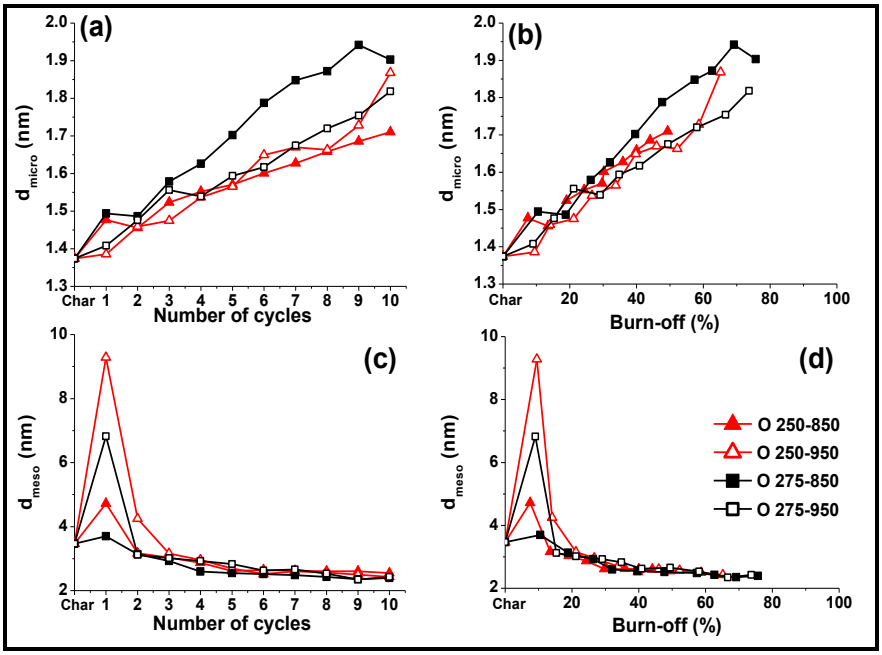

Figure 6.8. Micropore mean size versus number of cycles (a) and burn-off (b). And mesopore mean size versus number of cycles (c) and burn-off (d).

The pore size distribution is a key issue regarding the characterization of porous carbons and a number of methods have been developed for PSD analysis, the non-Local Density Functional Theory being widely used for the characterization of the porous structure of activated carbons and other porous materials.

In order to have a deeper knowledge on the generation of porosity, the NLDFT method was used to obtain the micropore size distribution from CO_2 isotherms and the micro and mesopore size distribution from N_2 isotherms. Figure 6.9 shows the results for five activated carbons prepared in different conditions, but all of them with S_{BET} values around 750 – 850 m^2g^{-1} and burn-off around 40 %. As can be observed from CO_2 NLDFT distribution, the microporosity pattern is very similar for all samples, with a distribution characterized by main peaks centered at 0.45, 0.55 and 0.88 nm in all cases, including the char. However, for N_2 NLDFT distributions there are some differences between the samples prepared at 850 and 950 ºC desorption temperature. The contribution of narrow mesoporosity is slightly lower for the 950 ºC samples, being essentially microporous and good candidates for their application as molecular sieves. For all samples a higher development of wide microporosity and very narrow mesoporosity (centered at 2.2 nm) respect to the starting char, can be observed. Finally, no significant differences were found in the pattern of mesoporosity within the 8 – 50 nm range, a great part of this porosity corresponding probably to that already existing in the starting char.

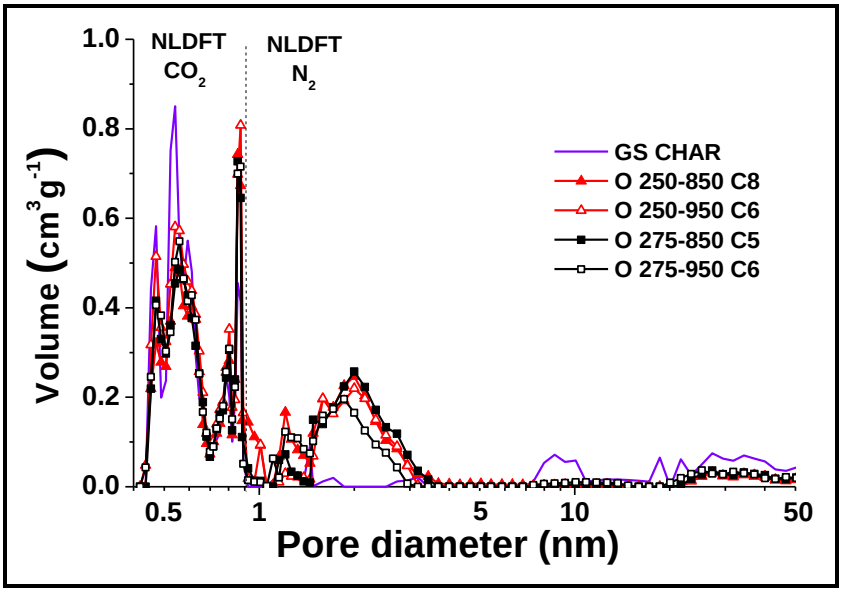

Figure 6.9. Pore size distribution by NLDFT method from CO_2 and N_2 isotherms for selected samples.

To complete the characterization of the activated carbons, the mesopore and macropore size distribution was obtained by mercury porosimetry within the 0.01 – 4 μm range (Figure 6.10). All the samples showed a similar pattern in the mesopore range whereas significant differences are observed regarding the macropores. Somewhat higher mesopore volumes and frankly higher macropore volumes were generated at 275 ºC oxidation temperature. This temperature, combined with 950 ºC for the desorption step, led to the highest development of macropores.

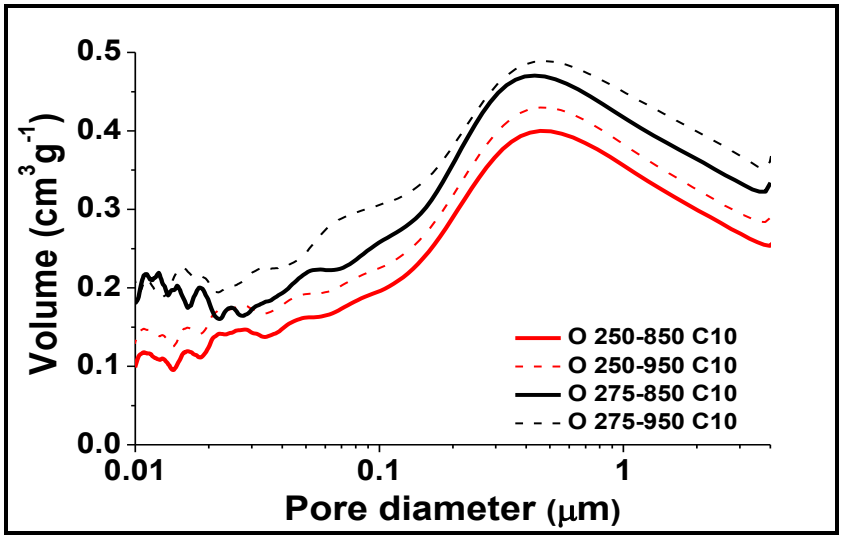

Figure 6.10. Macropore and mesopore size distribution between 0.01 and 4 μm for samples after 10 activation cycles.

6.3.5. Fourier transform infrared spectroscopy

Fourier transform infrared spectroscopy was used for the characterization of the surface functional groups of the activated carbons. Figure 6.11 shows the FTIR spectra of the char and the activated carbons after the fifth cycle of oxidation-desorption. At first sight, it is seen that all spectra are rather similar showing essentially the same peaks but with different intensities. The spectra show three main broad bands centered at 1070, 1500 and 3400 cm^{-1}. In general, a higher absorption intensity can be observed for the samples prepared at a desorption temperature of 850 ºC, except for the band around 1070 cm^{-1}, whose intensity is higher for samples oxidized at 275 ºC. In this wavenumber range the presence of oxygen groups is shown by the overlapping of bands in the 1300 to 900 cm^{-1} range, where γ(O—H) vibrations in ring ethers and primary C—O single bond stretching vibration from γ and δ lactone groups, aromatic and aliphatic ether, and epoxide structures occur [3].

The overlapping of absorption bands in the 1400 – 1700 cm^{-1} range are mainly due to the olefinic γ(C=C) vibrations, ν(C=C) stretching vibration and skeletal C=C vibrations in aromatic rings of some surface oxygen groups such as lactones and quinones. For the samples obtained at a oxidation temperature of 275 ºC is particularly significant the higher absorption of the peak c.a. 1625 cm^{-1}, which can be associated to olefinic ν(C=C) vibrations and aromatic skeletal stretching. The band centered around 3250 – 3500cm^{-1} region can be assigned to ν(O—H) and γ(O—H) vibrations in phenolic hydroxyl groups associated by hydrogen bonds [3]. It is remarkable that even after desorption at high temperature not all the surface oxygen groups created upon oxidation are removed and that these heat-treatment resistant groups build up on the activated carbon surface along the successive cycles.

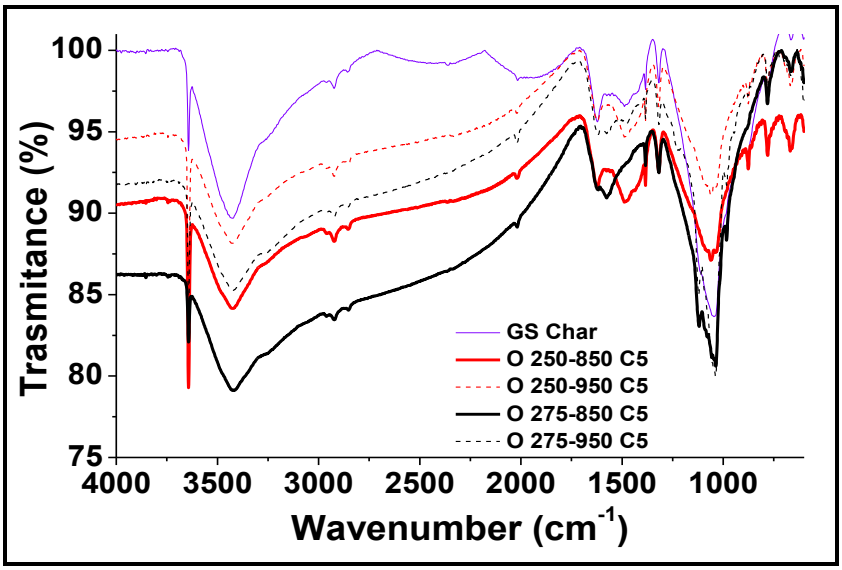

Figure 6.11. FTIR spectra of grape seed char and samples after 5 activation cycles.

6.3.6. Morphological analysis

The morphology of the activated carbons was evaluated by SEM, showing as the most relevant result that no important morphological changes were induced by the ozone treatment. The granular morphology of the starting seeds is maintained in the activated carbons along the activation cycles, even after 10 cycles (Figure 6.12), due to the controlled burn-off which seems to take place preferentially at the outer layer of the particles, as can be inferred from the size reduction observed in Figure 6.12. Likewise, changes in the texture at the outer surface can be observed, with a higher occurrence of large macropores, cracks and channels as the number of cycles is increased.

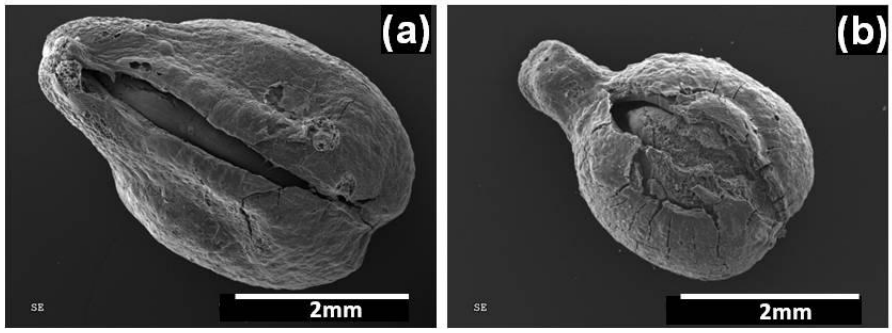

Figure 6.12. SEM micrographs of O 275-850 C5 (a) and O 275-850 C10 (b) activated carbons.

Figure 6.13 shows the SEM images of crushed particles showing that the pyrolysis led to a volatilization of the endosperm material leaving a low density structure in the inner portion of the char granules. Such low density structure can also be observed in the activated sample. It can also be seen that most of the mass of the activated carbon granules is allocated in the periphery. This structure can be of interest regarding potential applications implying mass transfer phenomena since the material combines granular

morphology and a short diffusion path, with a thickness of the outer layer around 200 μm.

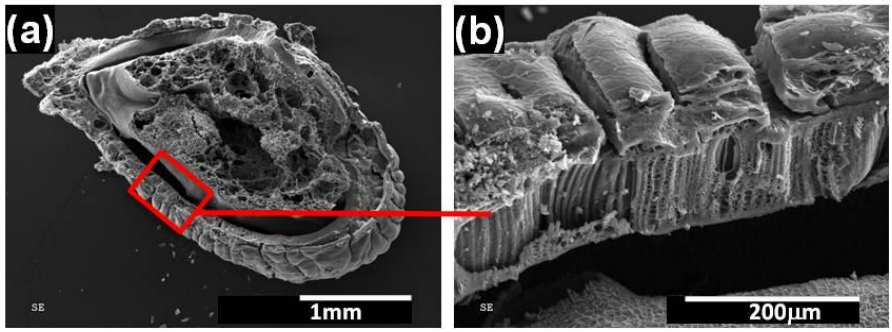

Figure 6.13. SEM micrographs of cross section of 275-850 C10 sample (a) and a detail of wall for 275-850 C10 sample (b).

References

[1] D. Jiménez-Cordero, F. Heras, N. Alonso-Morales, M.A. Gilarranz, J.J. Rodríguez. *Porous structure and morphology of granular chars from flash and conventional pyrolysis of grape seeds*. Biomass Bioenergy 2013; 54: 123 – 132.

[2] F. Heras, N. Alonso-Morales, M.A. Gilarranz, J.J. Rodríguez. *Activation of waste tire char upon cyclic oxygen chemisorption-desorption*. Ind. Eng. Chem. Res. 2009; 48(10): 4664 – 4670.

[3] P.M. Álvarez, J.F. García-Araya, F.J. Beltrán, F.J. Masa, F. Medina. *Ozonation of activated carbons: Effect on the adsorption of selected phenolic compounds from aqueous solutions.* J. Colloid Interface Sci. 2005; 283: 503 – 512.

[4] K.S.W. Sing, D.H. Everett, R.A.W. Haul, L. Moscou, R.A. Pierotti, J. Rouquerol, T. Siemieniewska. *Reporting physisorption data for gas/solid systems with special reference to the determination of surface area and porosity*. Pure Appl. Chem. 1985; 57(4): 603 – 619.

[5] M. Polyakov, M. Poisot, W.E. Maurits, T. Drescher, A. Lotnik, L. Kienle, W. Bensch, M. Muhler, W. Grunert. *Carbon-stabilized mesoporous MoS2 - Structural and surface characterization with spectroscopic and catalytic tools*. Catal. Commun. 2010; 12(3): 231 – 237.

[6] R. Mysyk, Q. Gao, E. Raymundo-Piñero, F. Béguin. *Microporous carbons finely-tuned by cyclic high pressure low-temperature oxidation and their use in electrochemical capacitors*. Carbon 2012; 50(9): 3367 – 3374.

CAPÍTULO 7 / CHAPTER 7

ACTIVACIÓN DE CHAR DE NFU CON OXIDACIÓN EN FASE LÍQUIDA

ACTIVATION OF WASTE TIRE CHAR IN LIQUID PHASE OXIDATION

7.1. Resumen / Abstract

En el presente capítulo se ha estudiado la activación de char de NFU mediante ciclos sucesivos de oxidación en fase líquida seguida por una etapa de desorción en atmósfera inerte a 650 ºC. En los experimentos previos realizados, los agentes oxidantes empleados fueron ácido nítrico, peróxido de hidrógeno y persulfato amónico. La oxidación con ácido nítrico y con peróxido de hidrógeno condujo a un mayor desarrollo de porosidad que la oxidación con persulfato amónico, por lo que éste último se excluyó para el resto del estudio. De los dos tamaños de partícula de la goma de NFU estudiados (1 y 2mm) el de 2mm resultó el más adecuado.

Se realizaron hasta 15 ciclos de activación a lo largo de los cuales se observó un aumento continuo del *burn-off*. Los mayores valores de *burn-off* se obtuvieron para los carbones activados con ácido nítrico. Se evaluaron dos concentraciones distintas (15 y 30%w) en los tratamientos con ácido nítrico y peróxido de hidrógeno, encontrándose que una mayor concentración conduce a un mayor *burn-off*, especialmente en el caso del peróxido de hidrógeno, pero no observándose diferencias notables en términos de la S_{BET} desarrollada por unidad de *burn-off*.

Se obtuvieron valores de S_{BET} en torno a 750 y 400 m^2g^{-1} en la activación con ácido nítrico y peróxido de hidrógeno, respectivamente. Los carbones activados preparados por activación con ácido nítrico mostraron mucha mayor contribución de microporosidad junto con presencia también mayor de mesoporos.

7.2. Materials and methods

The waste tire rubber was sieved in two different fractions of 1, and 2 mm of average particle diameter. The char used as starting material for cyclic activation with liquid phase oxidation was obtained by flash pyrolysis of the rubber from waste tires at 800 ºC for 20 min under nitrogen atmosphere at 100 $NmLmin^{-1}$ prepared in the pyrolysis furnace described in Chapter 2, according to the results of a previous work [1].

7.2.1. Samples characterization

The burn-off after each cycle was determined by sample weighting using the equation 2.1. Surface area and total pore volume of the samples were obtained by adsorption of N_2 at 77 K. The surface area was calculated from the N_2 isotherm using the BET equation and with the DR model, the t-method was used to obtain the micropore volume. The mesopore volume and average mesopore diameter was obtained by BJH method. The Non-Local Density Functional Theory was used to calculate the pore size distribution. The morphology of grape seeds char and activated carbons was analyzed by Scanning Electron Microscopy.

7.2.2. Cyclic activation conditions

The procedure for the oxidation step was different depending on the oxidant used. Oxidation with HNO_3 was carried out by boiling under reflux. Oxidation with H_2O_2 and $(NH_4)_2S_2O_8$ was performed at 20 ºC.

The desorption step was carried out in the furnace with manual control described in Chapter 2. The operating conditions for the desorption step in all the experiments were those found as optimum in Chapter 4 [2]: 650 ºC for 2 h with 100 $NmLmin^{-1}$ nitrogen flow and a heating rate of 10 $ºCmin^{-1}$.

The activated carbons were designated basis on the average particle diameter by the letters M (medium) and L (large) for samples with particle diameter of 1 and 2 mm, respectively. By the activating agent with the letters “N” for nitric acid, “H” for hydrogen peroxide and “AP” for ammonium persulphate, followed by the concentration of activating agent and the number of cycles applied, e.g. for sample M-H30 % C1, sample with initial particle size of 1mm was oxidized with H_2O_2 at 30 % and 1 activation cycle was completed.

7.2.3. Experimental program

The experimental work was carried out in two stages: previous tests and porosity development study. In the first set, different oxidizing agents and particle sizes were evaluated using a 5-cyles activation program. In the second series of experiments, different concentrations of the selected oxidants were tested in order to optimize the development of porosity. Table 7.1 summarizes the conditions used in both series of experiments.

Table 7.1. Conditions used in the activation experiments.

Rubber particle size (mm)	Oxidant	Concentration	Number of cycles
PREVIOUS TESTS			
1 / 2	NHO_3	65 %	5
1 / 2	H_2O_2	30 %	5
1 / 2	$(NH_4)_2S_2O_8$	1 M	5
POROSITY DEVELOPMENT STUDY			
2	NHO_3	15 % / 30 %	15
	H_2O_2	15 % / 30 %	15

7.3. Results

7.3.1. Burn-off in 5-cycle tests

In Figure 7.1 the variation of burn-off is plotted versus number of cycles, respectively. An almost linear increase of both parameters with the number of cycles applied was observed.

The burn-off values are significantly different for the different oxidants employed. The highest burn-off values were achieved with nitric acid (between 55 – 65 % after 5 cycles), while the lowest ones corresponded to hydrogen peroxide oxidation (c.a. 20 % after 5 cycles). For each oxidant, slightly lower burn-off was obtained with the largest particle size tested (2 mm), probably due to a lower penetration of the oxidant in the internal porous structure, although in the case of hydrogen peroxide the differences were very low.

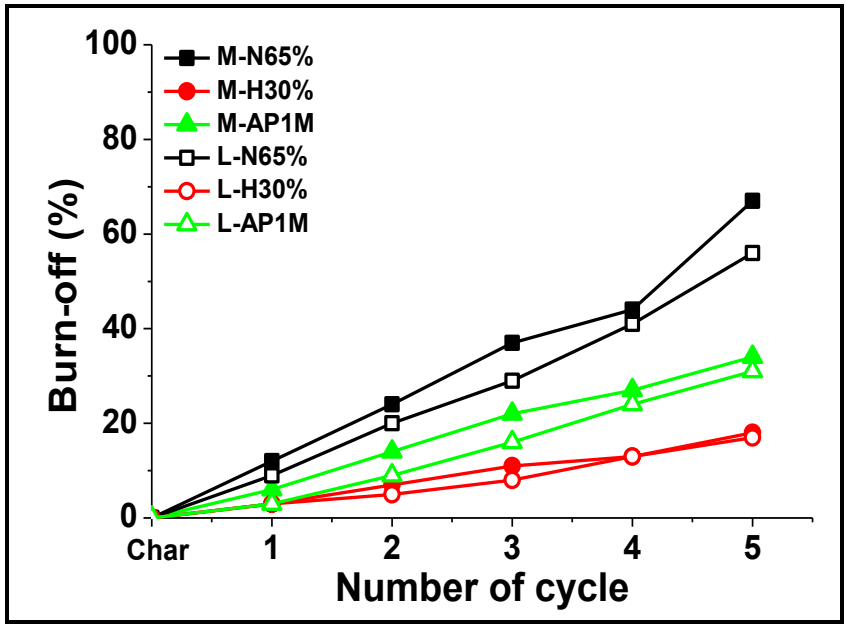

Figure 7.1. Evolution of burn-off upon activation cycles.

7.3.2. Specific surface area in 5-cycle tests

In Figure 7.2 is plotted the evolution of BET surface area in 5-cycle test and it can see that on the contrary of burn-off, BET surface area was less affected by the particle size of the starting rubber, suggesting that, in the case of largest particles, higher surface area is developed per unit of burn-off, at least during the cycles 1 to 3. In previous works using oxygen as oxidizing agent [2], the highest surface areas were obtained for the activation conditions that yielded the highest burn-off values. In the case of the liquid phase oxidants evaluated, nitric acid provided both the highest burn-off and BET surface area, 430 – 475 m^2g^{-1} after 5 cycles. However, ammonium persulphate provided significantly lower S_{BET} development (around 120 m^2g^{-1}) than hydrogen peroxide (180 – 190 m^2g^{-1}) in spite of the higher burn-off (28 – 30 % vs 17 %, respectively), probably because the large ammonium persulfate molecule provokes a more intensive attack on the external surface of the carbon.

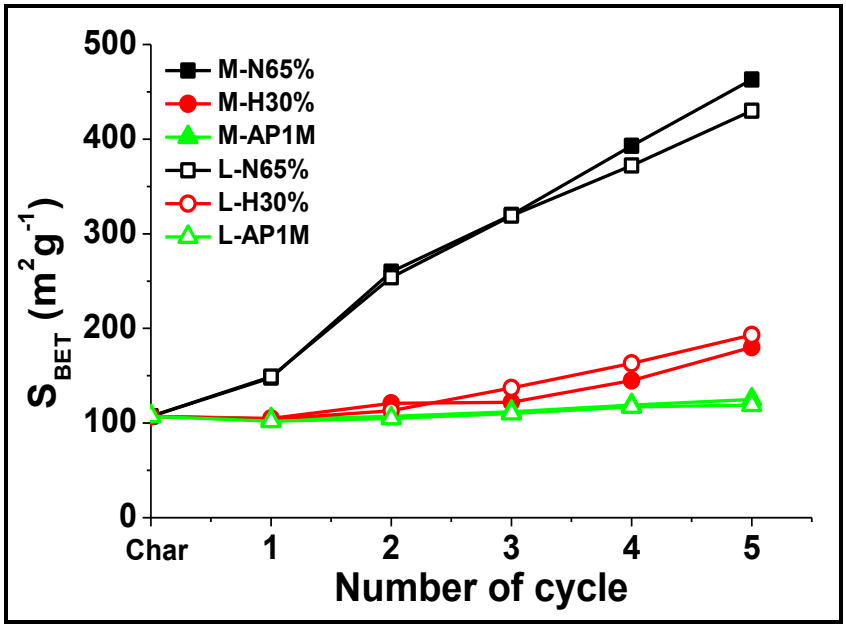

Figure 7.2. Evolution of BET surface area upon activation cycles.

7.3.3. Pore volume in 5-cycle tests

In Figure 7.3 the mesopore, narrow-mesopore and micropore volume developed along the activation cycles are depicted. Only nitric acid was able to generate micropores. This agent led also to a somewhat higher development of narrow mesoporosity (2 – 8 nm). These results confirm the lower mean pore size achieved with this oxidant (Figure 7.4). The ability of nitric acid to generate microporosity must be a key factor for further mesoporosity development upon micropore widening. As observed for burn-off and S_{BET}, the differences in micro and mesoporosity with the particle size were very low, but in general, a slightly higher results were obtained with the 1 mm fraction. In the following porosity development study, a carbon particle size of 2 mm was used and ammonium persulphate was disregarded due to the poorer porosity development.

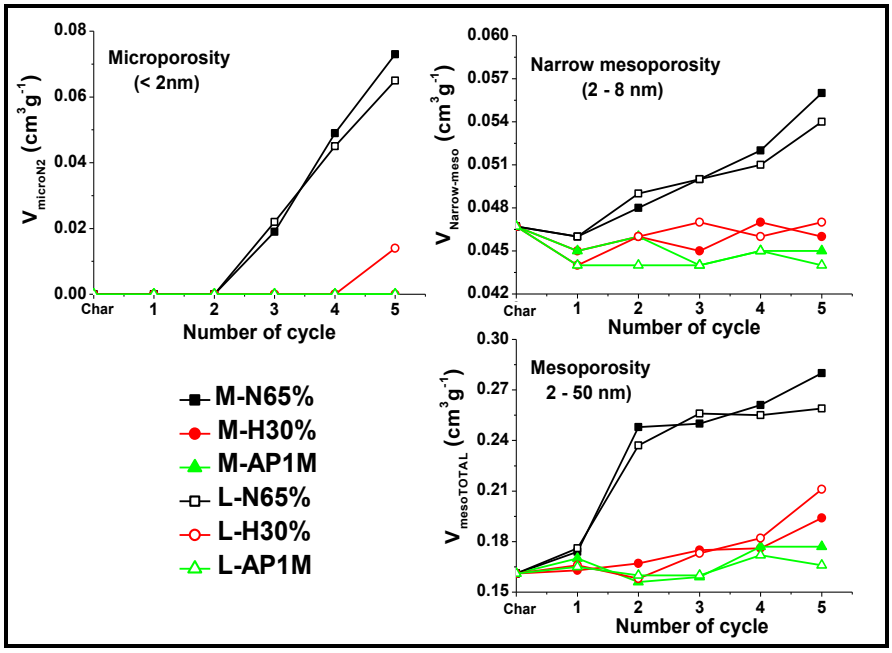

Figure 7.3. Evolution of micro and mesoporosity upon activation cycles.

7.3.4. Mean pore size in 5-cycle tests

Figure 7.4 shows the evolution of mean pore size of the carbons with the number of activation cycles applied. A sharp decrease took place after the first activation cycle, indicating a substantial change of the porous structure towards a higher contribution of microporosity and narrow mesoporosity. The influence of particle size was negligible in the case of nitric acid and of low relevance with the two other oxidizing agents. Nitric acid led to the development of pores of significantly lower mean size (around 10 nm after the 5 activation cycles), while ammonium persulphate yielded the highest (higher than 30 nm), which may be due to the aforementioned diffusional constrains. A monotonical and small decrease of mean pore size was in general observed upon successive activation cycles, somewhat more pronounced in the case of H_2O_2.

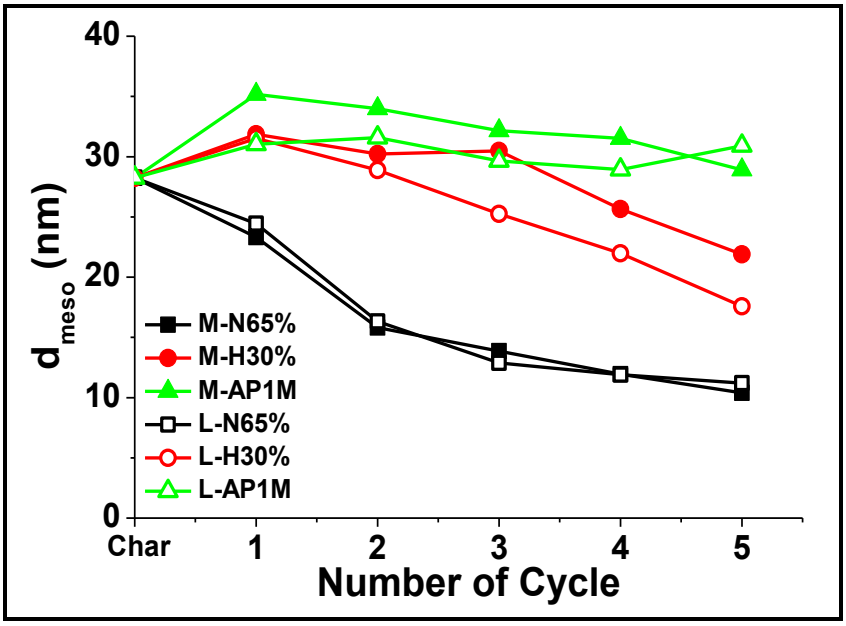

Figure 7.4. Evolution of mean pore size upon activation cycles.

7.3.5. Burn off in 15-cycle tests

For both nitric acid and hydrogen peroxide higher burn-off values were observed at the highest concentration tested (30 %) as can be seen in Figure 7.5, but the differences with respect to the results at the lowest concentration (15 %) was much higher with hydrogen peroxide. The evolution of burn-off along the activation cycles was very similar for nitric acid (both concentrations) and for 30 % hydrogen peroxide, with a nearly monotonical increase to reach values of about 90 % after 15 activation cycles. With 15 % H_2O_2 a lower burn-off increase per cycle was observed, more evident after the 4th cycle.

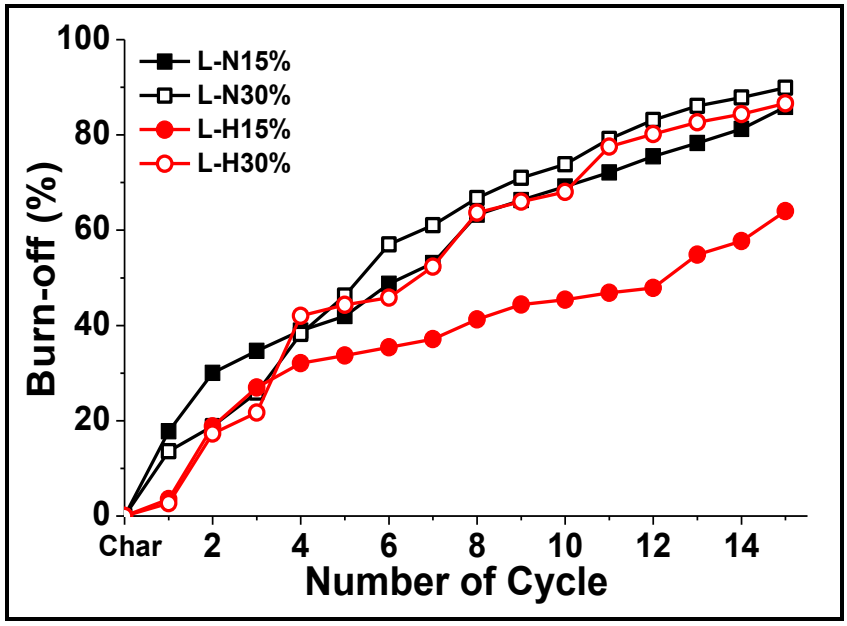

Figure 7.5. Evolution of burn-off along the activation cycles at different concentration of HNO_3 and H_2O_2.

7.3.6. Specific surface area in 15-cycle tests

In spite of the fairly similar evolution of burn-off upon activation with nitric acid and hydrogen peroxide at 30 %, a much higher development of BET surface area per cycle was observed in the activation with nitric acid (Figure 7.6). The specific surface area increases monotonically with burn-off up to 700 – 750 m^2g^{-1} after completion of the set of activation cycles applied. The differences among the activated carbons prepared at different nitric acid concentration are negligible up to the fifth cycle and then a gap of around 50 – 100 m^2g^{-1} is maintained along the following cycles. Hydrogen peroxide activation leads to lower porosity development and higher differences between the activated carbons prepared with 15 and 30 % concentration (around 400 and 280 m^2g^{-1} after 15 cycles, respectively). Therefore, nitric acid is substantially more effective than hydrogen peroxide in terms of surface area development. Moreover, nitric acid is also more efficient.

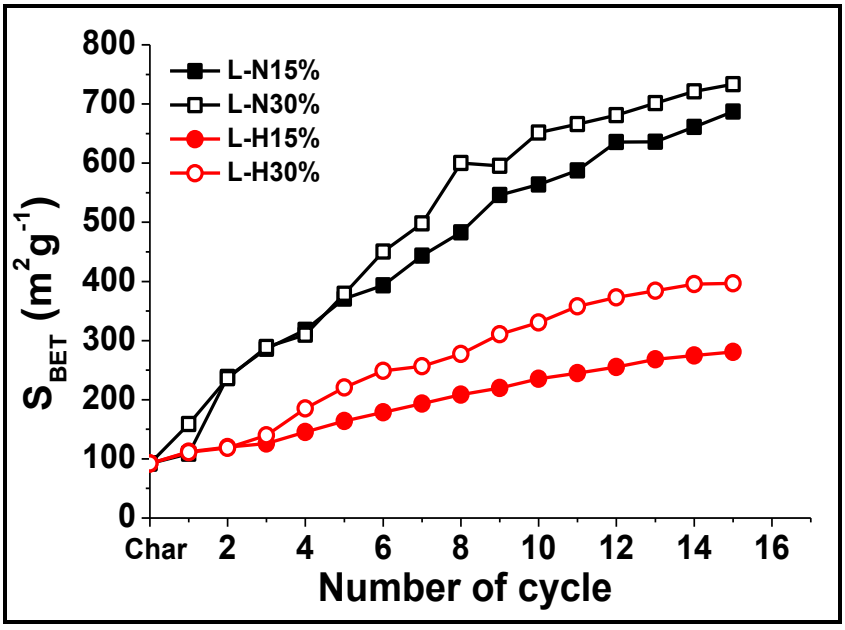

Figure 7.6. Evolution of S_{BET} along the activation cycles at different concentration of HNO_3 and H_2O_2.

Values of the Dubinin-Radushkevich specific surface area calculated from N_2 isotherms were also obtained for the sake of comparison with the reported in the literature. After 15 activation cycles with nitric acid at 15 and 30 % S_{DR} reached 1153 and 1031 m^2g^{-1} respectively, versus 577 and 952 m^2g^{-1} with H_2O_2 at the same concentrations. Values of 950 – 1500 m^2g^{-1} after 2 – 5 cycles and burn-offs of 20 – 39 % have been reported [3] for the cyclic activation of sucrose and cellulose using H_2O_2 at 200 ºC and 135 bar and further decomposition at 900 ºC in inert atmosphere.

7.3.7. Pore volume in 15-cycle tests

The evolution of pore volume shows different dependence with the type of oxidant and its concentration as can be seen in Figure 7.7. The profiles for the whole and narrow mesoporosity are quite similar at the two concentrations, showing an increase throughout the activation series and giving highest pore volumes with 30 % HNO_3 followed by 30 % H_2O_2 (0.68 and 0.48 cm^3g^{-1}, respectively), noting that concentration is the key condition in mesopores generation. On the opposite, the micropore volume shows a maximum within the activation cycles 8 to 12 (about 0.18 cm^3g^{-1} after 8 and 12 cycles with 30 and 15 % HNO_3, respectively).

This evidences a destruction of micropores associated to a high burn-off, which is consistent with the stabilization or even slight increase of mean pore size in the last cycles (see Figure 7.8). The loss of micropore volume is more accused at an oxidant concentration of 30 %, consistent with the higher development of mesoporosity in the last cycles observed at this concentration.

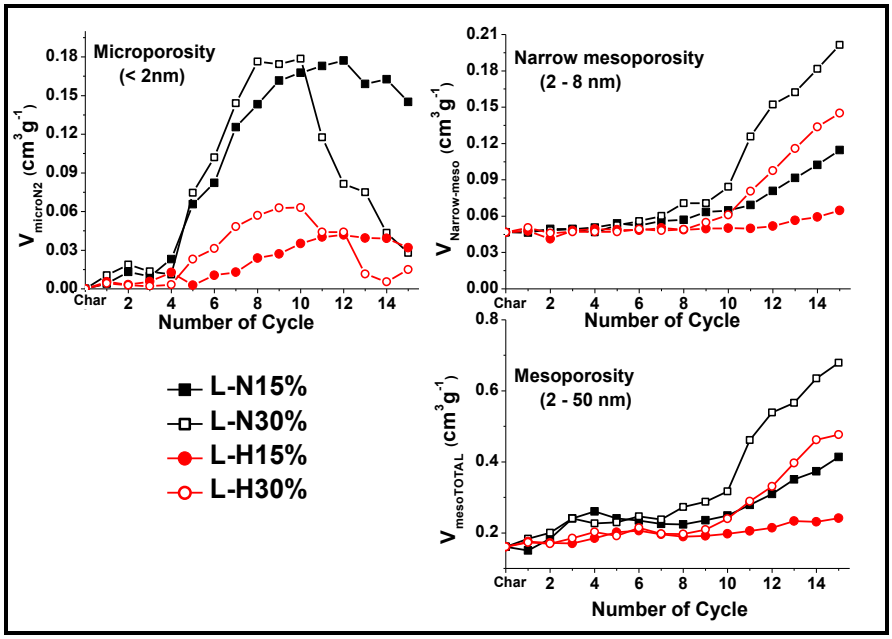

Figure 7.7. Evolution of micro and mesopore volumes upon activation cycles at different concentration of HNO_3 and H_2O_2.

7.3.8. Pore size distribution in 15-cycle tests

Figure 7.8 shows the evolution of mean pore size along the activation cycles with HNO_3 and H_2O_2 at the two concentrations tested. As can be seen, the variation is fairly small beyond the first cycle. For both oxidants lower mean pore sizes were obtained at 30 % concentration but the differences with concentration tend to decrease as activation proceeds, giving quite similar mean pore sizes after the 15 activation cycles (around 18 and 11 nm with H_2O_2 and HNO_3, respectively). The results obtained with nitric acid are very similar to those previously reported as obtained with air [2, 4], where mean pore sizes around 10 nm were achieved after 15 cycles.

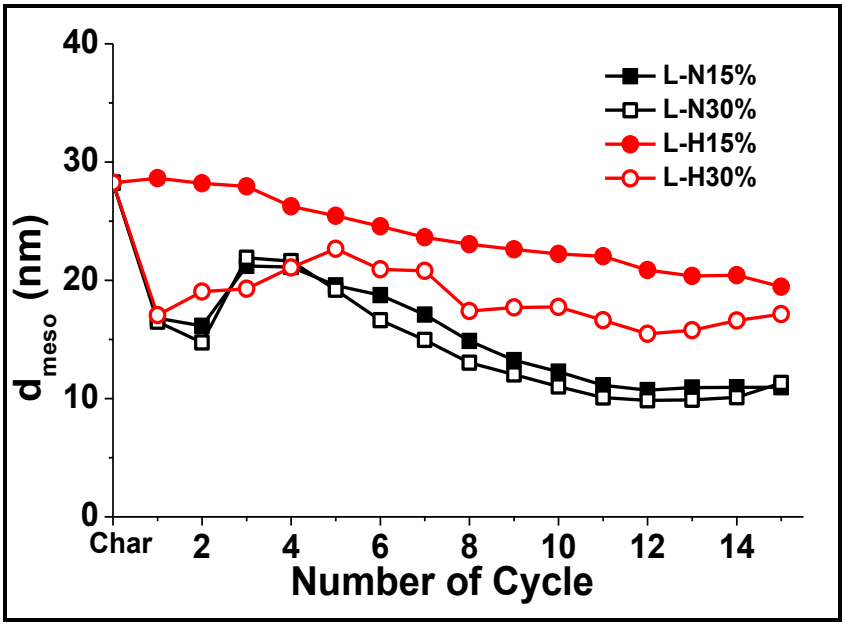

Figure 7.8. Evolution of mean mesopore size along the activation cycles at different concentration of HNO_3 and H_2O_2.

In order to have a deeper knowledge on the generation of porosity, the pore size distribution was calculated from N_2 isotherms by the NLDFT method for the WTR char and activated carbon samples after 15 activation cycles (Figure 7.9). As can be observed, the wide mesoporosity pattern is very similar for all activated carbons, especially for L-N15% C15 and L-H30% C15 samples with a pore diameter centered at 11, 29 and 34 nm, which shows a notable increment of pore diameter with respect to the initial char. The narrow mesoporosity shows a poor contribution compared to the adsorbed volume in the wide mesopore range, in agreement with the results in Figure 7.8. In the narrow mesopore range there are a clear differences between samples activated with nitric acid and hydrogen peroxide, showing the narrower distribution for carbons activated with HNO_3.

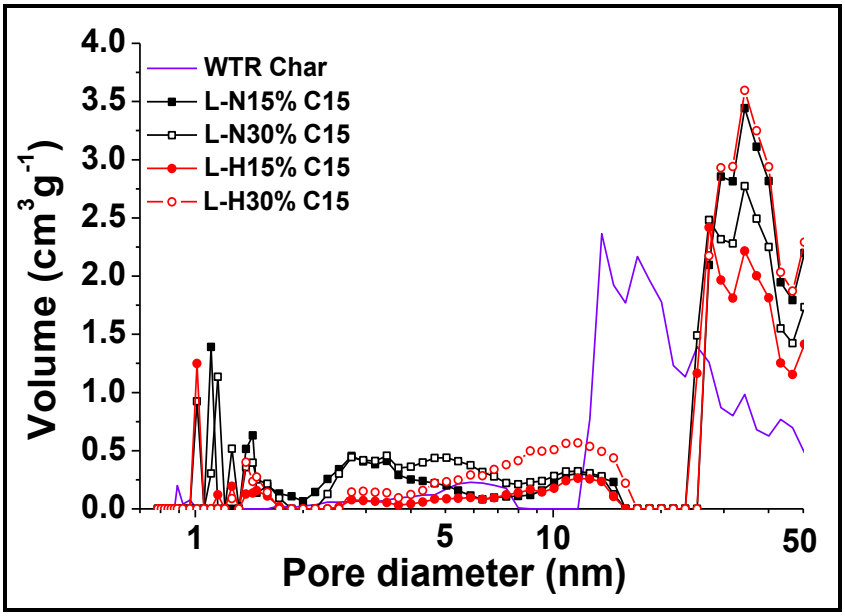

Figure 7.9. Pore size distribution by NLDFT method from N_2 isotherms for waste tire rubber char and the samples from L-N15%, L-N30%, L-H15% and L-H30% series after 15 activation cycles.

7.3.9. Morphological analysis

Figure 7.10 shows SEM images of activated carbons obtained at different activation conditions after 15 cycles, together with that of a starting char. It can be seen that an important reduction in particle size takes place during the activation process, which is more important in the case of the activation with 30 % HNO_3 due to the higher burn-off achieved after 15 cycles. The oxidation with nitric acid also results in a smother texture of the particles.

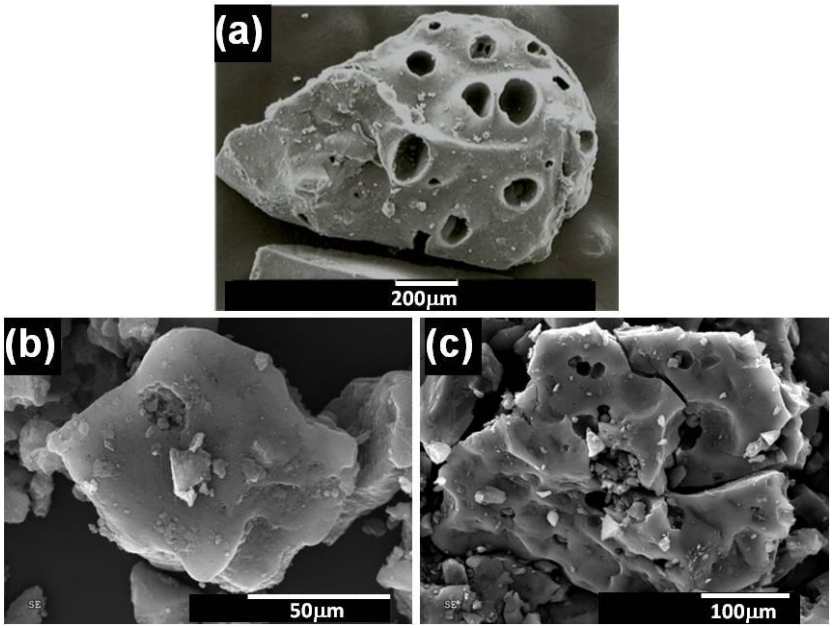

Figure 7.10. SEM images of (a) starting char, (b) activated carbon after 15 activation cycles with 30 % HNO_3 and (c) 30 % H_2O_2.

References

[1] N. Alonso-Morales, M.A. Gilarranz, F. Heras, V. González, J.J. Rodríguez. I*nfluence of operating variables on carbonization of waste tires*. 1st European Chemistry Congress, 2006, Bulgary.

[2] F. Heras, N. Alonso-Morales, D. Jimenez-Cordero, M.A. Gilarranz, J.J. Rodríguez. *Granular Mesoporous Activated Carbons from Waste Tires by Cyclic Oxygen chemisorption−Desorption*. Ind. Eng. Chem. Res. 2012; 51: 2609 – 2614.

[3] R. Mysyk, Q. Gao, E. Raymundo-Piñero, F. Béguin. *Microporous carbons finely-tuned by cyclic high pressure low-temperature oxidation and their use in electrochemical capacitors*. Carbon 2012; 50(9): 3367 – 3374.

[4] F. Heras, N. Alonso, M.A. Gilarranz, J.J. Rodríguez. *Activation of waste tire char upon cyclic oxygen chemisorption-desorption*. Ind. Eng. Chem. Res. 2009; 48(10): 4664 – 4670.

Capítulo 8 / Chapter 8

Activación de char de Semillas de Uva con Oxidación en Fase Líquida

---

Activation of Grape Seeds char in Liquid Phase Oxidation

8.1. Resumen / Abstract

En este capítulo, se han evaluado tres agentes oxidantes diferentes (HNO_3, H_2O_2, $(NH_4)_2S_2O_8$) y dos temperaturas de desorción distintas (850 y 950 ºC) en la activación de *char* de semillas de uva por sucesivos ciclos de oxidación en fase líquida seguida por desorción a alta temperatura. La evolución del *burn-off* y de la porosidad se han estudiado a lo largo de 10 ciclos de activación.

En los cinco primeros ciclos de activación con HNO_3 se observó un gran aumento de la superficie específica BET alcanzando valores superiores a 1200 m^2g^{-1} y con un *burn-off* inferior al 50 %. La activación con H_2O_2 y $(NH_4)_2S_2O_8$ condujo a un desarrollo de porosidad significativamente inferior que con ácido nítrico, alcanzando 600 y 800 m^2g^{-1} de superficie específica BET, respectivamente, para un *burn-off* equivalente.

El análisis de la distribución de tamaño de poro mostró que la generación de porosidad tiene lugar mediante la creación de nuevos microporos y por el ensanchamiento de los poros presentes en la muestra, en los casos de carbones activados preparados con HNO_3 y $(NH_4)_2S_2O_8$, mientras que cuando se usa H_2O_2 sólo se observa el ensanchamiento de los microporos estrechos presentes en el *char* inicial. Los carbones activados obtenidos son esencialmente microporosos, con una pequeña contribución de mesoporos. En el caso de los carbones activados con HNO_3 se ha obtenido un $V_{microN2}$= 0.69 cm^3g^{-1} y un $V_{mesoTOTAL}$= 0.07 cm^3g^{-1}, mientras que en la activación con $(NH_4)_2S_2O_8$ y H_2O_2 se han obtenido carbones activados con una muy baja contribución de mesoporos, con un volumen de mesoporo total de 0.04 y 0.01 cm^3g^{-1}, respectivamente.

La caracterización mediante SEM muestra que los carbones activados obtenidos mantienen la morfología granular de las semillas después de 10 ciclos de activación mostrando además una estructura hueca con un espesor de pared en torno a 200 μm.

8.2. Materials and Methods

The grape seeds char (GS Char) used as starting material was obtained by flash pyrolysis of the extracted seeds at 800 ºC for 2 h under nitrogen atmosphere, according to the results of Chapter 3 [1].

8.2.1. Samples characterization

The burn-off after each cycle was determined by sample weighting using the equation 2.1. Surface area and total pore volume of the samples were measured by 77 K N_2 adsorption/desorption and CO_2 adsorption at 273 K. The BET surface area of the samples was calculated from the N_2 isotherms using the Brunauer-Emmett-Teller equation, the t-method was used for the micropore volume and BJH method for mesopore mean size, whereas the Dubinin-Astakhov model was applied to CO_2 isotherms to obtain the S_{DA} and micropore mean size. The mercury intrusion porosimetry was used to determine the macropore volume. The Non-Lineal Density Functional Theory was used to calculate the pore size distribution.

Fourier transform infrared spectroscopy was used to characterize the main functional groups of the activated carbons surface. The morphology of grape seeds char and activated carbons was evaluated by Scanning Electron Microscopy.

8.2.2. Cyclic activation conditions

The oxidation step was different depending on the oxidant used. Oxidation with 30 % HNO_3 was carried out by boiling under reflux. Oxidation with 30 % H_2O_2 and 1M $(NH_4)_2S_2O_8$ was performed at 20 ºC.

The operating conditions for the desorption step in all the experiments were those found as optimum in Chapter 5: 850 and 950 ºC for 2 h using a

flow rate of 100 $mLmin^{-1}$ of nitrogen and a heating rate of 10 $ºCmin^{-1}$. The desorption step was carried out in the furnace with automatic control described in Chapter 2.

The activated carbons were designated by the activating agent with the letters “N” for nitric acid, “H” for hydrogen peroxide and “AP” for ammonium persulphate, followed by desorption temperature and the number of cycles applied, e.g. for sample H-850 C1, oxidation was carried with H_2O_2 at 850ºC of desorption temperature and 1 activation cycle was completed.

8.3. Results

8.3.1. Burn-off

Under all the combinations of oxidizing agent and desorption temperature tested, the burn-off increased almost linearly with the number of activation cycles applied (Figure 8.1). Likewise, burn-off showed, as a general trend, an increase with desorption temperature. The highest burn-off values were observed for the activated carbon series prepared with HNO_3, and the lowest for the H_2O_2 one.

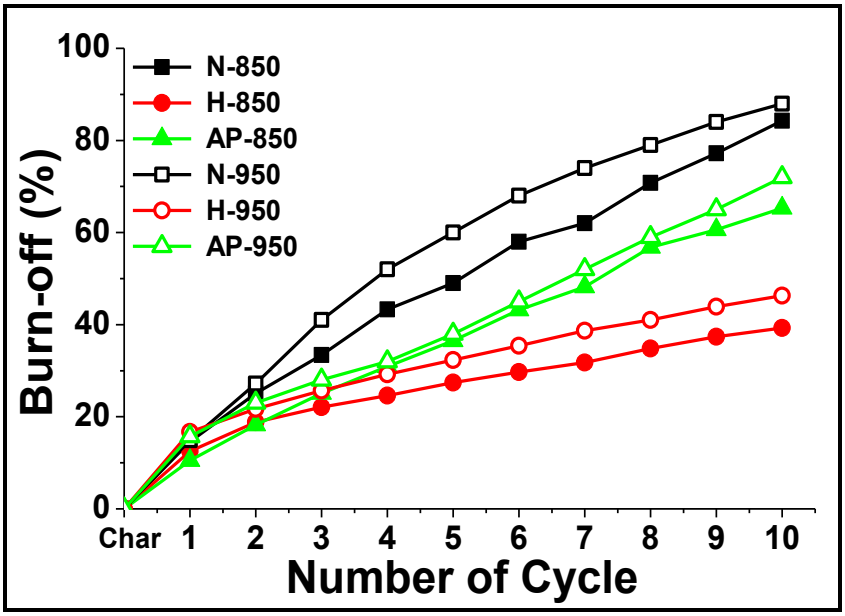

Figure 8.1. Burn-off vs number of activation cycles with different oxidizing agents and desorption temperatures.

8.3.2. Specific surface area

The starting char obtained from grape seeds used in this chapter was a mainly microporous with a S_{BET} of 47 m^2g^{-1} and a S_{DA} of 505 m^2g^{-1} (results of Chapter 3), denoting a frankly narrow microporosity according to the difference between both surface areas [1].

Figure 8.2 shows the development of surface area with the number of activation cycles. It can seen that a desorption temperature of 850 ºC leads to a S_{BET} development upon the first cycles higher than that observed at 950 ºC, in spite of the higher burn-off values achieved at this second temperature. This may be related with thermal stress leading to partial collapse of the microporous structure [2]. In the case of HNO_3 the development of porosity per cycle remained high up to the 5^{th} – 6^{th} cycle, reaching S_{BET} values above 1200 m^2g^{-1}. Beyond that the increase of S_{BET} was slower, due to the

coalescence of pores associated to high burn-off. Likewise, increasing the number of cycles decreases the differences in S_{BET} between the series of activated carbons prepared at the two desorption temperatures tested. After 10 activation cycles with HNO_3 a S_{BET} value around 1450 m^2g^{-1} was achieved.

With $(NH_4)_2S_2O_8$ and H_2O_2 as oxidizing agents, the development of S_{BET} was substantially lower, particularly when the desorption stage was carried out at 950 ºC, where the creation of S_{BET} was of low significance upon the five first cycles. The lowest S_{BET} development was observed for the H_2O_2 series, with S_{BET} values bellow 600 m^2g^{-1} after 10 activation cycles.

The evolution of S_{DA} shows higher values than S_{BET} during the first activation cycles, indicating a predominantly narrow microporosity of the resulting carbons. As burn-off increases new narrow microporosity is created and widening of existing pores takes place, being this more evident in the nitric acid series. With H_2O_2, the S_{BET} after ten activation cycles is still lower than 600 m^2g^{-1} and remains below S_{DA}, particularly at a desorption temperature of 950 ºC.

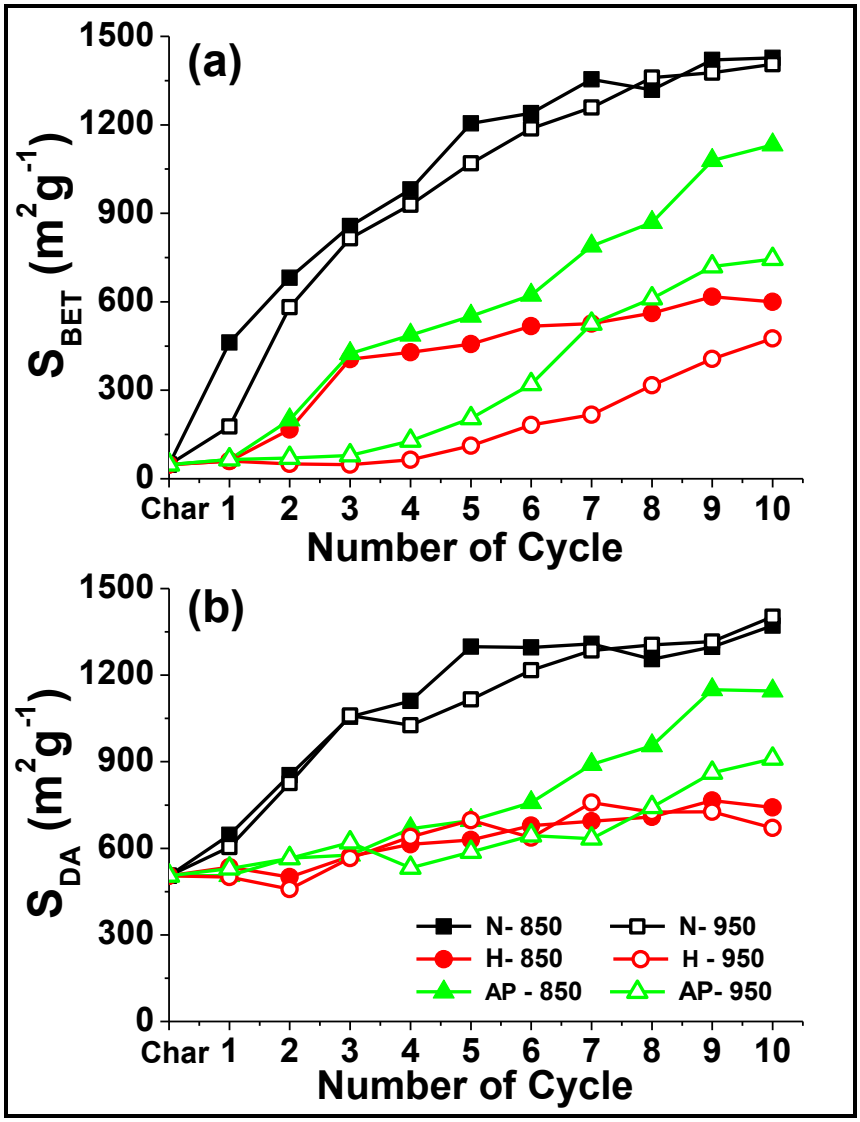

Figure 8.2. S_{BET} (a) and S_{DA} (b) development upon successive activation cycles.

Convenient operating conditions can be established in 5 activation cycles and a desorption temperature of 850 ºC for the HNO_3 series, leading to activated carbons with S_{BET} close to 1200 m^2g^{-1} at burn-off lower than 50 %. The generation of high surface area at a burn-off as low as possible is crucial for the sake of preserving the physical integrity of the particles, so that granular activated carbon can be obtained. For the $(NH_4)_2S_2O_8$ series around 8 cycles would be needed to obtain S_{BET} values close to 900 m^2g^{-1} at a burn-off c.a. 55 %. More modest values of surface area are obtained in the case of the H_2O_2 series, although these activated carbons can be of interest thanks to their pore size distribution with a predominantly narrow microporosity, as can be inferred from the comparison of the S_{BET} and S_{DA} values of Figure 8.2. Thus, these activated carbons may have potential application as molecular sieves.

8.3.3. Pore volume

As can be observed in Figure 8.3, very low mesopore volume was achieved under all the activation conditions tested, in contrast with the important development of microporosity occurred from the first activation cycle. An incipient development of mesopores can be observed beyond the first cycle for the HNO_3 series, and beyond the fourth cycle for the $(NH_4)_2S_2O_8$ one. That fairly modest generation of mesoporosity must be due to the widening of previously created micropores [3], as it was mentioned before. The development of mesopores was observed once the activated carbons achieved a micropore volume ($V_{microN2}$) of around 0.25 cm^3g^{-1}. It is remarkable that after 10 activation cycles the H–850 C10 sample showed quite a high micropore volume (0.69 cm^3g^{-1}) with a relatively low total mesopore one (0.067 cm^3g^{-1}). The carbons with a less developed porosity, i.e. the H_2O_2 series, show an almost negligible contribution of mesopores (around 0.017 cm^3g^{-1} at the most) which reinforces the aforementioned potential interest as molecular sieves, although further studies will be needed to check this.

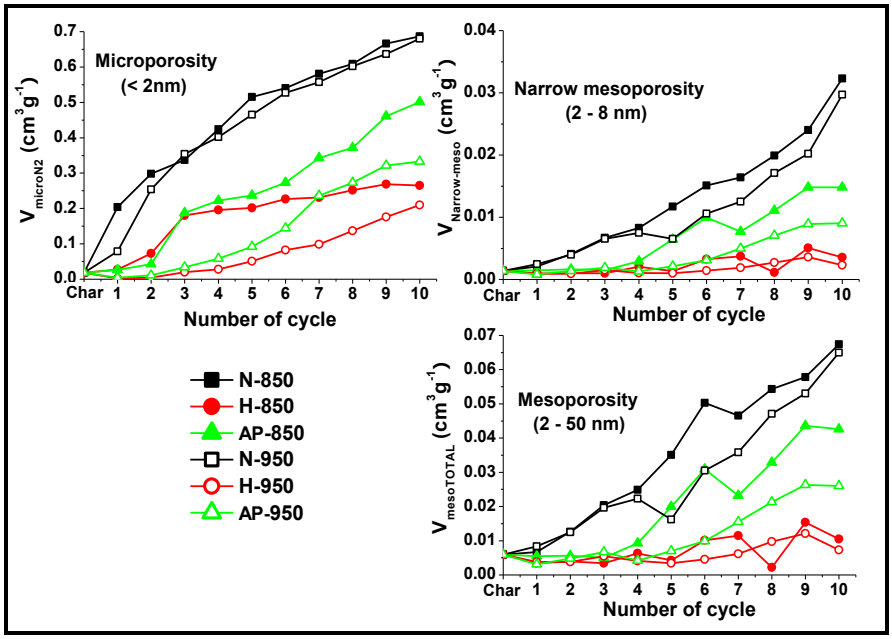

Figure 8.3. Pore volume development from N_2 adsorption isotherms along the cycles for different oxidizing agents and desorption temperatures.

Table 8.1 shows the macropore volume obtained from mercury porosimetry of the activated carbons prepared at desorption temperature of 850 ºC after 5 and 10 activation cycles. As can be seen, the number of oxidation-desorption cycles and the oxidizing agent also have a significant effect on the macroporosity of the resulting carbons. The macropore volume increases with the number of cycles applied and with burn-off being appreciably higher in the HNO_3 series [4].

Table 8.1. Macropore volume from mercury porosimetry between 0.01 and 4 μm after 5 and 10 activation cycles.

	V_{macro} (cm^3g^{-1})		
	N-850	**H-850**	**AP-850**
Char		0.707	
Cycle 5	0.347	0.293	0.309
Cycle 10	0.551	0.386	0.455

8.3.4. Pore size distribution

To learn more in depth on the porous structure of the activated carbons prepared, their pore size distribution was obtained. As a first approach Figure 8.4 shows that the mean micropore size increases with the number of activation cycles (and, consequently burn-off), while the mean mesopore size decreases. The decrease in mean mesopore size can be ascribed to the formation of narrow mesopores by coalescence of micropores upon burn-off. At burn-off values above 50 % the mean mesopore size becomes quite similar for all the carbons obtained, approaching to 2 nm, the upper limit of micropores.

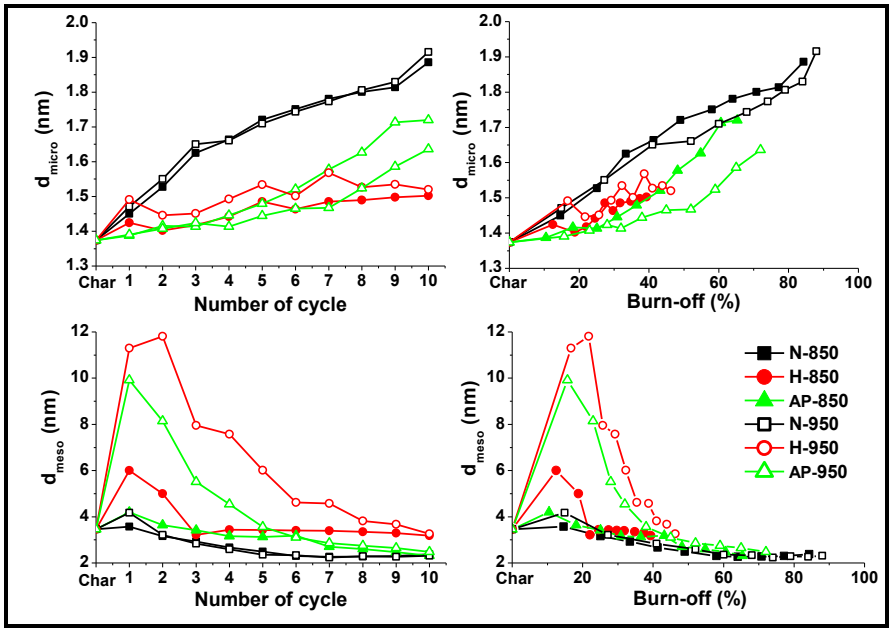

Figure 8.4. Mean micropore and mesopore size versus number of cycles and burn-off.

The non-local Density Functional Theory is widely used for the characterization of the porous structure of activated carbons and other porous materials. In Figure 8.5 the micropore and mesopore size distributions calculated by the NLDFT method from CO_2 and N_2 adsorption, respectively, are depicted for three selected carbons (one of each series with 850 ºC of desorption temperature) obtained at similar values of burn-off (around 40 %). As can be observed, the CO_2-NLDFT distribution is very similar for the three samples and falls essentially within the micropore range in agreement with the nature of the porosity of these carbons so far discussed. Their PSD seems to be determined in some extent by that of the starting char within the micropore range. On the contrary, in the mesopore range there are clear differences between the sample activated with HNO_3 and the two other, particularly looking at the narrower mesopores (below 3 nm). No significant differences can be found in the pattern of mesoporosity within the 8 – 50 nm

range, being this porosity initially present in the starting char. Summarizing, the activated carbons of essentially microporous nature have a heterogeneous micropore size distribution centered at 0.45, 0.55 and 0.88 nm and the sample activated with HNO_3 also at 1.8 nm.

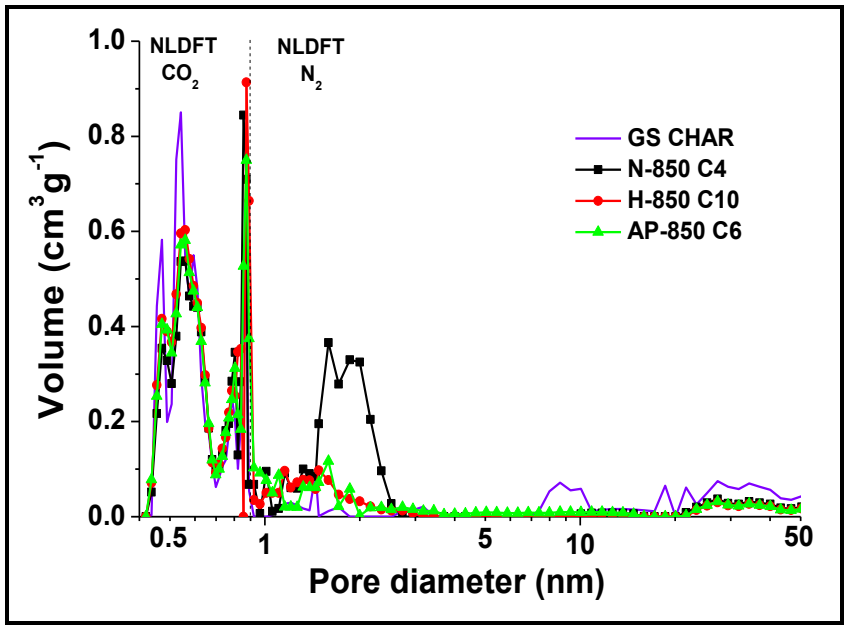

Figure 8.5. Pore size distribution by NLDFT method from CO_2 and N_2 isotherms for selected carbon samples.

8.3.5. Fourier transform infrared spectroscopy

Fourier transform infrared spectroscopy was used for the characterization of the main functional groups of the activated carbons surface. The spectra for the three series (Figure 8.6) were quite similar, showing essentially the same main peaks although with different intensities that increase with the number of cycles, so it can be interpreted in terms of progressive increase of the type and quantity of functional groups on the surface of the activated carbons. Therefore, the desorption at high temperature does not remove all the surface oxygen groups created upon oxidation and the most heat-resistant groups build up on the activated carbon surface. The overlapping of bands in the 1300 to 900 cm^{-1} range probe the presence of C—O bonds in various chemical surroundings, where γ(O—H) vibrations in ring ethers and primary C—OH occur [5, 6]. Likewise, bands in the vicinity of 1350 cm^{-1} ascribable to δ(O—H) and γ(C=O) vibrations. Relevant bands can also be found around 3600 cm^{-1}, assessed to non-bonded OH groups, and at 3225 and 3350 cm^{-1}, which correspond to γ(O—H) vibrations in hydroxyl groups. Olefinic γ(C=C) vibrations and skeletal C=C vibrations in aromatic rings can be responsible for the overlapping of bands in the 1700 – 1400 cm^{-1} range [5].

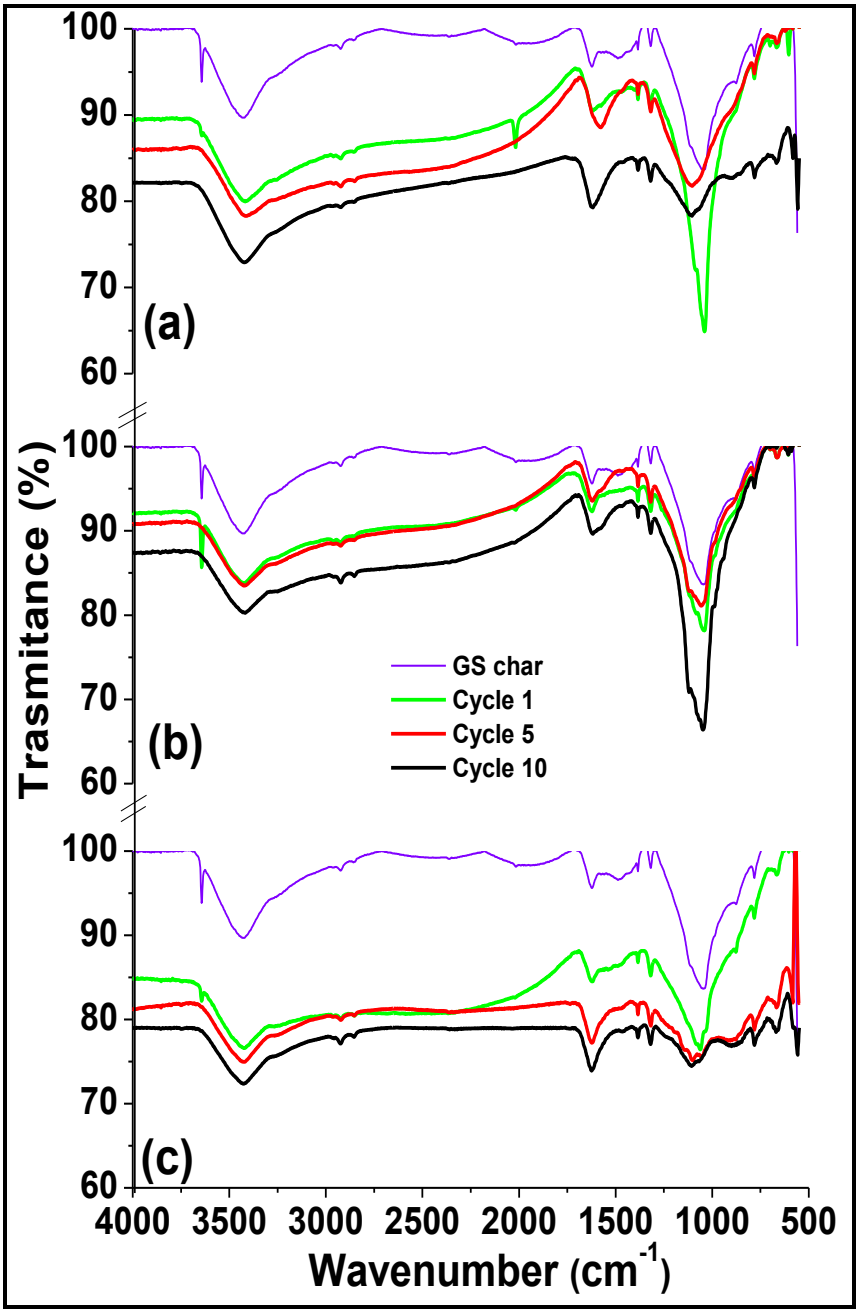

Figure 8.6. FTIR spectra of N-850 series (a), H-850 series (b), AP-850 series (c).

8.3.6. Morphological analysis

The morphology of the activated carbons was evaluated by SEM, showing that the granular structure was maintained along the cycles independently of the oxidizing agent used (Figure 8.7). Furthermore, there is also a reduction in size with respect to that of the starting seed along the cycles. It can also be observed that the samples activated with H_2O_2 and $(NH_4)_2S_2O_8$ have a higher prevalence of cracks on the outer surface.

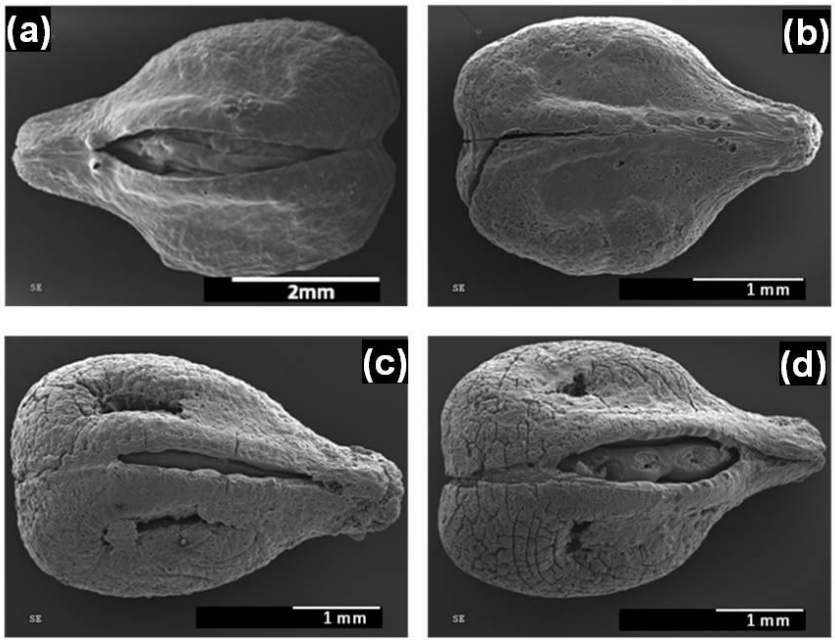

Figure 8.7. SEM micrographs of char from grape seed (a), N-850 C10 sample (b), H-850 C10 sample (c) and AP-850 C10 sample (d).

Figure 8.8 shows SEM images of crushed particles showing the hollow core structure of the carbon particles after 10 activation cycles with HNO_3 as activating agent. The hollow structure results from the volatilization of the albumen and embryo during the pyrolysis stage and is maintained along the activation. The activated carbon has most of the carbonaceous material allocated in a shell thickness of around 300 μm, being that an interesting feature since the granular material would combine easy handling and low pressure loss for packed bed applications with a convenient structure as adsorbent due to short diffusion path [7].

It can be observed that after 10 activation cycles both the outer layer and the carbonized tissue in the inner of the particle have been partially removed compared to the char (see SEM images of Figures 3.10 and 8.8). Likewise, a more open structure can be observed, in agreement with the larger volume of macropores determined by mercury porosimetry (Table 8.1). Such macropores can act as convenient channels for diffusion in adsorption applications.

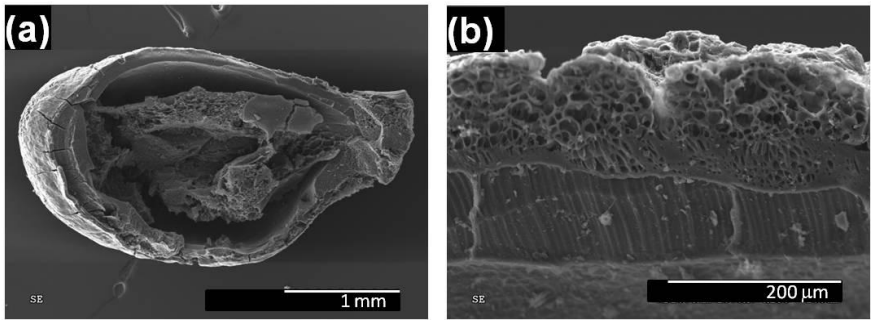

Figure 8.8. Cross section (a) and detail of wall of N-850 C10 sample (b).

References

[1] D. Jiménez-Cordero, F. Heras, N. Alonso-Morales, M.A. Gilarranz, J.J. Rodríguez. *Porous structure and morphology of granular chars from flash and conventional pyrolysis of grape seeds*. Biomass Bioenergy 2013; 54: 123 – 132.

[2] M. Polyakov, M. Poisot, W.E. Maurits, T. Drescher, A. Lotnik, L. Kienle, W. Bensch, M. Muhler, W. Grunert. *Carbon-stabilized mesoporous MoS2 - Structural and surface characterization with spectroscopic and catalytic tools*. Catal. Commun. 2010; 12(3): 231 – 237.

[3] A.NA. El-Hendawy. *Influence of HNO_3 oxidation on the structure and adsorptive properties of corncob-based activated carbon*. Carbon 2003; 41: 713 – 722.

[4] W.M.A.W. Daud, W.S.W. Ali. *Comparison on pore development of activated carbon produced from palm shell and coconut shell*. Bioresource Technology 2004; 93: 63 – 69.

[5] P.M. Álvarez, J.F. García-Araya, F.J. Beltrán, F.J. Masa, F. Medina. *Ozonation of activated carbons: Effect on the adsorption of selected phenolic compounds from aqueous solutions.* J. Colloid Interface Sci. 2005; 283: 503 – 512.

[6] L. Stobinski, B. Lesiak, L. Kövér, J. Tóth, S. Biniak, G. Trykowski, J. Judek. *Multiwall carbon nanotubes purification and oxidation by nitric acid studied by the FTIR and electron spectroscopy methods.* Journal of Alloys and Compounds 2010; 501: 77 – 84.

[7] M.J. Prauchner, F. Rodríguez-Reinoso. *Chemical versus physical activation of coconut shell: A comparative study.* Micro Meso Mater 2012; 152: 163 – 171.

Capítulo 9 / Chapter 9

Aplicación de carbones activados obtenidos a partir de Semillas de Uva como material de partida para electrodos usados en Supercapacitores

---

Application of Grape Seeds-based activated carbons as starting material for electrodes used in Supercapacitors

9.1. Resumen / Abstract

En este capítulo se estudia el almacenamiento electroquímico de energía en varios carbones activados utilizados en la preparación de electrodos usados para capacitores.

Para ello, se han usado tres series de carbones activados obtenidos mediante el método de activación cíclica de oxidación-desorción partir de char de semillas de uva. De las series activadas en fase gas, se han seleccionado la serie A275-850 activada con aire y la serie O275-850 activada con ozono, mientras que de las series activadas en fase líquida se eligió a la serie N850.

Mediante una adecuada selección de las condiciones de operación (método de oxidación y número de ciclos) es posible modificar el volumen y la distribución de tamaño de poro de los carbones activados y así, determinar la influencia de las propiedades texturales de estos carbones sobre el comportamiento electroquímico de supercapacitores simétricos carbón-carbón cuando se opera en diferentes electrolitos acuosos. Los resultados muestran que aunque la densidad de energía puede mejorarse utilizando electrolitos neutros, a causa de la mayor estabilidad de la ventana de voltaje que con los electrolitos ácidos o básicos, es importante adaptar las propiedades texturales de los carbones activados para mejorar la difusión de los iones dentro de los poros para asegurar la carga de la doble capa a elevadas densidades de corriente para alcanzar altas densidades de potencia.

9.2. Materials and Methods

The grape seeds char (GS Char) used as starting material was obtained by flash pyrolysis of the extracted seeds at 800 ºC for 2 h under nitrogen atmosphere, according to the results of Chapter 3 [1].

Three series of activated carbons from the char obtained were prepared by cyclic oxidation-desorption using three different oxidation procedures. In two activation series gas phase oxidation was employed, using air (21 % oxygen) and ozone (300 mgh^{-1} in air flow of 50 $mLmin^{-1}$) as activating agents: series A275-850 and O275-850, respectively (Chapters 5 and 6). The oxidation step of each cycle was carried out at 275 ºC for 2 h and a gas flow of 100 $mLmin^{-1}$ while the desorption step was carried out at 850 ºC for 2 h under a flow rate of 100 $mLmin^{-1}$ of nitrogen. Conditions for the switch from oxidation to desorption step were 10 $ºCmin^{-1}$ heating rate under nitrogen flow. For the last activation series a liquid phase oxidation was employed using boiling HNO_3 (30 %, v) under reflux for 20 min, N850 series. After oxidation, the samples were washed with distilled water until neutrality and dried in a muffle furnace at 105 ºC. Desorption step was carried out at same conditions that gas phase oxidation series (850 ºC, 2 h and 100 $mLmin^{-1}$ N_2 flow) (Chapter 8). For all experimental conditions, 3 to 7 activation cycles were performed in each series.

9.2.1. Chemical and Textural Characterization

The composition of activated carbons was analyzed by elemental analysis and X-ray photoelectron spectroscopy.

Surface area and total pore volume of the samples were measured by adsorption of N_2 at 77K and CO_2 at 273K. The surface area of the samples was calculated from N_2 isotherms using Brunauer-Emmett-Teller equation and the t-method for the micropore volume, whereas DA model was applied to CO_2 isotherms to determine surface area and the ultramicropore volume.

The $V_{microN2}/V_T$ ratio was used to assess the contribution of micropores to the total pore volume. The non-local density functional theory method was used to calculate both micropore and mesopore size distribution and the average micropore size was calculated by Stoeckli equation.

9.2.2. Electrochemical characterization

Electrode preparation and assembly of the supercapacitors was described in Chapter 2.

The electrochemical performance of the materials was evaluated in three aqueous electrolytes Na_2SO_4 0.5 $molL^{-1}$, KOH 6 $molL^{-1}$ and H_2SO_4 1 $molL^{-1}$ by cyclic voltammetry at 2 mVs^{-1} and galvanostatic charge/discharge at first using 200 mAg^{-1} in different range of maximum operating voltage: 0.6 – 2.0 V for Na_2SO_4 and 0.6 – 1.4 V for KOH and H_2SO_4, and later at a scan rate of 10 mVs^{-1} with only one voltage value and a variable current density from 100 to 30000 mAg^{-1}.

To obtain the ESR and the EDR, the impedance spectroscopy was carried out in 100 kHz to 300 mHz interval.

9.3. Results

9.3.1. Chemical and textural characterization

The composition of activated carbons obtained after 1, 4, 7 and 10 activation cycles is summarized in Table 9.1. In spite of all series was obtained from the same precursor, differences in composition of the activated carbons obtained were observed depending on the activating agent used. The Carbon percentage profiles along the activation process were similar for series activated in gas phase, showing a decrease with the activation cycles, especially for A275-850 C10 sample that shows the lower carbon mass fraction (52 %). In return, the N850 series shows a higher carbon mass fraction, increasing up to cycle 7 for decrease from that point.

The oxygen mass fraction for series activated in gas phase was higher, showing a trend to increase along the cycles while lower values and a decreasing profile was observed for N850 series. The Nitrogen mass fraction trend to increase along the activation cycles for all series although the values obtained are higher for N850 series.

Respect to the minor elements, only the presence of calcium, phosphorus and potassium in samples activated in gas phase even 10 activation cycles was noteworthy.

Table 9.1. Composition of activated carbons obtained by activation with air, ozone and HNO_3 after 1, 4, 7 and 10 activation cycles.

Sample	C (%)	H (%)	N (%)	S (%)	O (%)	P (%)	Ca (%)	K (%)
A275-850 C1	79.85	0.65	1.46	0.00	4.40	0.42	1.15	0.00
A275-850 C4	73.35	0.61	1.50	0.01	7.13	1.31	1.82	0.00
A275-850 C7	71.38	0.57	1.65	0.03	6.85	--	--	--
A275-850 C10	52.06	0.73	1.85	0.00	13.00	1.78	2.65	1.26
O275-850 C1	79.69	0.65	1.44	0.00	4.47	0.78	1.49	1.49
O275-850 C4	74.99	0.61	1.48	0.02	5.92	0.81	1.30	0.00
O275-850 C7	72.49	0.70	1.57	0.02	7.07	0.76	1.15	0.03
O275-850 C10	72.52	0.66	1.59	0.00	7.10	0.74	1.37	0.58
N-850 C1	82.48	0.59	1.81	0.00	4.13	0.67	0.77	0.44
N-850 C4	86.66	0.50	2.83	0.26	2.28	0.00	0.00	0.00
N-850 C7	88.42	0.49	3.80	0.12	2.25	--	--	--
N-850 C10	74.59	1.09	9.22	0.14	1.59	0.00	0.00	0.00

The N_2 adsorption-desorption isotherms for the activated carbon series are compiled in Figure 9.1. For all the samples, type I isotherms with a sharp increase of N_2 adsorption at low relative pressures were obtained. That means a general microporous structure for all the activated carbons but it can also be observed that adsorption capacity within a given series is strongly influenced by the number of cycles applied.

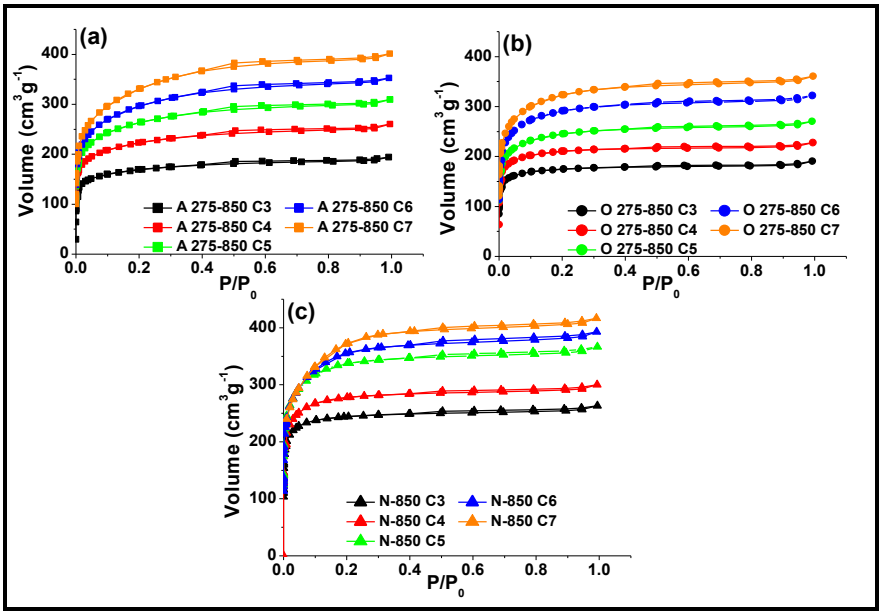

Figure 9.1. N_2 adsorption-desorption isotherms for carbons activated with (a) air, (b) ozone and (c) HNO_3.

The use of the different oxidants affects all the aspects of porous texture of the activated carbons, as evidenced by the results of different textural properties calculated from N_2 and CO_2 isotherms (Table 9.2).

Table 9.2. Textural parameters of the activated carbons.

Sample	S_{BET} (m^2g^{-1})	S_{DA} (m^2g^{-1})	L_0 (nm)	V_{mesoN2} (cm^3g^{-1})	$V_{microN2}$ (cm^3g^{-1})	$V_{microCO2}$ (cm^3g^{-1})	$V_{microN2}/V_T$ (%)
A275-850 C3	594	668	0.882	0.028	0.261	0.254	90.3
A275-850 C4	786	868	0.925	0.043	0.344	0.350	88.9
A275-850 C5	937	1021	1.202	0.051	0.413	0.432	89.0
A275-850 C6	1061	1127	1.391	0.063	0.467	0.494	88.2
A275-850 C7	1124	1260	1.476	0.081	0.498	0.582	86.0
O275-850 C3	614	790	0.761	0.012	0.269	0.312	95.8
O275-850 C4	741	947	0.778	0.021	0.328	0.385	94.1
O275-850 C5	840	1066	0.924	0.027	0.378	0.454	93.4
O275-850 C6	1004	1297	1.133	0.034	0.449	0.579	93.0
O275-850 C7	1121	1524	1.167	0.041	0.499	0.704	92.3
N-850 C3	857	1056	0.889	0.020	0.337	0.429	94.3
N-850 C4	981	1111	1.003	0.025	0.424	0.462	94.5
N-850 C5	1205	1239	1.147	0.035	0.515	0.559	93.6
N-850 C6	1240	1296	1.210	0.050	0.540	0.570	91.5
N-850 C7	1354	1309	1.301	0.047	0.581	0.583	92.6

For the three experimental series, the samples showed a constant increase in surface area along the activation cycles, both in S_{BET} and in S_{DA}. S_{BET} results was similar for the series oxidized in gas phase (1124 and 1121 m^2g^{-1} for air and ozone respectively after seven activation cycles applied), while oxidizing with HNO_3 higher porosity development was achieved (1354 m^2g^{-1} of S_{BET} after seven activation cycles). However, differences between gas-phase oxidants become significant for S_{DA}, with values of 1260 and 1524 m^2g^{-1} for air and ozone respectively, after the whole series of cycles. When nitric acid is used as oxidizing agent, S_{DA} values obtained are intermediate between air and ozone and very similar to S_{BET}. As a general conclusion it is possible to say that the porosity development with air and nitric acid is similar in terms of both S_{BET} and S_{DA} (slightly higher using nitric acid) while higher S_{DA} than S_{BET} can be achieved when ozone is used as oxidizing agent.

The results of specific surface area discussed above are in concordance with the values obtained for the average micropore size (L_0), that increased along the cycles for all the experimental conditions tested. Series showed highest S_{DA} values, that means higher microporosity development, also showed lowest L_0 (1.167, 1.301 and 1.476 nm for ozone, nitric acid and air respectively) after seven activation cycles. The air oxidation leads to the widest dispersion of pore sizes. Instead, the narrowest range of average pore size was achieved in ozone oxidation.

The simultaneous increase of micro and mesoporosity that can be deduced from S_{BET} and S_{DA} results discussed above was corroborated attending the monotonical increase of the volume of mesopores and micropores for the three experimental series. However, this increase does not occurs to the same extent for meso and micropores, as evidenced by the much higher increase values of mesopore volume than micropore volume and the increase of L_0 with the cycles applied. To support that the degree of microporosity from N_2 isotherm, calculated as $V_{microN2}/V_T$ (where V_T is $V_{microN2}$ + V_{mesoN2}), is presented in Table 9.2. The decrease of this factor with the activation cycles (90 – 86 % for air oxidation and 96 – 92 % for ozone and

nitric acid oxidation), even with the microporous nature of the samples, illustrates that the increase of mesoporosity takes place sharper than the increase of microporosity, agreeing to L_0 decrease. This fact can be explained by a enlarging of micropores and the pore wall destruction as a result of gasification [2, 3] or a thermal stress, that could induce a collapse of the microporous structure leading to the formation of mainly mesopores [4].

This observation can be also supported by the pore size distribution results obtained from the N_2 and CO_2 adsorption isotherms by the NLDFT method (Figure 9.2). In this figure, the results of PSD for three selected samples are compared (A275-850 C5, O275-850 C6 and N850 C4): one of each experimental series with similar S_{BET} (between 900 – 1000 m^2g^{-1}). The three samples show very similar PSD in the ultramicropore region (between 0.4 and 0.9 nm) with peaks at 0.45, 0.55 and 0.88 nm. This may suggests that the ultramicropore structure is not conditioned by preparation conditions but predetermined by the char. However, for NLDFT distribution calculated from N_2 isotherm (pore diameter higher than 1 nm) some differences between the samples can be seen, although the distribution profiles are centered in a narrow mesopore range (1.5 to 6 nm) for all samples. N850 C4 sample have the narrowest distribution (centered at 1.8 nm), followed by the O275-850 C6, centered at 2 nm, and finally the A275-850 C5 have the widest PSD, centered at 2.1 nm. Finally, no significant differences can be found in the pattern of mesoporosity in the 8 – 50 nm range, probably because of this porosity was present in the starting char.

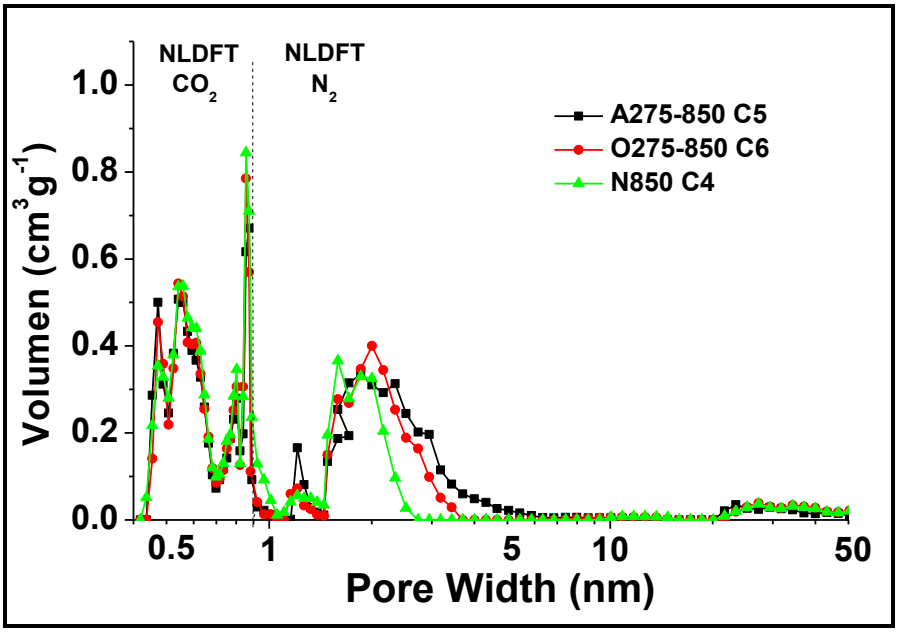

Figure 9.2. Pore size distribution by the NLDFT method from N_2 and CO_2 isotherms for selected samples with S_{BET} between 900 – 1000 m^2g^{-1}.

In conclusion, if the textural properties were summarized along the activation cycles for the different oxidant agents, Figure 9.3 shows that the most effective method for developing specific surface area using the smaller number of cycles is the HNO_3 based one. Figure 9.3 also show that even if air and ozone activation result in similar surface areas within cycles, air activation develops ultramicroporosity (see $V_{microCO2}$) and microporosity (see $V_{microN2}$) in the same extent since ozone oxidation drives to materials with more ultramicroporous character. For HNO_3 activation, the $V_{microCO2}$ are also slightly higher than the $V_{microN2}$.

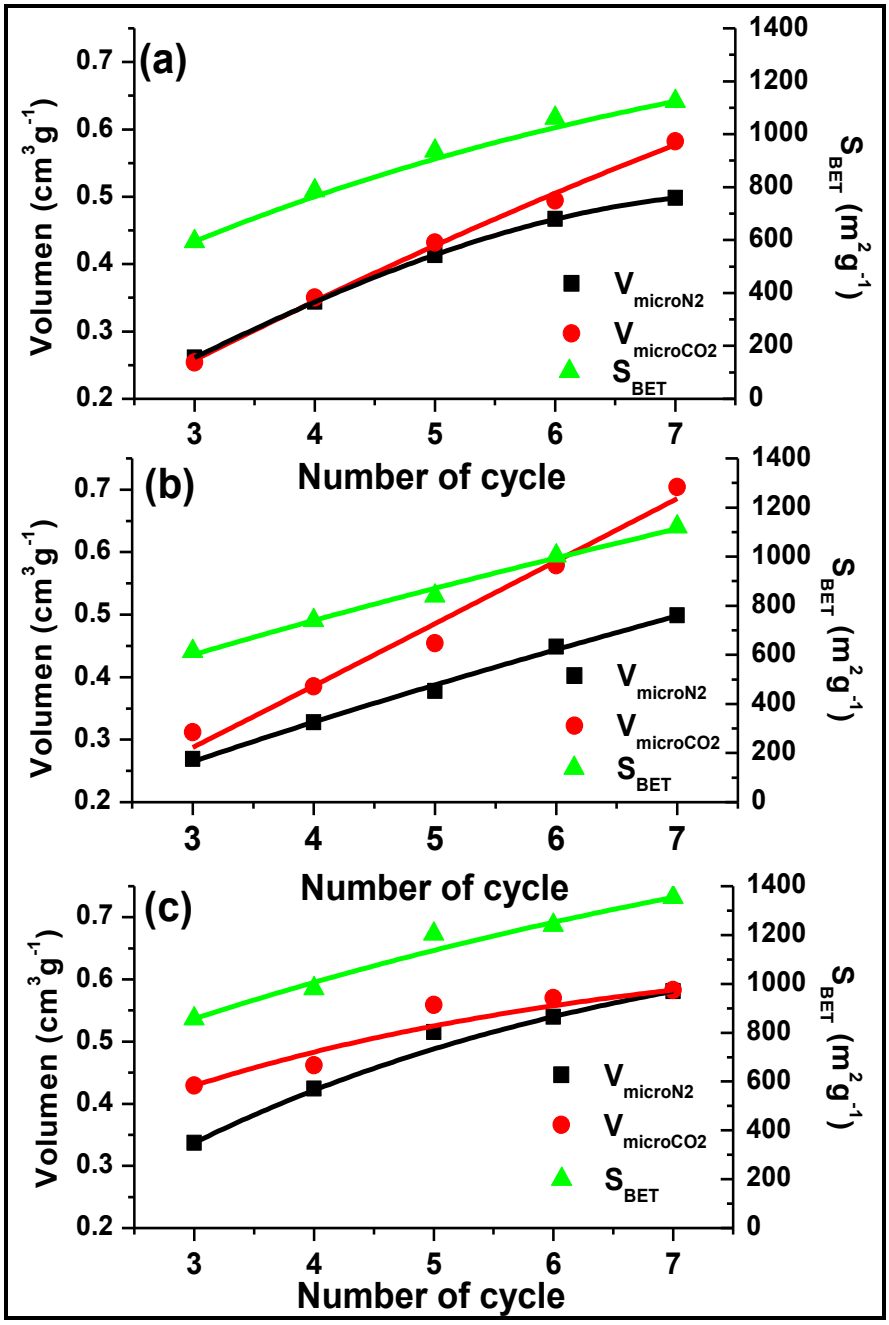

Figure 9.3. Micropore volume and BET surface area versus number of cycle for (a) air, (b) ozone and (c) HNO_3 series.

As a consequence, Figure 9.4 shows that if the BET surface area is presented versus the average pore size for the three series of porous materials, besides of the increase of L_0 follows the order air > ozone > HNO_3 series. That means that air oxidation drives to a more important widening of the porosity along activation cycles than ozone activation and even more than HNO_3 one.

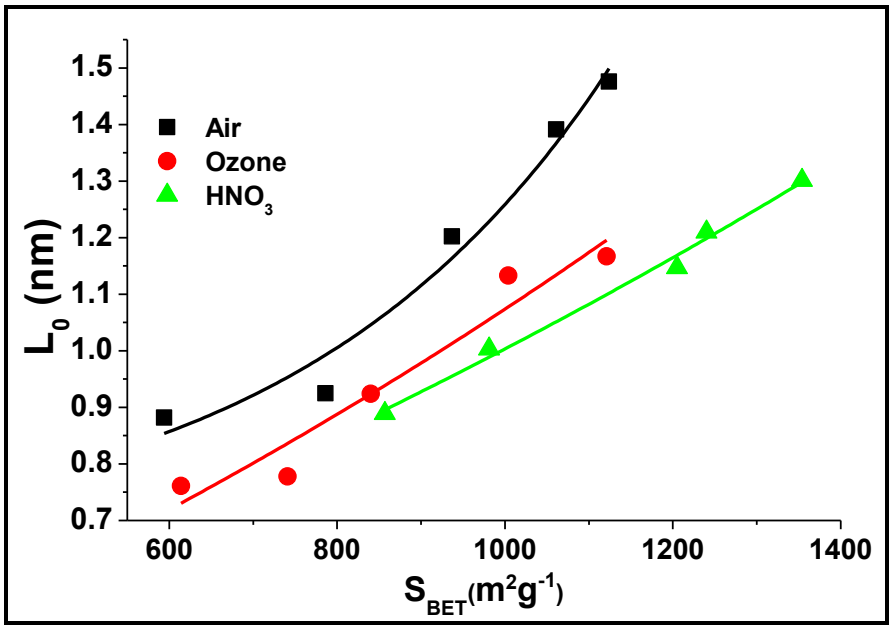

Figure 9.4. Average pore size versus BET surface area.

So by adequate selection of operating conditions (oxidation procedure and number of cycles) it is possible to tune the volume and pore size distribution of activated carbons. In such a way, those materials are very good candidates for studying the influence of carbon textural properties on the electrochemical behavior of carbon-carbon symmetric supercapacitors operating in different aqueous electrolytes.

9.3.2. Electrochemical characterization

Firstly, the materials are characterized as electrode activated carbons in symmetric two electrode capacitors by cyclic voltammetry, using a voltage range from 0.6 to 2.0 V for Na_2SO_4 and from 0.6 to 1.4 V for KOH and H_2SO_4 at a constant rate of 2 mVs^{-1} and by galvanostatic charge/discharge, at a constant current density of 200 mAg^{-1}. Figure 9.5 shows the plots of these techniques for the O275-850 C5 sample in Na_2SO_4 as example (for the rest of the samples, the diagrams were very similar). The CV curves exhibit a typical capacitor behaviour showing a nearly rectangular shape for cell voltages up to 1.0 V. For higher cell voltages, the deviation to the rectangular shape is related to pseudocapacitive reversible reactions taking place at the positive and the negative electrode i.e. fast redox reactions between the oxygen surface functionalities and the electrolyte at the positive electrode and redox reactions related to the reversible electrosorption of hydrogen at the negative one [5]. In the same direction, galvanostatic charge/discharge curves demonstrate a pure capacitive behaviour, with straight lines, at cell voltages up to 1.0 V. For values higher than 1.0 V, there is a distortion of the linearity associated to the above mentioned pseudo-capacitive effects.

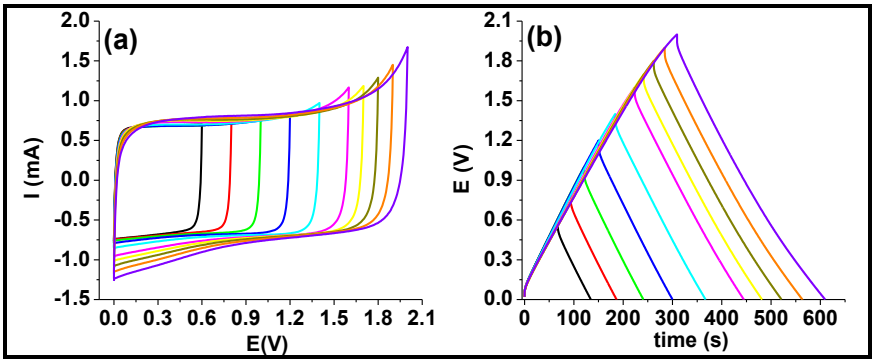

Figure 9.5. (a) Cyclic voltammetry and (b) galvanostatic charge/discharge in Na_2SO_4 for O275-850 C5 sample.

These experiments allowed selecting the optimum operating voltages using for each electrolyte to be used in the further characterization of the samples. In particular, this maximum operating cell voltage has been determined from the efficiency (calculated as the ratio between the discharge and charge times obtained from the galvanostatic charge/discharge) which must be higher than 98 %. The voltages chosen were 1.8 V for Na_2SO_4, 0.8 V for KOH and 1.0 V for H_2SO_4.

The gravimetric capacitance values calculated by galvanostatic charge/discharge at the maximum cell voltage for each electrolyte, plotted versus the S_{BET} for the three series of activated carbons are shown in Figure 9.6. In general, the lowest values of capacitance are obtained using Na_2SO_4 as electrolyte while H_2SO_4 gave highest results. These differences can be explained due to the difference in conductivity of the electrolyte i.e. 80, 800 and 1000 $mScm^{-1}$ for Na_2SO_4, KOH and H_2SO_4 respectively. For Na_2SO_4 and KOH as electrolytes, Figure 9.6 shows that there is not a relationship between the capacitance and the specific surface area. However, in H_2SO_4, there is an increase of the capacitance when increasing S_{BET} for all the series of activated carbons. The last is the expected behaviour and the reasons for do not obtaining the same in Na_2SO_4 and KOH are probably also related to conductivity issues.

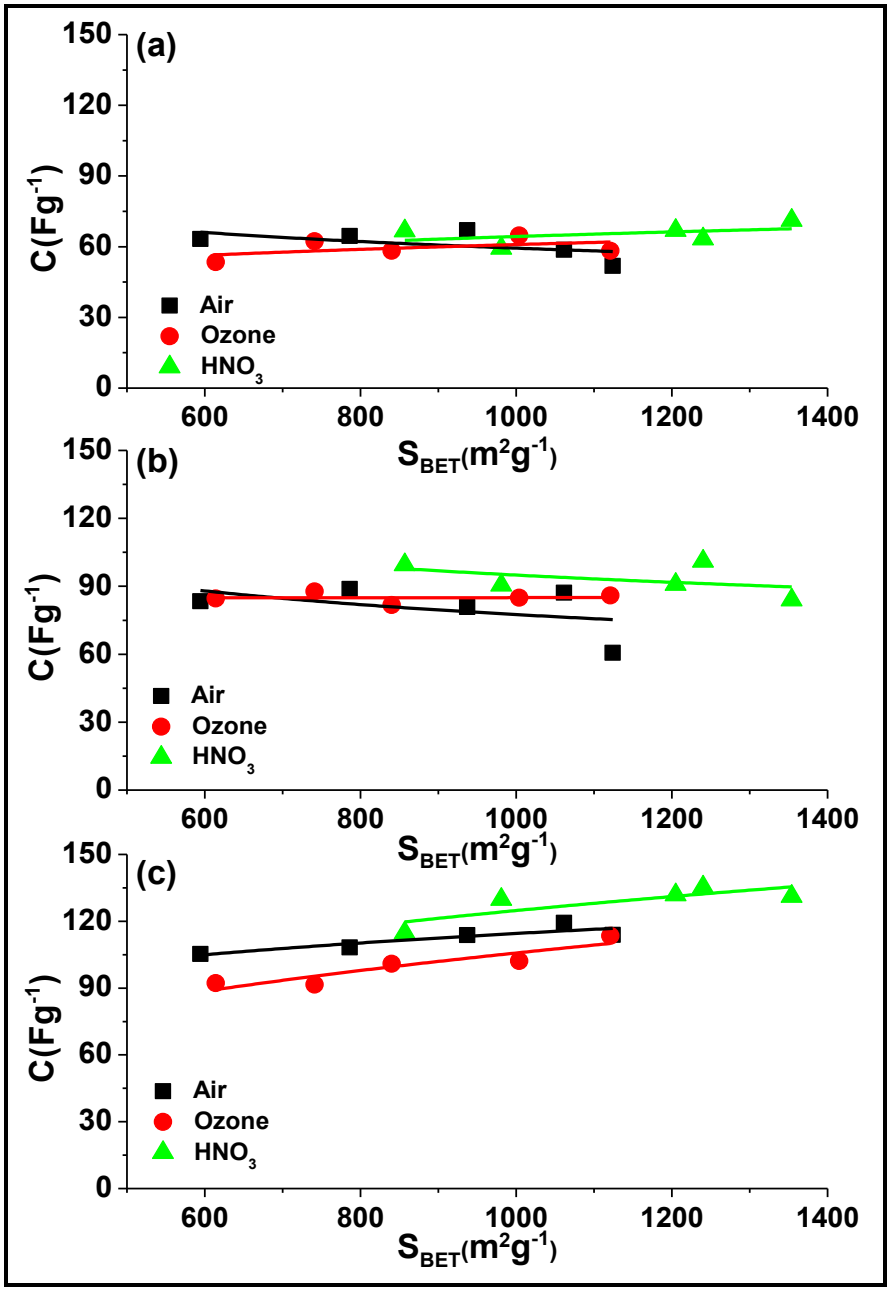

Figure 9.6. Gravimetric capacitance of the three series of activated carbons vs. BET surface area. The results were obtained by galvanostatic charge/discharge at 200 mAg^{-1} with a voltage of (a) 1.8 V in 1 $molL^{-1}$ Na_2SO_4, (b) 0.8 V in 6 $molL^{-1}$ KOH and (c) 1.0 V in 1 $molL^{-1}$ H_2SO_4.

In order to explore such possiblitiy, impedance spectroscopy has been performed over the grape seeds carbon based supercapacitors in all the electrolytes. Table 9.3 collects the equivalent series resistances (ESR) which are obtained from the high frequency limit (10kHz) of the impedance spectrum and is related to the sum of the ohmic resistances of the electrode materials, contacts and electrolyte.

Table 9.3. Electrical series resistance for the three series of activated carbons.

Sample	ESR (Ω)		
	Na_2SO_4	KOH	H_2SO_4
A3	1.473	0.721	0.728
A4	1.507	0.604	0.509
A5	1.342	0.632	0.510
A6	1.776	0.655	0.482
A7	1.208	0.579	0.571
O3	1.084	0.426	0.701
O4	1.125	0.915	0.728
O5	1.549	0.537	0.473
O6	1.363	0.708	0.633
O7	1.344	0.726	0.523
N3	1.415	0.694	0.439
N4	1.454	0.636	0.471
N5	1.368	0.671	0.537
N6	1.486	0.525	0.452
N7	1.245	0.528	0.490

The table shows that ESR values, whatever the carbon material, in each electrolyte follow the inverse trend to their conductivity i.e. $ESR_{Na2SO4} > ESR_{KOH} > ESR_{H2SO4}$. Moreover, the ESR does not depends on the electrode material as for each electrolyte the values are nearly constant. Hence the porous texture variations through the activation cycles do not modify the conductivity of the carbon material.

From the impedance spectroscopy can be also extracted the equivalent distributed resistance (EDR) which is mainly related to the diffusion of ions into the charge storing material and is obtained from the so-called Nyquist plots (representing the real part of the resistance versus the imaginary one) by extrapolating the nearly linear low frequency region down to the real part axis.

Figure 9.7 shows that EDR depends on the electrolyte used and on the micropore volume of the carbon electrode material. For a highly conductive electrolyte as H_2SO_4 there is almost no relationship between the EDR and the micropore volume, indicating that the ions easily diffuse into the micropores whatever their size. However when the electrolyte is less conductive, as for KOH or Na_2SO_4, is observed an increase of the resistance when the micropore volume increases. Such effect is more visible for the less conductive electrolyte i.e. Na_2SO_4, indicating that there is a kinetic barrier for the ions to diffuse into the microporous when the mobility of the ions in the electrolyte is low. Moreover, the fact that this effect is more marked for the HNO_3 series is related with (i) the higher microporosity developed in comparison to the other two carbon series (see Figure 9.3) and (ii) the smaller amount of oxygen surface functionalities (see Table 9.2) and therefore to the worst wetability of the carbon electrode surface.

Therefore, the reasons why is not observed the same increase of the capacitance vs S_{BET} when using Na_2SO_4 or KOH as electrolyte than when using H_2SO_4 (Figure 9.6) is related to the increase of the ions diffusion resistance to penetrate de porosity in such media when developing the surface and therefore the micropore volume.

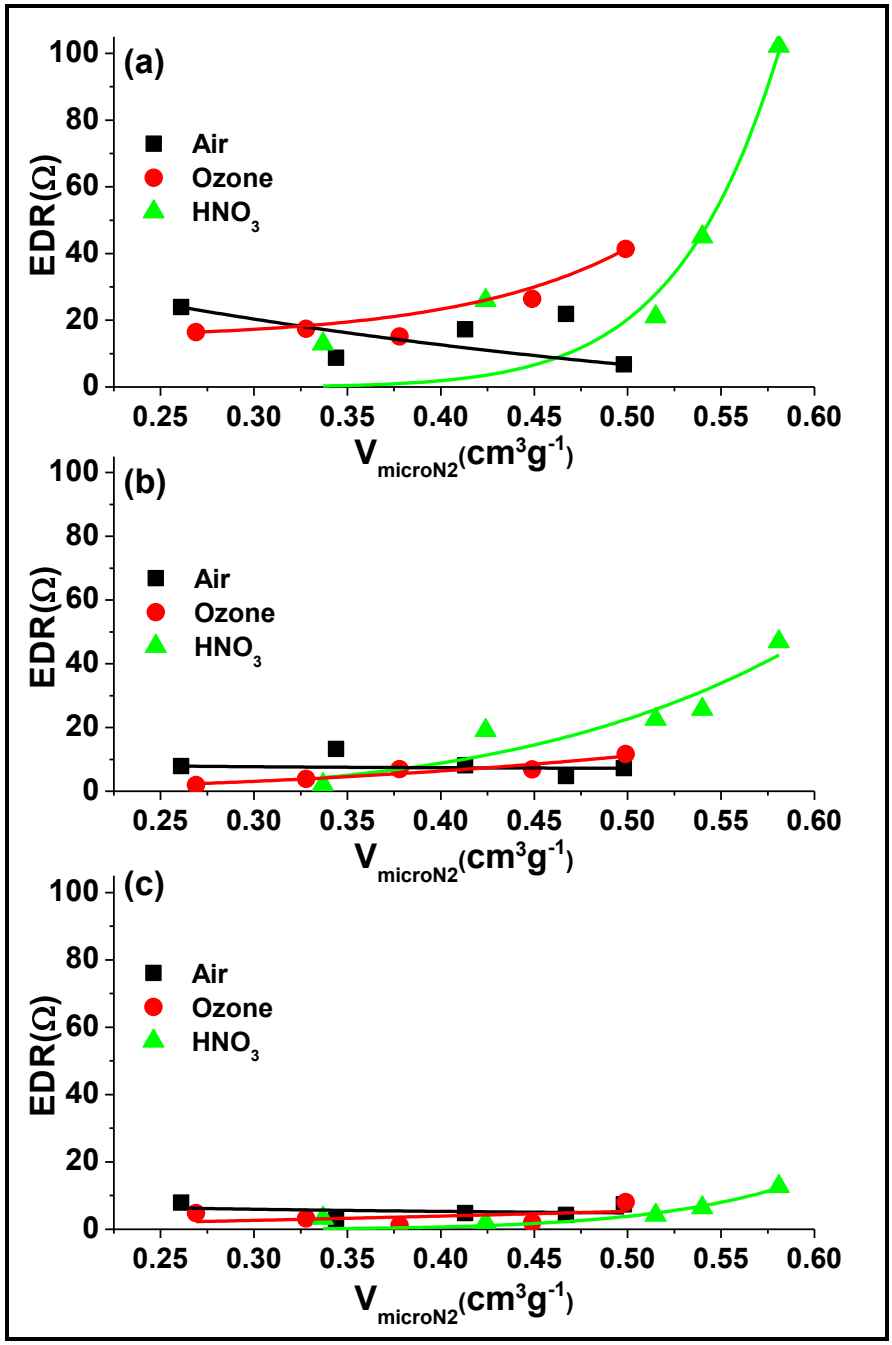

Figure 9.7. EDR results obtained by impedance spectroscopy of the three series of activated carbons vs. micropore volume in the three electrolytes: (a) Na_2SO_4, (b) KOH and (c) H_2SO_4.

In addition, when using H_2SO_4 as electrolyte, where kinetic effects do not much apply, Figure 9.6 shows that the three series of carbon follow the same ascendant trend of C vs S_{BET} but capacitance values are slightly different. The fact that the gravimetric capacitance values for the same value of surface area follow the order HNO_3 > Air > Ozone series, that is related to their different textural properties. Firstly, HNO_3 series present higher amount of micropores for accommodating the charges than the other two series (Figure 9.3). Secondly, comparing ozone and air series, even if the developed specific surfaces within activation cycles are similar, for the air series the micropores volumes obtained by N_2 and CO_2 adsorption are close since for the ozone series the micropore volume obtained by CO_2 adsorption is larger than the one obtained by N_2 adsorption. Such results indicate that for the ozone series the micropores are narrower than for the air one [6] as is also confirmed by the smaller L_0 values calculated for the ozone series (see Figure 9.4). Therefore, the small size of the micropores for the ozone series could induce a kind of ion sieving which could explain that the gravimetric capacitances are smaller than for air series.

In order to better asses the effect of the porous texture on the electrochemical performance of porous carbons in aqueous electrolytes, Figures 9.8, 9.9 and 9.10 present the specific capacitance as a function of the average pore size obtained in the three electrolytes at different current densities. For small current densities i.e. 200 mAg^{-1}, the known trend in which the specific capacitance increases for average pore sizes smaller than 1 nm [7, 8] is obtained independently of the electrolyte used for the supercapacitors built with all the carbon series. Such results confirm that the double layer is more efficiently formed in pores of this size [7, 8]. Moreover, the less effective character of larger pores versus the double layer formation is reflected on the decrease of the Cs when increasing L_0. The differences in Cs within the carbon series for the same electrolyte are related to the differences in porous texture already discussed above.

However, keeping in mind that supercapacitors are power devices, it is necessary to explore the electrochemical behaviour during fast charging i.e. at high current densities. Figures 9.8, 9.9 and 9.10 show that by increasing the current density, the Cs vs L_0 becomes an straight line when Na_2SO_4 is used as electrolyte since the same trends than at small charge densities are found for KOH and H_2SO_4. Such results are in concordance to the EDR results presented in Figure 9.7. In fact, as the diffusion of ions inside the micropores is kinetically unfavourable in the case of a low conductive electrolyte as Na_2SO_4, this effect will be more visible when faster the charge-discharge of the supercapacitor is done. Therefore, for electrolytes as Na_2SO_4, small micropores have an enhancing effect on the capacitance for low current densities but they have a negative effect on the capacitance when increasing the charge density. This is also the reason why the current density has the most detrimental effect on the capacitance of the carbon materials of the ozone series in reason of their smaller micropores size.

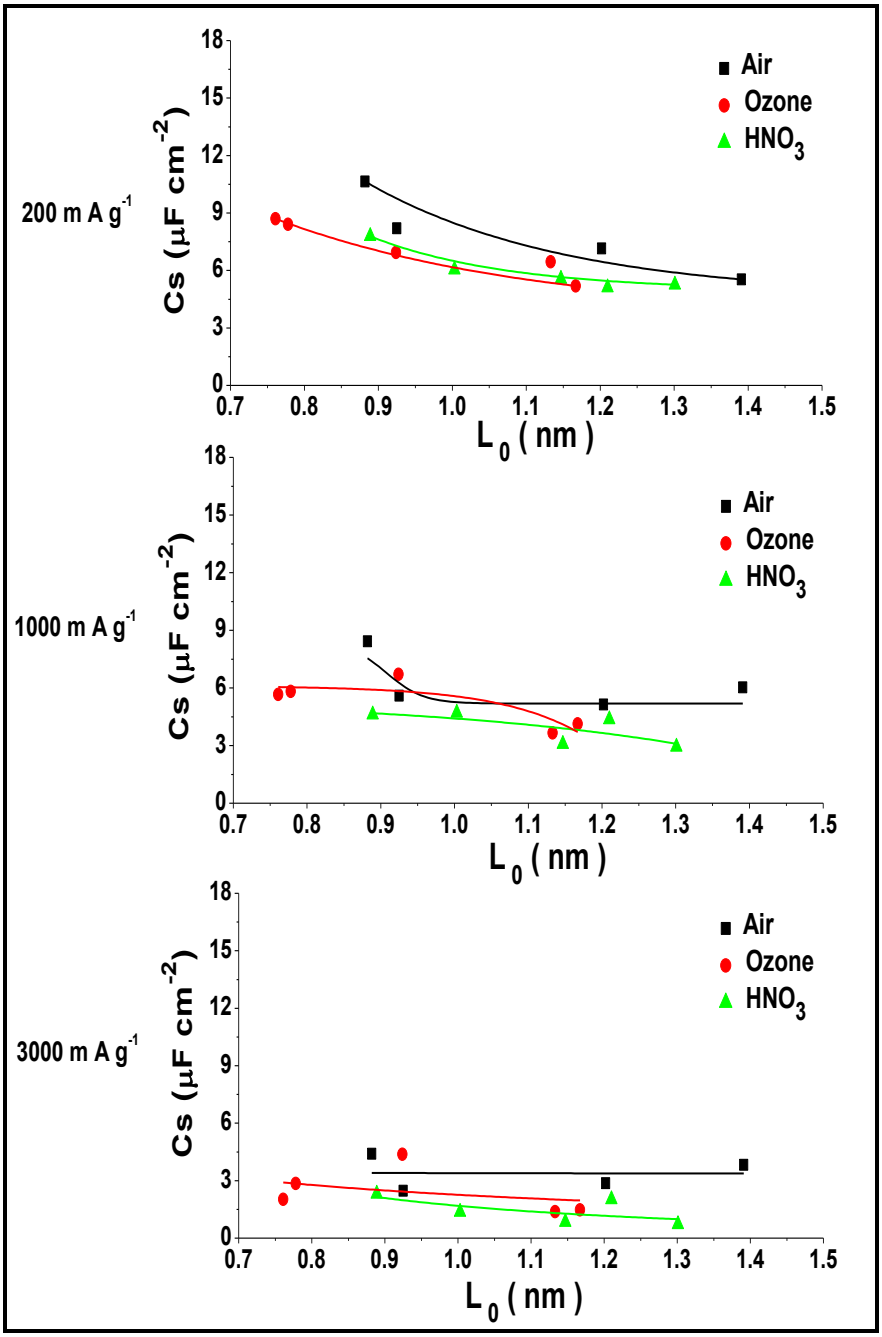

Figure 9.8. Specific capacitance vs L_0 at different current densities in Na_2SO_4.

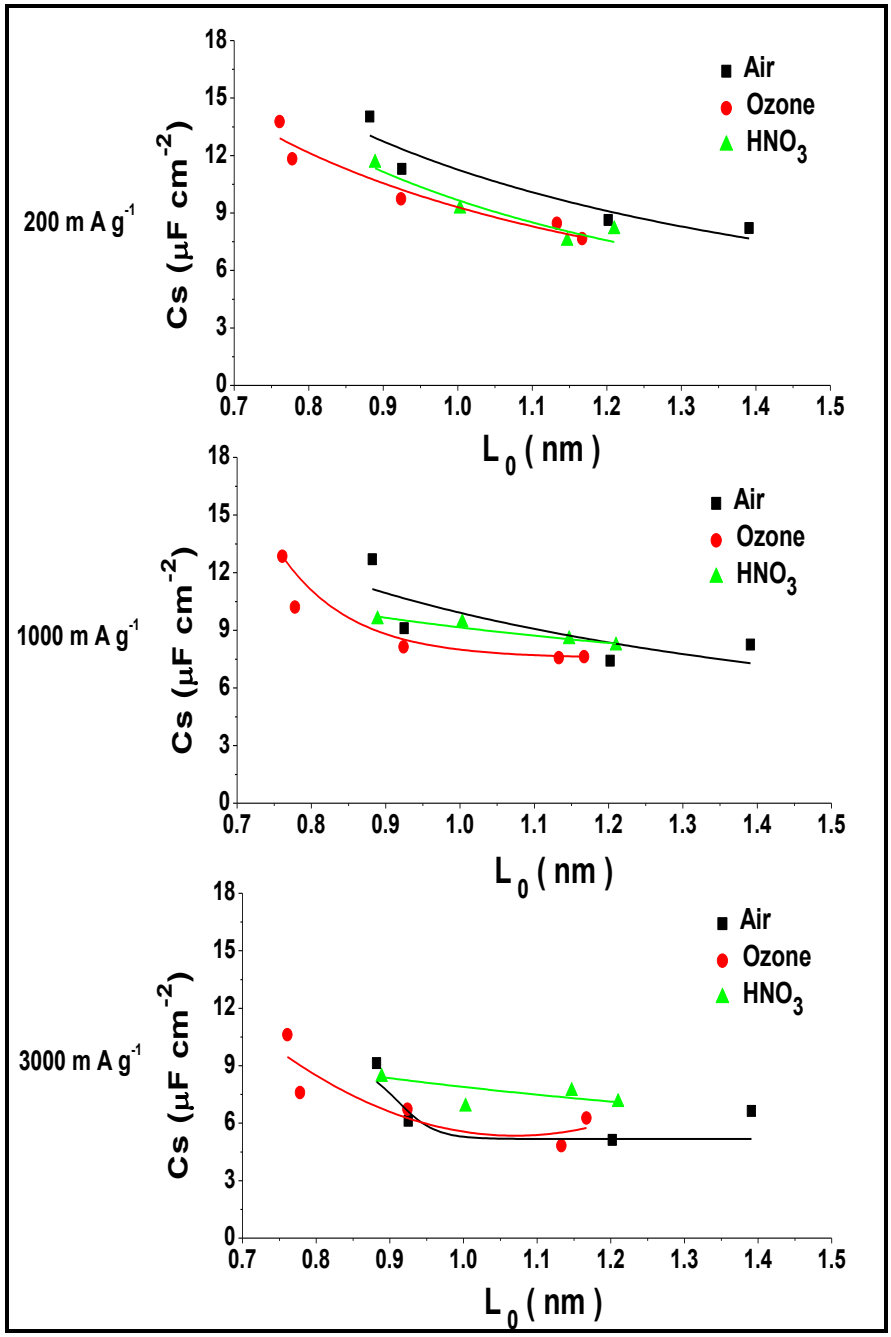

Figure 9.9. Specific capacitance vs L_0 at different current densities in KOH.

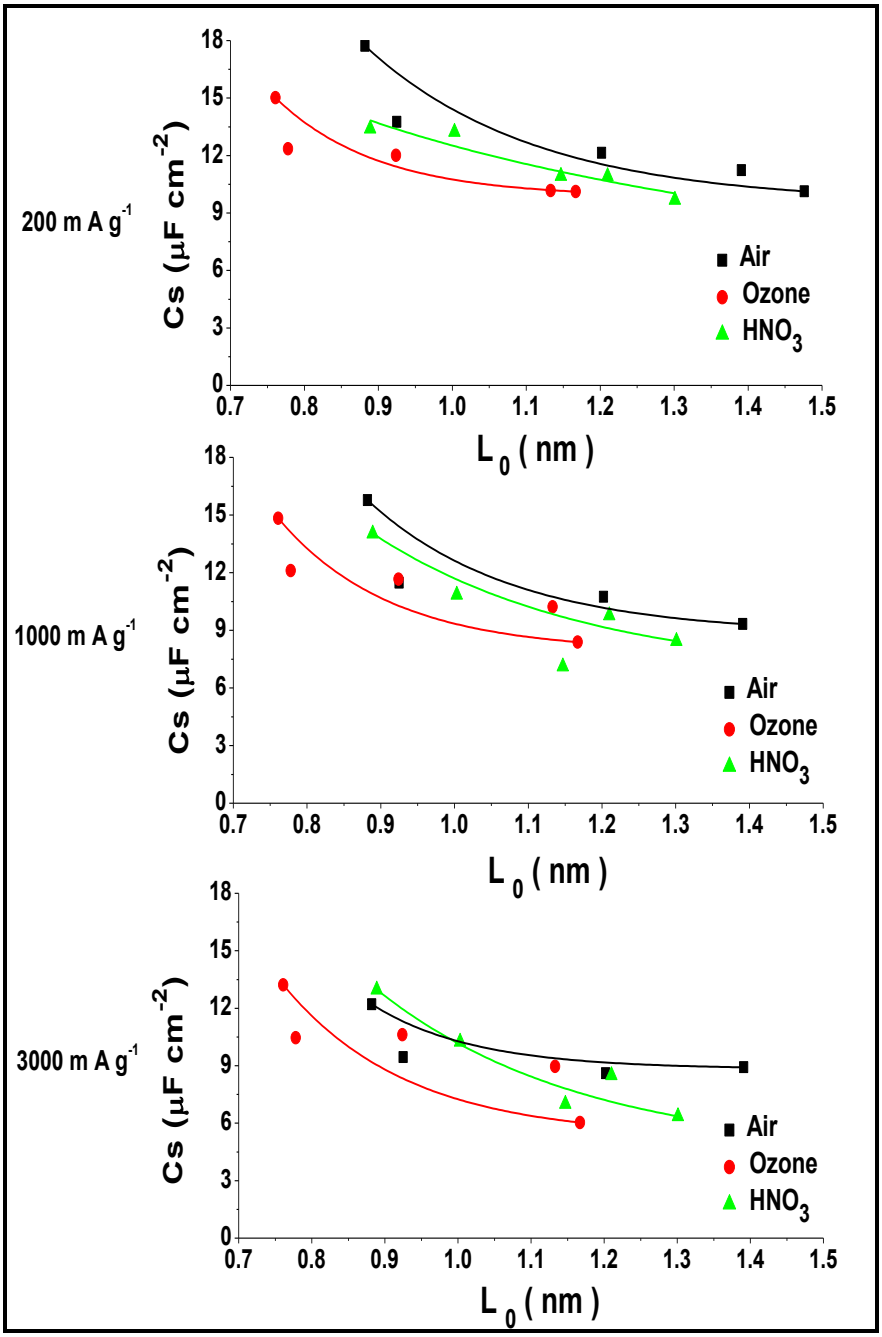

Figure 9.10. Specific capacitance vs L_0 at different current densities in H_2SO_4.

In the same direction, if the capacitance retention (expressed as the percentage of the capacitance obtained at low current densities) is plotted versus the current density for one sample of each series having a similar specific surface area i.e. A275-850 C5, O275-850 C6 and N850 C4 with S_{BET} ~1000 m^2g^{-1} (Figure 9.11), it can be observed that the most pronounced capacitance lost is always obtained when using Na_2SO_4 as electrolyte. Moreover, the results presented in Figure 9.10 confirm that a narrow microporosity can be a disadvantage when operating at high current densities in a poorly conductive electrolyte as Na_2SO_4. In particular, the differences between electrolytes are more marked for the N850 C4 carbon having a smaller average pore size i.e. 1.0 nm than for the sample A275-850 C5 having a wider one i.e. L_0 of 1.2 nm, even if they have the same specific surface area.

Therefore, although energy density can be improved using neutral electrolytes in reason of their higher stability potential window than the acidic or basic ones, it is important to adapt the porous texture of the carbon material for improving the ions diffusion inside the porosity for assuring the charging of the double layer at high current densities to attain high power densities.

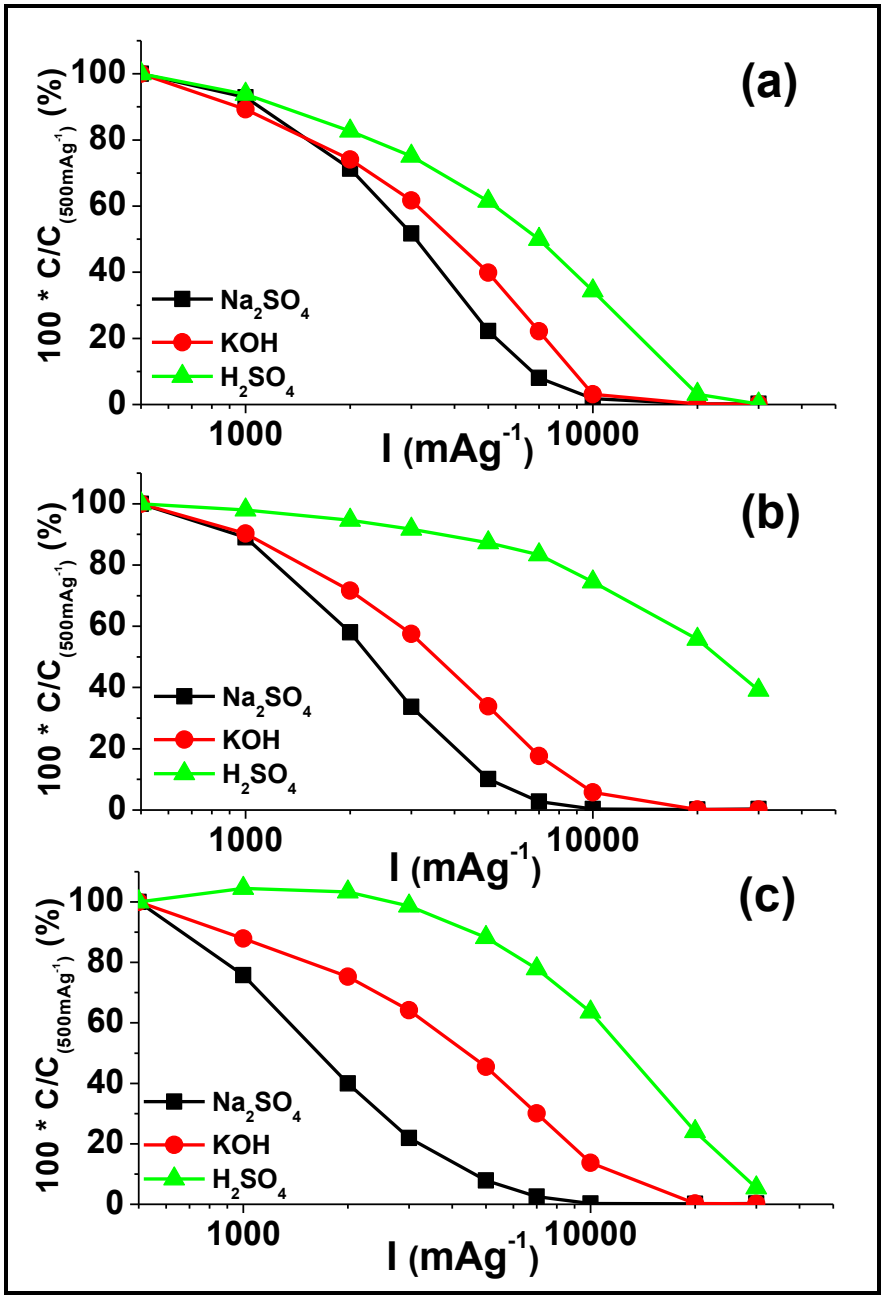

Figure 9.11. Capacitance vs current density plots obtained by galvanostatic charge/discharge with a voltage 1.8 V in Na_2SO_4, 0.8 V in KOH and 1.0 V in H_2SO_4 for activated carbons (a) A275-850 C5, (b) O275-850 C6 and (c) N850 C4.

In this sense Figure 9.12 depicts the Ragone plots for the supercapacitors built with the three samples of the different series having similar specific surface areas but different average pore sizes. It is clear that for small powers, corresponding to small current densities and high discharge times, the energy density is always higher in Na_2SO_4 independently of the porous texture of the electrode active material in reason of the higher cell voltage. For the same reasons, the less performing electrolyte is always KOH because the low cell voltage that can be used. Such differences are more visible when using the carbon with smaller average pore size i.e. N850 C4 as electrode material. In fact, higher values of maximum extractable values (E_{max}) can be obtained for the N850 C4 based supercapacitor than for the A275-850 C5 one in Na_2SO_4 as is reported in Table 9.4. However, for small discharge time ranging between 10 s and 1 s which is usually the operation range for a supercapacitor, the advantages of using the high stability potential window Na_2SO_4 are not visible anymore. In particular, for the N850 C4 based supercapacitor the extractable energy at a given power is now smaller in Na_2SO_4 than in H_2SO_4 as electrolyte. Table 9.4 shows that for the N850 C4 supercapacitor, only 36 % of the maximum energy is retained at 10 s discharge time in Na_2SO_4 since 94 % is done in H_2SO_4. Contrarily, for the A275-850 C5 based supercapacitor, having a smaller E_{max} in Na_2SO_4 than N850 C4, 65 % of this energy can be kept at 10 s. Therefore higher energy and power densities can be extracted at small times for the A275-850 C5 supercapacitor than for the N850 C4 one. Moreover, contrarily to the N850 C4 supercapacitor, the A275-850 C5 one presents more important E(10 s) values in Na_2SO_4 than in H_2SO_4.

Hence, for taking profit of all the advantages of a non corrosive, high energy potential window electrolyte as Na_2SO_4, it is necessary to use carbon materials having a micropore size enough narrow to ensuring the efficiency of the double layer formation for giving high energy densities but not too much narrow for avoiding diffusion problems of such a poor conductive electrolyte inside the porosity and to keep enough energy at high power densities.

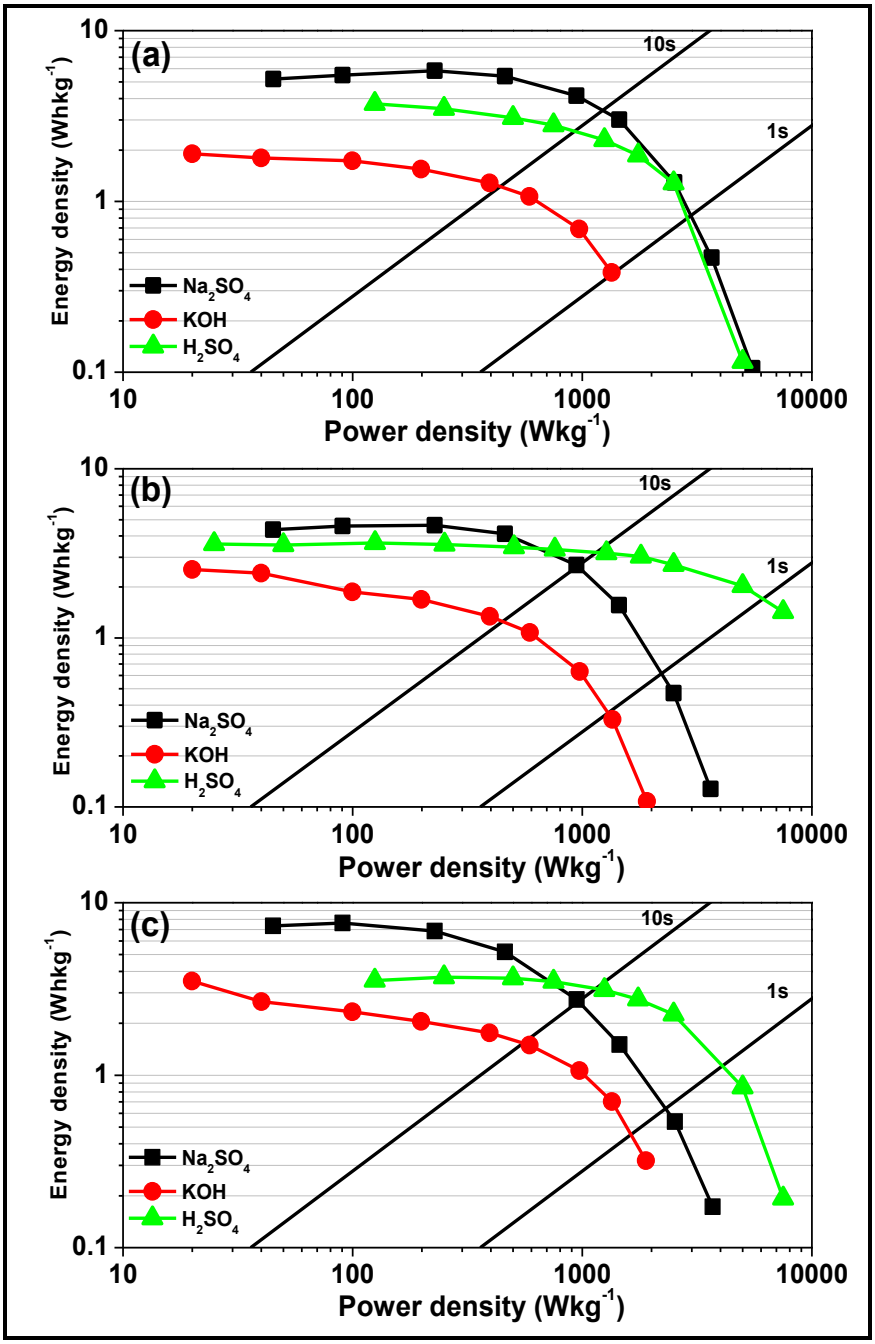

Figure 9.12. Ragone plot for supercapacitors operating in Na_2SO_4, KOH and H_2SO_4 using as electrode active material (a) A275-850 C5, (b) O275-850 C6 and (c) N850 C4.

Table 9.4. Maximum energy (obtained at a current density of 200 mAg^{-1}), energy and power density in 10 s for A275-850 C5 and N850 C4 samples.

Electrolyte	A275-850 C5			N850 C4		
	E_{max} (Wh kg^{-1})	E(10s) (Wh kg^{-1})	P(10s) (W kg^{-1})	E_{max} (Wh kg^{-1})	E(10s) (Wh kg^{-1})	P(10s) (W kg^{-1})
Na_2SO_4	5.5	3.6	1176	7.6	2.7	945
H_2SO_4	3.7	2.7	843	3.5	3.3	1049
KOH	1.8	1.3	351	2.7	1.7	473

References

[1] D. Jiménez-Cordero, F. Heras, N. Alonso-Morales, M.A. Gilarranz, J.J. Rodríguez. *Porous structure and morphology of granular chars from flash and conventional pyrolysis of grape seeds*. Biomass Bioenergy 2013; 54: 123-132.

[2] K.S.W. Sing, D.H. Everett, R.A.W. Haul, L. Moscou, R.A. Pierotti, J. Rouquerol, T. Siemieniewska. *Reporting physisorption data for gas/solid systems with special reference to the determination of surface area and porosity*. Pure Appl. Chem. 1985; 57(4): 603 – 619.

[3] P.M. Álvarez, J.F. García-Araya, F.J. Beltrán, F.J. Masa, F. Medina. *Ozonation of activated carbons: Effect on the adsorption of selected phenolic compounds from aqueous solutions.* J. Coll. Int. Sci. 2005; 283(2): 503 – 512.

[4] E. Raymundo-Piñero, F. Béguin. Interface science and technology, Volume 7. Chapter 6: Application of nanotextured carbons for supercapacitors and hydrogen storage. Academic Press 2006. P. 293 – 308.

[5] F. Béguin, E. Raymundo-Piñero, E. Frackowiak. *Carbons for electrochemical energy storage and conversion systems*. Chapter 8: Electrical double-layer capacitors and pseudocapacitors. CRC Press; 2010. P. 334.

[6] D. Cazorla Amorós, J. Alcañiz Monge, M.A. de la Casa Lillo, A. Linares Solano. *CO_2 as an adsorptive to characterize carbon molecular sieves and activated carbons*. Langmuir 1998; 14(16): 4589 – 4596.

[7] J. Chmiola, G. Yushin, Y. Gogotsi, C. Portet, P. Simon, P.L. Taberna. *Anomalous Increase in Carbon Capacitance at Pore Sizes Less Than 1 Nanometer*. Science 2006; 313(5794): 1760 – 1763.

[8] E. Raymundo-Piñero, K. Kierzek, J. Machnikowski, F. Béguin. *Relationship between the nanoporous texture of activated carbons and their*

capacitance properties in different electrolytes. Carbon 2006; 44(12): 2498 – 2507.

CONCLUSIONES

CONCLUSIONS

Conclusiones

El estudio sobre la obtención de materiales carbonosos a partir de neumáticos fuera de uso y semillas de uva mediante pirólisis y activación por ciclos de oxidación-desorción, y su posterior aplicación en el almacenamiento de energía, ha dado como resultado las conclusiones que se recogen a continuación.

Por lo que se refiere a la pirólisis de semillas de uva, la extracción previa del aceite que contienen y la velocidad de calentamiento no tienen una influencia clara ni en el rendimiento ni en la composición elemental. Por el contrario, la temperatura de pirólisis muestra una influencia importante sobre la superficie específica, alcanzándose valores máximos de S_{BET} y S_{DA} a 600 – 800 ºC y 800 ºC, respectivamente. Asimismo, los valores de superficie específica son mayores en el caso de las muestras preparadas mediante pirólisis flash.

El *char* obtenido en las condiciones óptimas de pirólisis (800 ºC, FH) posee una S_{DA} de 505 m^2g^{-1}, una S_{BET} de 47 m^2g^{-1}, una distribución de tamaño de poro bimodal con micro y macroporosidad ($V_{microCO2}$ = 0,2 cm^3g^{-1} y V_{macro} = 0,7 cm^3g^{-1}), tiene morfología granular y muestra una buena resistencia a la atrición, que va aumentando conforme se van desgastando las capas externas de la partícula.

La activación por ciclos de oxidación-desorción es un método eficaz para desarrollar porosidad, tanto en el *char* obtenido a partir de neumáticos fuera de uso, como de semillas de uva, y que permite obtener materiales granulares. Las condiciones de activación pueden ser ajustadas para proporcionar un equilibrio entre superficie específica y *burn-off* y un tamaño medio de poro determinado.

La activación de *char* de neumáticos fuera de uso ha proporcionado carbones activados fundamentalmente mesoporosos. En la activación con aire, el tamaño de partícula inicial y la temperatura de desorción afectan

significativamente al *burn-off* y a las propiedades texturales de los carbones activados obtenidos. Los mayores *burn-offs* se obtienen para los tamaños de partícula extremos (L y S) y para las temperaturas de desorción mayores (650 y 750 ºC). El S_{BET}, en general, aumenta con el número de ciclos, destacando la serie L-A650, que presenta diferencias notables respecto al resto de series desde el tercer ciclo. El tamaño medio de poro desciende desde el primer ciclo para todas las series, alcanzando valores entre 12 y 30 nm tras 6 ciclos y en torno a 10 nm tras 20 ciclos, con una mayor contribución de los mesoporos de mayor tamaño para las muestras preparadas a temperaturas de desorción altas. El análisis del volumen de poro muestra que la mesoporosidad aumenta paulatinamente desde el primer ciclo, mientras que el microporo comienza a desarrollarse a partir del 4º ciclo. Los resultados de la caracterización por TPO indican que la aplicación de 20 ciclos de activación conduce a la completa eliminación del carbón más reactivo presente en el *char* inicial, lo que puede estar relacionado con el desarrollo inicial de mesoporosidad.

El mayor desarrollo de superficie específica en la activación con aire de *char* de neumáticos se ha obtenido para un tamaño de partícula inicial de 2 mm y una temperatura de desorción de 650 ºC (serie L-A650), alcanzándose valores de S_{BET} cercanos a 600 m^2g^{-1} para un *burn-off* en torno al 45 % y manteniéndose la morfología granular del *char*.

De los oxidantes en fase líquida evaluados (HNO_3, H_2O_2 y $(NH_4)_2S_2O_8$) en la activación de *char* de neumáticos fuera de uso, la oxidación con ácido nítrico y con peróxido de hidrógeno condujo a un mayor desarrollo de porosidad que la oxidación con persulfato amónico. Tras 15 ciclos de activación se observó un aumento continuo del *burn-off*, que fue mayor para los carbones activados con ácido nítrico. Al evaluar la concentración del oxidante, se ha encontrado que una mayor concentración conduce a un mayor *burn-off*, especialmente en el caso del peróxido de hidrógeno, aunque no se han observado diferencias notables en términos de S_{BET} por unidad de *burn-off*. El análisis del volumen de poros muestra que la mesoporosidad

aumenta de manera destacada en los primeros ciclos para las series activadas con ácido nítrico, y en menor medida para las activadas con peróxido de hidrógeno y persulfato amónico, mientras que el microporo se desarrolla sólo para las series tratadas con ácido nítrico y a partir del 3º ciclo. Para las series de muestras obtenidas con concentración de oxidante al 30 % se produce un colapso de los microporos a partir del ciclo 10, que se corresponde con un aumento notable del volumen de mesoporo a partir de ese punto. El tipo de oxidante utilizado no afecta al tamaño medio de poro, pero la concentración de oxidante sí muestra influencia.

La activación con HNO_3 y H_2O_2 al 30 % permitió alcanzar el mayor desarrollo de S_{BET} con valores de 750 y 400 m^2g^{-1} y un tamaño medio de poro de 12 y 17 nm, respectivamente, pero a costa de valores de *burn-off* del 90 %.

La activación con aire de *char* de semillas de uva ha permitido obtener principalmente sólidos micro y macroporosos. Los valores más altos de *burn-off*, S_{BET} y S_{DA} se obtuvieron por la combinación de las temperaturas de oxidación y desorción más altas (275–850 y 275–950 ºC), aunque las temperaturas de oxidación bajas conducen a un mayor desarrollo de porosidad por unidad de *burn-off*. También se ha observado que la porosidad se desarrolla principalmente en la etapa de desorción. Los carbones activados obtenidos presentan una distribución de tamaño de poro heterogénea. La muestra A275-950 C8 presenta los valores de superficie específica más elevados, con S_{BET} y S_{DA} cercanos a 1300 m^2g^{-1} y con un *burn-off* del 70 %, conservando la morfología granular inicial de las semillas y mostrando una buena resistencia mecánica durante los test de atrición.

En la activación con ozono de *char* de semillas de uva, el *burn-off*, el S_{BET} y el S_{DA} aumentan de forma lineal con el número de ciclos aplicados; los mayores valores se han obtenido para la combinación de temperaturas de oxidación-desorción de 275–850 ºC. Todas las muestras obtenidas presentan una distribución de tamaño de poro heterogénea centrada en 0,45, 0,55, 0,88 y 2,2 nm. Los espectros de FTIR del *char* y los carbones

activados obtenidos tras 5 ciclos de activación son similares en su patrón, aunque es destacable que las muestras poseen grupos oxigenados superficiales resistentes al tratamiento a alta temperatura en atmósfera inerte. La muestra con mayor desarrollo de superficie específica (O275-850 C7) alcanza valores de S_{BET} en torno a 1200 m^2g^{-1} y S_{DA} superior a 1500 m^2g^{-1} para un *burn-off* inferior al 60 %, con $V_{microN2}$, $V_{mesoTOTAL}$ y V_{macro} de 0,52, 0,055 y 0,45 cm^3g^{-1}, respectivamente.

En la activación en fase líquida de *char* de semillas de uva, el *burn-off* y la superficie específica aumentan casi linealmente conforme aumentan los ciclos de activación, siguiendo el siguiente orden $HNO_3 > (NH_4)_2S_2O_8 > H_2O_2$. En general, los *burn-off* son mayores en los carbones preparados a una temperatura de desorción de 950 ºC, mientras que los mayores valores de superficie específica se obtienen a temperaturas de 850 ºC. Los espectros de FTIR de las series desorbidas a 850 ºC muestran bandas centradas en 1050, 1700 y 3450 cm^{-1} que indican que la desorción a alta temperatura no elimina todos los grupos superficiales oxigenados creados en la oxidación. El mayor desarrollo de superficie específica se consigue en la activación con ácido nítrico tras sólo 5 ciclos de activación y empleando una temperatura de desorción de 850 ºC, llegándose a valores de S_{BET} y S_{DA} superiores a 1200 y 1300 m^2g^{-1}, respectivamente, con *burn-offs* en torno al 50 %. Para valores de *burn-off* equivalentes a éste, las muestras activadas con H_2O_2 y $(NH_4)_2S_2O_8$ desarrollaron unos valores máximos de S_{BET} de 600 y 800 m^2g^{-1}, tras 10 y 7 ciclos, respectivamente. Los carbones activados obtenidos por activación en fase líquida de char de semillas de uva son principalmente micro y macroporosos con una pobre contribución de mesoporos, principalmente cuando se utiliza ácido nítrico como oxidante.

Las diferentes variantes del método de activación por ciclos de oxidación-desorción proporcionan un buen desarrollo de porosidad en los dos materiales estudiados, en comparación con el *char* de partida, y mantienen la morfología granular tras numerosos ciclos de activación. El tipo de porosidad desarrollada depende del agente oxidante empleado y del *char*

de partida. El *char* de neumáticos fuera de uso desarrolla micro y mesoporosidad, tanto cuando se activa con oxidantes en fase gas como cuando se utilizan oxidantes en fase líquida. Por su parte, los carbones activados procedentes de *char* de semillas de uva presentan fundamentalmente macro y microporosidad, con una contribución muy baja de mesoporos, especialmente cuando la activación se realiza con ácido nítrico u ozono.

Los carbones activados obtenidos a partir de semillas de uva se han utilizado para preparar supercapacitores. Se seleccionaron carbones activados preparados por activación con aire, ozono y ácido nítrico atendiendo a su distribución de tamaño de poro principalmente microporosa. Al comparar el comportamiento electroquímico de las tres series de carbones activados en electrolitos neutro, básico y ácido se han obtenido mayores valores de capacitancia gravimétrica en H_2SO_4 mientras que los resultados más bajos se obtuvieron en Na_2SO_4. Por otra parte, la relación entre la capacitancia gravimétrica y las propiedades texturales de los carbones activados está dominada por problemas de conductividad. De hecho, cuando disminuye la conductividad del electrolito hay un aumento de la resistencia de los iones a la difusión dentro de los poros. Como consecuencia, el aumento de la S_{BET} y el volumen de microporos sólo tiene un efecto positivo sobre la capacitancia cuando se usa un electrolito de elevada conductividad como el H_2SO_4.

Con respecto al efecto del tamaño de poro sobre los rendimientos electroquímicos, se ha obtenido que para densidades de corriente bajas, la capacitancia específica aumenta para tamaños de poro medio menores a 1 nm, independientemente del electrolito y de los carbones activados utilizados en los supercapacitores. Estos resultados confirman que la doble capa es más eficiente en poros de ese tamaño. En cambio, cuando aumenta la densidad de corriente, poros demasiado pequeños tienen un efecto negativo sobre la capacitancia cuando se usa un electrolito con una conductividad baja como el Na_2SO_4. Por consiguiente, para potencias bajas, la densidad de

energía siempre ha sido mayor en Na_2SO_4 que en los electrolitos ácidos o básicos, a causa del elevado voltaje de la celda. Sin embargo, para tener beneficios de todas las ventajas de un electrolito como el Na_2SO_4 (no corrosivo y con un rango de voltaje de elevada energía) es necesario adaptar las propiedades texturales de los carbones activados con tamaños de microporos suficientemente grandes para mejorar la difusión de los iones dentro de los poros para alcanzar elevadas densidades de potencia.

Conclusions

The study on the preparation of carbonaceous materials from waste tires and grape seeds by pyrolysis and cyclic activation of oxidation-desorption, and on their application in energy storage, has led to the conclusions commented below.

With respect to the pyrolysis of grape seeds, the extraction of seed oil and the heating rate do not have a clear influence neither in yield non in elemental composition of the char. Conversely, the pyrolysis temperature shows an important influence on specific surface area, which reach maximum values of S_{BET} and S_{DA} around 600 – 800 ºC and 800 ºC, respectively. Likewise, the specific surface area values are higher in samples prepared by flash pyrolysis.

The char obtained in at the optimum pyrolysis conditions (800 ºC, FH) has a S_{DA} around 505 m^2g^{-1}, a S_{BET} of 47 m^2g^{-1} and a bimodal pore size distribution with micro and macroporosity ($V_{microCO2}$ = 0.2 cm^3g^{-1} and V_{macro} = 0.7 cm^3g^{-1}). The char presents granular morphology and shows good resistance to attrition, which increases when the external layers of particle are abraded.

The activation process by oxidation-desorption cycles is an effective method to develop porosity in the char obtained from waste tires and grape seeds that also allows to obtain granular materials. The activation conditions can be adjusted to provide control on pore size and a balance between specific surface area and burn-off.

The activation of waste tire char provided mainly mesoporous activated carbons. In the activation with air, the size of initial particle and the desorption temperature affected significantly burn-off and textural properties of the activated carbons obtained. The highest burn-offs values were obtained for extreme particle sizes (L and S) and for the highest desorption temperatures (650 and 750 ºC). The S_{BET}, in general, increased with the number of cycles applied. The series L-A650 showed notable differences with respect to the

other series from the third activation cycle. The average pore size decreased from the first cycle for all series, reaching values between 12 and 30 nm after 6 activation cycles and around 10 nm after 20 activation cycles, with a higher contribution of wider mesoporous for samples prepared at the highest desorption temperatures. The analysis of pore volume shows that mesoporosity increases gradually from the first cycle, while microporosity develops from 4th cycle. The results of TPO characterization indicate that the application of 20 activation cycles leads to the complete elimination of the most reactive carbon present in the initial char, which may be related to the initial development of mesoporosity.

The highest specific surface area development during the activation with air of waste tire char is achieved for samples with an initial particle size of 2 mm and for a desorption temperature of 650ºC (L-A650 series). Thus, S_{BET} values close to 600 m^2g^{-1} with a burn-off around 45 % and granular morphology are obtained.

With respect to the liquid phase oxidants evaluated (HNO_3, H_2O_2 and $(NH_4)_2S_2O_8$) in the activation of waste tires char, the oxidation with nitric acid and hydrogen peroxide led to a higher porosity development than ammonium persulphate oxidation. For 15 activation cycles a steady increase of burn-off was observed, which was higher for activated carbons obtained by nitric acid oxidation. It was found that a higher concentration of oxidant agent led to higher burn-off, especially in the case of hydrogen peroxide, although no significant differences were observed in terms of S_{BET} per burn-off unit. The pore volume analysis showed that the mesoporosity increased significantly in the first cycles for the series of samples activated with nitric acid, and in a minor extent for the series activated with hydrogen peroxide and ammonium persulphate. The development of micropores was only significant for the series activated with nitric acid and from 3rd cycle. For the series of samples obtained with 30 % oxidant, a collapse of micropores is produced from cycle number 10, which correspond with a significant increase of mesoporous

volume at this point. The type of oxidant used did not affect the average pore size, whereas it was influenced by the concentration of oxidant.

The activation of waste tires char with 30 % HNO_3 and 30 % H_2O_2 led to the highest development of S_{BET} with values of 750 and 400 m^2g^{-1} and a average pore size of 12 and 17 nm, respectively, but with burn-off values around 90 %.

The activation with air of grape seeds char resulted mainly micro and macroporous solids. The highest values of burn-off, S_{BET} and S_{DA} was obtained by the combination of high oxidation and desorption temperatures (275–850 and 275–950 ºC), although the lower oxidation temperatures lead to a higher porosity development per burn-off unit. It was also observed that the porosity is mainly developed in the desorption stage. The activated carbons obtained present a heterogeneous pore size distribution. The A275-950 C8 sample exhibits the highest specific surface area, with S_{BET} and S_{DA} values close to 1300 m^2g^{-1} and with burn-offs around 70 %, while keeping the granular morphology of initial seeds and showing a good mechanic resistance during attrition tests.

In the activation with ozone of grape seeds char, the burn-off, the S_{BET} and the S_{DA} showed a gradual increase with the number of activation cycles applied; the highest values were obtained for a oxidation and desorption temperature of 275 and 850 ºC, respectively. The samples obtained present a heterogeneous pore size distribution centered at 0.45, 0.55, 0.88 and 2.2 nm. The FTIR spectrum of char and activated carbons obtained after 5 activation cycles are similar in pattern. It is remarkable that the activated carbon samples have surface oxygen groups resistant to high temperature treatment in inert atmosphere. The sample with the highest specific surface area development (O275-850 C7) reached S_{BET} values around 1200 m^2g^{-1} and S_{DA} values above 1500 m^2g^{-1} for a burn-off lower than 60 %, with $V_{microN2}$, $V_{mesoTOTAL}$ y V_{macro} of 0.52, 0.055 and 0.45 cm^3g^{-1}, respectively.

In the liquid phase activation of grape seed char, the burn-off and specific surface area increased gradually along the activation cycles, the values being dependent on the type of oxidant in the following order HNO_3 > $(NH_4)_2S_2O_8$ > H_2O_2. In general, the burn-off values were higher for the activated carbons prepared at desorption temperatures of 950 ºC, while higher values of specific surface area were obtained at desorption temperature of 850 ºC. The FTIR spectrum of series subjected to desorption at 850 ºC showed bands centered at 1050, 1700 and 3450 cm^{-1} that indicate that desorption at high temperature do not eliminate completely the surface oxygen groups created in oxidation stage. The higher specific surface area development was achieved in the activation with nitric acid with only 5 activation cycles and at a desorption temperature of 850 ºC, reaching S_{BET} and S_{DA} values above 1200 and 1300 m^2g^{-1}, respectively, with burn-off values around 50 %. For burn-off values equivalent to this last, the samples activated with H_2O_2 and $(NH_4)_2S_2O_8$ developed a maximum values of S_{BET} of 600 and 800 m^2g^{-1}, after 10 and 7 activation cycles, respectively. In activation by liquid phase oxidation of grape seeds char were favors both micro and macropores development especially when oxidation were carried out with nitric acid.

The different conditions studied for cyclic oxidation-desorption oxidation provide a good development of porosity for waste tires and grape seeds char, while maintaining the granular morphology of the material after several activation cycles. The type of pores developed depends on the oxidant used and the starting char. The waste tires char developed mainly micro and mesoporosity upon both gas phase and liquid phase oxidation. The activated carbons obtained from grape seeds char exhibit mainly macro and mesoporosity, with a very low contribution of mesopores, especially when the oxidation is carried out with nitric acid or ozone.

The activated carbons obtained from grape seeds char were used to prepared electrodes used in supercapacitors. This activated carbons prepared by activation with air, ozone and nitric acid were selected attending

to their mainly microporous character. By comparing the electrochemical performance of the three series of carbons in a neutral, basic and acidic electrolyte (Na_2SO_4, KOH and H_2SO_4) it has been shown that the highest values of gravimetric capacitance for a same electrode active material were obtained in H_2SO_4 while the lowest were shown in Na_2SO_4. Moreover, the relationship between the gravimetric capacitance and the textural parameters of the electrode material is also mastered by conductivity issues. In fact, when decreasing the conductivity of the electrolyte there is an increase of the ions diffusion resistance to penetrate the micropores. As a consequence, the increasing of the specific surface area and of the micropore volume have only a positive effect on the capacitance when using the electrolyte with the highest conductivity, i.e. H_2SO_4.

Regarding the effect of the pore size on the electrochemical performances, it has been shown that for small current densities, the known trend in which the specific capacitance increases for average pore sizes smaller than 1 nm is obtained independently of the electrolyte used for the supercapacitors built with all the carbon series. Such results confirm that the double layer is more efficiently formed in pores of this size. However, when increasing current densities, such small pore sizes have a negative effect on the capacitance when using a poorly conductive electrolyte as Na_2SO_4. Consequently, for small powers the energy density is always higher in Na_2SO_4 than in the acidic or basic electrolyte independently of the porous texture of the electrode active material in reason of the higher cell voltages. However, for taking profit of all the advantages of a non-corrosive, high energy potential window electrolyte as Na_2SO_4 it is necessary to adapt the porous texture of the carbon material with micropore sizes large enough for improving the ions diffusion inside the porosity for attaining high power densities.

ANEXOS

APPENDICES

Appendix 1. Nomenclature

AC	Activated carbon
ANOVA	Analysis of variance
BET	Brunauer – Emmet – Teller
BJH	Barret – Joyner – Halenda.
BO	Burn-off (%)
C	Capacitance (Fg^{-1})
Cs	Specific capacitance (μFcm^{-2})
CV	Cyclic voltammetry
DA	Dubinin-Astakhov
$\mathbf{d_{meso}}$	Mean mesopore size (nm)
$\mathbf{d_{micro}}$	Mean micropore size (nm)
DR	Dubinin-Radushkevich
EA	Elemental analysis
EDLC	Electric double-layer capacitor
EDR	Equivalent distributed resistance (Ω)
$\mathbf{E_{max}}$	Maximum energy (obtained at $200mAg^{-1}$ of current density) ($Wh\ kg^{-1}$)
ESR	Equivalent series resistance (Ω)
FTIR	Fourier transform infrared spectroscopy
GA	Galvanostatic charge/discharge
GS	Grape seed
I	Current density (mAg^{-1})
ICP-MS	Inductively coupled plasma mass spectrometry
$\mathbf{L_0}$	Mean micropore size calculated by Stoeckli equation (nm)
NLDFT	Non-Local Density Functional Theory
$\mathbf{NLDFT_{CO2}}$	Non-Local Density Functional Theory applied to CO_2 isotherms
$\mathbf{NLDFT_{N2}}$	Non-Local Density Functional Theory applied to N_2 isotherms
NOU	Net oxygen uptake (%)

PSD	Pore size distribution
P/P_0	Relative pressure
S_{BET}	Specific surface area calculated from BET equation (m^2g^{-1})
S_{DA}	Specific surface area calculated from DA model (m^2g^{-1})
S_{DR}	Specific surface area calculated from DR model (m^2g^{-1})
SEM	Scanning electronic microscopy
SSA	Specific surface area (m^2g^{-1})
TGA	Thermogravimetric analysis
TPD	Temperature programmed desorption
TPO	Temperature programmed oxidation
V_{macro}	Macropore volume (cm^3g^{-1})
$V_{microCO2}$	Micropore volume from CO_2 isotherm (cm^3g^{-1})
$V_{microN2}$	Micropore volume from N_2 isotherm (cm^3g^{-1})
$V_{Narrow\text{-}meso}$	Narrow mesopore volume (cm^3g^{-1})
$V_{mesoTOTAL}$	Mesopore total volume (cm^3g^{-1})
V_T	Total pore volume ($V_{microN2} + V_{mesoN2}$) (cm^3g^{-1})
XPS	X-ray photoelectron spectroscopy
WTR	Waste tire rubber

Appendix 2. Diffusion of results

Scientific publications:

- F. Heras, N. Alonso-Morales, D. Jiménez-Cordero, M.A. Gilarranz, J.J. Rodríguez. *Granular mesoporous activated carbons from waste tires by cyclic oxygen chemisorption desorption*. Ind. Eng. Chem. Res. 2012; 51: 2609 – 2614.

- D. Jiménez-Cordero, F. Heras, N. Alonso-Morales, M.A. Gilarranz, J.J. Rodríguez. *Porous structure and morphology of granular chars from flash and conventional pyrolysis of grape seeds*. Biomass Bioenergy 2013; 54: 123 – 132.

- D. Jiménez-Cordero, F. Heras, N. Alonso-Morales, M.A. Gilarranz, J.J. Rodríguez. *Development of porosity upon physical activation of grape seeds char by gas phase oxygen chemisorption-desorption cycles.* Chem. Eng. J. 2013; (submitted).

- F. Heras, D. Jiménez-Cordero, M.A. Gilarranz, N. Alonso-Morales, J.J. Rodríguez. *Activation of waste tires char by cyclic liquid-phase oxidation*. Unpublished results 2013.

- D. Jiménez-Cordero, F. Heras, N. Alonso-Morales, M.A. Gilarranz, J.J. Rodríguez. *Gas phase oxidation with ozone for the preparation of granular activated carbons from grape seeds by cyclic oxidation-desorption*. Unpublished results 2013.

- D. Jiménez-Cordero, F. Heras, N. Alonso-Morales, M.A. Gilarranz, J.J. Rodríguez. *Preparation of granular activated carbons from grape seeds by cycles of liquid phase oxidation and thermal desorption.* Fuel Proc. Tech. 2013; (submitted).

- D. Jiménez-Cordero, F. Heras, M.A. Gilarranz, E. Raymundo-Piñero. *Study on application of grape seeds-based activated carbon as electrode material and their capacitance properties in different electrolytes.* Unpublished results. 2013.

National and international congresses:

- F. Heras, D. Jiménez-Cordero, M.A. Gilarranz, N. Alonso-Morales, J.J. Rodríguez. *Cyclic oxygen chemisorption-desorption for the activation of waste tires char.*

3rd International Conference for Energy Storage/ Conversion and Environment Protection (CESEP). Torremolinos, Málaga (Spain). October 2009.

(Poster presentation)

- D. Jiménez-Cordero, F. Heras, M.A. Gilarranz, N. Alonso-Morales, J.J. Rodríguez. *Control del desarrollo de porosidad en la activación de char de neumáticos mediante ciclos de quimisorción / desorción de oxígeno.*

10th Reunión del Grupo Español del Carbón. Gerona (Spain) May 2010.

(Oral presentation)

- F. Heras, D. Jiménez-Cordero, M.A. Gilarranz, N. Alonso-Morales, J.J. Rodríguez. *Control of the porosity development in waste tires char activation by cyclic oxygen chemisorption-desorption.*

The Annual World Conference on Carbon. Clemsom (USA) July 2010.

(Poster presentation)

- F. Heras, N. Alonso-Morales, D. Jiménez-Cordero, M.A. Gilarranz, J.J. Rodríguez. *Granular mesoporous activated carbons from waste tires by cyclic oxygen chemisorption-desorption.*

The Annual World Conference on Carbon. Shangai (China) July 2011.

(Poster presentation)

- D. Jiménez-Cordero, F. Heras, M.A. Gilarranz, N. Alonso-Morales, J.J. Rodríguez. *Preparation of adsorbents by pyrolysis of grape seeds.*

The Annual World Conference on Carbon. Shangai (China) July 2011.

(Oral presentation)

- F. Heras, D. Jiménez-Cordero, M.A. Gilarranz, N. Alonso-Morales, J.J. Rodríguez. *Oxidación en fase líquida para la activación de char de neumáticos fuera de uso mediante ciclos de quimisorción / desorción de oxígeno.*

11th Reunión del Grupo Español del Carbón. Badajoz (Spain) October 2011.

(Oral presentation)

- D. Jiménez-Cordero, F. Heras, M.A. Gilarranz, N. Alonso-Morales, J.J. Rodríguez. *Control del desarrollo de porosidad en la activación de char de semillas de uva mediante ciclos de quimisorción / desorción de oxígeno.*

11th Reunión del Grupo Español del Carbón. Badajoz (Spain) October 2011.

(Oral presentation)

- D. Jiménez-Cordero, F. Heras, M.A. Gilarranz, N. Alonso-Morales, J.J. Rodríguez. *Activation of grape seeds char by oxygen chemisorption – desorption finding activation conditions.*

The Annual World Conference on Carbon. Krakow (Poland) June 2012.

(Poster presentation)

- D. Jiménez-Cordero, F. Heras, M.A. Gilarranz, N. Alonso-Morales, J.J. Rodríguez. *Development of porosity in the activation of grape seeds char by cyclic oxygen chemisorption-desorption.*

The Annual World Conference on Carbon. Krakow (Poland) June 2012.

(Oral presentation)

- D. Jiménez-Cordero, F. Heras, M.A. Gilarranz, N. Alonso-Morales, J.J. Rodríguez. *Development of porosity upon physical activation of grape seeds by gas phase ozone chemisorption-desorption cycles.*

The Annual World Conference on Carbon. Rio de Janeiro (Brazil) July 2013.

(Poster presentation)

- D. Jiménez-Cordero, F. Heras, M.A. Gilarranz, N. Alonso-Morales, J.J. Rodríguez. *Liquid phase oxidation for the preparation of granular activated carbons from grape seeds by cyclic oxidation-desorption.*

The Annual World Conference on Carbon. Rio de Janeiro (Brazil) July 2013.

(Poster presentation)

- D. Jiménez-Cordero, F. Heras, M.A. Gilarranz, N. Alonso-Morales, J.J. Rodríguez. *Control del desarrollo de porosidad en la activación con ozono de char de semillas de uva mediante ciclos de oxidación / desorción.*

12th Reunión del Grupo Español del Carbón. Madrid (Spain) October 2013.

(Poster presentation)

- D. Jiménez-Cordero, F. Heras, M.A. Gilarranz, N. Alonso-Morales, J.J. Rodríguez. *Oxidación en fase líquida para la preparación de carbones activos granulares a partir de char de semillas de uva por ciclos de oxidación-desorción.*

12th Reunión del Grupo Español del Carbón. Madrid (Spain) October 2013.

(Poster presentation)

Notes


UAM
UNIVERSIDAD AUTONOMA
DE MADRID